ISOTOPIC STUDIES OF AEROSOL SULPHATE AND AMMONIUM IN THE MARINE ATMOSPHERE

CHENG-TING LIN

A thesis presented to the School of Environmental Sciences, University of East Anglia, in the candidature for the degree of Doctor of Philosophy

September 2010

ABSTRACT

Studies carried out in this thesis focus on measuring the isotopic composition and ionic composition of atmospheric aerosol samples. Aerosol filters were obtained for seven cruises travelling down the Atlantic Ocean from the UK to Cape Town, South Africa; across the Atlantic from the U.S. to Europe; and around Montserrat.

Aerosol analyses for sodium, potassium, calcium, ammonium, sulphate, nitrate and methanesulfonic acid (MSA) was carried by ion chromatography. Results are used in conjunction with five-day air parcel back trajectories to consider sources of aerosol ions, particularly sulphate and ammonium.

Isotopic analysis for aerosol sulphate used using barium sulphate precipitation and isotope ratio mass spectrometry (IRMS). A new method was developed, based on McIlvin & Altabet (2005) and Zhang et al. (2007) to allow accurate measurements of ammonium isotopes composition on small sample sizes using IRMS with an analytical precision of 0.2‰ for triplicate measurements.

Sulphate isotopic composition ranges from +6 to +20‰. Based on isotopic composition of sources the relative importance of anthropogenic (0% to 80%); biogenic (11% to 90%) and seasalt sulphate (0.6% to 60%) were estimated. Maximum anthropogenic contributions were observed near continents in the Northern Hemisphere (60~80%) and maximum biogenic contributions over the remote North and South Atlantic. For the first time the ratio of MSA/biogenic sulphate from DMS oxidation in the atmosphere is directly estimated; the MSA/bio SO_4 ratio ranges from 0.1 over the tropical Atlantic to 0.7 in the remote South Atlantic.

Aerosol ammonium isotopic composition ranges from -12 to +14 ‰. The data was used to perform segregation into two sources, similar to sulphate. For the majority of sampling locations, anthropogenic ammonium is dominant but, the biogenic source becomes significant in the South Atlantic, and in tropical waters, exceeding 50%.

Acknowledgement

Firstly, I owe my deepest gratitude to Tim Jickells for his enthusiasm, patience, never-ending support, supervision and, most of all, inspiration over the past 4 years. I must also thank my co-supervisors, Alina Marca-Bell, Alex Baker, Peter Liss and Simon Kelly for their continuous support on all aspects.

This thesis would not have been possible without Tim Lesworth and Alex Baker, who have provided me with all the samples and data presented in this thesis, and I have ended up with a dataset sufficient for a PhD without having to collect samples myself. I could not have gone through ammonium isotope analysis so smoothly without the help of Laura Bristow, Alison Bateman and Alina Marca-Bell. Thanks to Simon Kelly for providing help on sulphate isotope analysis from beginning to the end. Thanks also to Kimberly Wright, who has helped my ion chromatograph analysis. Also to Tom Bell, in particular, for the inspiration for one of the most important graph plots in this thesis. Thank you also for the guidance and help on statistics.

I would especially like to thank all my friends for continuous support, in particular my landlord Colin Bevan - thank you for the numerous delicious cooking. Shintaro Yanagi, Ricardo Correia and Jonatan Sánchez Martín all deserve a special mention. Lastly, to my family for their continuous encouragement. None of this would have been possible without your support.

LIST OF CONTENTS

List of Figures

List of Tables

Chapter 1: Introduction

In this chapter background information on the field of the thesis will be presented. This chapter will aid the descriptions and explanations listed in the later chapters. This thesis focuses entirely on aerosol chemistry in general and the isotopic composition of aerosol sulfur and nitrogen as sulfate and ammonium specifically. A general introduction will be provided before getting into the details this thesis focuses on.

1.1 Aerosol Formation

Aerosols refer to the fine particles suspended in the atmosphere derived from a number of sources. In general, significant contributors are wind-borne dust, sea spray and volcanoes (Raes et al., 2000). Ever since the industrial revolution, anthropogenic inputs such as combustion of fossil fuels and biomass have also become a significant factor to the overall context (Table 1.1). Aerosols represent an important part of the geochemical cycle and atmospheric transport.

Table 1.1 An estimated global particle emission to the atmosphere (Raes, 2000)

	Source strength (Tg yr^{-1})
Sea salt	
Total	5900
0–2 μm	82.1
2–20 μm	2460
Soil dust	
< 1 μm	250
1–10 μm	1000
0.2–2 μm	250
2–20 μm	4875
Organic carbon	
Total	69
Biomass burning	54.3
Fossil fuel	28.8
Terpene oxidation	18.5
Black carbon	
Total	12
Biomass burning	5.6
Fossil fuel	6.6
Sulfate (as H_2SO_4)	
Total	150
Natural	32
Anthropogenic	111
Nitrate	11.3[a]
Ammonium	33.6

Table 1.1 lists out some of the most dominant sources of particles in the atmosphere forming aerosols. Sea spray from whitecaps and soil dust from inland or desert regions are two major sources of aerosol. Biogenic and anthropogenic sources are also significant.

Primary aerosols are particles such as sea spray or soil dusts that are introduced into the atmosphere through mechanical processes, for example sea spray and soil particles. Several species of aerosol are not released into the atmosphere directly, but formed in the atmosphere as secondary aerosols. The formation of secondary aerosols is through the reaction of gases in the atmosphere, which then either aggregate into clusters to form small particles or attach onto other existing particles (O'Dowd and Leeuw, 2007). An example is the emission of SO_2 which is oxidised to sulfuric acid in the atmosphere (equation 1.1 & equation 1.2) and

can then either form aerosol sulfuric acid or reacts with ammonia to form ammonium sulfate (equation 1.3).

$SO_{2\,(g)} + H_2O_{\,(l)} <-> H^+_{\,(aq)} + HSO_3^-{}_{(aq)}$ **Equation 1.1**

$HSO_3^-{}_{(aq)} + OH^-_{\,(aq)} \rightarrow 2H^+_{\,(aq)} + 2SO_4^{2-}{}_{(aq)}$ **Equation 1.2**

$2NH_{3\,(aq)} + H_2SO_{4\,(aq)} \rightarrow (NH4)_2SO_{4\,(aq)}$ **Equation 1.3**

Apart from their sources and origin, aerosols have also been classified by their size. A relative wide range of aerosol sizes, from a few nanometres to tens of micrometers, can be found (Raes et al., 2000), and classified into two separate categories. Aerosol particles with a diameter larger than 1μm are classified as coarse mode aerosol; particles that are smaller than 1μm are categorized into fine mode aerosol. Although smaller particles in the order of a few nanometres are found, they grow into larger aggregates (<1μm) very rapidly through nucleation and coagulation, hence are not classified into another category (Raes et al., 2000). It is worth noting that each mode are formed in different ways and have characteristic chemistry (figure 1.1)

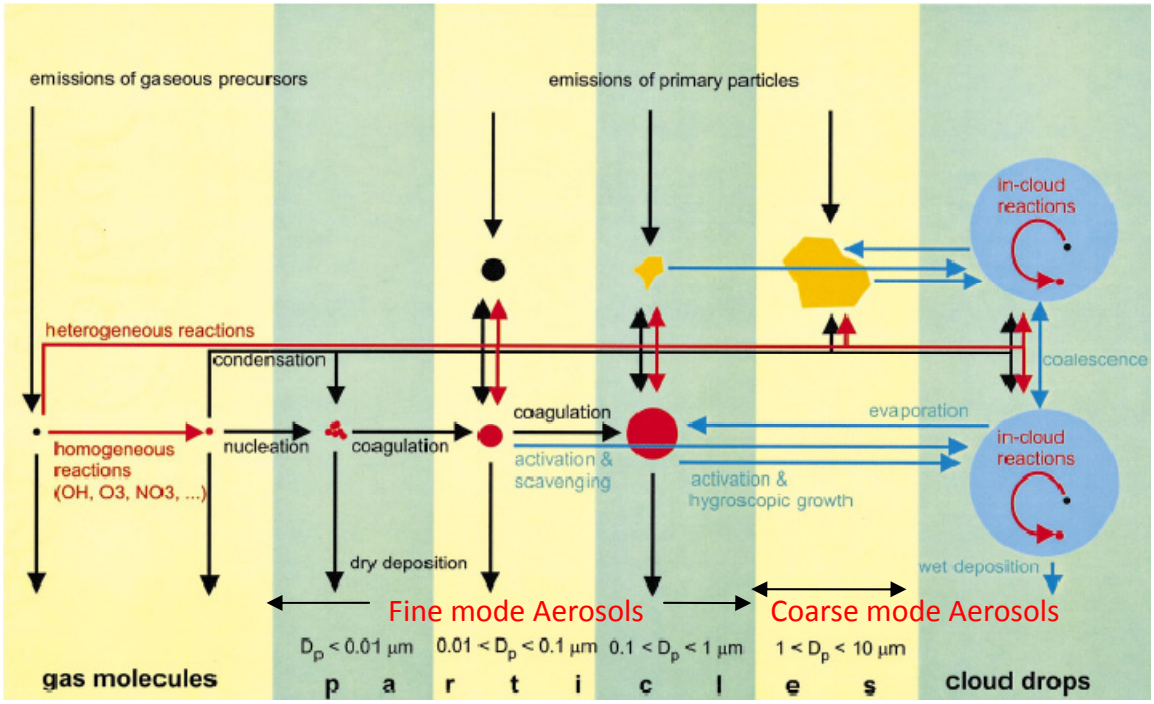

Figure 1.1 A schematic summarising the growth of aerosol particles (Raes et al. 2000).

1.2 Aerosol and Climate Change

Aerosols play a crucial role in the climate system globally, and contribute significantly to the atmospheric geochemistry. Complex reaction pathways have been identified to be very important in the cycling of several major chemicals in the natural system. The formation of aerosol is also known to be related to cloud formation, which in term affects cloud cover. This will have an influence on the cloud albedo, which is one of the factors affecting global temperature controls (TAR, Ramaswamy et al., 2003).

The potential effect of aerosols on climate change was highlighted by the Intergovernmental Panel on Climate Change, or IPCC for short, in their Third Assessment Report (TAR, Ramaswamy et al., 2003), occupying two out of fourteen chapters dedicated to the description and evaluation of aerosols. However, there are still a lot of unknowns and

uncertainties to be researched in this topic, particularly on the reaction pathways, which are complex and intertwined with one another throughout the system, making it more difficult to evaluate. Nevertheless, the effect of aerosol on cloud cover and global temperature has attracted much research interest, and in the TAR it is suggested that clouds influence global temperature control and may play a crucial role in the ongoing global warming debate (Figure 1.2).

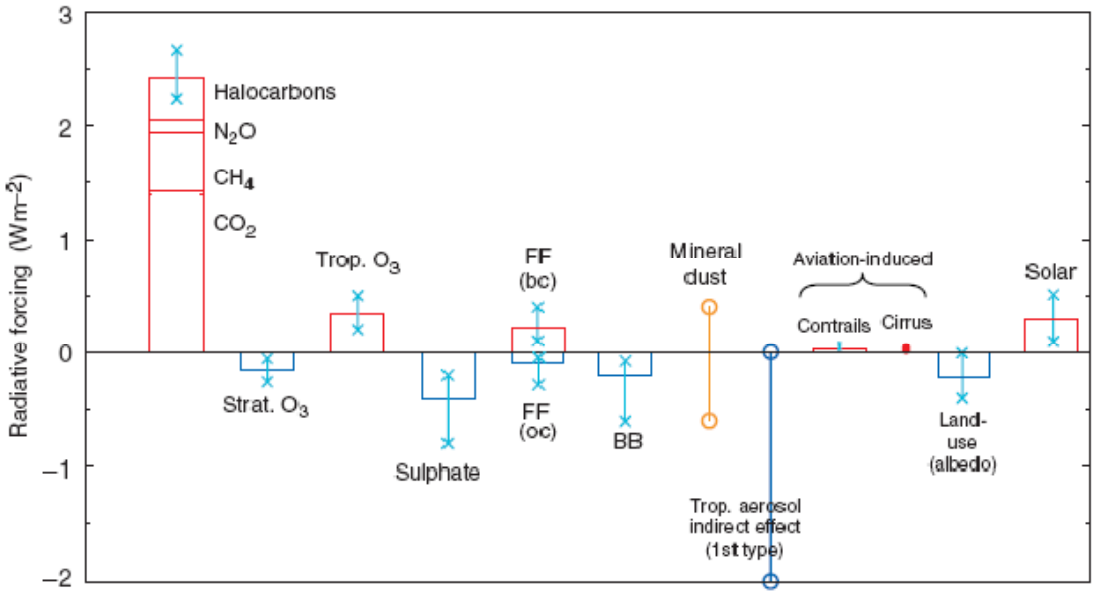

Figure 1.2 Global, annual mean radiative forcings (Wm^{-2}) affected by a number of agents for a period of pre-industrial to about 2000 B.C. in present. FF indicates fossil fuel combustion and BB represents biomass burning. Taken from IPCC TAR (Ramaswamy et al., 2003).

In figure 1.2 above, it can be seen that aerosol may have a negative radiative forcing, having a similar magnitude, but opposite to the forcings by a combination of CO_2, CH_4, N_2O and halocarbons. The mechanism of such negative forcing will be described later, but it is important to identify that, in theory, the influence by aerosols may become a negative feedback system to the global temperature rise, ultimately dampening the greenhouse warming effect. However, it is also clear from figure 1.2 that the uncertainties associated

with the indirect effect of aerosol are particularly large, reflecting that much still need to be studied in the subject.

1.3 Aerosol Chemistry

This thesis will be focusing entirely on the chemistry of the marine aerosol system, analyzing aerosol filter samples from a number of cruises. The filters are analysed for the major ions sodium, potassium, calcium, ammonium, chloride, nitrate, sulfate and methanesulfonic acid (MSA). In this section the sources of these ions will be discussed. Only aerosol components that are important to the marine atmospheric cycle will be mentioned. Separating samples into fine and coarse mode can also make better estimates of deposition fluxes, since coarse mode aerosols will deposit faster than fine ones due to their size (Baker et al. 2007; Raes et al., 2000), and sodium & magnesium ions are usually used as tracers of the source (Keene et al., 1986). Further details on the sampling of aerosols will be described in the methodology chapter. Although aerosol species are classified into coarse and fine modes, this alone is not sufficient to evaluate natural and anthropogenic perturbations that have seasalt, biogenic and anthropogenic sources of certain species such as sulfate. A numerical correction that separates seasalt from non-seasalt fraction of sulfate enables in-depth analysis of aerosol and the evaluation of the potential anthropogenic input. The mechanism of this correction is discussed later.

Among the aerosol components mentioned above, sea spray is found predominantly in

coarse mode aerosol samples and hence rapidly deposits (Raes et al., 2000). Seasalt aerosol has essentially the same composition as seawater (Keene et al., 1986). Input of terrestrial dust is also an important coarse mode aerosol component and this carries with it the chemical composition of soils. In this study non-seasalt calcium is a convenient tracer of dust. Calcium can be found frequently in rocks such as calcite, aragonite, limestone, chalk, to a lesser extent gypsum ($CaSO_4$), and others in the form of carbonate ($CaCO_3$). It represents a major component and is hence a suitable tracer of soil dust (Andrews et al., 2004), although the concentration of calcium in soils will vary from place to place, which does limit the quantitative use of this tracer. These soils can be lifted into the air to form aerosols, particularly from desert environment. Reactions of $CaCO_3$ with sulfuric acid in the atmosphere will reduce acidity and form $CaSO_4$.

The sources of potassium are well defined, and predominantly from sea spray and biomass burning. If the sea-spray component is corrected for, non-seasalt potassium is a good tracer for biomass burning (Andreae & Merlet, 2001). Potassium is a crucial nutrient for plants, used for protein synthesis and the opening-closing of stomata. Potassium is therefore found in high concentrations in plant cells. Therefore although potassium is also found in salts and minerals, the combustion of biomass will result in a large input of non-seasalt K into the atmosphere.

A combination of sulfate and methanesulfonic acid (MSA) has provided a means to measure and analyse biogenic sulfur species, derived from the oxidation of dimethylsulfide (DMS)

in the atmosphere, and this is discussed extensively later. The nitrogen species of ammonium and nitrate are potential tracers for agricultural activities, such as fertilizers and combustion of biomass (see chapter 1.4). Ammonium is believed to have a relatively weak but potentially important marine source (Jickells et al., 2003). A summary of aerosol sources and their tracer is presented below (Table 1.2).

Table 1.2 A short summary of some major marine aerosol species analysed in this thesis.

Tracer	**Source**	**Reference**
Sea Spray (Na)	White caps & wind	Andrews et al. (2004) Keene et al. (1986)
Calcium	Desert dust ($CaCO_3$ + $CaSO_4$)	Baker et al. (2006)
Potassium	Biomass Burning	Andreae (1983) Andreae & Merlet (2001)
Ammonium	Agricultural practices Biomass burning Marine (weak)	Baker et al. (2006) Andreae & Merlet (2001)
Sulfate	Fossil fuel combustion, Oxidation of DMS (biogenic) Volcanoes Seasalt	Andrews (2004)
Nitrate	Derivative of NO_x from industrial/biomass combustion (reaction 1.4.1) Lightning strikes	Andrews (2004) Duce et al. (2008)
Methanesulfonic Acid (MSA)	Oxidation of DMS (biogenic)	Charlson et al. (1987)

1.4 The Nitrogen Cycle

The global nitrogen cycle is very important from many perspectives. Reactive species of nitrogen act as reaction radicals in several important atmospheric chemical reactions. Nitrogen species deposits from the atmosphere in the form of nutrients required for primary production (Gruber & Galloway, 2008), and become a crucial component for chemical pathways taking place such as the production of enzymes and formation of amino acids. It is worth noting that without anthropogenic perturbations, the amount of nitrogen available is limited. This makes nitrogen one of the limiting factors controlling net primary productions, hence having an effect on species further up the food chain (Gruber & Galloway, 2008). Since the introduction of artificial fertilizers to enhance agricultural yield, the nitrogen cycle has been heavily affected, resulting in an enrichment of nutrients to the natural system, causing environmental problems such as eutrophication in lakes and estuaries. The increase of nitrogen in the natural systems has also contributed to the loss of stratospheric ozone via the production of N_2O (Galloway et al., 2003). An assessment of the anthropogenic impact on the natural system will be discussed later. This thesis will focus predominantly on the coastal and marine nitrogen cycle, whilst describing pathways on land where necessary.

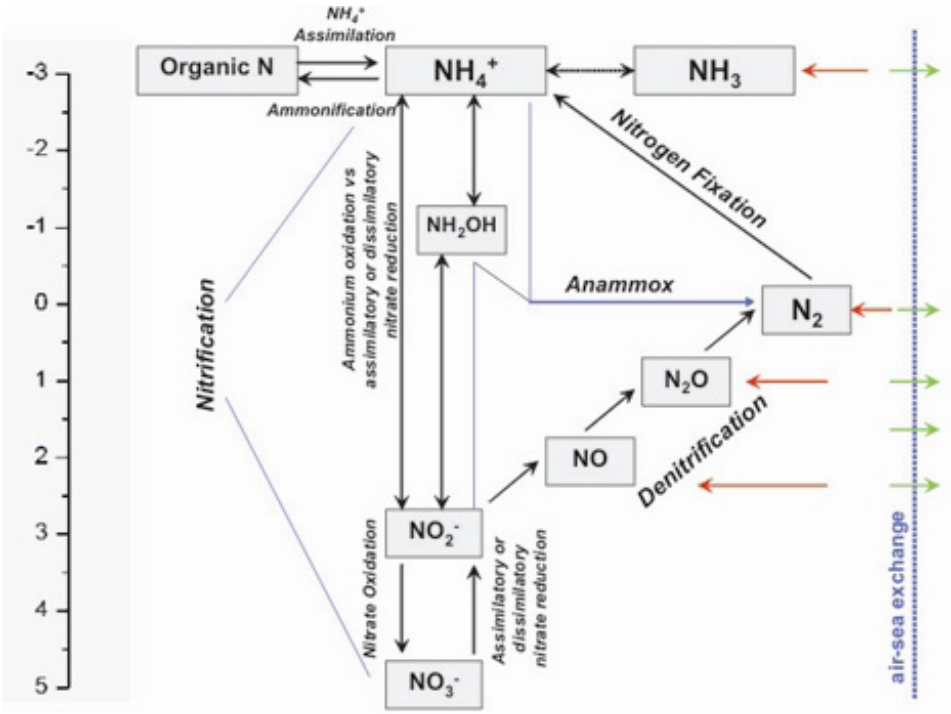

Figure 1.3 A schematic diagram of different species of nitrogen in marine and coastal system. Specific processes that take place in the transformation are noted, and the oxidation states are plotted against corresponding species. Schematic is taken from Purvaja et al. (2008).

Figure 1.3 presents nitrogen species that exist in the coastal and marine system, in aqueous form in the ocean or as gaseous states in the atmosphere. Within the species mentioned in the diagram, there are three species that are particularly important in the whole nitrogen cycle (Andrews et al., 2004): nitrogen gas (N_2) has an oxidation state of zero, nitrate (NO_3^-) has an oxidation state of plus five (5+), and ammonium (NH_4^+) has an oxidation state of minus three (3-). Nitrogen as a gas (N_2) is kinetically stable due to its nitrogen triple bond, and therefore requires a lot of energy in order to be assimilated by nitrogen-fixing bacteria, which exist where nitrogen gas is the only source of nitrogen in the area. Lightning and nitrogen-fixing micro-organisms are two major natural sources of nitrogen fixation in terrestrial and aquatic systems. Ammonium is produced by the decomposition of organisms, either dissolved in water or trapped on the surface of soil particles (Andrews et al., 2004).

Ammonium are then absorbed by plants and microbes, or oxidised to nitrite and ultimately nitrate.

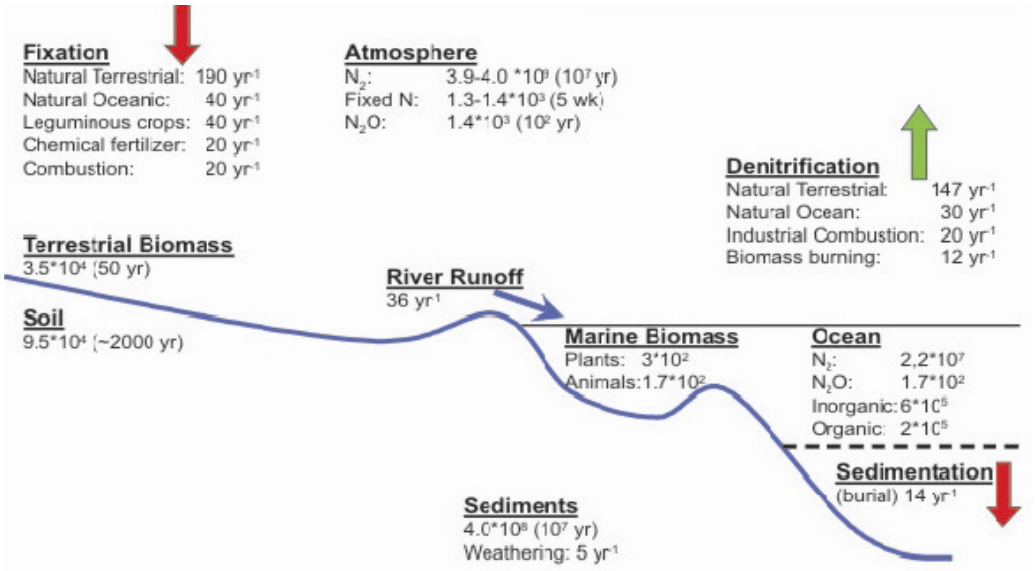

Figure 1.4 Global nitrogen fluxes, reservoirs (Purvaja et al., 2008). The sizes are given in Tg (10^{12}g) and fluxes in $TgNyr^{-1}$. The terminology Tg and TgN are not shown in the schematic. Residence times within the relevant environmental compartment are given in brackets.

Figure 1.4 provides supplementary information to figure 1.3. By referring to the fluxes, reservoirs and residence times, one can assess individual processes in more detail. It can be seen that the natural fluxes of nitrogen are still dominant over anthropogenic influences, such as the natural flux from terrestrial and marine system with a natural N_2 fixation rate 230 $TgNyr^{-1}$ and anthropogenic fixation 80 $TgNyr^{-1}$, although such budgets are rather uncertain. For example, Gruber & Galloway (2008) suggested a relatively larger anthropogenic fixation compared to the natural one. However, the accumulation of nitrogen by anthropogenic activities is certainly significant in all budgets, having potential harmful effects that are mentioned above.

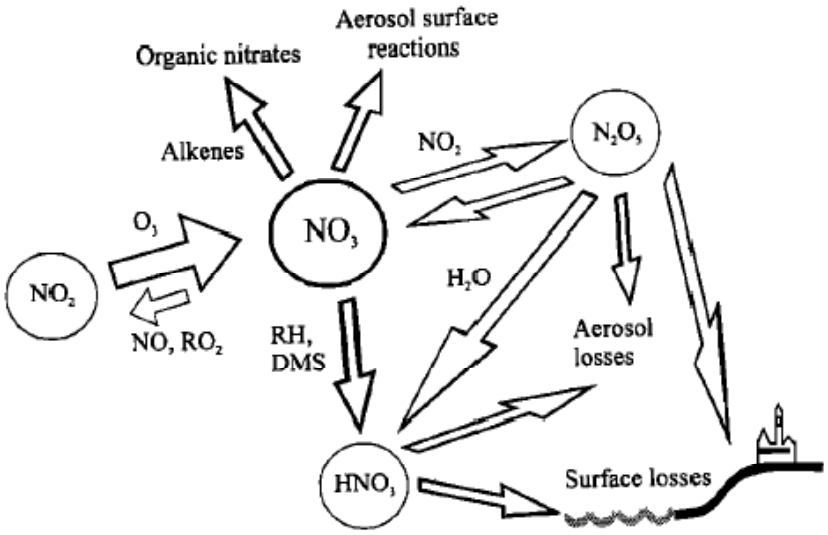

Figure 1.5 A simple schematic of nitrate cycling in the atmosphere and possible reaction pathways (Allan et al., 2000)

As noted above, the nitrate radical (NO_3) is an important oxidant in the atmosphere (alongside with OH and O_3). Figure 1.5 provides a general picture of the nitrate radical reaction pathways in the marine atmosphere, and describes processes in more detail compared to figure 1.3. The oxidation of organic materials by microorganisms will produce ammonia gas (NH_3), which subsequently oxidize to nitrite (NO_2^-) and then nitrate (NO_3^-), as shown in figure 1.3.The majority of nitrate in the marine atmosphere will be expected to be found in coarse mode aerosols due to the photolysis (equation 1.4) of nitrate during daytime into N_2O_5 (Andreae & Crutzen, 1997). This then reacts with water vapour in the air to form nitric acid (equation 1.6), which is associated with sea spray and found in the coarse mode (equation 1.7). In the absence of seasalt in the terrestrial environment, ammonium nitrate (NH_4NO_3) is formed (equation 1.8), which is categorized as fine mode aerosol (Raes et al., 2000). However this will dissociate in the remote marine atmosphere due to the presence of seasalt, which removes HNO_3 and cause a displacement in the equilibrium

(equation 1.8) to release NH_3 and HNO_3. Hence in the marine atmosphere nitrate is predominately found in the coarse mode, with minor concentrations found in the fine mode (Baker et al., 2006).

$NO_2 + O_3 \rightarrow NO_3 + O_2$ **Equation 1.4**

$NO_3 + NO_2 + M \rightarrow N_2O_5 + M$ **Equation 1.5**

$N_2O_5 + H_2O \rightarrow 2HNO_3$ **Equation 1.6**

$HNO_{3\,(g)} + NaCl_{\,(s)} <-> HCl_{\,(g)} + NaNO_{3\,(s)}$ **Equation 1.7**

$NH_4NO_3 <-> NH_3 + HNO_3$ **Equation 1.8**

Where *M* represents a third body that does not react, *(g)* refer to gas phase and *(s)* is particulate phase. Arrow <-> indicates equilibria reaction.

Ammonia & ammonium (NH_x) in the marine system is believed to exist in four different states in a "multi-phase" system, NH_4^+ dissolved in seawater, NH_3 in aqueous form, NH_3 as a gas, and particulate ammonium as aerosol in the atmosphere (Quinn et al., 1990). Exchange of NH_3 between the atmosphere and ocean is believed to be temperature dependant, with the ocean being a source of NH_3 to the atmosphere at low latitude and sink at high altitude regions (Johnson et al., 2008), in the absence of other factors such as local pollution. NH_x species in the atmosphere are important in several processes. Ammonia gas, as a base, will react with the acidic species of sulfate (as sulfuric acid) to form ammonium sulfate aerosol particle, which is the most abundant form of NH_x in the atmosphere. These particles are also important in cloud formation, as cloud condensation nuclei (Johnson & Bell, 2008). Hence, ammonium is found to be directly related to non-seasalt sulfate (section 1.1). The reaction between ammonia and sulfuric and nitric acids therefore couple the biogeochemical nitrogen and sulfur cycles. This applies particularly to non-seasalt sulfate

both from anthropogenic sources and from oxidation of DMS (Johnson & Bell, 2008). Since DMS is produced by biogenic processes from phytoplankton in the ocean, ammonium may be important in the interaction of biogeochemical nitrogen and sulfur cycle.

1.5 The Sulfur Cycle

Sulfur is an important component in the global biogeochemical cycles, and is probably one of the most perturbed cycles by anthropogenic activities.

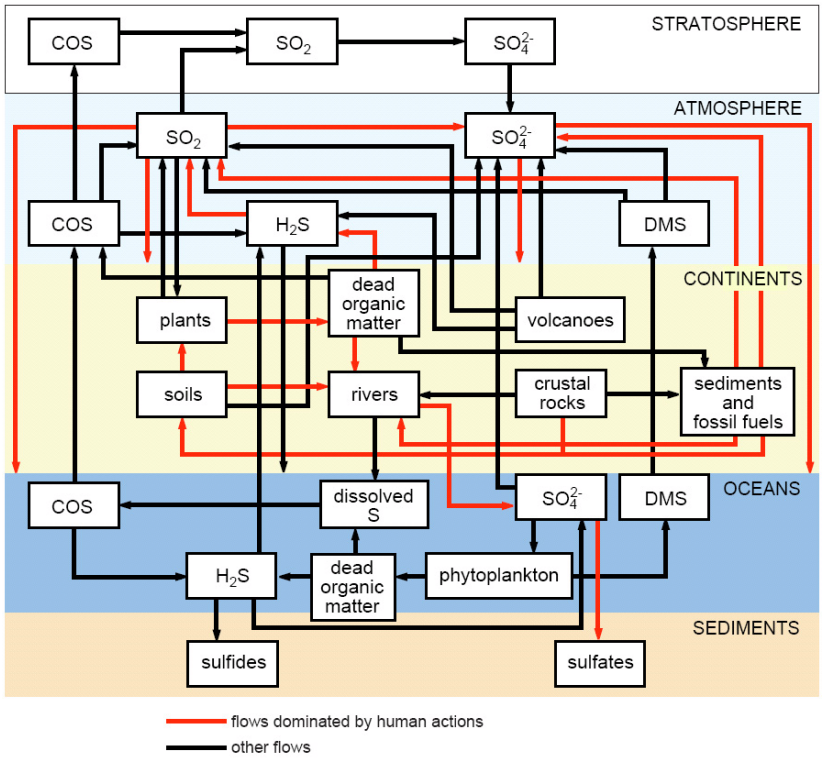

Figure 1.6 A schematic summary of the global sulfur cycle, highlighting processes heavily affected by anthropogenic activities. Schematic is taken from Smil (2007).

Figure 1.6 summarizes the biogeochemical processes of sulfur in 5 different components of the Earth system, each with dominant processes and sulfur species. On the continent, component of sulfur exists naturally in soils, and is assimilated by plants as a trace nutrient. Sulphide (S^{2-}) minerals are also a reservoir of sulfur, and among different minerals pyrite

(FeS_2) is the most commonly found (Andrews et al., 2004). Sulfur within minerals can be mobilized either via physical or chemical weathering processes. Mining will result in the exposure of pyrite to oxygen, which is subsequently oxidized to sulfate (S^{6+}) and can result in acid mine drainage problems.

Algae and phytoplankton will also take up sulfate as a nutrient necessary for growth, and for marine phytoplankton, dimethylsulfide (DMS) is produced. DMS comes from the breakdown of dimethylsulfoniopropionate (DMSP), which is produced by the metabolic process of marine phytoplankton. DMS will oxidize to form sulfate and methylsulfonic acid (MSA) in the atmosphere (von Glasow & Crutzen, 2004) and MSA is used as a tracer for biogenic activities. This process of DMS oxidation is potentially important to the climate regulation as will be discussed later.

The decomposition of organisms by bacteria will also produce sulfur in the form of hydrogen sulfide (H_2S), mainly in marine sediments. H_2S will then either precipitate into sulfide minerals such as FeS_2, or be oxidised to form sulfate. Volcanoes are also another source of H_2S in the atmosphere, and this sulfur is subsequently removed to the surface or oxidised into sulfur dioxide (SO_2) and then deposited as sulfate.

In the atmosphere, sulfate is an important component in controlling the acidity of the atmosphere. Sulfuric acid (H_2SO_4) is a source of strong acidity in the atmosphere in comparison to the weaker carbonic acid from the dissolution of carbon dioxide (CO_2). Ammonia, or ammonium in solution, is alkaline, hence counteracts the acidity and make the

atmosphere less acidic. Sulfate is therefore often found to be coupled with ammonium, as mentioned above in section 1.4.

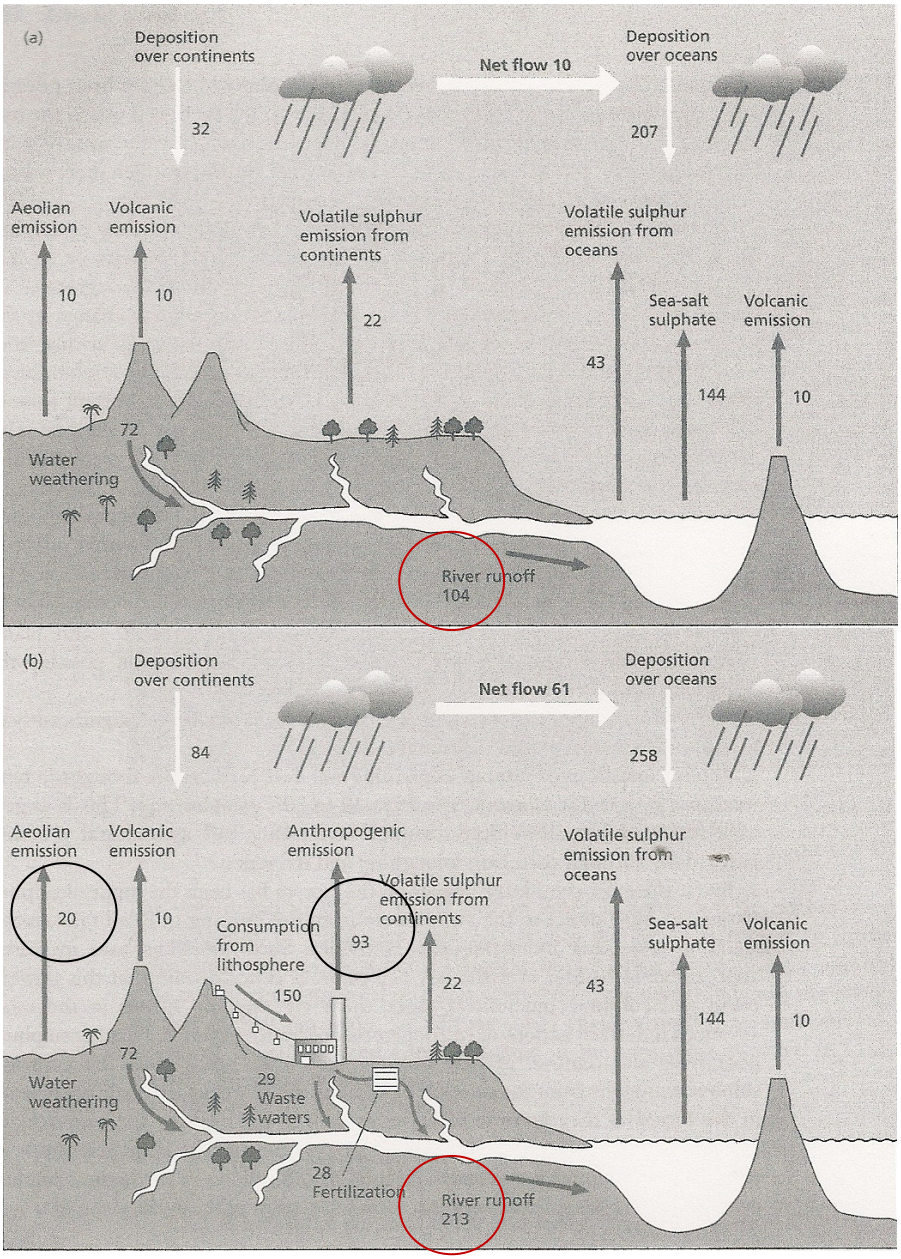

Figure 1.7 A summary for the reservoirs and fluxes of sulfur. (a) represents the natural sulfur cycle prior to any anthropogenic perturbations and (b) shows the sulfur in the mid-1980s. Fluxes between reservoirs are in $TgSyr^{-1}$ (Andrews et al., 2004). See text for explanation of circles.

Figure 1.7 highlights the effect of anthropogenic emissions of sulfur on the natural sulfur cycle. From figure 1.7, (a) is referred to as natural and (b) anthropogenic + natural sources.

Around 103 $TgSyr^{-1}$ (marked with black circles in diagram b, 93 + 21 = 103) of anthropogenic sulfur is emitted to the atmosphere compared to natural sulfur. Waste, fertilizers and river runoff has introduced sulfur into the aquatic system by 109 $TgSyr^{-1}$ (marked with red circle, 213 – 104 = 109). The deposition onto continents and oceans has also each increased by about 50 $TgSyr^{-1}$.

Sulfate is also known to act as cloud condensation nuclei (CCN) for marine clouds (Charlson et al., 1987), and cloud cover is one of the factors controlling global albedo and temperature (Ramaswamy et al., 2003). Understanding the role of clouds in the warming and cooling of the planet and how it changes in the present warming world is one of the biggest uncertainties climate change researchers face (Ayers et al., 2007). The interaction between marine biogenic aerosols and global climate was first introduced by Charlson et al. (1987), when they hypothesised a feedback system that acts as a planetary thermostat (Hubert, 2007). This hypothesis has become known as the CLAW hypothesis (Charlson et al., 1987) and attracted much research focus. This paper has also stimulated scientists to collaborate in their individual fields, and recognise the unique interdisciplinary linkages among different components in the global biogeochemical system.

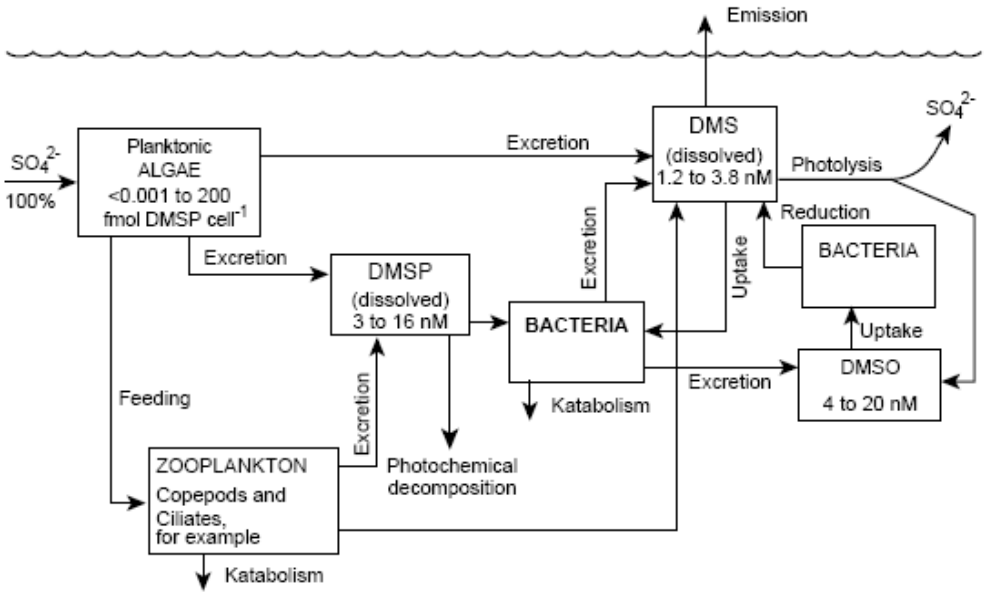

Figure 1.8 A schematic diagram of the processes that control DMS production and other related sulfur species in the surface ocean (Andreae & Crutzen, 1997).

According to the CLAW hypothesis, the major source of CCN over marine environments come from DMS, which is an organic sulfur compound contributing to the smell of the sea. As mentioned above, DMS is derived from DMSP, which is an osmolyte that is essential in some types of phytoplankton and algae (Malin & Kirst, 1997). The overall cycling of DMS and its precursors within the ocean is complex and involves productions by algae and subsequent degradations by bacteria (figure 1.8). There are two ways DMS can be lost from the surface ocean, firstly through physical ventilation into the atmosphere, where further oxidation takes place. Another way is the photochemical and microbial breakdown in the water column (Charlson et al., 1987).

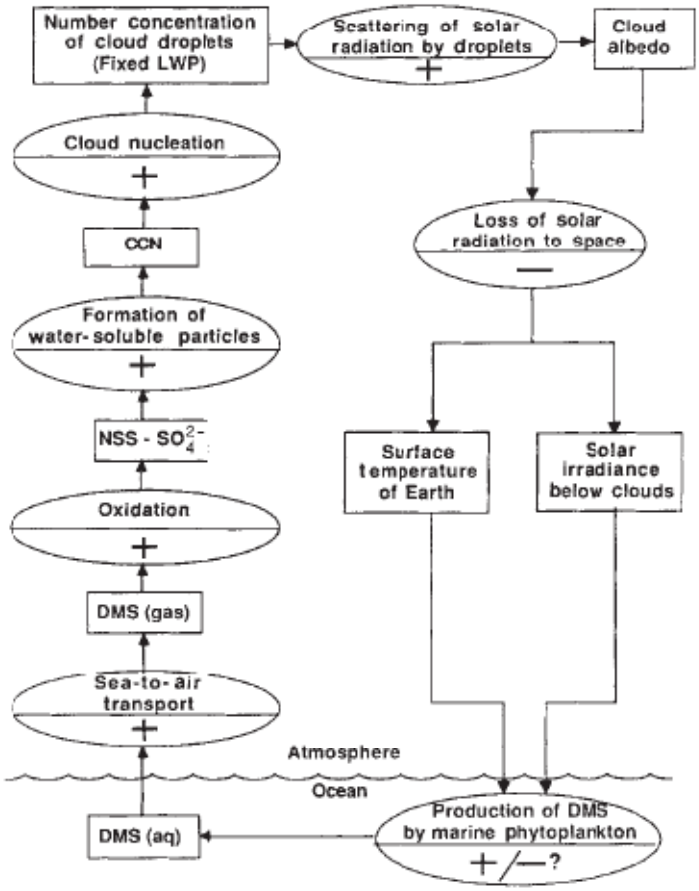

Figure 1.9 A proposed feedback system involving the production and removal of DMS in the marine environment (Charlson et al., 1987).

Figure 1.9 is a schematic representation of the CLAW hypothesis. In this hypothesis an increase in available energy form the sun will result in the warming of ocean as well as stimulate photosynthesis, which could enhance phytoplankton growth. This will produce more DMS and could result in an elevated aerosol sulfate in the atmosphere. Elevated CCN will then cause an increase in cloud cover, increase in albedo and induce a temperature drop. This negative feedback system has many assumptions and uncertainties (Charlson et al., 1987), which can have multiple consequences. For example, if the warming of ocean was significant enough to cause reduced phytoplankton population due to stratification and nutrient limitation, then the whole feedback system will act in the directly opposite way and

result in an increased warming effect. The reason for the uncertainties can be explained by the complexity of the natural system, which has several interdisciplinary components that have to be considered. In short, the hypothesis seems to be too complicated to be subjected to simplistic tests (Liss et al., 2007), and unless multi-disciplinary connections inherent in the CLAW hypothesis are more thoroughly studied, scientists will be unable to assess climate change risks to coupled marine systems, let alone considering appropriate mitigation or adaptation strategies (Ayers et al., 2007). A recent study by Woodhouse et al. (2010) stated that very large changes in DMS flux will be required to have any significant effect on CCN, and concluded that the CLAW feedback could be very weak.

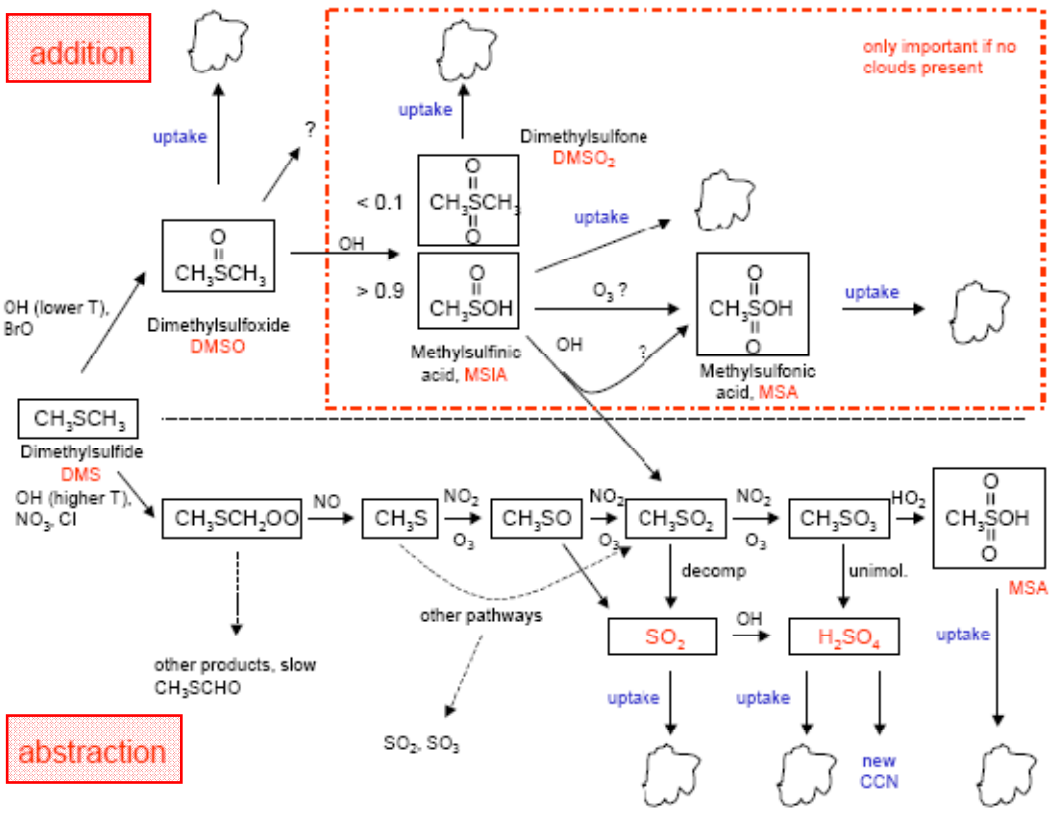

Figure 1.10 Proposed schematics of DMS oxidation reactions in the atmosphere (von Glasow & Crutzen, 2004).

Figure 1.10 provides a detailed process for the oxidation of DMS in the atmosphere, illustrating the complexities of the process. Between the two pathways, addition and abstraction, addition will only be important in cloud-free regions. This is because the process requires the hypobromite radical (BrO^-), which is produced by the photolysis of ozone, catalyzed by atmospheric bromine (von Glasow & Crutzen, 2004). Since photolysis is limited by cloud cover, addition is only effective where no clouds are present. As for the abstraction process, nitrogen dioxide (NO_2) is involved as well as the hydroxyl (OH^-) radical, which is present in both pathways. Sulfuric acid and MSA are produced at the end of the process, and sulfuric acid can be ionically bonded to ammonium, forming sulfate. Both sulfate and MSA are relatively stable in atmosphere, and are measured consistently as tracers of the sulfur cycle. MSA, especially, is used to trace biogenic activities because of the advantage over non-seasalt sulfate of having a unique DMS source. The relative production of MSA and sulfate (as sulfuric acid in the atmosphere) as end products of the DMS oxidations are determined by temperatures and the oxidants available during the process (Von Glasow et al., 2004).

A study by Ayers et al. (1991a) made seasonal measurements of CCN, DMS and MSA around the remote Southern Ocean, in an attempt to test the CLAW hypothesis and the role of the DMS source. The result showed similar seasonal fluctuations of DMS to MSA and non-seasalt sulfate. Ayers updated the measurements by measuring CCN, DMS and MSA together (Ayers & Gras, 1991b), and similar relationships were observed. These authors

concluded that their results were consistent with the CLAW hypothesis, i.e. that DMS emissions do significantly reflect CCN production.

1.6 Sulfur Isotopes in the Marine Environment

Isotopic analysis is one of the most important ways of evaluating the varying processes of natural geochemical cycles. Isotopes of an element differ in mass due to different numbers of neutrons, but otherwise have essentially the same chemical properties. Chemical and physical processes will often favour a certain mass of the same element in a molecule, and will fractionate into different compositions of the same molecule, resulting in different isotopic compositions in products compared to reactant. Measuring the isotopic composition of certain molecules, ions or atoms can be used to help understand processes in the geochemical cycle. In this thesis, only the isotopic composition of sulfur as sulfate and nitrogen as ammonium in fine mode aerosol samples are measured, hence the focus of background descriptions here will concentrate mostly on sulfate and ammonium. More details on the isotopic analysis of sulfate and ammonium will be described in chapter 2. The isotopic composition of sulfur as sulfate measures the ratio between a relative atomic mass of 34 and 32 sulfur ($^{34}S/^{32}S$). This is expressed as parts per thousand or parts per mil (‰ $\delta^{34}S$) relative to the Cañon Diablo troilite standard (Rees et al., 1978), or CDT in short (formula 1.9).

$$\delta^{34}S = \left[\frac{\left({}^{34}S/{}^{32}S\right)_{sample}}{\left({}^{34}S/{}^{32}S\right)_{standard}} - 1\right] \times 1000$$

Formula 1.9

Various studies, for example, Norman et al. (2006), Wadleigh (2004) and McArdle et al. (1995, 1998), have measured the isotopic composition of sulfate ($\delta^{34}S$) in atmospheric aerosols from various sources. The sources of sulfate in aerosols have very different $\delta^{34}S$ values relative to the accuracy and precision of the analysis and hence it is possible to trace the source of sulfate in atmospheric aerosols using isotopic analysis (figure 1.11). In this study, with the AMT cruises in particular, cruise tracks provide samples expected to be from distinctive sources, from the heavily polluted European region to the pristine area of the Southern Atlantic. The detailed cruise information will be presented in the methodology chapter.

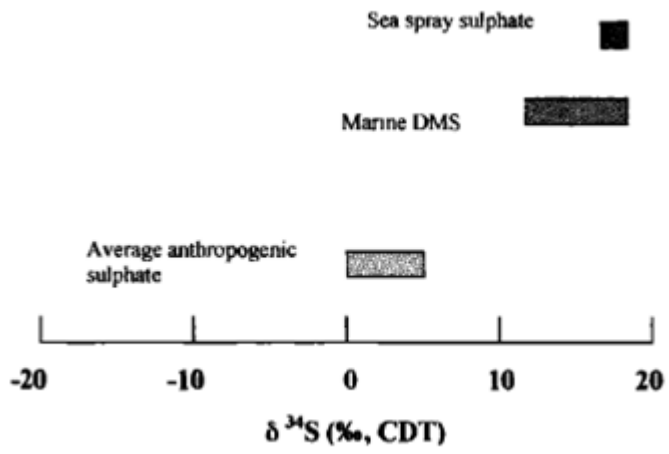

Figure 1.11 Variations in $\delta^{34}S$ values from sulfur sources that are considered in this thesis (Wadleigh et al., 2001).

Figure 1.11 provides a summary of $\delta^{34}S$ values measured from different sources. The isotopic composition of seasalt sulfate is a stable value of 21‰, while the $\delta^{34}S$ value for

DMS, classified as biogenic sulfur, ranges from +15‰ to +20‰. The value from combustion of fossil fuels has a $\delta^{34}S$ value of around +1‰ to +8‰. A summary of the major sources of sulfate in atmospheric aerosol samples are listed below in table 1.3. It is worth noting that equations in Wadleigh (2004) will be used in the data processing of sulfate isotopes in this study, because she presents formula to theoretically segregate sulfates into three components: seasalt, biogenic and anthropogenic. This will be described in more detail in the methodology chapter.

The reasons that cause the difference in isotopic compositions from different sulfur sources are well understood. Seasalt sulfates in aerosols sampled originate from ocean waters removed from marine environments by wind. In the marine geochemical cycle, two processes dominate the isotopic fractionation of sulfate: the bacterial sedimentary processes at the bottom of the ocean producing mainly FeS and FeS_2 from sulfate reduction, and the reduction of sulfate to sulphide via bacterial reduction in the water column (Thode, 1991). These processes have a tendency to favour the lighter sulfur isotopes, resulting in the ocean water sulfate rich in the heavier isotopes (Thode, 1991). The formation of sulfate evaporites over time is believed to influence the $\delta^{34}S$ values of ocean water sulfate and evaporate sulfates vary from +10‰ to +30‰ through geological time (Rees, 1970). At the present day the sulfur isotopic composition of sulfate has value of +21‰, with negligible change with depth within in ocean (Rees, 1978)

The isotopic value of marine biogenic sulfur (DMS) is not very well constrained, and the

theoretical value of biogenic sulfate was estimated to be between +14‰ and +22‰ (Calhoun et al., 1991). This estimate was later constrained to +18±2‰ in a study by Patris et al. (2000), also used by Wadleigh (2004).

Fossil fuels originate from decomposed organic matter, and have a wider range of isotopic compositions, depending on various factors, such as temperature, and the types of organic matter decomposed (Thode, 1991). Petroleum has a wide $\delta^{34}S$ values from -10‰ to +40‰, while sulfur in coals exist as pyrite and organic sulfur (Thode, 1991). A general average representing fossil fuel combustions is shown below in table 1.3.

Table 1.3 A summary of $\delta^{34}S$ values measured from different sources of sulfate.

Source of sulfur	$\delta^{34}S$ values (‰)	Reference
Seasalt	+20 ~ +22	McArdle (1995)
	+21	Norman et al. (2006) Rees (1978) Wadleigh (2004)
Biogenic (DMS)	+15 ~ +20	Norman et al. (2006)
	+16 ~ +20	Wadleigh (2004)
Anthropogenic	+4 ~ +8 (fossil fuel combustion)	Norman et al. (2006)
	+5 ~ +7 (anthropogenic emission)	Patris et al. (2000)
	+1 ~ +5 (anthropogenic end member)	Wadleigh (2004)

1.7 Nitrogen Isotopes in the Marine Environment

Isotopes of nitrogen as ammonium are also measured in similar ways to those of sulfur. For the isotopic composition of nitrogen as ammonium, the ratio of two isotopes of N are calculated (formula 1.10), one with a relative atomic mass of 14 and another 15 ($^{15}N/^{14}N$).

The composition is expressed relative to the internationally agreed standard, atmospheric N_2 gas, with a $\delta^{15}N$ value set as 0‰. More details will be described in chapter 2.

$$\delta^{15}N = \left[\frac{\left({}^{15}N/{}^{14}N\right)_{sample}}{\left({}^{15}N/{}^{14}N\right)_{standard}} - 1\right] \times 1000$$

Formula 1.10

There are numerous studies concentrating on measuring the isotopic composition of nitrogen species, nitrate in particular, in terrestrial regions and the hydrosphere, and ammonium is comparatively less studied. Ammonium as an aerosol species, can originate from multiple sources, described in section 1.4, with the dominant anthropogenic source from animal waste and a natural emission from degrading organic matter on land and in the oceans. Ammonium from fertilisers is believed to have $\delta^{15}N$ values close to 0‰ (Heaton, 1986), due to the fact that commercial production of fertiliser utilises atmospheric N_2.

Table 1.4 A short summary of the isotopic composition of ammonia/ammonium from different sources by varying studies.

$\delta^{15}N$ (‰)	Source	Reference
-7 to +2	Coal combustion	Russell et al. (1998)
-5 to -10		Heaton (1986)
+9 ± 4	Vehicle	Yeatman et al. (2001)
-2 to +12	Aerosol over USA	Heaton (1986)
-12 to -6	Urban sewage	Liu et al. (2008)
-5 to +5	Fertilizer	Russell et al. (1998)
-5 to 0	Agricultural	Liu et al. (2008)
-15 to +28	Animal excreta	Russell et al. (1998)
+22	Chickens	Yeatman et al. (2001)
+14 to +21	Pigs	
+11 to +18	Cows	
-5 to 0	Soil	Russell et al. (1998)
+2 to +7	Ocean NH_4^+	Russell et al. (1998)
-3 to +7	Pretoria rainfall, South Africa	Heaton (1986)
-5.9 to 0	Rainfall (high lightning activities)	Heaton (1987)
-8.3 to +8.6	Rainfall	Russell et al. (1998)
-19 to -5.5	Urban Rainfall	Liu et al. (2008)
-15 to +10	Rainfall	Rolff et al. (2008)
-16 to +22	Rainfall	Xie et al. (2008)
-1.7 to -22	Rainfall	Xiao et al. (2002)

The large range of values for atmospheric of ammonium is illustrated in table 1.4. It is rather difficult to distinguish one source from another in one aerosol sample, unless the sample has travelled over regions of a single dominant source. The wide range of rainwater values is due to the large variations of environments in which rainwater deposits ammonium and nitrate onto land. In this study, the sources that contribute to the ammonium in the samples are assumed to be separated into marine and anthropogenic sources, with a rather unclear separation in between. Details for the separation are described in chapter 2 and analysed data will be shown in chapter 3.

1.8 Thesis outline

In this thesis aerosol samples collected around the oceans are analysed for major ions, MSA and sulfate & ammonium isotopic compositions in an attempt to evaluate the relative significance of natural and anthropogenic sulfate & ammonium in the remote marine environment.

- In chapter 2 the sampling and analytical methods are presented.
- In chapter 3 the results of the aerosol isotopic analyses are presented.
- In chapter 4 the aerosol major ions and MSA results are presented and used to present an initial partitioning of different sulfate sources (seasalt, biogenic and anthropogenic) from isotopic measurements.
- In chapter 5 various datasets are synthesized focusing particularly on the coupling of the S and N cycles, the relative importance of various sulfate sources and the utility of MSA as a biogenic sulfate tracer.
- In chapter 6 a short summary will be given, based on the data presented in this thesis, focusing particularly on the aerosol sulfate and ammonium isotopic analyses.

Chapter 2: Methodology

This chapter will describe different analyses used in this study, including ion chromatography and isotopic analysis of sulfate and ammonium. Background will be presented as an introduction into the methods, and steps will be described in detail. Corrections performed will also be mentioned, followed by appropriate references.

2.1. Ion Chromatography Method

2.1.1 Introduction

This chapter will describe methods used to measure the concentration of some chosen ions in the aerosol filter sampled on several cruise tracks. General background information will be given on the aerosol samples analysed in this thesis. It should be noted that all of the aerosol samples from 6 different cruises were not sampled in person. Instead, samples are provided by Tim Lesworth (Lesworth, 2007) and Alex Baker (Research Fellow, UEA). It must also be noted that throughout this study, only fine mode filters are used where available (exceptions described below).

2.1.2. Description of Cruises

Table 2.1 A summary of cruises from which data were analysed in this study.

Cruise	Dates	Sample Provider	Origin	Destination
AMT15	17th Sep – 29th Oct 2004	Tim Lesworth	UK	Cape Town, South Africa
AMT17	17th Oct – 28th Nov 2005	Tim Lesworth	Clyde, UK	Cape Town, South Africa
JC18	4th Dec – 14th Dec 2007	Alex Baker	Montserrat	Montserrat
36N	1st May – 15th Nov 2008	Tim Lesworth	St. Georges, Bermuda	Lisbon, Portugal

Table 2.1 above summarises the general information for cruises from which samples were analysed in this study, and detailed cruise tracks will be presented in the discussion chapter where appropriate.

2.1.3. Sample Extraction and Analysis

In order to analyse the concentrations of ions in aerosol filters, the cold sonication method is used in this study (Lesworth, 2007). The method used is identical to that in Lesworth's thesis. One quarter of a filter is used for one batch of measurement. The quarter filter is cut into squares of approximately 1 x 1 cm size into 50ml centrifuge tube (pre-rinsed in milli-Q water containing 10% HCl, rinsed again with milli-Q and dried in the oven). 25ml of Milli-Q water is added and the solution sonicated for one hour in a water bath at room temperature. The sample is then filtered through a 0.6μm syringe filter using a 50ml pre-rinsed syringe into another 50ml centrifuge tube. The filtered solution (aerosol extract) will be preserved in the fridge for up to a week; if not analysed within the period, the samples are frozen for

longer storage times. It should be noted that aerosol sample filters are frozen for long term storage, and should only be extracted into solution when analysis is to be performed.

The instrument used to measure the ionic concentration of aerosol extracts is the ion chromatography analyser. Figure 2.1 represents a brief schematic of this system.

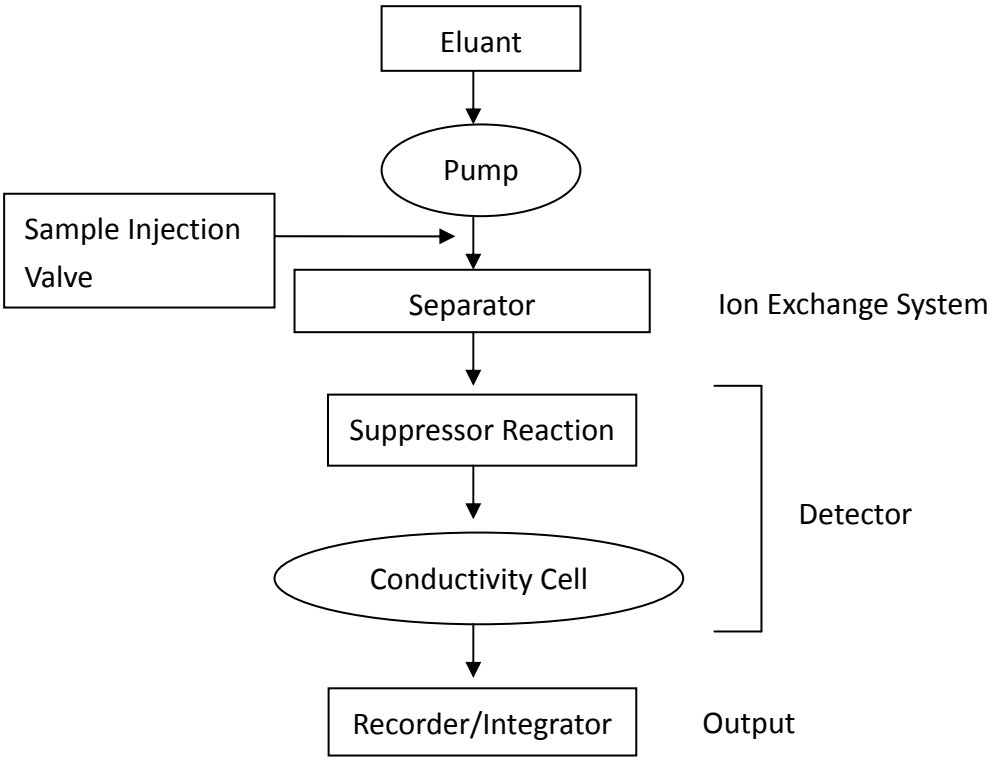

Figure 2.1 Schematic of the chromatography system (Lesworth, 2007).

Ion chromatography refers to "the analysis of ions and polar molecules, achieved by separating individual ions from one another from a complex mixture based on their charge, which is detected by the means of conductivity" (Fritz et al.,2000). As figure 2.1 shows, throughout the analysis, the samples are carried through the system using a mobile eluant liquid, usually milli-Q (ultra pure) water or KOH or MSA at low concentration. More specifications on the eluant used will be described later. The major ions within the sample

will then undergo separation in the separation column, which is filled with ion exchange resin. In this study, high performance ion chromatography (HPIC for short) is used, which utilise the fact that different ions in the liquid will have different conductivities compared to one another, thus allow the system to separate individual ions. Within the detector, the suppressor will reduce the conductivity of the mixture of samples and eluant, to enhance the effectiveness of the conductivity sensor. The suppressor works by chemically reducing the conductivity of the eluant before entering the detector column. When individual groups of ions pass through the conductivity detector, peaks will be observed. The area under the peak is integrated in the computer (connected to the analyser) and output can be obtained quantitatively. By analysing a set of reference solution with desired concentrations in replicates within the same batch as the samples, the concentration of samples can be calculated by plotting the actual concentration of the reference against the integrated area under the peak that is measured and can be comprehensively compared to the area of the peak from samples with unknown concentrations of the ion.

The cations and anions were analysed on a dual Dionex DX600/DX320 ion chromatograph. Due to limited volume of samples available in some cases, a single channel Dionex ICS2000 was also used, which measures anions only. The DX600 uses KOH and milli-Q water as eluant for the anion side and 40mM MSA and milli-Q water for the cation side. Similar to the anion side of DX600, the ICS2000 uses KOH and milli-Q water.

When analysing MSA within the normal anion sample analysis, the peak appears at around 5

minutes into the run (26 minutes for one sample run), and can be confused for other similar ions which also appear very closely in time to MSA, such as acetic acid. Such disturbance will require MSA to be analyzed using a specially-designed program to enhance the peak observed for MSA. By elongating the run time for one sample run, the peaks that are close together can be separated further away from one another, thus making identification of a MSA possible. However, this will sacrifice sensitivity, since individual ions will be forced to stay in the detector for longer, thus flatten out the peaks detected. It is therefore necessary to balance between detect ability and sensitivity when measuring MSA.

Within the batch of measured samples are sets of standard solutions of known concentration, designed to be used as calibration references to the sample solutions which have unknown ionic concentration.

Table 2.2 The concentration of major ions and chemicals used to make up the stock standard solution for ion chromatography measurements in this study.

Ion	Na^+	Ca^+	K^+	NH_4^+	Cl^-	NO_3^-	SO_4^{2-}	MSA
Chemicals Used	NaCl	$CaCl_2.(2H_2O)$	KCl	NH_4Cl	NaCl	$NaNO_3$	K_2SO_4	MSA (99.9% ultra pure)
Conc. (µM)	600	150	50	100	600	200	200	15

The stock solution is made by weighing individual chemicals on a digital balance. They are then transfer into a 250ml volumetric flask and filled with milli-Q water. Each batch of standard solution consists of six sets of concentrations, made up by serial dilution of the stock standard solution described in table 2.2, with the last set made up of milli-Q water only,

which is treated as blank. After the analysis, six consecutive standards are used to produce a straight line calibration graph of concentration (calculated from actual weight) against integrated peak area (measured) graph, with an intercept of zero. In addition to the routinely made reference solution, in order to enhance the standardisation of the measurement, a well-characterised UEA internal standard is included in every batch measured. This provides quantitative comparisons to past datasets that have the same standard included in the batch. This standard is prepared independently from standards produced in this study, and provides a mean of comparison should the standard preparation steps are not appropriate or incorrect. It should be noted that apart from the measurements of MSA, most ion chromatograph data were provided by Alex Baker. For some samples, only a limited amount of filter was available, and this sometimes limits the range of analyses and replicates. Major ions for this study such as ammonium and sulfate were also measured during the measurements of MSA. These data were compared to that provided, and found to be similar to one another (figure 2.2). Other comparisons have similar trends to that presented in figure 2.2, and are therefore not shown in this thesis. With confidence that the two sets of data are comparable derived from such comparison, the data from MSA measurements can be used to compare to other ion chromatograph data that are provided by Alex Baker. The two analyses were done some time apart on separate batches from the same main filter and hence figure 2.2 also provides evidence on the integrity of samples during storage.

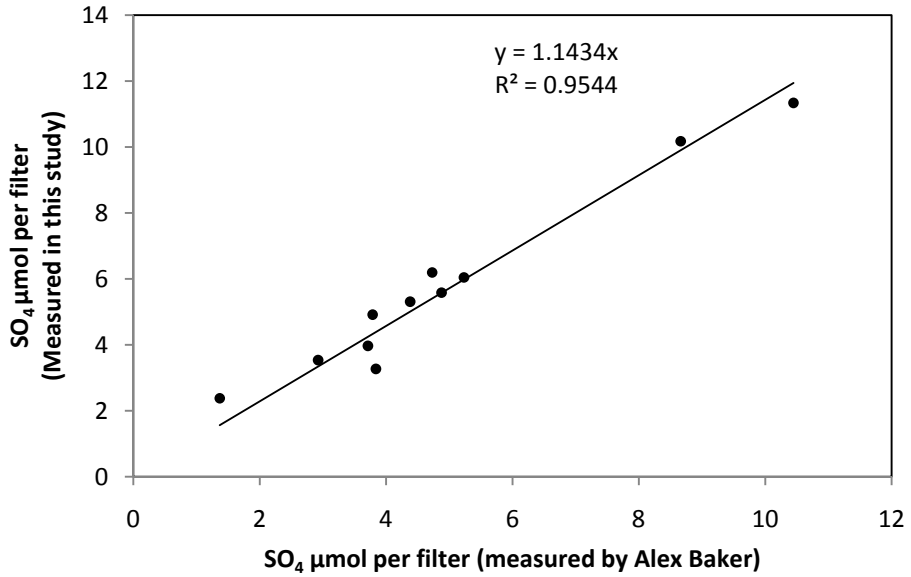

Figure 2.2 A graph comparing the micro-moles of sulfate present in one filter, measured in this study against measurements by Alex Baker. Samples plotted are taken from AMT15 cruise, sample 19-29.

The detection limits (for calculation method see below) are obtained during the calculation of the ionic concentrations, and is referred to as the instrumental detection limit of the ion chromatography analyser. In calculating the average concentrations and other data manipulations, samples calculated to be below the detection limit are given an estimate that is set to be 75% of the detection limit for the batch. This is an arbitrary number chosen for consistency with data obtained from Alex Baker. It is also found that no more than 20% of the samples are below detection. Although further statistical treatment can be applied for estimated values below detection limits, this thesis will only look at the general trend of ions, not quantifying them in any detail. Therefore for samples below the calculated detection limit, a simple substitution method is applied.

Table 2.3a Calculated mean detection limits for individual ions from Lesworth (2007).

	Ion (μM)						
	Na^+	Ca^+	K^+	NH_4^+	Cl^-	NO_3^-	SO_4^{2-}
Fine Mode	7.2	5.1	8.2	10.1	11.0	2.3	3.3

Table 2.3b Calculated mean detection limits for individual ions in this study.

	Ion (μM)						
	Na^+	Ca^+	K^+	NH_4^+	Cl^-	NO_3^-	SO_4^{2-}
Fine Mode	26.3	8.8	6.8	12.7	23.4	6.3	4.2

By comparing the detection limits calculated from table 2.3a and 2.3b, the values obtained are similar for most ions. The detection limit of MSA is 3.8±1.7 μM before the program described above is applied (p33, section 2.1.3). After the program has been implemented, the detection limit has improved to 1.2±0.4 μM. It should be noted that such improvement should be explained by the better separation of the peaks during measurements, rather than an increase in instrumental sensitivity.

2.1.4. Calculation of Ion Concentrations in Extracts

As technology advances, it becomes easier to obtain the output data from analysers. The Dionex HPIC system used in this study displays the correlation/regression line for the standard solutions measured, and gives the concentration of ions for every sample in a single spreadsheet. However, the use of the supplied software can limit the analysts' subsequent data processing and hence here the raw peak area output is used and processed in a spreadsheet. Using this method, the calculation becomes more thorough and easy to identify

errors that maybe involved, while providing statistical confidence to the calculations of the concentration for professional purposes. Much of the calculation procedures involved are described in great detail in chapter 5 of Miller & Miller (2005), and only key equations will be shown in this thesis.

In order to calculate the concentration of ions in extracts, the standard solutions are first used to create a calibration graph. An example is shown below in figure 2.3.

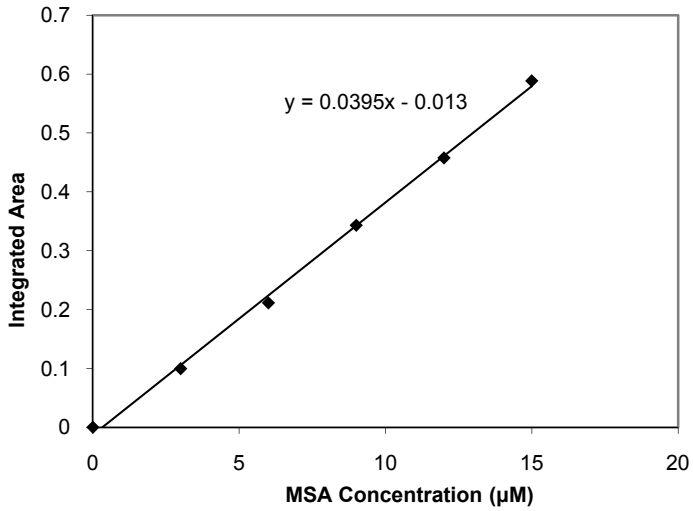

Figure 2.3 A calibration for MSA in this study. The measured integrated area under the peak is plotted against the actual concentration of the standard.

The usual regression line equation is used in this calculation:

$$y = bx + a$$

where y will be the integrated peak area, x the concentration of standard, a is the value of blank (last standard in the series containing only milli-Q water and assumed to have 0 µM concentration), and m the gradient.

By re-arranging the equation:

$$x = \frac{(y-a)}{b}$$

The concentration of ions in sample extracts can then be calculated subsequently.

In order to calculate the analytical error, an equation in Miller & Miller (2005) is used:

$$S_{xo} = \frac{S_{y/x}}{b}\sqrt{1 + \frac{1}{n} + \frac{(y_0-\bar{y})^2}{b^2 \sum_i (x_i-\bar{x})^2}}$$

where y_o is the experimental value from which x_o is to be determined, S_{xo} is the estimate of standard deviation of x_o. $S_{y/x}$ is a value that estimates the random errors in the instrumental signal i.e. y direction. The number of calibration points i.e. standards measured is described as the term n. Averages of instrumental signal and concentration are shown as $\bar{y}$ and $\bar{x}$ respectively. The sequence of standards calculated in the batch is shown as x_i, meaning the i^{th} sample with x concentration in the calibration.

Detection limit will help to define whether the signal measured is a genuine peak contributed by ions or just an instrumental error. Any values lie above the limit can be considered to be genuine.

$$Limit\ of\ Detection = y_B + 3S_B$$

where y_B is the signal of the blank during the analysis and S_B is the standard deviation derived from the calculation of the blank value.

Since Milli-Q (ultra pure) water is used as blank in every batch of analysis, the value of y_B is effectively zero, and therefore the detection limit will usually be three times the standard deviation of the blank value.

Instrumental drift should also be accounted and corrected for in the calculation. In order to counter the instrumental drift, samples are run in groups of around 15, with a complete set of standard solutions at the top and bottom of the series. Assuming that the instrumental drift through the sample is linear:

$$Concentration = \left(C_a \times \frac{N - n + 1}{N + 1}\right) + \left(C_b \times \frac{n}{N + 1}\right)$$

where C_a is the concentration from the first set of calibration, and C_b the second set. N is the total number of samples in the entire batch analysed, and n represents the position of the samples in the batch, and this position take all blanks and standards run into account. E.g. 5^{th} sample in the batch with 3 blanks and 5 standards before it will be n = 13.

2.1.5. Calculation of Atmospheric Concentrations & Sea-salt Corrections

Multiple filter blanks were collected during every cruise, and these blanks help to correct the ion chromatography data by subtracting analytes derived from sources such as the filter papers or the extraction motor, in order to obtain the actual ionic concentration present in the atmospheric aerosol. This calculation converts concentration in solution extracts to concentration in volumes of air, which is measured in conjunction when filters are sampled.

$$Atmospheric\ Concentration = \frac{4 \times c \times V_e \times 10^{-3}}{V_a}$$

where c is the measured concentration of ions in µmol/l, V_e is the volume of the extract (25ml in this study), this is multiplied by 4 since only one quarter of the filter is used for the analysis. V_a is the volume of air that has passed through the filter in the collector (units in m^3).

As described in the introduction chapter, some ions such as sulfate have seasalt and non sea-salt sources, and it is non-seasalt (nss) component of ions that are of interest in many studies. Keene et al. (1986) have introduced a method to remove the seasalt signal by referring the ratio of ion species to Na^+, the most suitable representative of seasalt because of its high concentration in seawater, low concentration in other sources and its limited chemical reactivity in the atmosphere:

$$NSS\ Concentration = c - \left([Na^+] \times \frac{[S_{sw}]}{[Na^+{}_{sw}]}\right)$$

Where c is the total atmospheric concentration of ions measured, $[Na^+]$ is the atmospheric concentration of sodium measured, $[S_{sw}]$ is the concentration of the ion species in seawater and $[Na^+{}_{sw}]$ is the average concentration of sodium in seawater.

The concentrations of ions in seawater have been well defined by many studies and are described below in table 2.4.

Table 2.4 A list of ion concentrations in seawater used during seasalt corrections in this study (Stumm & Morgan, 1996).

Ion	Na^+	K^+	Ca^{2+}	SO_4^{2-}
Concentration (mM)	468	10.2	10.2	28.2

As shown in table 2.4, the ratio can be easily obtained by dividing the concentration of the desired ion species by the concentration of sodium. By removing the seasalt signal, a variety of data analysis can be carried out, especially for potassium and sulfate, which are heavily involved in anthropogenic processes, as described in the introduction.

2.2 Isotopic Measurements

In this section a general introduction to the instruments used for isotopic analysis will be given. The terminologies for calculating the isotopic composition of desired species are described in chapter 1.6 and 1.7, and descriptions of the instruments used will be discussed in this section.

2.2.1 Introduction to Mass Spectrometry

In order to measure the ratio between isotopes of a species, isotope ratio mass spectrometer (IRMS) is used. Firstly it should be noted that the mass spectrometer will only function under vacuum, often by the order of 10^{-6} to 10^{-9} mm Hg pressure (Faure & Mensing, 2005). The mass spectrometer consists of three components, the source, electromagnet and the collector. At the source, samples will be ionized into ions and entrained into ion beams by bombarding electrons at the molecule. The ion beam is then accelerated into the electromagnet by applying a field of high electric voltage. The adjustable magnetic field will have an effect on the positively charged ion beam and deflects the ions according to their isotopic masses i.e. lighter isotopes will be deflected more significantly compared to the heavier isotopes. The collector is made up of a metal cup covered by a slit metal plate. The slit plate is arranged to only allow isotopes of the same masses to pass through, while others with different isotopic masses are blocked by the earthed plate and effectively removed. The ionizing electron beam, electric field for acceleration and the electromagnet can be optimised using various parameters to effectively measure the desired masses of the

isotopes analysed (Faure & Mensing, 2005). It should be noted that a source of known gas with exceptionable purity (either as supplied or after chemically cleaning) must be introduced into the IRMS as a carrier gas. An example of the need for high purity would be measuring nitrous oxide (N_2O) in the presence of atmospheric carbon dioxide (CO_2); both have isotopic species of mass 44, 45 and 46, and hence the carrier gas must be CO_2 free. A schematic of the mass spectrometer is shown below in figure 2.4.

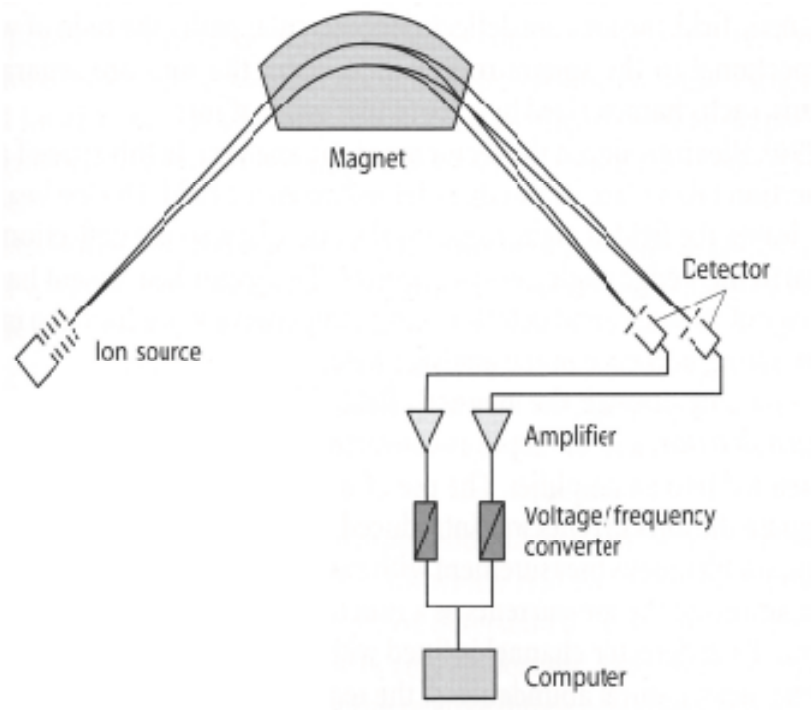

Figure 2.4 A schematic of mass spectrometer (Hoefs, 2004).

Two types of IRMS are used in this study. For the measurement of ammonium isotopes, a duel inlet system is used. This system measures samples in conjunction with reference gas in pairs by applying a switch valve. The analysis uses an inert helium gas as a carrier for samples and reference materials through the system. For the measurement of sulfate isotopes, a continuous flow inlet system is used. This system works by carrying both the sample and reference gas using a helium carrier gas (Kendall & McDonnell, 1998). This is achieved by

injecting the reference gas before the sample gas is introduced. Sufficient time is allowed to avoid any disturbance to the sample analysis by the reference gas. More on the mechanics of the duel inlet system will be described below.

2.2.2 Isotopic Analysis of $\delta^{34}S$

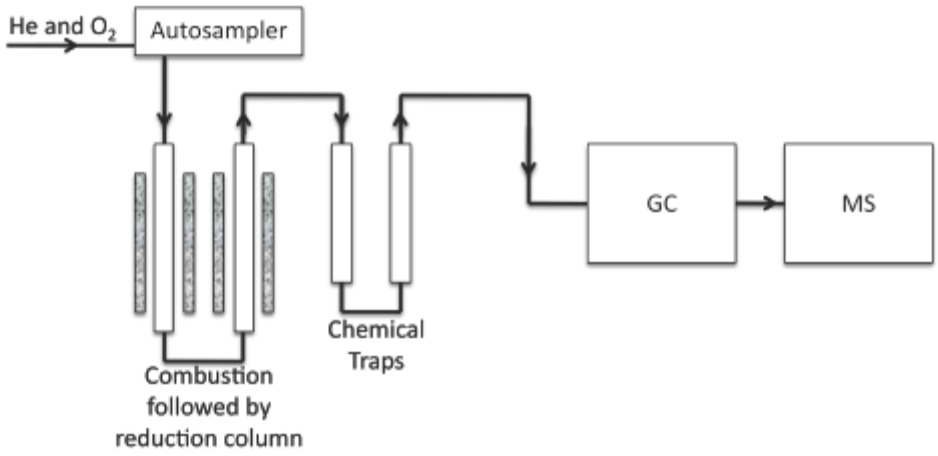

Figure 2.5 Schematic of the sample preparation system Vario ELIII connected to the mass spectrometer PDZ-Europa 20-20. Furnaces are presented as shaded blocks. Schematic is by the courtesy of Laura Bristow (2009).

For the analysis of $\delta^{34}S$, a Vario ELIII (Elemental Analyser) is connected to the PDZ-Europa 20-20 (IRMS). From figure 2.5, samples are dropped into the combustion column by the auto-sampler, when the previous one has been analysed by the mass spectrometer. The samples are heated at a stable temperature of 950°C, and combusted into gaseous forms (in the case of sulfate analysis in this study, SO_2). The gaseous samples are then passed through a reduction column (600°C) to remove other components that are not desired. The following chemical traps remove any water present in the gas. The pure, clean gaseous sample is then passed to the mass spectrometer (MS). A GC column separates gases by their stationary phase (coating of column) and mobile phase (carrier gas),

producing a separation between different sample compounds that pass into the MS with intervals, and allows measurements of multiple compounds in one single batch run.

2.2.3 Isotopic Analysis of $\delta^{15}N$

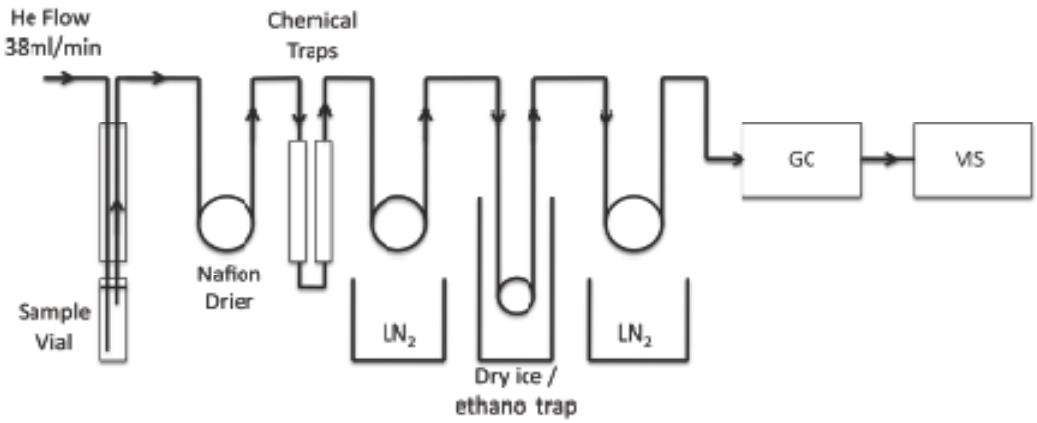

Figure 2.6 A schematic of the automated preparation system TGII for ammonium isotopic composition measurements. The shorthand LN_2 indicates liquid nitrogen. Schematic is by the courtesy of Laura Bristow (2009).

For the analysis of $\delta^{15}N$, a TGII preparation system is utilised (figure 2.6). The sample vials contains N_2O sample gases, produced from procedures that are described later. The needle transfers helium carrier gas (flow rate approx. 40ml/min) into the vial, bubbling the liquid and transport N_2O samples to the nafion drier, where water is removed. The chemical traps remove H_2O, CO_2 and organic compounds present in the samples. The first loop is immersed into liquid nitrogen; this effectively traps and concentrates the sample gases (N_2O) within the steel trapping loop. Other non-condensable gases such as N_2 are not fixed by the cryo-trap and are subsequently vented into the atmosphere. Prior to the first trap being lifted and sample gas released, the second trap is immersed in liquid N_2 for 15 seconds to cool down to the condensation temperature, so as to avoid a leak of sample gas through the

system. In between the dry ice / ethanol trap, which stays consistently at -80°C, will condense any H_2O that is not removed by nafion drier and the chemical traps.

After 150 seconds (starting from 0 seconds at the beginning of the run) the second cryo-trap is lifted from the liquid nitrogen. This warms the sample in the 2^{nd} trap, returning it to the gas phase and it is then flushed by the helium into the GC column (described above), where N_2O is separated from CO_2 (both have isotopic masses 44, 45 and 46). The MS can then measure $\delta^{15}N$ of N_2O independently from other disturbances. The cyro-traps reduce the time required for a single measurement from 30min to 15min, due to the ability to condense N_2O samples in trapping loops while another is been analysed. Instead of running one sample for 24 minutes, by fixing the sample gas within the cyro-trap, when sample 1 has passed through to the mass spectrometer, sample 2 can be on its way to be fixed by the second trap, while the auto-sampler will start preparing for the sample 3. After the analysis, sample 2 can be released from the cyro-trap into the GC and then MS, while sample 3 will be fixed and sample 4 can be prepared by the auto sampler. This half the running time of samples from 24 to 12 minutes. It should be noted that by programming the analyser in this way, the first sample analysed by the MS will always be atmosphere air (while the first sample is fixed in cyro-trap), and is ignored during data processing.

2.3 Methodology for the Analysis of δ34S of Sulfate Aerosols

This section will describe in detail the methodologies used to measure the isotopic composition of sulfate in fine mode aerosol extracts. A barium chloride precipitation method is widely used among scientists to measure sulfate isotopes in a variety of fields, and in this study methodological steps were adapted from the thesis and papers by Nicola McArdle (McArdle 1993, McArdle et al. 1995 & McArdle et al. 1998). The procedure adapted from Wadleigh (2004) to distinguish different sources of sulfate in the aerosol samples by using ion chromatography in conjunction with isotopic data of sulfate is described in chapter 3.

2.3.1 Precipitation and Isotopic Analysis

The methodology is adapted from multiple papers from the same author, Nicola McArdle (McArdle 1993, McArdle et al. 1995 & McArdle et al. 1998). The method is simple and is time efficient at the same time and involves concentrating the sulfate as barium sulfate solid by adding barium to aerosol extracts.

$$Ba^{2+}_{(aq)} + SO_4^{2-}{}_{(aq)} \rightarrow BaSO_{4\,(s)}$$

Due to concentration limitation of isotopic analysis (1/4 aerosol filter per sample), replicate sample analysis is generally not possible, and a quarter of an aerosol filter producing 25ml of aerosol extract will only precipitate enough barium sulfate for one analysis. There are the occasional aerosol extracts with comparatively high concentration of sulfate that will allow replicates to be measured, but the majority are only analysed once. In addition, instead of the normal methods of collecting the precipitate on a filter paper and combusting it for isotopic

analysis, in this study a simpler method is devised in an attempt to extract the precipitate into tin capsules for analysis and to reduce the amount of CO_2 produced during the combustion of filter papers, which will affect data quality. The tin capsules allow samples to be loaded directly into the auto-sampler for the elemental analyzer and onto the mass spectrometer.

Before the precipitation of an aerosol extract, 0.25ml of 0.1M HCl is added to adjust the pH, in order to inhibit the reaction between atmospheric CO_2 and barium chloride, producing barium carbonate. This ensures that all available barium chloride ($BaCl_2$) is used to precipitate sulfate ions in the aerosol extract.

The volume of barium chloride required is not fixed among batches, due to the variation of the concentration of sulfate among samples and the amount of $BaCl_2$ added was adjusted to ensure excess Ba^{2+} was introduced. A sample with the highest concentration of sulfate (based on ion chromatographic analyses completed prior to isotopic analysis) is selected, and barium chloride is added at a 1.5 times molar amount to sulfate. Other samples in the same batch will use that volume to ensure excess barium is added, and to make precipitation process more time efficient and provide more consistent blanks.

After the precipitation, the sample is left between 12-24 hours at room temperature to allow precipitation of sulfate. The sample is then centrifuged at 4000rpm for 30 minutes, and the liquid extracted using a large volume pipette, leaving as much precipitate as possible. The samples are then dried and re-suspended again using 140µl of milli-Q water, which is transferred to a tin capsule and dried in the oven for analysis on the mass spectrometer.

2.3.2 Corrections

The data is firstly corrected for instrumental drift. During the analysis, usually of approximately 12 to 15 samples, a standard reference material is analysed, usually in triplicate. In the case of sulfate analysis of this study, NBS-127 is used (see below). After the batch has completed, the positions of the reference materials against the measured values of reference materials are plotted. This will show the changes in the measured values with varying positions i.e. time. Since the reference materials will only have a single value, and changes along the position of the plot can be recognised as instrumental drift. A line of best fit is applied, and the measured value will be mathematically drift corrected relative to the standard reference value. In most cases the best fit relationship of the standard drift will not be linear over the whole sample run, therefore a set of standards will be chosen and all samples (include the chosen standards) enveloped by the standards will be mathematically adjusted up or down from the best fit line. Only samples that lie between the corrected reference material triplicates will have the correction applied and effectively be corrected for drift. Those in the majority where drift is minimal will have no correction applied to either the reference materials or the samples.

Apart from the general drift correction, an oxygen correction is also performed. This takes into consideration possible interferences of the oxygen isotopes within the samples measured, in the case of SO_2 (from sulfate) ^{18}O (Holt & Kumar, 1991). This interference arises because the presence of ^{18}O could increase the mass of SO_2 and could be mistaken for

higher $\delta^{34}S$.

Other reference materials, which in this study are IAEA-SO-5 (+0.5±0.2‰$_{VCDT}$) and IAEA-SO-6 (-34.1±0.2‰$_{VCDT}$), are measured along with NBS-127 (+20.3±0.4‰$_{VCDT}$). All three reference materials are barium sulfate solids with very different $\delta^{34}S$ values. The measured (after been drift corrected and calculated for $\delta^{34}S$) values of IAEA-SO-5, IAEA-SO-6 and NBS-127 are plotted against the expected values. A line of best fit is drawn, and is expected to have a gradient of 1 and intercept of 0, or be close to it, assuming no fractionation during isotopic analysis e.g. incomplete combustion of sample solids. The equation obtained by the best fit line can then be applied to the samples measured and allow the correction of $\delta^{34}S$ values.

In the case of measuring samples that are potentially low in sulfate concentrations, errors can arise in the isotopic analysis. A set of barium sulfate standards can therefore be run in the batch. The set will consist of sulfate of different weight e.g. from 0.1mg to 2mg, and analysed for their isotopic composition. The weight of the sulfate standards are then plotted against the measured isotopic composition. Such graph is usually not linear, with a threshold of around 0.5mg, below which the isotopic composition increases rapidly towards infinity. By applying a best fit curve, the equation can be used to correct for the heavy isotopic composition observed in samples that contain very little barium sulfate precipitate. Based on measured concentrations, it was concluded that all samples were above the threshold of 0.5mg barium sulfate and therefore the correction was not needed. It should be also noted

that although the isotopic composition of barium sulfate remains consistent with increasing mass, if excess sulfate is loaded into the combustion chamber, incomplete combustion will occur, and subsequently affect other samples that follow afterwards. In this study a threshold of 2mg is chosen, above which the precipitates are separated into multiple tin capsules after the centrifuge step, before being dried in the oven and weighed. All of the replicates reported in this study are produced under such circumstances.

2.3.3 Reference Material & Sensitivity

Throughout this part of the study, NBS-127 is used consistently as the primary standard reference material. It is a barium sulfate with an international recognised value of +20.3‰$_{VCDT}$ (Halas & Szaran, 2001). Sufficient reference materials are run alongside sample materials to ensure the confidence of corrections/calculations for sample sulfur isotopic composition. A summary for the calculated isotopic value of NBS-127 was shown in figure 2.7, with an average value of 21.17‰$_{VCDT}$ ± 1.26‰$_{VCDT}$. This demonstrates the accuracy and precision of the analyses based on the standard reference material (particularly given the wide range of environmental variability seen in S isotopic compositions) and samples were not corrected for the small difference between the measured and reported value of the reference material. It is worth noting that there is a particular batch (reference 55 to 77) with outstanding precision compared to other batches.

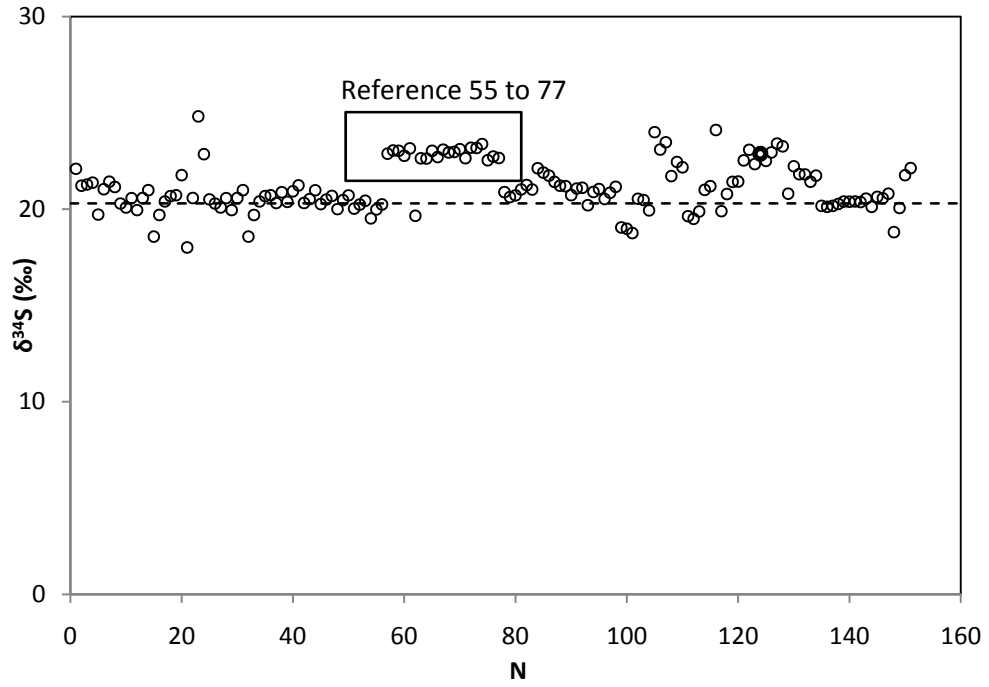

Figure 2.7 A summary for the calculated isotopic value of NBS-127 run in a total of 8 batches of aerosol samples.

In addition, tin capsules containing no materials are placed at the beginning of the sample batch as blanks. The sizes of the samples measured are directly proportional to the size of the integrated area under the peak, and during this study the blank values stayed consistently and significantly small compared to samples and reference materials (blank vs. sample size usually 1/100 to 1/1000). It can be concluded that instrumental blank correction is not necessary in this study.

Apart from the precision obtained by summarising measured $\delta^{34}S$ values for NBS-127 reference materials, some of the aerosol samples measured have enough sulfate in the solution to produce replicates. For AMT15 samples those would represent aerosols sampled near the Saharan regions, and 36N will have aerosols sampled near the US/Europe continent, and will be described in more detail in chapter 4. The deviations of replicas range from

+0.1‰$_{VCDT}$ to +0.8‰$_{VCDT}$ (average 0.4‰$_{VCDT}$), and agree with deviations obtained from other studies (±0.3‰ in McArdle et al., 1998 and ±0.5‰ in Norman et al., 2006).

2.4 Methodology for the analysis of $\delta^{15}N$ of ammonium in aerosols

2.4.1 Introduction

The following section will describe methodologies used to measure the isotopic composition of ammonium in aerosol extracts. There are two major reference papers that are used, with most of the procedure and steps adapted from them. Combined together they provide a methodology that is both sensitive and accurate. One is a paper from Zhang et al. (2007), which describes a method to consistently convert ammonium to nitrite, and McIlvin et al. (2005) which presents a method to convert nitrite into nitrous oxide gas, which is used for the isotopic analysis.

2.4.2 Background

There are other methods that have been utilized to measure the isotopic composition of ammonium, of which Holmes et al. (1998) and Lehmann et al. (2001) are two well known methodologies.

Holmes et al. (1998) measure ammonium using a diffusion method. In an environment of controlled temperature and under continuous shaking, ammonium ions are released from solution and trapped on H_2SO_4 impregnated filters, which are further combusted for the nitrogen isotopic analysis. Because diffusion is a physical process through which

isotopically lighter ammonium ions are preferentially separated from the heavier ones, corrections must be applied to account for this fractionation effect, which increases the uncertainty of the isotopic data. The methodology has many disadvantages and large errors. For example, the shaking process is very time consuming and usually takes several weeks to completion. Recovery of ammonia is variable, thus introducing uncertainty to the results. In the study, volume of sample (determined by the concentration of ammonium) needed also becomes a problem, because several litres of individual samples are often required.

Lehmann et al. provide a more efficient method than Holmes et al. By passing the sample solution through a Poly-Prep cation exchange resin columns by gravity flow, ammonium ions are trapped in the resin, which was dried and combusted for isotopic analysis. However, although it is efficient in terms of time taken to produce samples, there are still a number of uncertainties being brought forward. The physical process of absorption induces a fractionation effect similar that for diffusion, leading to possible inaccurate results. The recovery rate can be affected by other ions competing with ammonium during the absorption process, which also introduces uncertainty to the isotopic results. It is worth noting that Jickells et al. (2003) adapted this method to measure the nitrogen isotopic composition of ammonium.

Apart from the uncertainties that are pointed out above, those two methods share a common possible source of error, which is the efficiency of the combustion during isotopic analysis. Since in both methods NH_4 is combusted to form N_2, insufficient combustion is likely to

cause N-isotope fractionation.

Zhang et al. (2007) & McIlvin et al. (2005) together present a method that improves upon the above two methodologies in many ways, particularly in terms of efficiency of the reaction, the final sensitivity of the method and the speed of the analysis. The isotopic analysis of aerosol ammonium used in this study is based on the one developed by Zhang et al. (2007) for the analysis of seawater and freshwater ammonium. Only a small amount of ammonium is required in their study (0.5 to 10 μM concentrations in 20ml).

2.4.3 Conversion of ammonium to nitrite

2.4.3.1 Background

Zhang et al. (2007) suggested a method that can be used to measure the ^{15}N isotopic composition of ammonium at concentrations down to few micro-molar (μM), much lower than achieved efficiently by past studies. This method is based on the oxidation of ammonium (NH_4^+) to nitrite (NO_2^-) and the subsequent conversion of nitrite to nitrous oxide (N_2O) gas, which is used for isotopic analysis. There is a specific requirement that the concentration of NH_4^+ must not exceed 10μM, over which the oxidation of NH_4^+ to NO_2^- will not be efficient under the condition used. They also suggested that it is essential to keep the pH of reactants in a narrow optimum range for the oxidation to work efficiently. As noted earlier, this method was developed for marine & freshwater ammonium. Chapter 2.4.3.2 to 2.4.3.4 describes the adapted version for fine mode aerosol extracts.

2.4.3.2 Measuring nitrite

Because the ^{15}N measurement of ammonium involves its conversion to nitrite, it is necessary to ensure that the aerosol does not contain nitrite. Thus prior to the isotopic measurement of ammonium, the nitrite component of the aerosol sample solution must be measured. Nitrite concentration was measured using a colorimetric method. The same method was applied to determine the concentration of nitrite resulting from the oxidation of ammonium and thus calculate the yield of ammonium oxidation.

The colorimetric method of Parsons et al. (1984) is used throughout this study. This is based on the reaction of NO_2^- with sulphanilamide and *N*-(1-naphthyl)-ethylenediamine dihydrochloride (NED). This reaction will only work under acid conditions and to produce a magenta-coloured product, which is measurable at 543nm wavelength using a photo-spectrometer. In order to measure the concentration of nitrite on the photo-spectrometer, a calibration curve must be done prior to the measurement of samples. A range of nitrite concentration solutions were prepared using serial dilution of a stock nitrite solution with much higher concentration.

Solutions at all concentrations were measured in triplicate, as well as the aerosol solutions. The photo-spectrometer measures the amount of visible light absorbed by the solutions, which is directly proportional to the nitrite concentration. Based on the standards, a calibration curve can be plotted (figure 2.8).

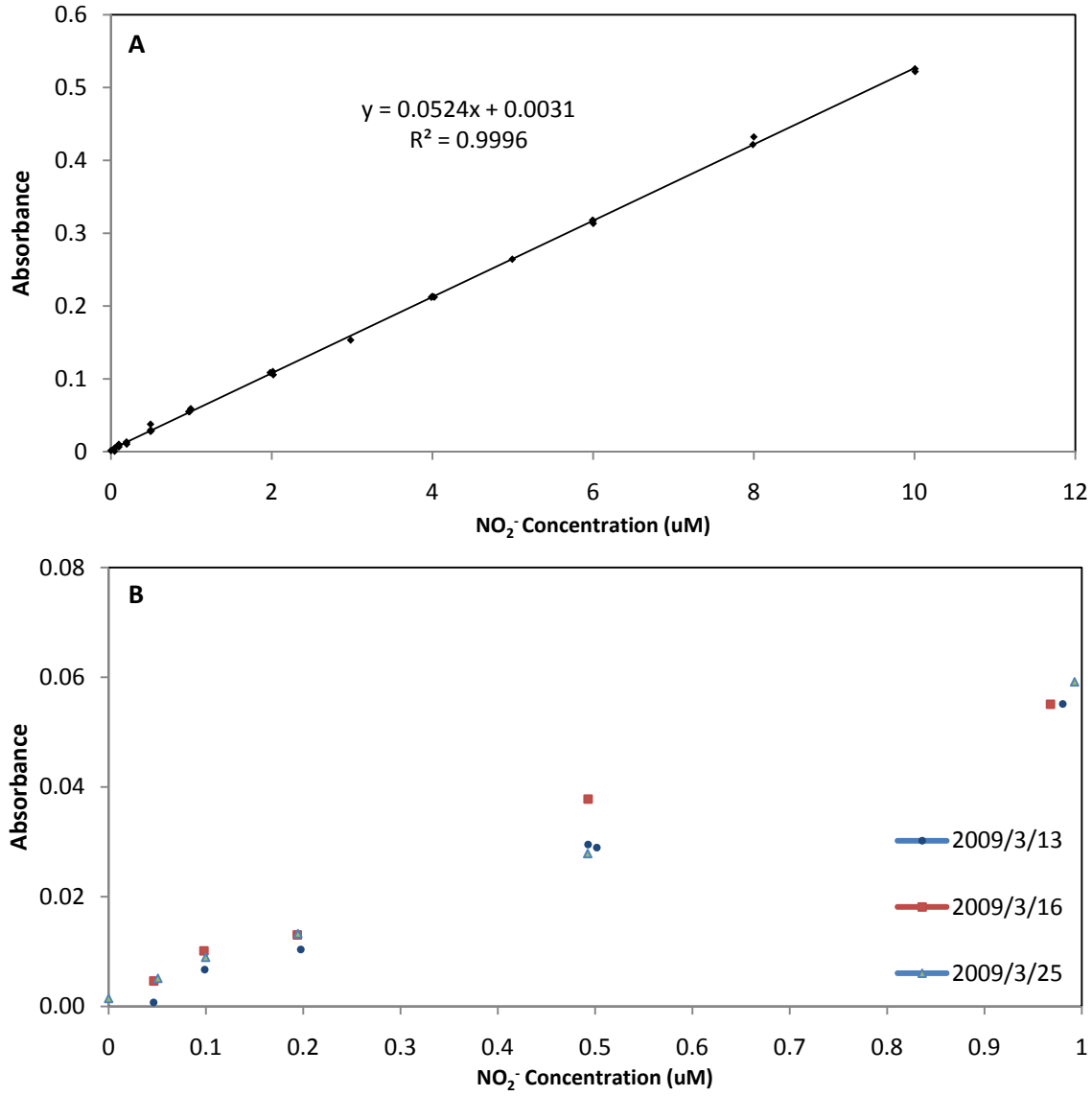

Figure 2.8 Calibration curve: (A) absorbance plotted against nitrite concentration from 0 to 10µM and (B) magnified plot of absorbance plotted against nitrite concentration from 0 to 1µM. Different symbols represent different days when the standard solutions were measured.

Using the equation for the calibration line (figure 2.8) the concentration of nitrite in samples can be calculated:

Absorbance = 0.0524 × (nitrite concentration) + 0.0031

Nitrite concentration = (Absorbance – 0.0031) / 0.0524

The value of the blank is given by the y-intercept, which suggests minor contribution from the milli-Q water used to make up the standard solutions. Taking into consideration the three

sets of data, at concentrations of 0.05, 0.1 and 0.2μM, the standard deviation of the absorbance was ±0.002, suggesting a sensitive measurement with very good detection limit.

2.4.3.3 Removal of nitrite

The presence of nitrite has the potential to interfere with the isotopic analysis of ammonium since the method will ultimately analyze both NH_4^+ and NO_2^- present together. It is only necessary to remove nitrite from aerosol extracts when the NH_4^+ / NO_2^- ratio is smaller than 50 because below this ratio the impact of NO_2^- will become significant. Since the addition of reagents to remove the nitrite will contribute to an additional isotopic blank value, this step is only utilised where the impact of nitrite is significant. The removal of nitrite involves the addition of sulfanilic acid. The resulting diazonium salt formed is then destroyed by heating in a boiling water bath.

There is very little data on aerosol nitrite, because it is usually considered a minor species. Aerosol extracts from cruise AMT15, 17 and JC18 were therefore analyzed for nitrite, and the results are shown below in table 2.5.

Table 2.5 Concentration of all major nitrogen related ions from 3 different cruise aerosol samples. The concentrations of NO_2^- were measured using the colorimetric method, while NH_4^+ and NO_3^- were measured using ion chromatography.

Sample	Concentration (uM)			Ratio
	NH_4^+	NO_3^-	NO_2^- (mean)	NH_4^+/NO_2^-
AMT15				
8	102	20	0.15	662
15	74	14	0.08	895
16	149	11	0	
19	124	13	0	

20	56	13	0.16	345
21	163	16	0	
22	67	13	0	
24	29	12	0	
25	20	12	0.06	341
26	14	11	0	
27	60	14	0.08	775
28	22	7	0.23	98
29	17	9	0.07	240
AMT17				
11	90	8	0	
12	81	9	0.34	236
13	61	10	0	
16	79	11	0.38	208
17	185	11	0.02	8327
19	104	14	0.11	981
27	106	7	0.05	2329
JC18				
3	3.0	0.9	0	
4	1.8	0.5	0	
5	1.6	0.5	1.27	1.26
6	9.0	0.7	0	
7	4.7	1.0	0.15	31.3
9	3.7	1.5	6.44	0.57
10	2.2	2.0	0.06	36.7

Note that in table 2.5 there are several samples with no associated NH_4^+ / NO_2^- values, because those samples have nitrite concentrations below the detection limit of the photo-spectrometer, and are assumed to have no nitrite. The table also shows that the ratios are usually much larger than 50 and very variable, suggesting that it is not be necessary to carry out the nitrite removal. This improves the isotopic results as less reagents were used, therefore giving a lower blank value. It is worth noting that the ratio is smaller than the desired 50 for all samples from cruise JC18. However, this is due to an unusually low

ammonium concentration instead of an increase in nitrite concentration. The reason for the low ammonium measured for all JC18 samples is unknown.

2.4.3.4 Oxidation of ammonium to nitrite

The oxidation of ammonium to nitrite is achieved by chemical oxidation. The reagents used in this study are described in great detail in Zhang et al. (2007), and will not be mentioned here. There are several factors controlling this reaction (see below), which are described in the paper by Zhang et al. (2007). In order to efficiently convert ammonium to nitrite, all factors must be kept at an optimum range. In the reaction ammonium reacts with a hypobromite (BrO^-) solution in alkaline conditions forming nitrite under vigorous shaking. The hypobromite is formed from Br_2 (equation 2.4.3.4.2) generated from the reaction of bromate and bromide (equation 2.4.3.4.1). When the oxidation is complete, sodium arsenite solution is added to remove any excess BrO^-.

At the time the ammonium oxidation to nitrite was finished, the conversion rate of this reaction was calculated by measuring the nitrite concentration colorimetrically (chapter 2.4.3.2) after the oxidation of known ammonium concentration solutions.

$$BrO_3^- + 5Br^- + 6H^+ \rightarrow 3Br_2 + 3H_2O$$ **Equation 2.4.3.4.1**

$$Br_2 + 2NaOH \rightarrow NaBrO + NaBr + H_2O$$ **Equation 2.4.3.4.2**

$$BrO^- + NH_4^+ + 2OH^- \rightarrow NO_2^- + 3H_2O + 3Br^-$$ **Equation 2.4.3.4.3**

The factors controlling the effectiveness of oxidation of ammonium to nitrite are: (a) the amount of BrO^- solution added, (b) reaction time and (c) the starting concentration of the

NH_4^+ solution. Zhang et al. (2007) have tested and presented their optimum conditions to obtain maximum conversion efficiency, but their approach was re-evaluated here for the new application to aerosol samples.

At the method testing stage, ammonium stock solution was made using analytical grade ammonium sulfate. The nitrite stock solution, used for the calibration of the photo-spectrometer, was made using analytical grade sodium nitrite. All weighing was carried out using a micro-balance with an accuracy of 0.0001 milli-gram (mg) using tin foil weighing capsules. Stock solutions at a concentration of 1000μM (this applies to both NH_4^+ and NO_2^- standards) were made up in volumetric flasks and stored at room temperature for no more than one week.

2.4.3.4.1 Optimum concentration of ammonium

In the tests to confirm optimum concentration for conversion of ammonium to nitrite, the ammonium stock solution (1000μM) was used to make up a range of solutions at concentrations of 2, 5, 7.5, 10, 20, and 80μM in quintuplicate. 2ml of hypobromite solution was added to every sample, and shaken on a bottle shaker for 30 minutes. Sodium arsenite was added immediately after shaking to remove excess BrO^- and the solution analyzed for nitrite on a photo-spectrometer. Concentrations of nitrite were then calculated using the calibration line shown in figure 2.8. Using the calculated theoretical concentration of nitrite based on the known starting concentration of ammonium the conversion yield was

calculated each time. Conversion rates are presented in figure 2.9, which indicates a sharp drop in yield above 10µM ammonium concentration, with a higher variability below 5µM concentration. A consistent recovery of approximately 80% can be achieved within the range 5 to 10µM. In the study by Zhang et al. (2007), the optimised conversion was also achieved between 5 and 10µM, though a stable conversion of 90-100% was achieved instead of the 80% in this study, even though identical conditions were adopted.

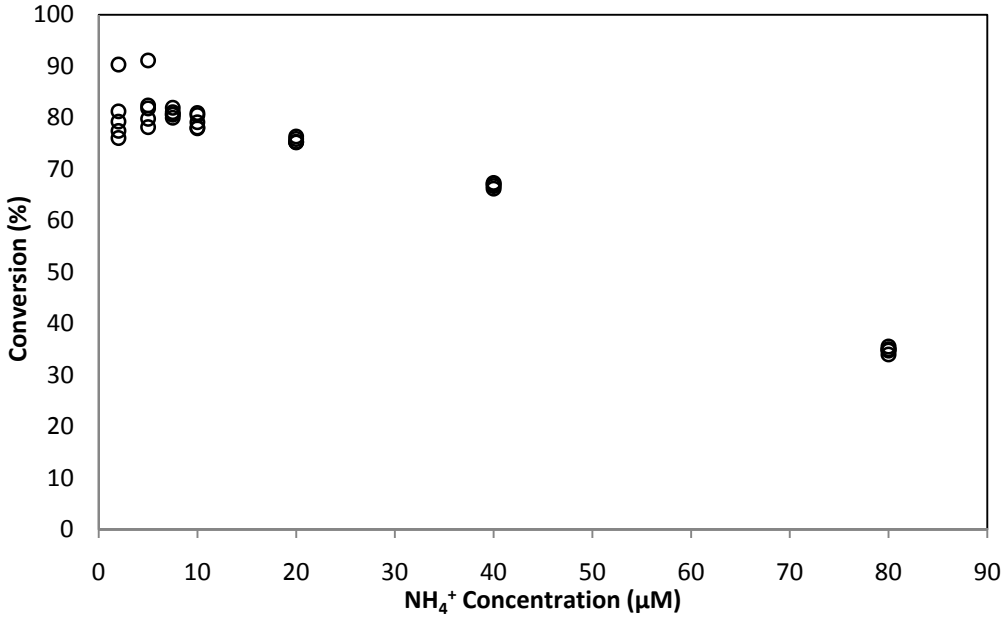

Figure 2.9 Changes in oxidation yield with varying ammonium concentrations.

2.4.3.4.2 Optimum oxidation time

Testing the optimum oxidation time of ammonium to nitrite was done in a similar way to the previous section. This time, the concentration of ammonium in samples was kept at 5µM (within the optimum range). As before, 2ml of BrO^- solution was added, and oxidation times at 15, 30, 60 and 120 minutes were considered. The ammonium to nitrite conversion rates was calculated and the results are presented in figure 2.10. The result shows consistent

conversion rates at 30 minutes, above or below which the yield becomes more variable, which introduces larger isotopic variability to the conversion step. Zhang et al. (2007) has a stable conversion (at 90-100%) within the same time range of 30-60 minutes.

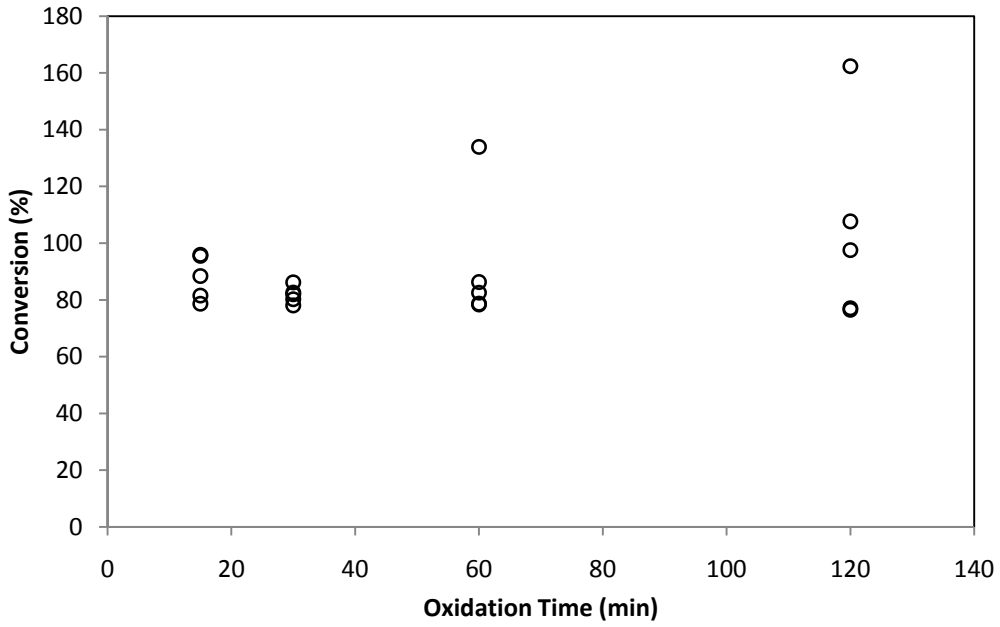

Figure 2.10 Changes in oxidation yield with varying oxidation duration (15, 30, 60 and 120 minutes respectively).

2.4.3.4.3 Optimum amount of oxidizing agent

The procedure was once again repeated to test the volume of BrO^- solution needed to maximize yield. Samples of 5μM ammonium concentration were made, to which variable volumes of BrO^- solution were added at a ratio of a quarter, half, one and double compared to the standard 2ml added during tests run above, which means 0.5, 1, 2 and 4 ml respectively. They were all shaken for 30 minutes and measured for nitrite. The conversion rates are shown in figure 2.11, which indicate that the yield decreases when more than 2ml of the BrO^- solution is added, and below this volume the yield becomes more variable. These parameters (including the test described above) show great similarities with the study by

Zhang et al. (2007).

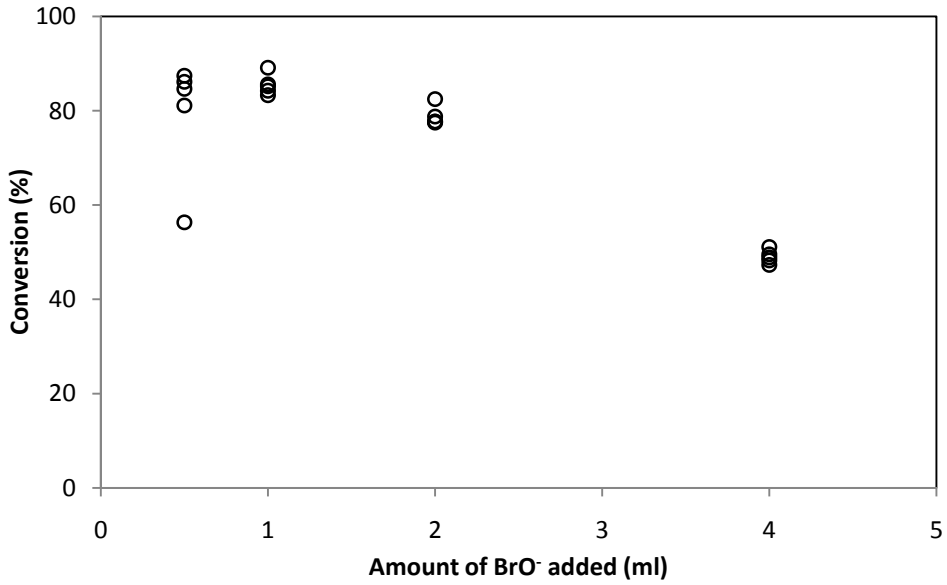

Figure 2.11 Changes in oxidation yield with varying volumes of BrO^- solution added (0.5, 1, 2 and 4 ml respectively).

2.4.3.4.4 Conclusions from optimum tests

The tests described in section 2.4.3.4.1 to 2.4.3.4.3 show that the oxidation step will stabilize at an 80% conversion rate when 1-2ml of hypobromite solution is added to ammonium solution at a concentration of 5µM, with an optimum reaction time of 30 minutes. By Comparison, Zhang et al. (2007) were able to achieve a 90-100% conversion over an ammonium concentration range of 5-10µM, with the addition of 2ml BrO^- solution and an oxidation time of 60min. They have also noted that the addition of 1ml BrO^- may provide better yield, which can also be seen in figure 2.11. However, their subsequent experiments indicate that reducing the volume of BrO^- solution did not give consistent results, thus this volume was kept at the originally used volume of 2ml (Zhang et al., 2007). Scaling up sample and reagent volumes may be anticipated to yield good conversion but for this

analysis a sample concentration of 5μM NH_4^+ is suitable, representing only a few millilitre (or less) of aerosol extract. Although this will allow for isotopic replicate measurement to improve precision, in this study, single measurements are made due to limitation on sample volumes.

2.4.4 Isotopic Measurements of NH_4^+ in the form of Nitrous Oxide gas

2.4.4.1 Conversion of NO_2^- to N_2O gas

The final stage of the reaction involves converting nitrite to N_2O for isotopic analysis. After the removal of excess hypobromite solution, the nitrite is converted to N_2O gas by Hydrazoic acid (HN_3), which is formed using a 1:1 solution of acetic acid (20% concentration) and sodium azide solution (2M concentration). The reaction is highly pH sensitive (McIlvin et al, 2005), with an optimum pH condition of 4.5 in this study.

$$H_2NO_2^+ + HN_3 \xrightarrow{\text{slow}} N_3NO + H_2O + H^+ \xrightarrow{\text{fast}} N_2O + N_2$$ **Equation 2.4.4.1.1**

Extra care is required during this procedure, as sodium azide is an extremely explosive chemical, and to reduce this hazard it is stored as a solution (2M concentration), as which it is stable. Hydrazoic acid is also a highly toxic chemical, so can only be handled in a Class 1 fume cupboard.

After the conversion of ammonium to nitrite, the solution is transferred to crimp sealed 20ml vials, with the solution amount sufficient to contain 20nmol of N. When needed the azide solution (HN_3), is freshly made using acetic acid (20%) and 2M azide solution, in 1:1 ratio. It is always made shortly before using it, and is not stored.

The stock azide-acetic acid solution is placed in crimp sealed vials and purged with N_2 gas at 50-60 ml/min speed for 20 minutes with a gas outlet needle inserted in order to remove any N_2O produced by nitrite in the reagents. It should be noted that an electronic flowmeter is not used to measure the N_2 flow rate because of potential toxic gas remaining inside the meter after usage. A soap film bubble flowmeter was used instead to prevent the problem.

Tests for finding the right amount of acidic azide solution show that for every 4ml of sample solution (5μM NH_4^+), 350μl of azide-acetic acid solution needs to be added to reach the optimum pH between 4 and 5. After the stock azide-acetic acid solution is purged with N_2 for 20 minutes, the appropriate volume of this stock azide-acetic acid solution is added to each sample, using a gas-tight syringe via the crimp-sealed septum. The solution is then shaken and left for 30 minutes. In order to minimize leakage of N_2O gas the vials are stored upside down for this period. The acid is then neutralised using 350μl of 10M sodium hydroxide (NaOH) to increase the pH, in order to terminate further production of hydrazoic acid, which is a potential hazard when the samples are put through the mass spectrometer.

2.4.4.2 Isotopic Measurement of N_2O

When measuring N_2O gas for its isotopic composition, the reference material becomes important, since there is no N_2O gas international standard. In order to work out the isotopic composition of samples, multiple ammonium international standard materials are measured in conjunction with the samples. IAEA N1 (+0.4‰), USGS25 (-30.4‰) and USGS26 (+53.7‰) are all international standards for ammonium, with a known isotopic value. After

all ammonium samples and international standards are converted to N_2O gas on the azide step, they are all measured against an internal lab standard N_2O gas (20ppm N_2O).

It is then assumed to have an isotopic composition of 0‰ since industrial production of N_2O gas involves the use to atmospheric nitrogen gas ($\delta^{15}N = 0‰$).

Pairs of N_2O lab internal standard gas are inserted every 10-12 samples within the batch, so that they can be used to assess possible instrumental drifts.

Measured isotopic values are plotted against the accepted value for the above mentioned three standards, and a calibration line is calculated using this data. By referring to equation 2.4.4.1.1, the isotopic composition of N in N_2O can be determined. Of the 2N in the N_2O gas, one N will be from the ammonium and the other N from azide, which is produced using ammonia gas originated from atmospheric N_2, which is an international standard with an isotopic value of 0‰.

One test of the accuracy of a method is to plot the measured versus known values of independently analysed (i.e. calibrated using other standards) standard reference materials. In conventional analyses such a plot should approximate to a graph with a slope of one and an intercept of zero, or if there is a finite blank this intercept represents the blank. In this isotopic analysis the situation is slightly more complex. The first reason for this is that isotopic values can range from positive to negative values and hence the plot looks rather more complex, although the same principle applies and the y intercept approximates to the blank. The second reason specific to the N_2O analysis is that half of the N comes from the

azide with a value of zero and the other half comes from the ammonium standard. Therefore the measured value will be the numerical average of the ^{15}N of the standard and the azide which has an isotopic value of 0‰. This will reduce the measured value to exactly half of the observed value of the standards and hence the plot of measured vs. known will have a slope of 0.5 not 1.0.

Replicates of the three international reference materials are measured in every batch of samples. Laboratory measurements show small variations for the calibration lines run in different batches. Results for standards are very close to theoretical predictions - slope values ranges from 0.46 to 0.47, and the intercept very close to zero (figure 2.12).

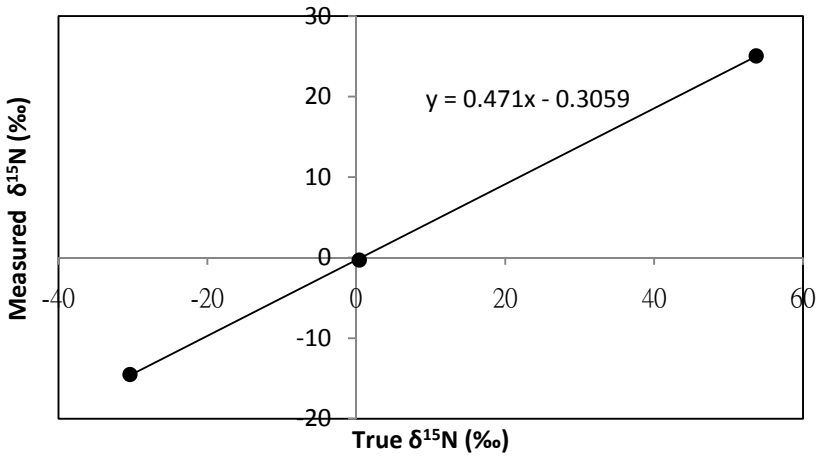

Figure 2.12 An example of the measured isotopic composition of ammonium standards plotted against true isotopic compositions. Regression line plotted using the true and measured values of IAEA-N1, USGS-25 and USGS-26.

As described above, the ammonium conversion to nitrite step is tested using a photo-colorimeter. In order to test the azide conversion step (nitrite is converted to N_2O gas), three nitrites (lab standards) with known isotopic compositions are used together with ammonium samples in the same batch. The nitrite lab standards are Fisher $NaNO_2$, Sigma

$NaNO_2$ and Fisher KNO_2. These nitrite lab standards were calibrated using an ANCA EA coupled on-line with a Europa 20-20 IRMS (Bristow, 2009), a similar system used for sulfate isotopic analysis (combustion of solid samples to IRMS).

The values are compared in the same way as ammonium standards, and the slope for measured vs. actual values is again expected to be close to 0.5. Laboratory measurements give an average slope around 0.49 and intercepts close to zero (e.g. figure 2.13). This indicates an accurate measurement with good precision and insignificant blank values. It should be noted that nitrite standards will only be used as a reference to test the azide method, and cannot be used in any data analysis, because the processing of these samples does not include all the analysis steps for ammonium conversion to nitrite. Specifically, as no hypobromite solution is added to the nitrite standards, the alkalinity originated from the hypobromite solution will not be present, resulting in a pH difference between nitrite standards and ammonium samples/standards. Measurements show a pH of 3.8 for ammonium samples/standards through both steps (ammonium conversion to nitrite and nitrite conversion to N_2O gas) and a value of 2.2 for nitrite standards (nitrite conversion to N_2O gas only). Therefore when adding the azide solution, the reaction condition will be different, even though the pH is proven to be suitable for effective conversion.

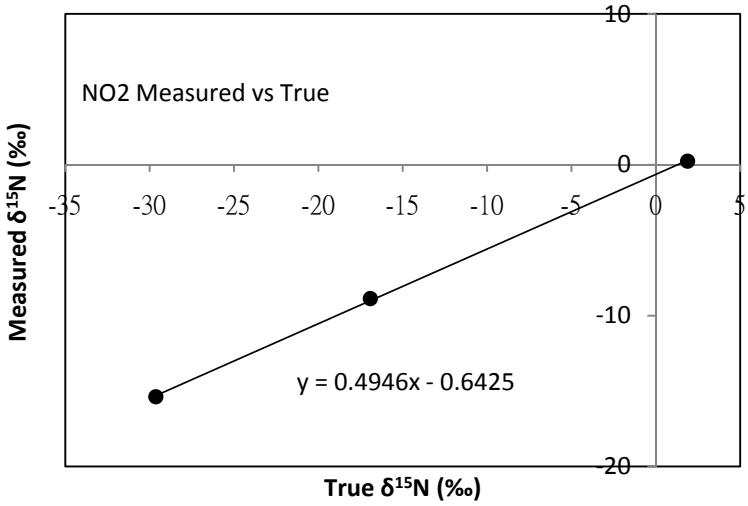

Figure 2.13 An example of the measured isotopic composition of nitrite standards plotted against the true isotopic compositions.

2.4.5 Data Processing and Calculation

This chapter will cover procedures taken to process output data from the mass spectrometer. Examples will be provided alongside the formulas used presented. Some important equations were adapted from McIlvin et al. (2005) as will be noted.

2.4.5.1 Raw Data

There are numerous data available from the mass spectrometer after measurements of a batch of samples. Similar to the Dionex analysis, the isotopic composition can be internally calculated and presented on the computer, but does not provide estimates of the precision or uncertainties involved in the calculation. Therefore raw data are extracted onto a spreadsheet and calculations carried out. The total beam area (integrated area under peak) reflects the size of the peak i.e. amount of gas sample analysed. There are five isotopomer species of N_2O (table 2.4.5.1.1), and two ratios (molecular masses 45/44 and 46/44) are measured for N_2O gas samples.

Table 2.6 The abundance of isotopomer for N_2O gas.

Mass	Species
44 (most abundant)	$^{14}N^{14}N^{16}O$
45	$^{14}N^{15}N^{16}O$, $^{15}N^{14}N^{16}O$ & $^{14}N^{14}N^{17}O$
46	$^{14}N^{14}N^{18}O$

2.4.5.2 Drift Correction

Similar to the sulfate isotope drift correction, the order that the samples are run (N) is plotted against the ratio (mass 45/44 and mass 46/44 in two separated correction graph, instead of a single correction graph for mass $^{34/32}S$). As noted earlier samples of the laboratory N_2O internal standards are interspersed throughout the sample run. A best fit line (or curve) is generated and an equation of the line calculated for the analyses of these N_2O samples and the reference materials and samples are corrected according to their position in the batch.

2.4.5.3 Calculation of $\delta^{15}N$

After the ratio of 45/44 and 46/44 are corrected for drift, the relative δ value can be calculated. Identical to equation 1.7.1 in the introduction chapter (section 1.7), $\delta^{45}N_2O$ and $\delta^{46}N_2O$ can be calculated.

$$\delta^{45\ (and\ 46)}N_2O_{sample} = (R_{sample} - R_{standard}) / R_{standard} \quad x100 \qquad \textbf{Equation 2.4.5.3.1}$$

After the calculation of $\delta^{45}N_2O$ and $\delta^{46}N_2O$, the real isotopic value of $\delta^{15}N$ can be calculated using the equation from McIlvin's paper (2005).

$\delta^{15}N_{sample} = \delta^{45}N_2O_{sample}\,[1 + {}^{17}R_{std} / (2^{15}R_{std})] - \delta^{17}O\,[{}^{17}R_{std} / (2^{15}R_{std})]$ **Equation 2.4.5.3.2**

where $^{17}R_{std} = 0.037\,99$, $^{15}R_{std} = 0.367\,65$, *and* $\delta^{17}O = 0.52\,\delta^{18}O$ (McIlvin & Altabet, 2005).

Both mass 44 and mass 46 N_2O have $^{14}N^{14}N$ (table 2.4.5.1.1), and the calculation of $\delta^{46}N_2O$ involve the ratio of mass $^{46}N_2O$ ($^{14}N^{14}N^{18}O$) / $^{44}N_2O$ ($^{14}N^{14}N^{16}O$), essentially $^{18}O/^{16}O$, and therefore $\delta^{46}N_2O$ can be effectively considered as $\delta^{18}O$.

By using equation 2.4.5.3.1 and 2.4.5.3.2, $\delta^{15}N$ can be calculated by using $\delta^{45}N_2O$ and$\delta^{46}N_2O$.

2.4.5.4 Blanks and Correction

Blanks are also measured to determine the contribution of reagents to the total isotopic value. One set is run through both the oxidation step (NH_4^+ to NO_2^-) and the azide conversion step, while the other is only put through the azide step. This will test the size of the blanks for corrections. Theoretically, blanks that go through the azide step only will have a smaller contribution to the final measured compositions, since fewer chemicals are added. Measurements confirm that blanks for the calculation of oxidation + azide conversion step has a larger value compared to the azide only step blanks. It should be noted that for blanks made during azide only step are made in milli-Q water only (the oxidation + azide conversion blanks contains hydroxide), so the difference of pH noted above for nitrite standards will also apply for this set of blanks. Measurements suggest that overall blanks (oxidation of NH_4^+ to NO_2^- + azide conversion to N_2O) contribute a signal equivalent to approximately 10% of the sample. Blank values are subtracted from the overall value to obtain the actual value. An average precision of 0.2‰ is obtained from replicates of standards in this study.

2.4.5.5 Storage tests

Due to the amount limitation of the international standards of ammonium, it is necessary to test how effectively ammonium reference materials can be stored without significant fractionation. Nitrite standards are very difficult to store even in frozen state (Bristow, 2009), but little is known for ammonium standards stored in frozen state, therefore measurements were carried out the test the effectiveness of frozen storage for ammonium standards, since freezing was the standard preservative method for aerosol samples. It should be noted that due to the limitation of time, the storage test could only be undertaken at a time range of about two months. In order to minimize possible fractionation from escape of water vapours during the freezing/defrosting process, standards were kept in crimp-sealed vials to prevent gas leakage. In the latest measurement, frozen standards made on the 7th of April, 2009 were measured against fresh standards at 28th May, 2009 (figure 2.14).

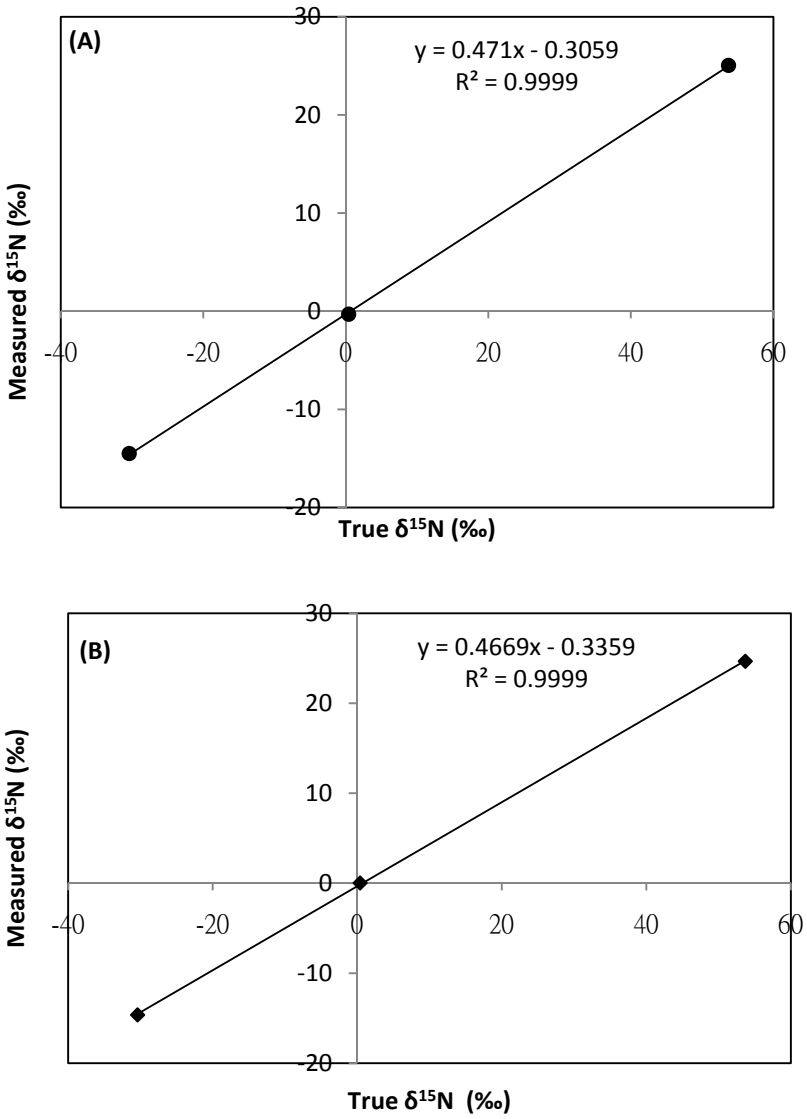

Figure 2.14 Frozen (from 09.Apr.2009 to 28.May.2009) ammonium standards (A) plot of measured against true isotopic composition, compared with (B) fresh ammonium standards.

Figure 2.14 above shows that there is only a minor difference in both the gradient and y-intercept between fresh and stored standards. This suggests that provided with suitable conditions, the samples can be stored in the freezer for at least 52 days (approximately 2 months), without significant changes in their isotopic composition.

Chapter 3: Sulfur & Nitrogen Isotopes in Aerosols

In this chapter, data obtained from aerosol samples will be presented. The isotopic composition of sulfate and ammonium in samples are calculated as described in the methods chapter, and further calculation will be presented below, in an attempt to further utilize the dataset available.

3.1 Sulfur Isotopic Composition of Sulfate

As described in the introduction chapter, mass spectrometry provides a viable way to distinguish and trace sulfate aerosols from various sources. The distinctive isotopic compositions among different components of sulfate in the atmosphere have been used quantitatively (see introduction chapter) in several studies. In this thesis, and specifically in the processing of isotopic data in this chapter, three major end member compositions of sulfate will be used, referring to a paper by Wadleigh (2004) and discussed in the introduction chapter. The isotopic composition of seasalt sulfate is assumed to be at +21‰, biogenic sulfate +18 ± 2‰, and anthropogenic sulfate +3 ± 2‰. Those three values mentioned above will be used in various graphs and calculations that are described below.

3.1.1 Changes in $\delta^{34}S$ Along Cruise Tracks

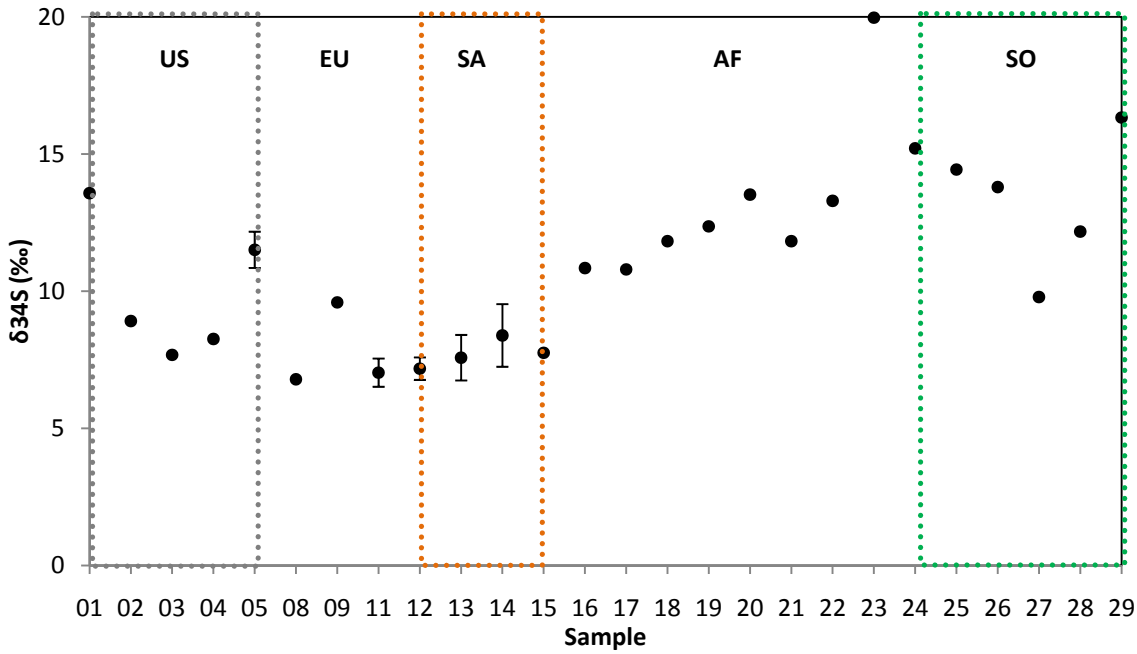

Figure 3.1 $\delta^{34}S$ variations for fine mode aerosol samples from AMT15 cruise. Available standard deviations are attached where replicates are measured. The colour shading and letter codes refer to classifications by five-day back trajectories (see below).

Five-day back trajectories are used to group samples into different categories: zone US represents air that has travelled close to or over North American region within the last five days; zone EU indicates air passing over Europe; zone SA represents air passing around the Saharan Desert, zone AF represents air passing over Southern Africa, and zone SO represents samples where the air has been over the Southern Ocean for the previous 5 days. If a line is drawn among points, it will not represent the changes in isotopic compositions among samples directly. This is because the distance between sample stations are not constant, and neither is the time around which they are sampled. If a solid line is drawn throughout the samples, it will imply something about the trend among samples, while the plot only describes the isotopic composition at each specific location.

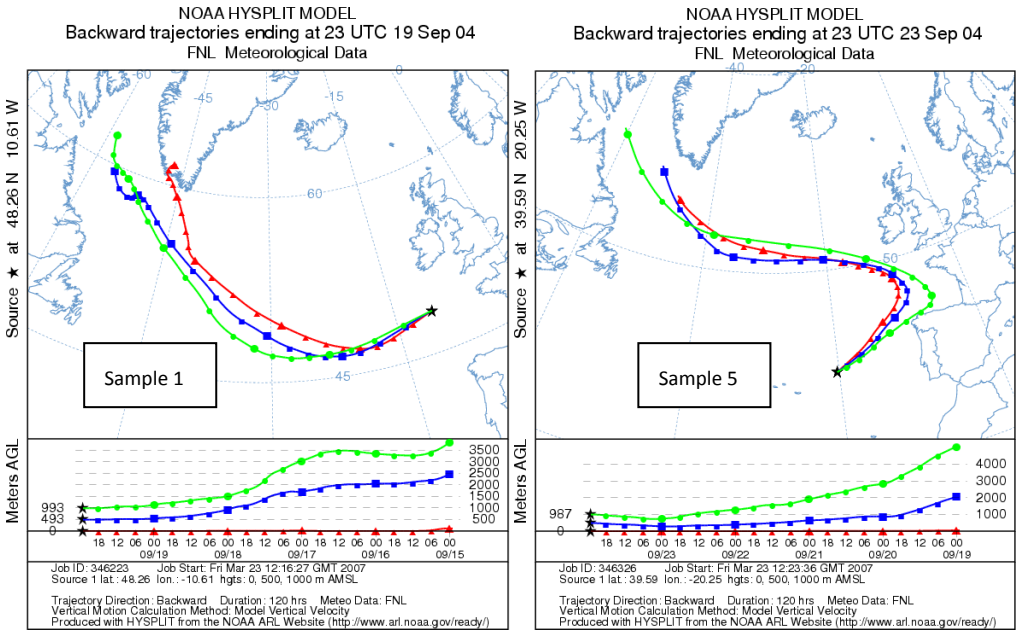

Figure 3.2 Five-day back trajectory for sample station 1 (left) and 5 (right) from cruise AMT15. Mid-point latitude coordinates are used in producing the trajectory.

The result for the AMT15 cruise is shown in figure 3.1. Trajectory examples are shown in figure 3.2 (see also appendix 1, section I). From figure 3.1, the isotopic composition of sample 1 is +13.6‰ (zone US), having a trajectory showing air travelling near the North America continent within the past five days. Similar trajectories are observed for sample 02 and 03, with decreasing isotopic values to 7.7‰ with the lowest value in sample 03. The trend then has an increase in sulfate isotopic values to +11.5‰ at sample 05, which is hard to explain by simply referring to the trajectory (figure 3.2), because the trajectory suggests a similar source region to samples 01 to 05. Fluctuation can be observed for samples categorized as EU, from +6.8‰ to +9.6‰. Saharan region samples have similar isotopic values of around +7‰ to +8‰ (zone SA). The isotopic compositions then gradually increase as the cruise travels further south down the Atlantic Ocean, reaching a maximum value of +20‰ at sample 23 (zone AF), with a trajectory showing air travelling entirely over the

Southern Atlantic Ocean, not touching land. The isotopic values then fluctuate around +10 to +16‰ thereafter (all SO) in areas considered as being remote from terrestrial sources. From those observations, some changes in $\delta^{34}S$ values can be explained. For the first four samples, air-mass back trajectories suggest anthropogenic sources from the American region despite being collected close to Europe producing a source of isotopically light sulfur, along with isotopically heavier biogenic and seasalt sulfate picked up around the remote North Atlantic Ocean. Sample 05 is expected to have a combination of anthropogenic sources from both American and European regions, though there is no way to quantify their distributions separately. It also has a considerable component of biogenic or seasalt, which results in the heavier isotopic composition in comparison to the rest of the European samples. In samples 05 to 15, European anthropogenic influences can be observed from the low $\delta^{34}S$ values. As the cruise progresses into the South Atlantic, into remote regions with less anthropogenic influence, seasalt and biogenic contributions become a more significant component relative to anthropogenic sources, resulting in heavier isotopic values. The lower value of $\delta^{34}S$ for sample 27 cannot be explained by 5-days back trajectories, which suggests air travelling over and around the sampling location for the past five days, in the middle of the South Atlantic Ocean.

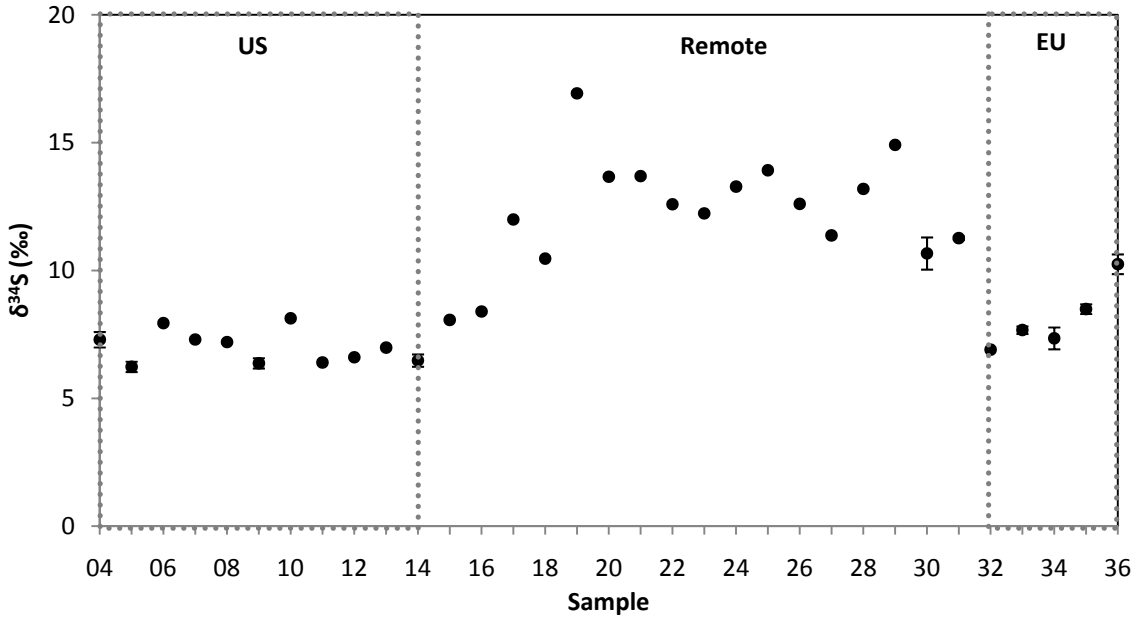

Figure 3.3 $\delta^{34}S$ variations for fine mode aerosol samples of 36N cruise. Available standard deviations are attached where replicates are measured. Similar to figure 3.1, coloured categories are based on 5-day back trajectories.

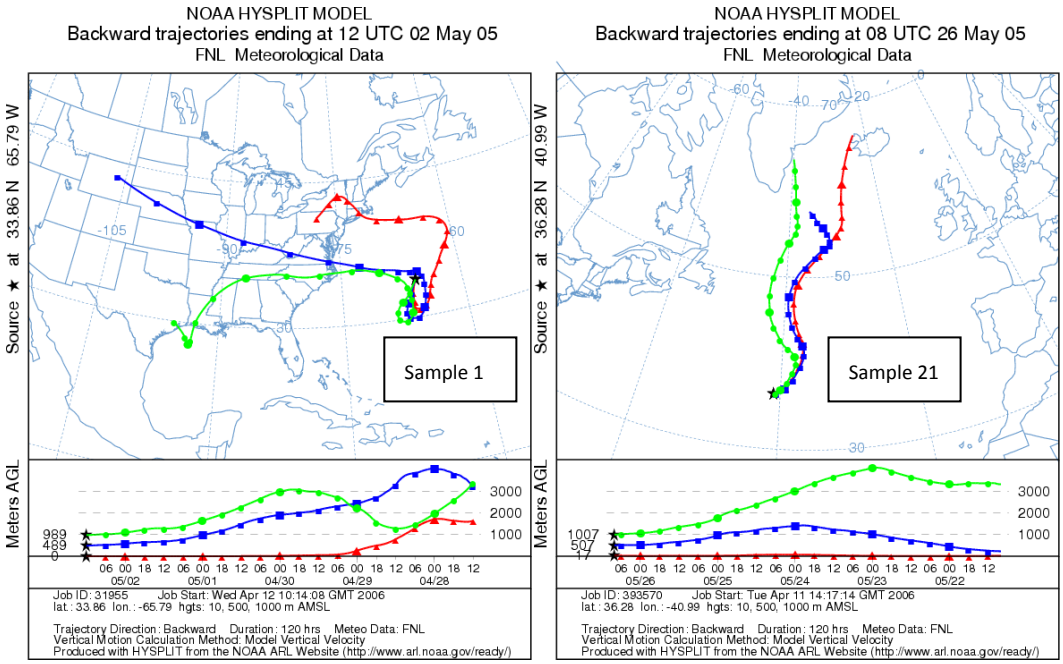

Figure 3.4 Five-day back trajectory for sample station 1 (left) and 21 (right) from cruise 36N. Mid-point latitude coordinates are used in producing the trajectory.

Figure 3.3 provides a simpler picture than the AMT15 cruise presented above. In general the samples near the US coast have isotopic composition of approximately +6‰ to +8‰.

Isotopic compositions of sulfate increase to around +10‰ to +16‰ as the cruise travels

further away from land, and decrease again to about +7‰ to +8‰ nearer the European coast. Based on those observations, it can be suggested that sulfate isotope signals are all lower than the value representing biogenic and seasalt sulfate (+18‰ and +21‰ respectively) along the transect, implying a significant anthropogenic sulfate contribution, particularly nearer the North America and European continents. In the middle of the transect (samples 16-31), sulfate isotope values are higher, suggesting less anthropogenic sulfate relative to a seasalt and biogenic source. These changes in isotope values are consistent with the 5-day trajectories (figure 3.4 see also appendix 1, section III), as can be seen from the categorization.

These two sets of complete data from two distinctive transect give a quantitative picture of attempts to trace the source of sulfate in aerosol samples. However, many samples are likely to contain sulfate from several sources. The $\delta^{34}S$ data on its own also cannot separate biogenic and seasalt sulfate sources, due to the mixing effect in the atmosphere and relatively close isotopic values for both component. Thus while these plots are instructive, they do not alone allow detailed quantitative interpretation. The subsequent sections consider ways to combine isotopic and atmospheric concentration data to further discriminate between different sulfate sources.

3.1.2 $\delta^{34}S$ and Percentage Seasalt Sulfate (PSS)

Considering the disadvantages mentioned above, another complementary approach is taken, by using the concentration of non-seasalt (nss) sulfate data together with the isotopic data.

With the additional nss sulfate information it is possible to separate biogenic and seasalt sulfate signals within samples.

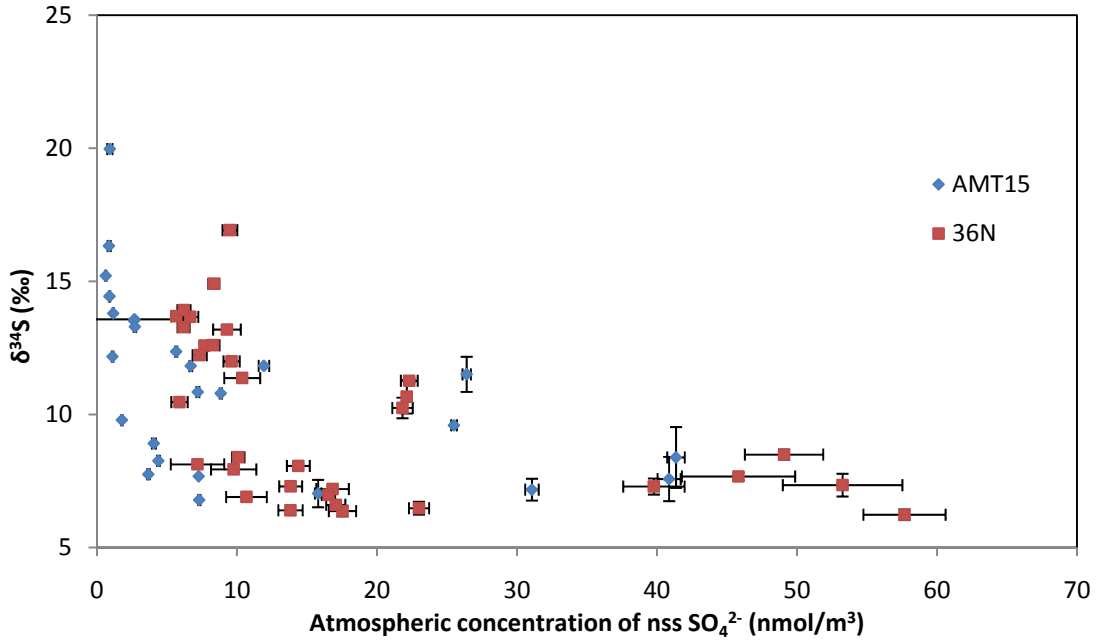

Figure 3.5 A plot of$\delta^{34}S$ measured against the atmospheric fine mode aerosol concentration of non-seasalt sulfate for cruise AMT15 and 36N. Standard deviations for nss sulfate are shown (horizontal error bar). For the isotopic dataset, error bars (vertical) are attached only where replicates are measured.

In figure 3.5, two sets of data from very different cruise tracks (AMT15 & 36N) are presented in a single plot of measured $\delta^{34}S$ against calculated nss sulfate. An increase in the concentration of nss SO_4 (with decreasing $\delta^{34}S$ values) implies an increase in anthropogenic or biogenic sulfate and/or a decrease in seasalt sources. Anthropogenic and biogenic sulfate can be distinguished by their different isotopic signatures (+18‰ for biogenic and +3‰ for anthropogenic sulfate sources, see above). Data points below +10‰ may be considered to be dominated by anthropogenic sulfate sources, similarly sulfate isotope values around 20‰ imply a biogenic or seasalt source, others between +10‰ to 20‰ suggest a complex mixing of all three components of sulfate.

A few observations can be made from figure 3.5 above. Data points from AMT15 generally have nss SO_4 concentration lower than 10 nmol/m^3. Samples from 36N, which is expected to have heavier anthropogenic influence compared to AMT15, have many points at around 10 nmol/m^3 or greater concentrations. This suggests that more samples from AMT15 are taken in a comparatively pristine region compared to 36N, resulting in the lower concentration of nss sulfate observed in the plot above. The 36N samples with high nss SO_4 concentrations are also generally characterized by low sulfur isotope values (+6‰ to +8‰), consistent with a significant anthropogenic component.

However figure 3.5 is still not able to be used to directly estimate the relative importance of different sulfur sources. However, by a modification of this approach, it is possible to achieve this goal by plotting sulfur isotope composition against the percentage seasalt concentration (figure 3.6).

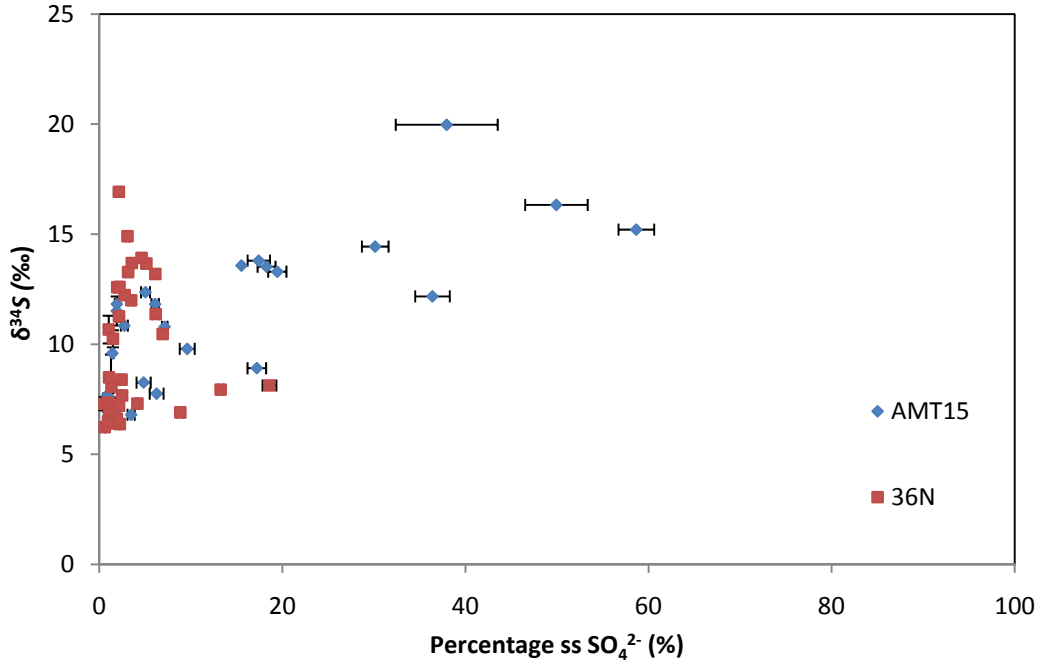

Figure 3.6 A plot of the isotopic composition of sulfate against percentage seasalt sulfate for samples of cruise AMT15 and 36N. Standard deviations for percentage seasalt sulfate are shown (horizontal error bar). For the isotopic dataset, error bars (y-axis) are attached only where replicates are measured.

It can be seen from figure 3.6 that not much can be concluded by simply plotting $\delta^{34}S$ against percentage seasalt sulfate (PSS). Samples from AMT15, especially those sampled near the Southern Ocean region, have a higher seasalt component i.e. higher PSS. They are considered to be made up of seasalt and biogenic components and smaller anthropogenic contributions. Data points that have PSS>30% are shown to have come from the South Atlantic, where biogenic activities and sea spray are dominant over anthropogenic influences. As for 36N, the cluster of samples with sulfur isotope values of 10‰ or greater are found to be sampled from the middle of the transect, away from the North American and European continents, close to the region where biogenic activities and seasalt source are potentially more important than anthropogenic influences. Samples with low PSS and isotopic values below 10‰ are substantially influenced by anthropogenic emissions. The

error bars provide confidence that changes or trends described above are not due to instrumental fluctuations.

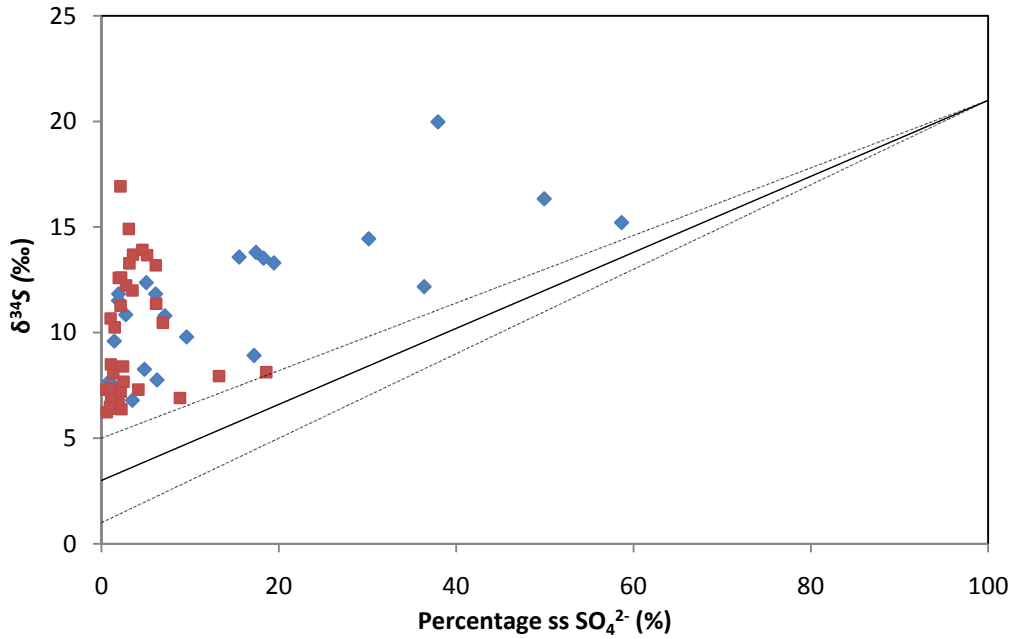

Figure 3.7 A plot of the isotopic composition of sulfate against percentage seasalt sulfate for samples of cruise AMT15 (blue rhombus) and 36N (red square). Seasalt (+21‰) and anthropogenic end member (+3± 2‰) points are connected using solid line for the average value, and the dotted lines join the values of single standard deviation around the average values. Error bars for individual pairs are not shown for clarity of the graph.

As mentioned above, the large differences of $\delta^{34}S$ values between anthropogenic and seasalt sulfate makes it easier to identify possible sources of sulfate. In the absence of a biogenic source, an assumption can then be made, that with a higher percentage of seasalt sulfate, isotopically heavier sulfate can be expected to be found, i.e. larger $\delta^{34}S$ values. Theoretically, when samples have 100% seasalt sulfate, the $\delta^{34}S$ value will be +21‰. Similarly, lighter sulfate is expected in heavily polluted area, with a $\delta^{34}S$ value approximately between 0 and +5‰ when the percentage of seasalt sulfate is 0%. For the $\delta^{34}S$ values of anthropogenic sulfate, a value of +3 ± 2‰ (Wadleigh, 2004) will be use in this

study. In the absence of a biogenic source, linear mixing between these end members would be expected.

In figure 3.7, three lines are drawn to show the theoretical values of $\delta^{34}S$ mentioned above, assuming mixing of seasalt and anthropogenic sulfate only. The solid line represents the suggested value for anthropogenic sulfate and the two dotted lines above and below uses the extremes of the standard deviations of the anthropogenic sulfate value (Wadleigh, 2004). Any sample which falls within the region between the dotted lines can be explained by simple mixing between seasalt and anthropogenic sulfate. Samples with high PSS and heavy sulfate are considered to be dominated by a sea spray source. Samples of comparatively lower positive isotopic compositions and low PSS can be considered to be dominated by anthropogenic influence.

On both cruise few, if any samples fall along the simple mixing line in figure 3.7 with most points falling above the mixing line. This indicates an additional contribution of sulfate emission (biogenic, DMS). It also suggests that significant amount of sulfates in almost all samples come from this source.

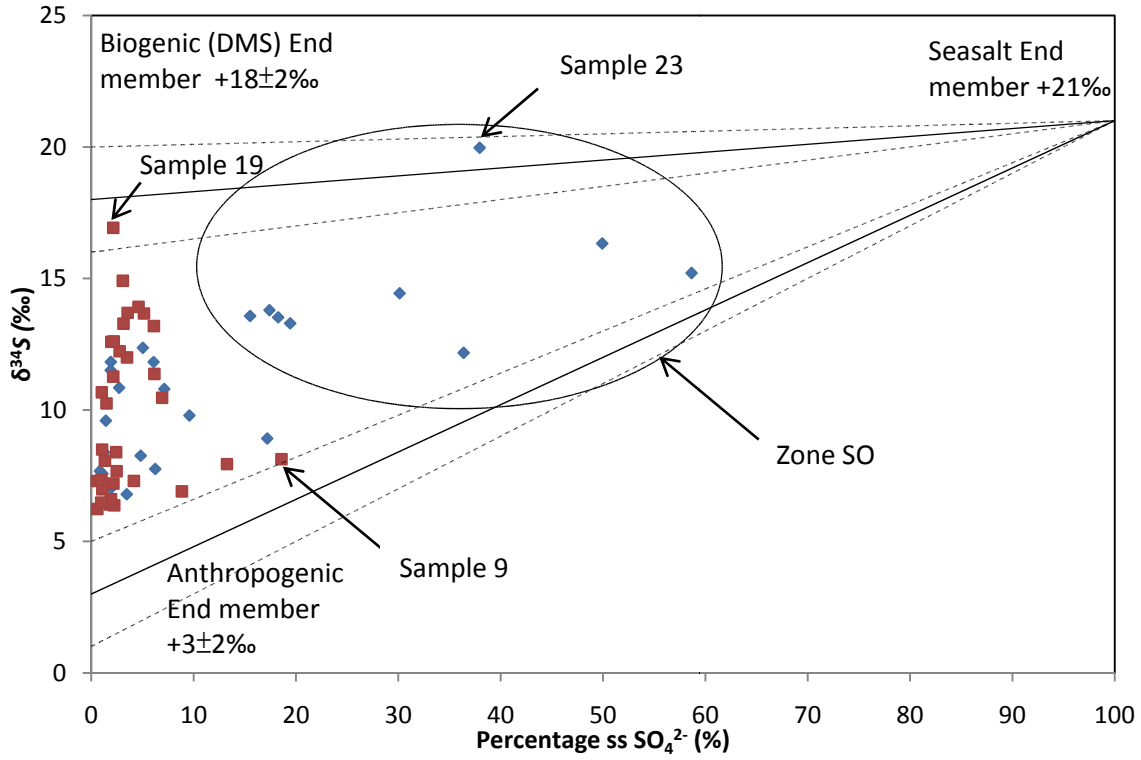

Figure 3.8 A plot of the isotopic composition of sulfate against percentage seasalt sulfate for samples of cruise AMT15 (blue rhombus) and 36N (red square). Biogenic (+18± 2‰), Seasalt (+21‰) and anthropogenic end member (+3± 2‰) points are connected using solid line for the average value and dotted lines for representing joining of standard deviation of average value deviations. Zone SO represents Southern Ocean. Error bars for individual pair are not shown for clarity.

Figure 3.8 is the most appropriate plot to describe the complex mixing process compared to figure 3.6 and 3.7. All data points lie within the triangle formed by connecting all three end member points together. This implies a complex three-way mixing process taking place for virtually all samples, with only a few points lie within the simple seasalt / anthropogenic mixing zone. Sample 23 from AMT15 cruise and sample 9 from 36N cruise are two samples that are close to being represented by simple mixing of two sulfur sources (figure 3.8). Nine samples that are circled in the plot and marked zone SO represent samples expected to have a major marine i.e. seasalt and biogenic sulfur sources, since all are collected around the Southern Ocean. The high percentage of seasalt and an isotopic composition range of +12‰

to +20‰ suggest a combination of three different sources, with seasalt and biogenic components more important than the anthropogenic source. In addition, all those 36N samples categorized as remote (figure 3.3) have $\delta^{34}S$ values larger than 10‰. However, those samples lie further left in the plot in figure 3.8, when compared to the AMT15 samples that are also classified as remote (zone SO). This suggests that although complex mixing is observed in both categories, 36N samples have less seasalt contribution in comparison to AMT15 samples. Sample 09 from 36N cruise has low PSS values and can be described by simple mixing between anthropogenic and seasalt sulfate sources, while sample 19 from 36N can be described by simple mixing between biogenic and seasalt sulfate sources.

By referring to the figure 3.8, the two cruises seem to have quite distinctive characteristics. Samples from AMT15, due to its cruise track, have a wide range of $\delta^{34}S$ values. Those with high PSS and $\delta^{34}S$ values are found to be sampled near the Southern Ocean, where the sulfate is predominantly from biogenic and seasalt sources. The majorities of data points do not lie within the anthropogenic zone, although the results in general do suggest a mixture of sulfate from all three different sources. For 36N, the samples all have low PSS and $\delta^{34}S$ value of +6‰ to +16‰. Samples that lie just above the theoretical anthropogenic region have sampling location near the coast of the US/Europe. As the cruise travels further away from the North American and European continents, heavier sulfates are found in samples, while the percentage of seasalt sulfate remains more or less constant. This implies an increasing input of sulfur from biogenic sources.

Figure 3.8 helps to describe the complex mixing process all samples have gone through. Although one or multiple components can be separated from the rest, it is still impossible to assess the contributions of each component in more detail. However, Wadleigh (2004) introduced an equation that made it possible to quantify different sources of sulfate. Detailed calculations will be presented subsequently.

3.1.3 Segregation of Sulfate Components

By using an equation (equation 4.1.3.1) from Wadleigh (2004), and a combination of isotopic and ion chromatography data, it is possible to calculate the atmospheric concentration of each sulfate components in every fine mode aerosol samples. Three sulfate end members (mentioned several times above) are once again used in the following equations.

$$\delta^{34}S_{meas} = \delta^{34}S_{bio}f_{bio} + \delta^{34}S_{anth}f_{anth} + \delta^{34}S_{ss}f_{ss} \quad \textbf{Equation 4.1.3.1}$$

$$\textit{and } f_{bio} + f_{anth} + f_{ss} = 1 \quad \textbf{Equation 4.1.3.2}$$

(Wadleigh, 2004)

Where $\delta^{34}S_{meas}$, $\delta^{34}S_{bio}$, $\delta^{34}S_{anth}$ and $\delta^{34}S_{ss}$ are the sulfur isotopic composition of measured, biogenic, anthropogenic and seasalt sulfate respectively. f_{bio}, f_{anth} and f_{ss} indicate the fraction of biogenic, anthropogenic and seasalt sulfate respectively of the total atmospheric concentration of sulfate, which adds up to 1.

Equation 4.1.3.1 provides the equation which can be rearranged to calculate f_{bio}, the biogenic fraction desired in this procedure. Biogenic sulfur calculation in this context will use end member values of +18±2‰ for $\delta^{34}S_{bio,}$ +21‰ for $\delta^{34}S_{ss}$ and +3±2‰ for $\delta^{34}S_{anth}$, values taken from Wadleigh (2004).

From Equation 4.1.3.1:

$$\delta^{34}S_{meas} = \delta^{34}S_{bio}f_{bio} + \delta^{34}S_{anth}f_{anth} + \delta^{34}S_{ss}f_{ss}$$

$$\delta^{34}S_{meas} = 18f_{bio} + 3f_{anth} + 21f_{ss} \quad \text{Substitute appropriate values}$$

From Equation 4.1.3.2:

$$f_{bio} + f_{anth} + f_{ss} = 1$$

$$f_{anth} = 1 - f_{ss} - f_{bio}$$

Overall:

$$\delta^{34}S_{meas} = 18f_{bio} + 3f_{anth} + 21f_{ss} \quad \textbf{Equation 4.1.3.3}$$

And

$$f_{anth} = 1 - f_{ss} - f_{bio} \quad \textbf{Equation 4.1.3.4}$$

By substituting f_{anth} from 4.1.3.4 into the f_{anth} in equation 4.1.3.3:

$$\delta^{34}S_{measured} = 18f_{bio} + 3(1 - f_{ss} - f_{bio}) + 21f_{ss}$$

$$\delta^{34}S_{measured} = 15f_{bio} + 3 + 18f_{ss}$$

$$f_{bio} = (\delta^{34}S_{measured} - 3 - 18f_{ss})/15 \quad \textbf{Equation 4.1.3.5}$$

Once the biogenic fraction of the samples is determined, the concentration of biogenic sulfur can be calculated by multiplying the biogenic fraction by the total concentration of sulfur, obtained from ion chromatography analysis.

$$Concentration\ of\ SO_4^{2-}{}_{(bio)} = Concentration\ of\ total\ SO_4^{2-} \times f_{bio} \quad \textbf{Equation 4.1.3.6}$$

By substituting f_{bio} from 4.1.3.5 into the f_{bio} in equation 4.1.3.6:

$$Concentration\ of\ SO_4^{2-}{}_{(bio)} = Conentration\ of\ total\ SO_4^{2-} \times \left[\frac{(\delta^{34}S - 3 - 18 * Fraction\ of\ Seasalt)}{15}\right] \quad \textbf{Equation 4.1.3.7}$$

$$where\ fraction\ of\ Seasalt = \frac{Concentration\ of\ seasalt\ Sulphate}{Concentration\ of\ total\ Sulphate} \quad \textbf{Equation 4.1.3.8}$$

By using equation 4.1.3.7, it is possible to calculate the concentration of biogenic sulfate in samples, using only $\delta^{34}S$ and the seasalt fraction. Once the concentration of biogenic sulfate is obtained, the concentration of anthropogenic sulfate can be easily obtained by subtracting the concentration of biogenic sulfate from the non-seasalt concentration of sulfate in that fine mode aerosol sample. This is a relatively new approach to studying sulfate in the atmosphere, and provides several interesting findings that will be described subsequently. In

addition, the calculation of error for biogenic sulfate is also done in several stages. Although the calculation is very straightforward, and follows the simple standard error propagation (Miller & Miller, 2005) described in the methods chapter, the equations are long, taking up several pages of space. They are therefore placed in appendix 2 for those who are interested in the evaluation of the relative standard deviations of sulfate components. In the graph plots that will be presented below involving these components, error bars for biogenic and anthropogenic sulfate will be shown based on these calculations.

To sum up, by re-arranging the equations in Wadleigh (2004), it is possible to segregate different sulfate sources from one another. Coupled with the atmospheric concentration, a histogram can be drawn to present the contribution of three distinctive sulfur sources to the total sulfate concentration in the aerosol.

3.1.4 The Biogenic Sulfate Data

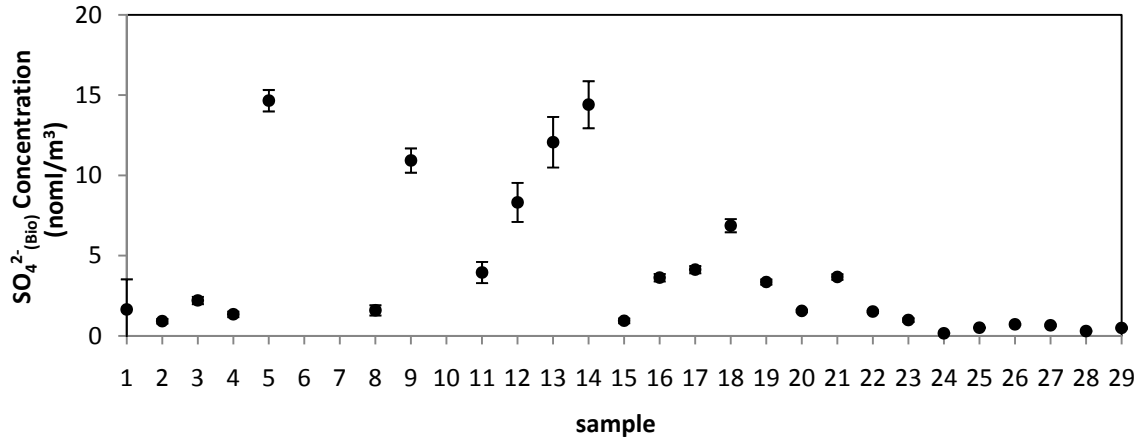

Figure 3.9 Atmospheric concentration of biogenic sulfate for individual sample stations on cruise AMT15. Standard deviations are attached where available.

Figure 3.9 above presents the concentration of biogenic sulfate for AMT15 aerosol samples. It should be noted that the line that is drawn between sample stations are neither

representative of the distance nor the sampling time interval. When compared to the overall sulfate (range from 42 nmol/m^3 at sample 14 to 1.7 nmol/m^3 at sample 29), the proportion of biogenic sulfate is quite significant. The relative proportions of the various sulfate components will be discussed in the next chapter.

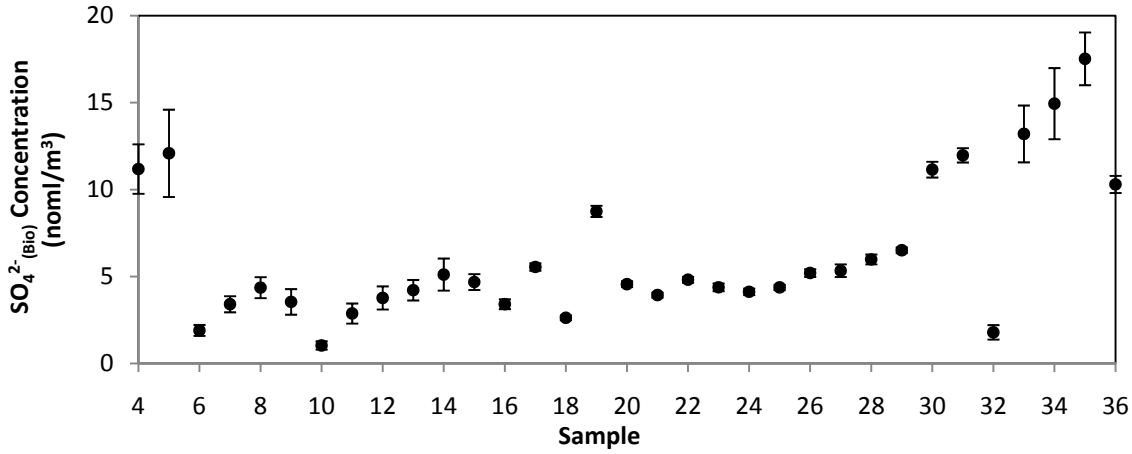

Figure 3.10 Atmospheric concentration of biogenic sulfate for individual sample stations on cruise 36N. Standard deviations are attached where available.

Similar to figure 3.9 above, figure 3.10 shows the changes in biogenic sulfate along the cruise for 36N aerosol samples. From this figure it can be concluded that biogenic sulfate concentration is high (apart from sample 32) at the beginning and end of the cruise (range from 10 to 20 nmol/m^3), which is close to the U.S and Europe respectively. In the middle of the remote North Atlantic, the concentration is comparatively low (range from 1 to 8 nmol/m^3). However, it is in the remote North Atlantic that biogenic sulfate is found to be significant compared to seasalt and anthropogenic sulfate. More details on this will be discussed in the next chapter.

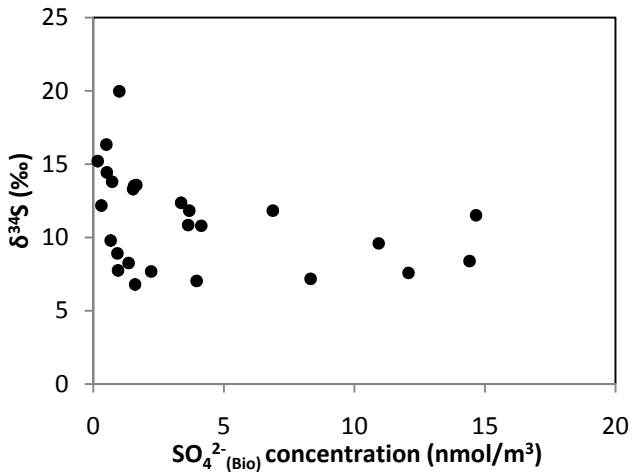

Figure 3.11 Variations in the isotopic compositions ($\delta^{34}S$) with different biogenic sulfate concentrations in the AMT15 atmospheric aerosol samples.

In figure 3.11 the overall isotopic composition of aerosol samples from AMT15 is plotted against the calculated biogenic components. It should be noted that figure 3.11 cannot be used to interpret the data further, since any trend observed is simply a result of the segregation calculations.

Segregated data for sulfate will not be shown here, and will instead be described in chapter 4, where the data is compared with ion chromatography data. This is believed to provide a clear picture on the changes in atmospheric sulfate concentrations according to the seasalt, biogenic and anthropogenic sources.

3.2 Nitrogen Isotopic Composition of Ammonium

As mentioned in the introduction chapter, although numerous studies have been done on the isotopes of nitrogen species in the atmosphere and ocean, the majority have chosen nitrite, nitrate or nitrous oxide (N_2O) gas as the main tracer. A paper by Jickells et al. (2003) is the only study that has measured marine atmospheric aerosol ammonium isotopes. They used

the resin method (see methodology), which is much less sensitive in comparison to that used in this study. Data that were presented in Jickells et al. (2003) will be used (with permission from the authors), and will be presented alongside data obtained in this study, due to the scarcity of the ammonium data present. The goal of the ammonium isotope analysis in this study was to develop a new method with better detection limit and precision than Jickells et al. (2003), and to evaluate if the trends suggested by Jickells et al. (2003) on ammonium isotope and concentration were correct. If the trends were correct, interpretations can be refined by the additional dataset measured, and sulfate and ammonium isotope data combined to evaluate the relative significance of natural and anthropogenic sulfur/nitrogen sources in fine more aerosol samples.

At the early stages of this study, due to the relative sensitivity and instrument limitations, only sulfate isotopes were analysed. It is not until the introduction of the azide method that convert nitrite to nitrous oxide (McIlvin et al., 2005), in conjunction with the conversion method by Zhang et al. (2007) that converts ammonium to nitrite, that made sensitive measurements of ammonium possible. This allows more samples to be measured in replicates and greater confidence in the results for low concentration samples. In this section, available aerosol samples from cruise AMT15 and JC18 are measured. Due to sample availability, only the latter halves of the AMT15 samples were available (sample 15-29). 12 samples are taken from JC18 cruise travelling around Montserrat. Samples from cruise JCR, which followed a similar cruise track to AMT15, are taken from Jickells et al. (2003).

3.2.1 Atmospheric Ammonium and $\delta^{15}N$

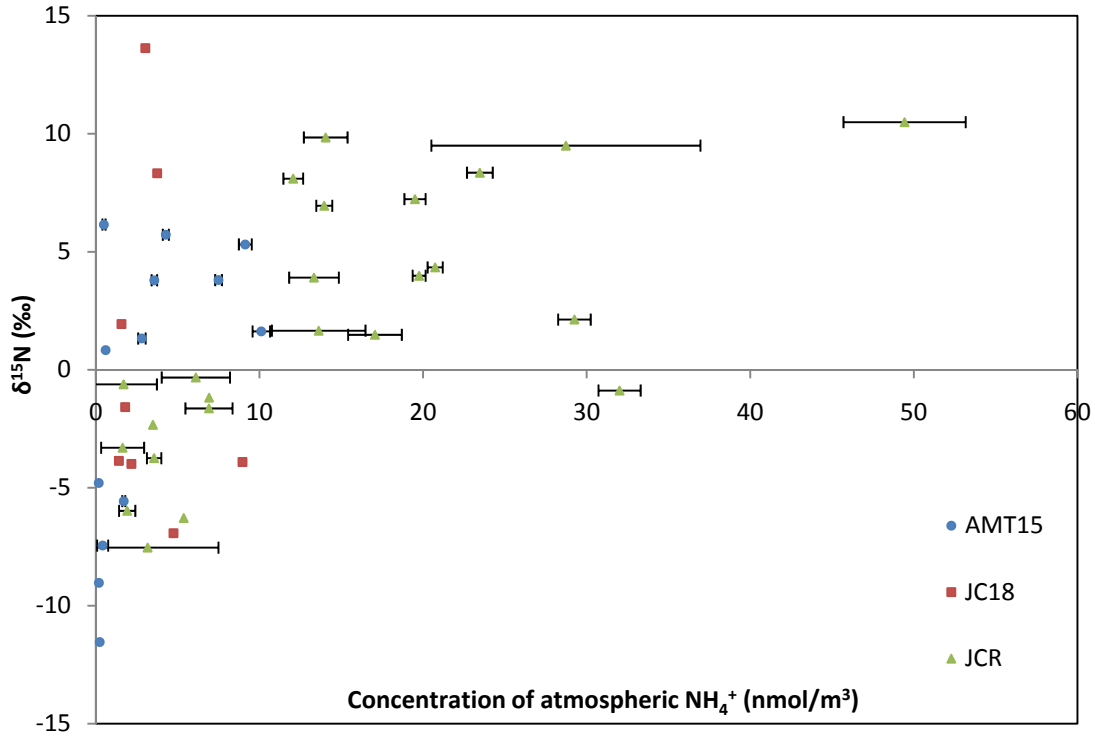

Figure 3.12 A plot of the isotopic composition of ammonium against measured atmospheric ammonium concentration, classified by individual cruises. Standard deviations are attached where available.

Figure 3.12 above shows the isotopic composition of ammonium against the concentrations of ammonium in aerosol samples from 3 cruises. From the graph alone, little information can be interpreted. There is a vague trend that increasing ammonium concentration seems to contribute to a increase in isotopic composition, which may be explained by increasing terrestrial input. This is of course an inevitable consequence of the assumptions used in calculating the percentages. The pattern in figure 3.12 shows considerable variability, also have low atmospheric ammonium concentrations. This is consistent with a relatively weak marine ammonia (Jickells et al., 2003; Johnson & Bell, 2008) source relative to anthropogenic emissions.

The wide range of isotopic composition from sources made it difficult to choose an end member based on literatures. Samples within a certain threshold of $\delta^{15}N$ and ammonium concentration in figure 3.12 can be chosen to give an approximate value for end members. However, large relative uncertainties have been introduced using this method. These uncertainties are predominantly contributed by the uncertainties from the definition of the threshold values and the calculation of end members, not those of individual sample analyses. This uncertainty may reflect natural variability within source regions or systematic difference between types of sources, e.g. biomass burning vs. animal waste. The data set here is too small to allow this to be determined. If this method is to be applied in the future instead of picking one data point and assume it to be representative, it may be possible to reduce the uncertainties in the end members by increasing the number of data points, i.e. analyse more samples. It should be noted that there could be a large natural variability in the end members, in contrast to sulfate because for sulfate the marine end members represent open ocean sulfur isotope composition which is essentially constant and even the observed range of anthropogenic sulfate isotope values is rather small.

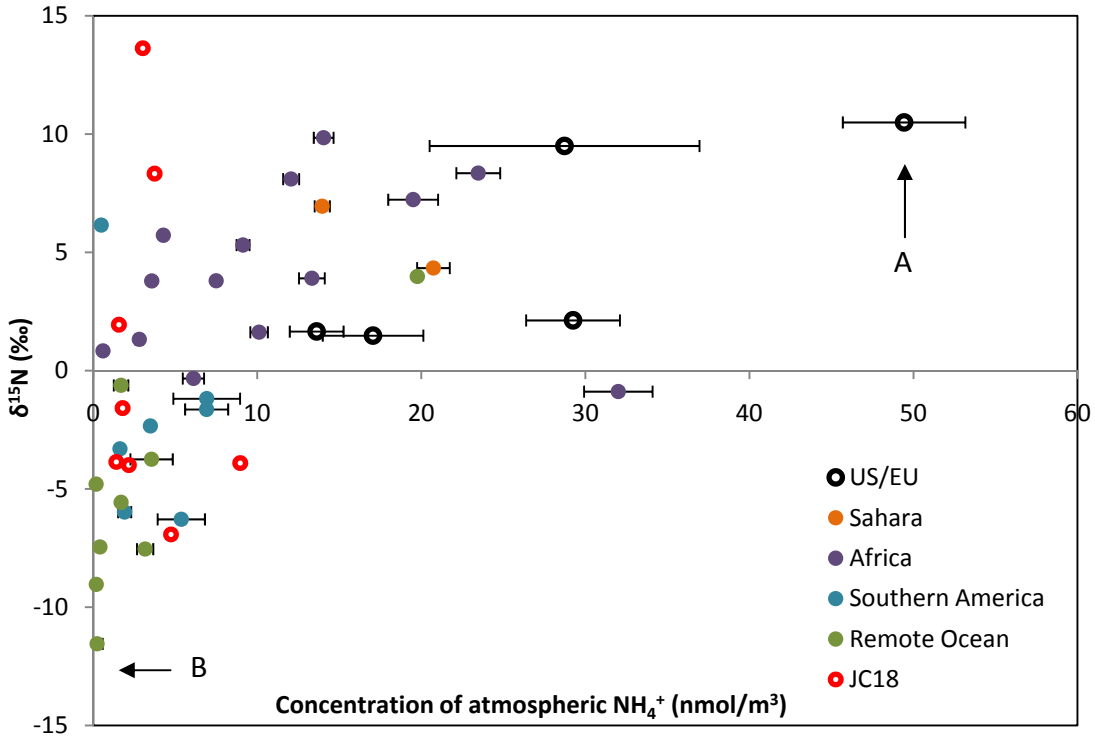

Figure 3.13 A plot of the isotopic composition of ammonium against measured atmospheric ammonium concentration, classified by regions based on five-day back trajectories.

Figure 3.13 above incorporates trajectory information into a graph of $\delta^{15}N$ vs. ammonium concentrations. It can be seen that samples from the US and EU regions have high concentrations of atmospheric ammonium, and have heavier isotopes compared to samples classified as remote ocean. This fits with the descriptions stated for figure 3.12, and furthermore presents Saharan, African, South America region samples which lie in between US/EU and remote ocean samples. Remote southern ocean samples are characterised by low ammonium concentrations and light isotopic composition.

Samples from JC18 are left out of the classification, because it is impossible to explain the changes in isotopic compositions among samples with similarly low ammonium concentrations with back trajectories.

Figure 3.13 is a more helpful graph in the determination of end members for segregation

calculations. Consider two extreme data points marked out by the arrows in figure 3.13 and their back trajectories compared with other samples.

Sample A was collected at the shortest distance to the European continent by five-day back trajectory among all other samples (sample 02 from cruise JCR, appendix 1, section V). Sample B, though was not collected closest to the remote Southern Ocean, but sampled air that travelled along the region where satellite picture suggests to have high chlorophyll i.e. biogenic activities (sample 29 from cruise AMT15, appendix 1, section I. see also figure 4.4 in section 4.3.2) and had not crossed land for at least 5 days before collection.

These two samples will therefore be assumed to be representative of anthropogenic and biogenic end members for the dataset presented in this thesis. Doing this will neglect the uncertainty in classifying samples into anthropogenic and biogenic groups based on their isotopic and concentration data and the associated high standard deviations derived during the calculation of end members . The only errors envolved in the calculation of relative errors of segregated values will be the standard deviations from isotopic measurements. As mentioned previously, replicate measurements of samples were not performed, and the deviations from reference materials will be applied instead. It should be noted that due to the excellent precision for the analysis of ammonium isotopes, the error bars presented will be small. However, this approach does ignore the issue fo uncertainty in end member concentrations..

Before exploring the segregation calculation, the individual cruise data sets are considered.

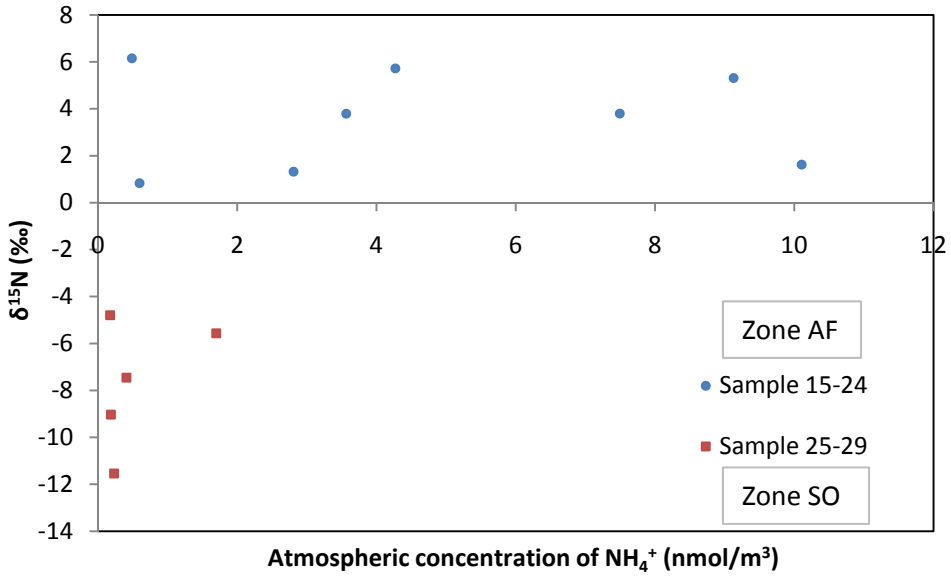

Figure 3.14 Nitrogen isotopic composition of ammonium plotted against the atmospheric fine mode aerosol concentration of ammonium for cruise AMT15 samples 15 to 29 except 17 and 18, due to sample limitation. For classification by trajectories, see figure 3.1 above.

Figure 3.14 separates AMT15 samples from the other two cruises. Data points are categorized according to their 5-day back trajectories, in exactly the same way as done in section 3.1 above. Samples 15 to 24 have their trajectories touching or close to the African continent, while samples 25 to 29 have air coming from the Southern Ocean for the last 5 days according to the trajectories. The two categories are separated from each other in a very distinctive way, and all of the samples from the Southern Ocean have a lighter isotopic composition of ammonium in comparison to those categorized as African, regardless of their atmospheric concentration of ammonium. This data is consistent with a marine source of ammonium for the Southern Ocean samples which is isotopically lighter compared to the continental sources. Samples considered to have more anthropogenic influence should have high ammonium concentration. They seem to have an isotopic composition regardless of the atmospheric concentrations of around +4 ± 2‰.

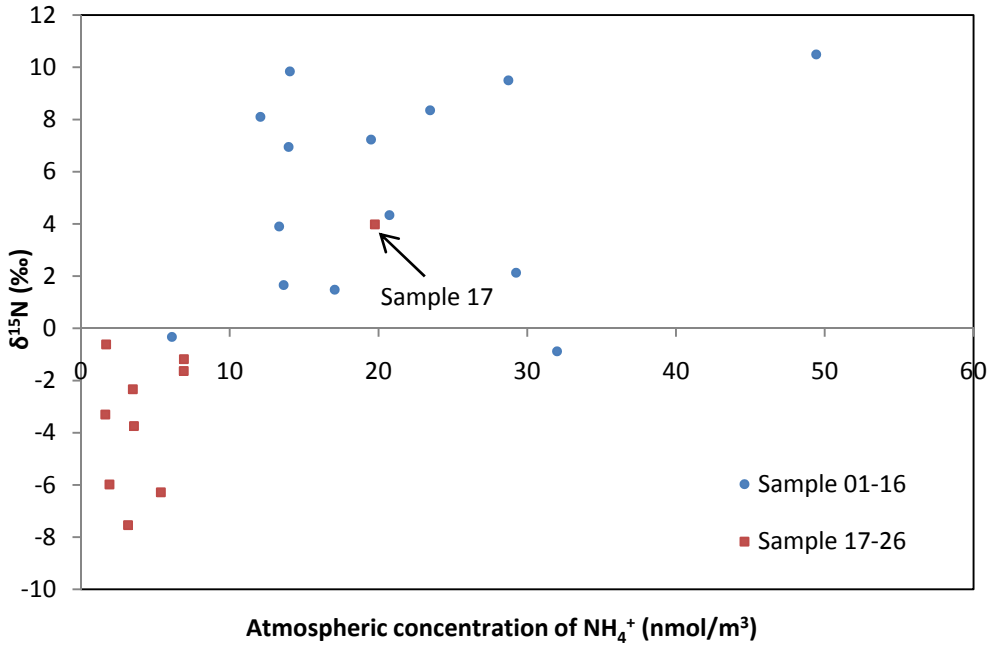

Figure 3.15 A re-plot of the nitrogen isotopic composition of ammonium plotted against the atmospheric fine mode aerosol concentration of ammonium for cruise JCR. Data were taken from Jickells et al. (2003).

Data used to plot figure 3.15 are categorized in the same way as AMT15 samples based on back trajectory data. The trend described above is also observed in this plot. Sample 01-16 have trajectories showing air coming from or touching the European and African continents. They are observed to have heavier isotope signals in comparison to the other set of data. The other set with trajectories from the South Atlantic/Southern Ocean is considered to have a more dominant marine influence, and have much lighter composition in comparison. There is only one sample (sample 17) that cannot be explained since it has a positive isotopic value, and classified as marine by its trajectory. It was sampled right in the middle of the Atlantic Ocean, roughly between Brazil and Angola, and trajectory shows that the air collected has travelled from near the continent, but has not touched any land within the past five days. The positive isotopic value of +4‰ suggests that there is an anthropogenic influence present,

and the relatively high ammonium concentration is consistent with a possible anthropogenic contribution to sample 17.

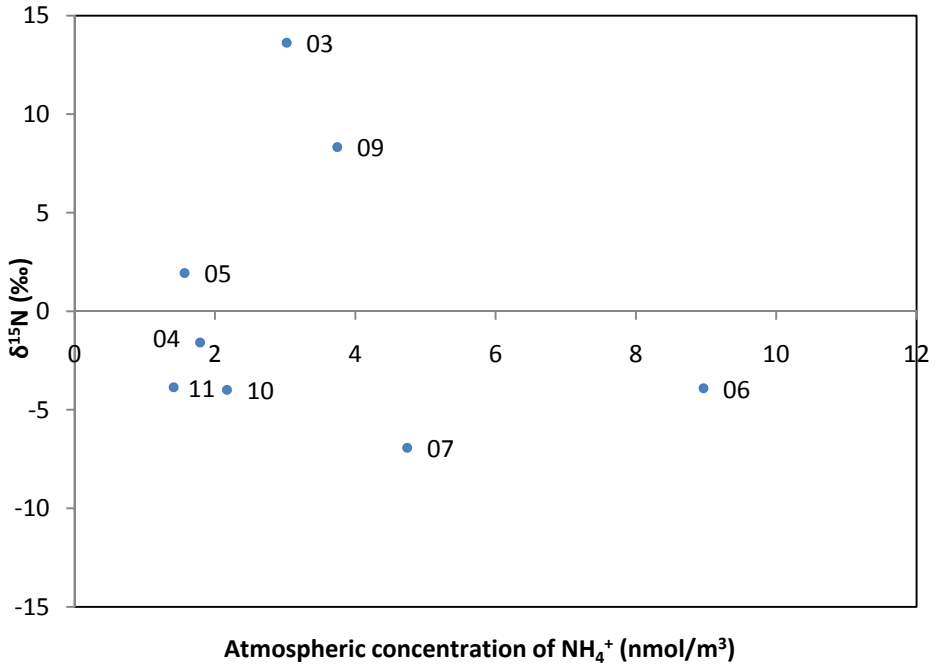

Figure 3.16 A plot of the $\delta^{15}N$ against the atmospheric concentration of fine mode ammonium for cruise JC18 samples. Individual sample points are marked on the graph.

Figure 3.16 shows the ammonium concentration data plotted against ammonium isotopic composition data. Samples 04, 05, 10 and 11 have low ammonium concentrations and an isotopic composition similar to the data obtained from AMT15 and JCR. Samples 06 and 07 have a comparatively higher ammonium concentration, but are isotopically light. This could be explained by an increase of marine biogenic emissions but more data would be required to confirm this. There could also be an isotopically light anthropogenic source of ammonium, such as coal combustion (-10‰ to +2‰) or fertilizer (-5‰ to +5‰) (see table 1.4).

Samples 03 and 09 have a heavy isotopic composition and comparatively low ammonium

concentration compared to other samples. Heavy ammonium isotopes seem to indicate a significant anthropogenic source, and from the literature, such isotopic value can only be contributed by animal excreta (chapter 1.7, table 1.4), although this might normally be expected to also give rise to high concentrations. Although for sample 03 this could be explained by an anthropogenic source from Antigua and Barbuda, and would suggest that sample 04 should be similarly influenced and it is not. As for sample 09, back trajectory suggests an anthropogenic source from the islands, although high concentrations would be expected along with the heavier isotopic composition.

3.2.2 Segregation of Ammonium Components

Procedures similar to the sulfate segregation (chapter 3.1.3) were performed to the ammonium dataset. Although there have been no attempts in the literature to suggest a formula in the mixing of ammonium from different sources in the atmosphere, the concepts described by Wadleigh (2004) can be used in this section. The propagation of errors will be described in the appendix.

Assume simple two-end member mixing between anthropogenic and a marine biogenic source for the mass of ammonium:

$$TN = BN + AN$$
$$BN = TN - AN \qquad \textbf{Equation 3.2.2.1}$$

where TN is the overall ammonium concentration, BN is the biogenic component and AN is the anthropogenic component of ammonium.

The isotopic composition is then given by:

$\delta^{15}N_T \times TN = \delta^{15}N_B \times BN + \delta^{15}N_A \times AN$ **Equation 3.2.2.2**

where $\delta^{15}N_T$, $\delta^{15}N_B$ and $\delta^{15}N_A$ represents the isotopic composition of total (i.e. measured ammonium isotope values), biogenic and anthropogenic ammonium respectively.

Substitute 3.2.2.1 into 3.2.2.2:

$\delta^{15}N_T TN = \delta^{15}N_B \times (TN - AN) + \delta^{15}N_A AN$

$\delta^{15}N_T TN = \delta^{15}N_B TN - \delta^{15}N_B AN + \delta^{15}N_A AN$

$\delta^{15}N_T TN = \delta^{15}N_B TN + AN(\delta^{15}N_A - \delta^{15}N_B)$

$AN(\delta^{15}N_A - \delta^{15}N_B) = \delta^{15}N_T TN - \delta^{15}N_B TN$

$AN(\delta^{15}N_A - \delta^{15}N_B) = TN(\delta^{15}N_T - \delta^{15}N_B)$

$AN = \frac{TN(\delta^{15}N_T - \delta^{15}N_B)}{(\delta^{15}N_A - \delta^{15}N_B)}$ **Equation 3.2.2.3**

$\%AN = \frac{AN}{TN} \times 100$ **Equation 3.2.2.4**

Substitute 3.2.2.3 into 3.2.2.4:

$$\%AN = \frac{TN(\delta^{15}N_T - \delta^{15}N_B)}{(\delta^{15}N_A - \delta^{15}N_B)} \times \frac{1}{TN} \times 100$$

$\%AN = \frac{(\delta^{15}N_T - \delta^{15}N_B)}{(\delta^{15}N_A - \delta^{15}N_B)} \times 100$ **Equation 3.2.2.5**

Equation 3.2.2.5 provides a way to calculate the percentage of anthropogenic ammonium in the aerosol samples. However, it should be noted that neither the isotopic composition of anthropogenic nor biogenic ammonium are well understood, and therefore must be assumed in order for the equation to work properly. By referring to figure 3.13, it was assumed that $\delta^{15}N$ for anthropogenic ammonium ($\delta^{15}N_A$) is +10.5‰ and biogenic ammonium ($\delta^{15}N_B$) -11.5‰. By referring to table 1.4 in the introduction chapter, the anthropogenic end member falls around the values measured in various studies apart from coal combustion and urban sewage, and the marine biogenic end member does not agree with any of the values described in table 1.4 (ocean NH_4^+ with a value between +2‰ to +7‰). The only similar study by Jickells et al. (2003) suggested a value for marine biogenic ammonium of

between -5‰ to -8‰.

As mentioned, there are no uncertainties data for isotopic data of samples ($\delta^{15}N_T$) due to lack of replicate measurements. Therefore, an instrumental uncertainty for the reference materials measured is used, which is ± 0.2‰.

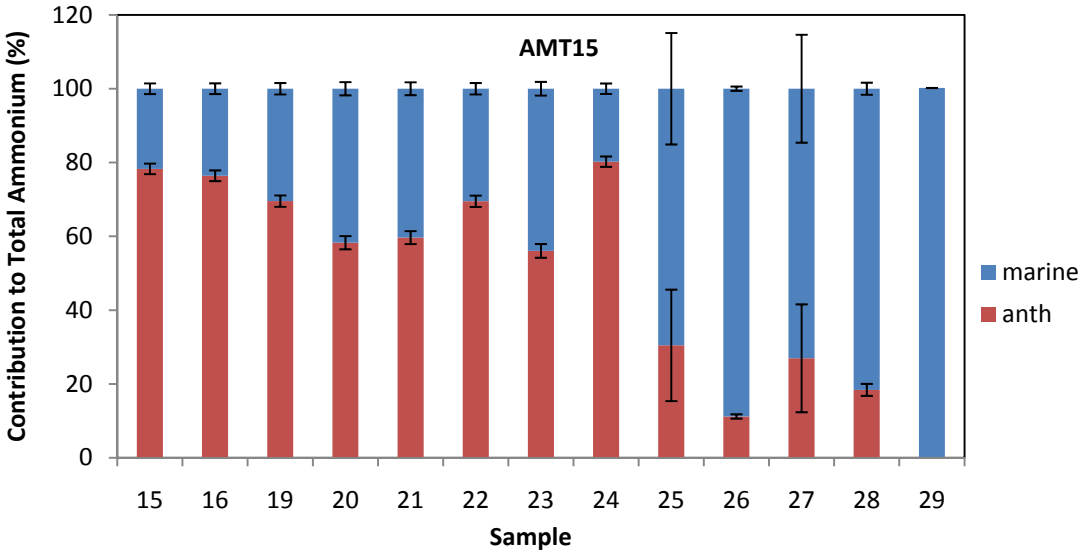

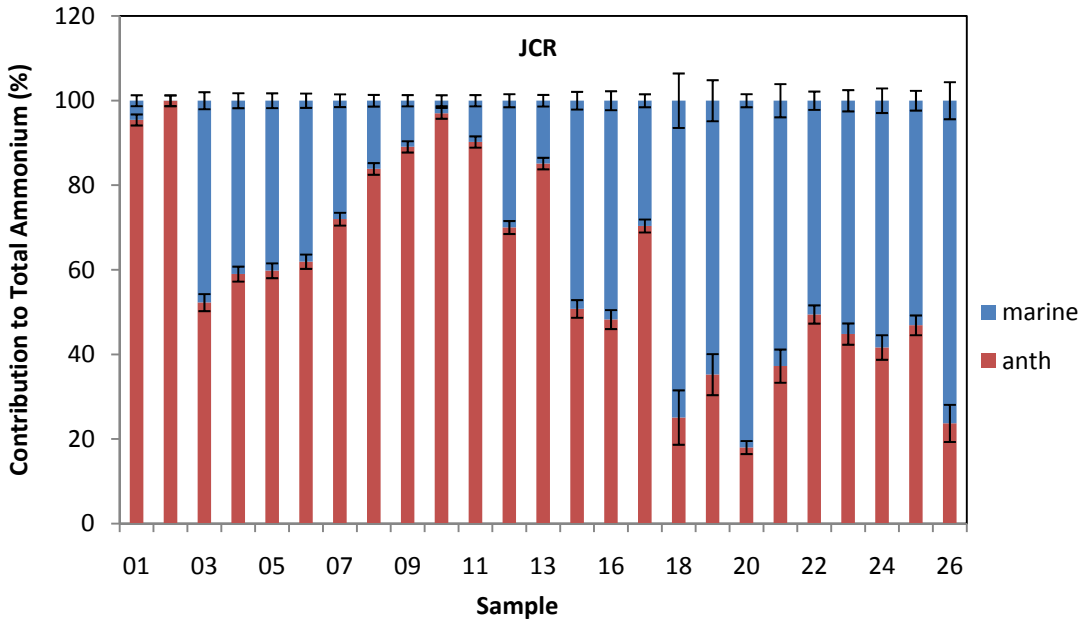

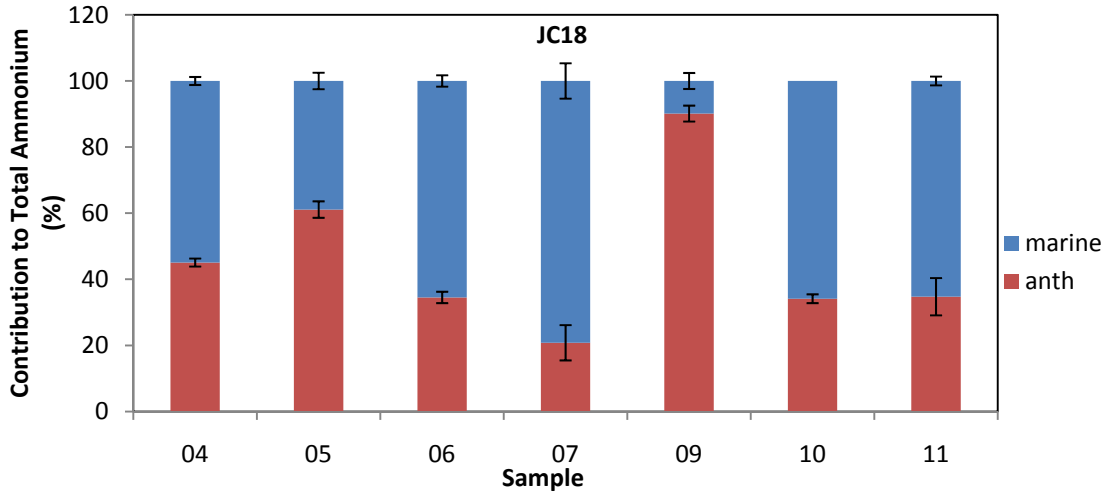

Figure 3.14 Histograms showing the contribution of marine biogenic and terrestrial anthropogenic component to the overall ammonium in the atmosphere for cruises AMT15, JCR and JC18 respectively.

Using the source segregation model described earlier, the relative contribution of marine and anthropogenic ammonium can be estimated. Figure 3.14 provides an alternative representation of the contribution of ammonium by sources similar to sulfate isotopes, representing the relative importance of anthropogenic and marine biogenic components (based on the assumption about end member sources discussed above), regardless of concentration. On AMT15 the data suggests a dominant anthropogenic source for samples 15 to 24, whilst samples 25 to 29 marine biogenic ammonium becomes more significant over the anthropogenic component. On JCR, Sample 01 and 02 have almost 100% anthropogenic ammonium, with sample 03 having approximately 45% marine biogenic component, decreasing down the cruise track to sample 10 and 11, where anthropogenic components become dominant again. Marine biogenic ammonium becomes more significant further down to the remote Southern Atlantic. These trends agree well with the back trajectories, providing confidence in the segregation attempt (Appendix 1, V. JCR).

On JC18, marine biogenic ammonium seems to be significant for sample 06, 07, 10 and 11, with sample 09 having 60 to 80% anthropogenic component. However, a valid explanation cannot be drawn by just referring to the back trajectories. While some of the samples from this region are consistent with the results from the open ocean samples, there are several anomalies and further work would be required to understand the causes of these differences.

3.3 Conclusion

In this chapter, isotopic compositions of sulfate and ammonium are compared to their respective atmospheric concentrations. Attempts have been made to separate sulfate and ammonium into different source components based on the isotopic and ion chromatography data, and has shown to provide a better picture of the aerosols analysed. It should be noted that the segregation of sulfate (similar to figure 3.14) will be shown in chapter 4. In general, both sets of data have shown to have significant anthropogenic component near continents, and the marine biogenic component is more important for samples collected in the remote ocean.

Chapter 4: Fluctuations of atmospheric ion concentration along cruise

4.1 Introduction

In this chapter the concentrations of aerosol ions in the marine atmosphere will be represented for all cruise aerosol samples analysed in this study. The factors driving the variation in aerosol ion concentration will be discussed. It should be noted that all the data presented in this thesis comes from fine mode aerosol samples unless stated otherwise. As a reminder, there are six cruise data sets that will be shown: three will come from The Atlantic Meridional Transect (AMT for short) cruise programme number 15 and 17. Another data set is from the 36 North cruise, followed by cruise JC18.

4.2 Forecasts & Expectations

Cruise samples (AMT cruises in particular) analysed share some characteristics in common, due to their similar air mass sources and origins. Forecasts and expectations of changes can be made to help interpreting the data. The distribution of sources has already been mentioned in chapter 1, and only a brief review will be given here.

Samples that represent air that has recently passed through European regions should have comparatively high concentration of anthropogenic ions, such as ammonium, non-seasalt sulfate and non-seasalt potassium. Among those three ions, non-seasalt (nss for short) sulfate is derived from the combustion of fossil fuels, DMS oxidation and volcanic activities; ammonium is a tracer for agricultural activities, and biomass burning results in an input in

nss potassium (Baker et al. 2006). The African Continent is expected to have a higher dust input, originating from desert regions, resulting in high concentrations of nss calcium aerosols (Baker et al. 2006). Southern Atlantic Ocean samples are expected to have the lowest non-seasalt ion concentrations throughout the cruise, due to the relatively pristine environment of the Southern Ocean. However, impacts from marine biological activities can also be expected, due to the upwelling of nutrient rich water in the Southern Ocean causing increases in the productivity (Baker et al. 2006). These expectations can be evaluated by combining aerosol data and air-parcel-back-trajectories.

In addition, sodium can serve as a tracer for environmental removal processes. The atmospheric concentration of sodium is dependent on the rate of production and removal. Production depends on wind speed, while removal depends on wet/dry deposition and mixing. It is therefore useful to consider changes in sodium to help interpret the data for ions. The general pattern of aerosol distribution will now be presented and interpreted using a combination of air parcel back trajectories, aerosol concentrations, inter element relationships and the patterns of emissions discussed above. The analytes of particular interest in this thesis (aerosol sulfate and MSA, sulfur isotopes and ammonium isotopes) are then considered in this context.

4.3 Cruise AMT 15

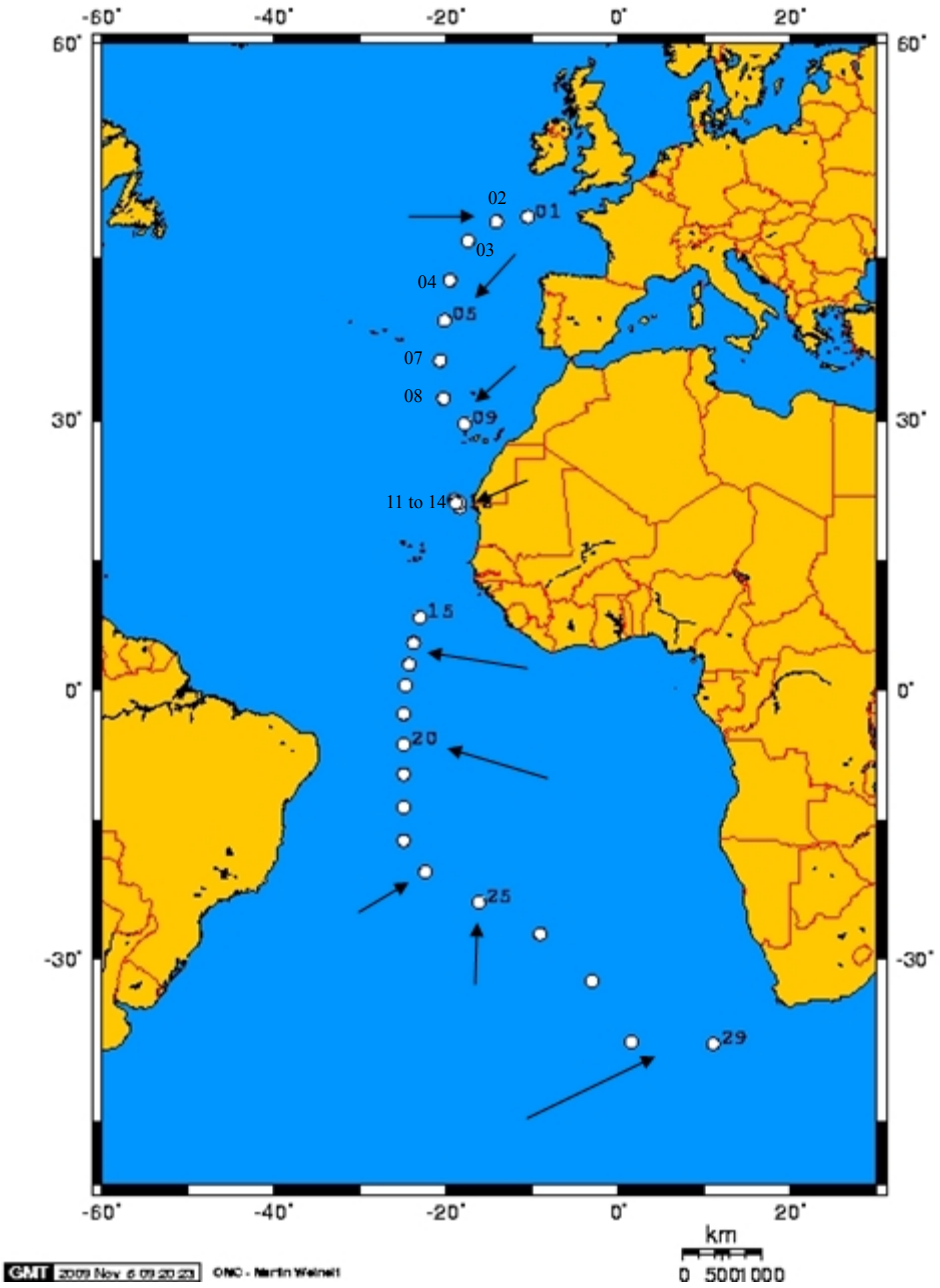

Figure 4.1 Cruise map for AMT15 based on mid-point latitude coordinates. The cruise started from sample 1, collected near the English Channel down to 29 near South Africa. Station numbers of selected stations are displayed at the top-right corner of the relevant sampling station. Sample 06 and 10 are instrumental blank samples and were not shown. Appropriate trajectories are shown by arrows.

Figure 4.1 presents a detailed map of sampling stations based on the coordinates measured at the middle of a sampling period for each samples. The atmospheric concentration represented in the following context will therefore represent the average concentration

during the sampling period. The arrows in figure 4.1 provide a picture of where the air comes from before being sampled, according to air-parcel back trajectories; it should be noted that the size/length of the arrow does not represent wind strength. More information is provided in the appendix. It must be noted that due to limited volume of samples, although all samples were measured for major ions, some of the samples were not analysed for Methane Sulfonic Acid (MSA).

4.3.1 Sodium, non-seasalt Calcium, Potassium and Sulfate

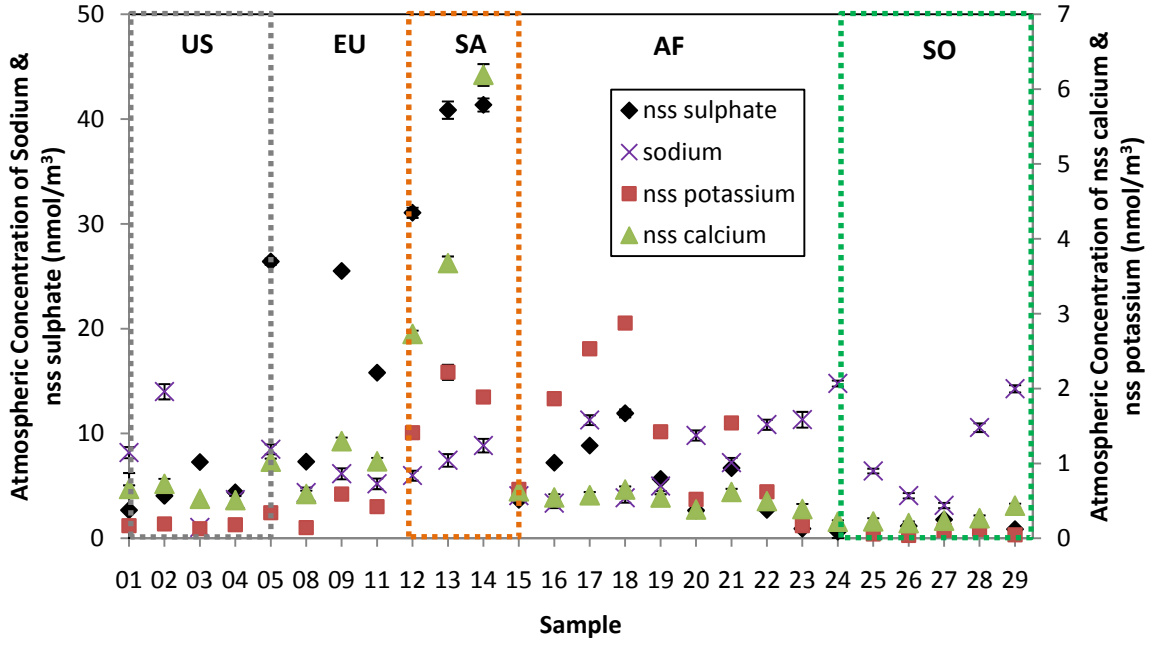

Figure 4.2 Atmospheric concentrations of sodium, nss sulfate, nss potassium and nss calcium for individual samples collected on AMT15. Concentrations of nss calcium & potassium have been plotted on the secondary y-axis to the right. Error bars of standard deviation are shown for each data points. Samples are categorized according to back trajectories (see text).

In figure 4.2 above, comparatively small standard deviations for measured concentrations give confidence that the fluctuations observed are not due to analytical uncertainties. It is worth noting that apart from sodium, the other three sets of error bars are derived from the calculations of non-seasalt concentration by error propagation.

Five-day back trajectories are used to group samples into different categories: zone US represents air that has travelled close to the North American Continent regions within the last five days; zone EU indicates air passing around Europe; zone SA represents air passing close to the Saharan Desert, zone AF represents air passing close to Southern Africa, and zone SO represents samples where the air has been over the Southern Ocean for the previous five days. These classifications depend entirely on the five-day back trajectories of individual samples, hence grouping samples that have passed over similar locations, instead of a geographical classification by sample collection location.

At zone SA, large concentrations of nss sulfate and nss calcium are observed. According to the classifications described above, this increase should be associated with a relatively increased emission (or reduced removal) from a combination of anthropogenic activities as well as the Saharan dust plume input. As Sultan & Janicot (2000) and Baker et al. (2006) suggests, a European contribution to these ions should also be considered in addition to emission from the Saharan region itself. This is because within the Saharan region, anthropogenic activities are small. Therefore high concentrations of anthropogenic-related ions over the Saharan region must consider air masses that flow east from Sahara, having passing close to Europe at some point during the five days period (effectively sample 12 to 14) before being sampled on the Atlantic. Hence these air masses potentially indicate both European and desert emission.

An increased influence of biomass burning can be traced between the samples stations 16 to

19 based on nss K. Samples in zone AF show an increase in nss K along with nss SO_4^{2-} which suggest biomass burning is an important source of nss SO_4 in air from South Africa (Baker et al., 2006), even though other sources can also contribute to nss SO_4^{2-}. More on the relationship between nss K and nss SO_4^{2-} will be discussed later. As the cruise moves down towards the Southern Ocean, decreased concentrations of many ions can be observed from the graph except for sodium. In zone SO, the concentrations of anthropogenic ions are comparatively low, indicating a more pristine environment with minor anthropogenic input.

4.3.2 Sodium, Ammonium, MSA and non-seasalt Sulfate

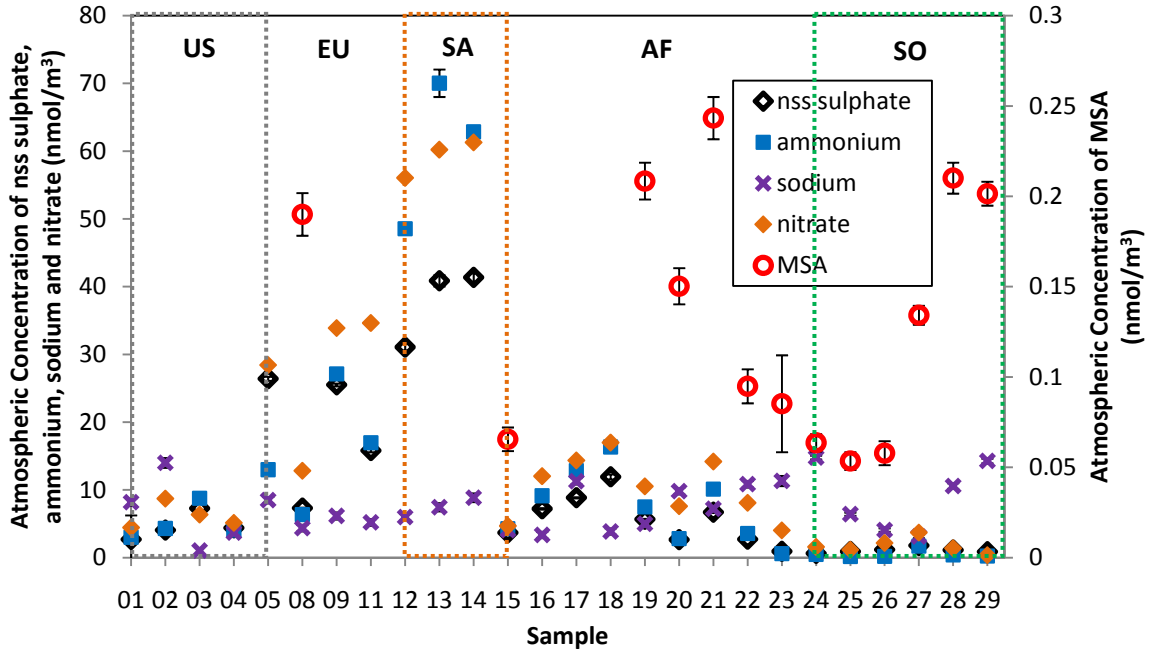

Figure 4.3 Ions (apart from Na) with possible link to processes of biogenic emission. All results are for fine mode aerosol except nitrate being coarse mode aerosol, due to the nature of the species. Concentrations of MSA are plotted on the secondary y-axis to the right. Error bars of standard deviation are attached to each ion data point. Samples are categorized by air mass again in the same way as those in figure 4.2.

Figure 4.3 highlights ions which may be linked to biogenic activities and nitrate with a major anthropogenic source. It should be noted that due to limitation of sample volume,

stations without MSA data indicate samples that were not analysed for the analytes.

Some trends can be observed in the graph above, which can be explained by back trajectories. Concentrations of nss SO_4^{2-}, NH_4^+ and NO_3^- in the US sector are relatively low, although higher than the samples in the SO category. This is probably due to anthropogenic input from the North American continent, as suggested by the trajectories. The long distance across the Atlantic Ocean results in dilution and removal of such signals, hence the low concentration. Samples collected further west have higher concentrations for many of these ions, and will be discussed in detail later for cruise 36N. A similar increase in ion concentrations due to anthropogenic activities can also be observed in zone EU.

In zone SA, the large increase in nss SO_4^{2-}, NH_4^+ and NO_3^- can be explained in the same way as described above, by a combination of dust plume input and a possible anthropogenic influence from European regions. These ions tend to behave similarly throughout the cruise and the relationship between the ions for the whole dataset is considered later (Chapter 6).

The concentration of ammonium, nitrate, non-seasalt sulfate and sodium are relatively low in the AF air mass, while relatively high concentrations of MSA are observed at sample 19 and 21, indicating air masses sampled have travelled over regions of high marine biogenic activities (and associated DMS emissions) within the previous five days (figure 4.3). Low concentrations of MSA from sample 22 to 24 indicate that the marine productivity is low, or rate of removal is high (figure 4.4), and trajectories show that the low concentrations are not due to samples that only travel for a short period around the ocean. For samples

classified as zone SO, low concentrations of both ammonium and nss sulfate are observed as expected if terrestrial sources of these ions dominate. There is a notable increase in the concentration of MSA from sample 26 to 29. Since low temperatures encourage the production of MSA relative to H_2SO_4 during DMS oxidation pathways (von Glasow & Crutzen, 2004), and the South Atlantic has relatively high phytoplankton activities (figure 4.4), low temperature and high productivity should stimulate the production of MSA. The pattern observed in figure 4.3 is logically linked to the patterns of productivity in the Southern Ocean. However, similar increase is not observed for nss SO_4^{2-}, which remain at small concentrations of around 1 nmol/m^3. This illustrates the complexity of interpreting nss SO_4 data which has multiple sources. Hence MSA is a better tracer for biogenic sulfur compared to nss sulfate, and this is explained further in chapter 5.

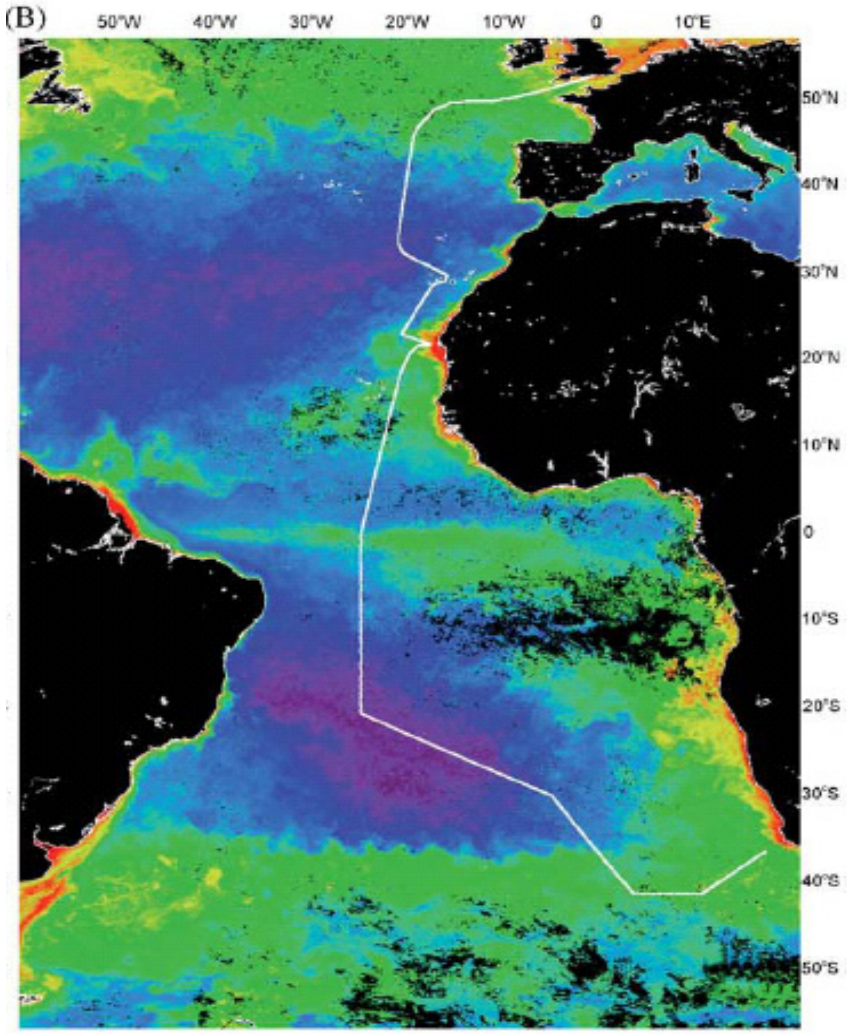

Figure 4.4 Satellite picture of the composite chlorophyll of the Atlantic Ocean (551N–551S by 601W–201E) during October 2004 (AMT15). The productivity is highest at red-coloured regions and lowest at purple-coloured regions.

4.3.3 Sulfate Aerosol and Different Sources

In the methodology chapter, an equation adapted from Wadleigh's paper (2004) provides a means to segregate sulfate aerosol concentration into different sources, using a combination of isotopic and ionic concentration data. The sulfate isotope data is presented in chapter 3. Here the relative distributions of the three sulfur sources to the total sulfur (based on the sulfate isotope result) are presented.

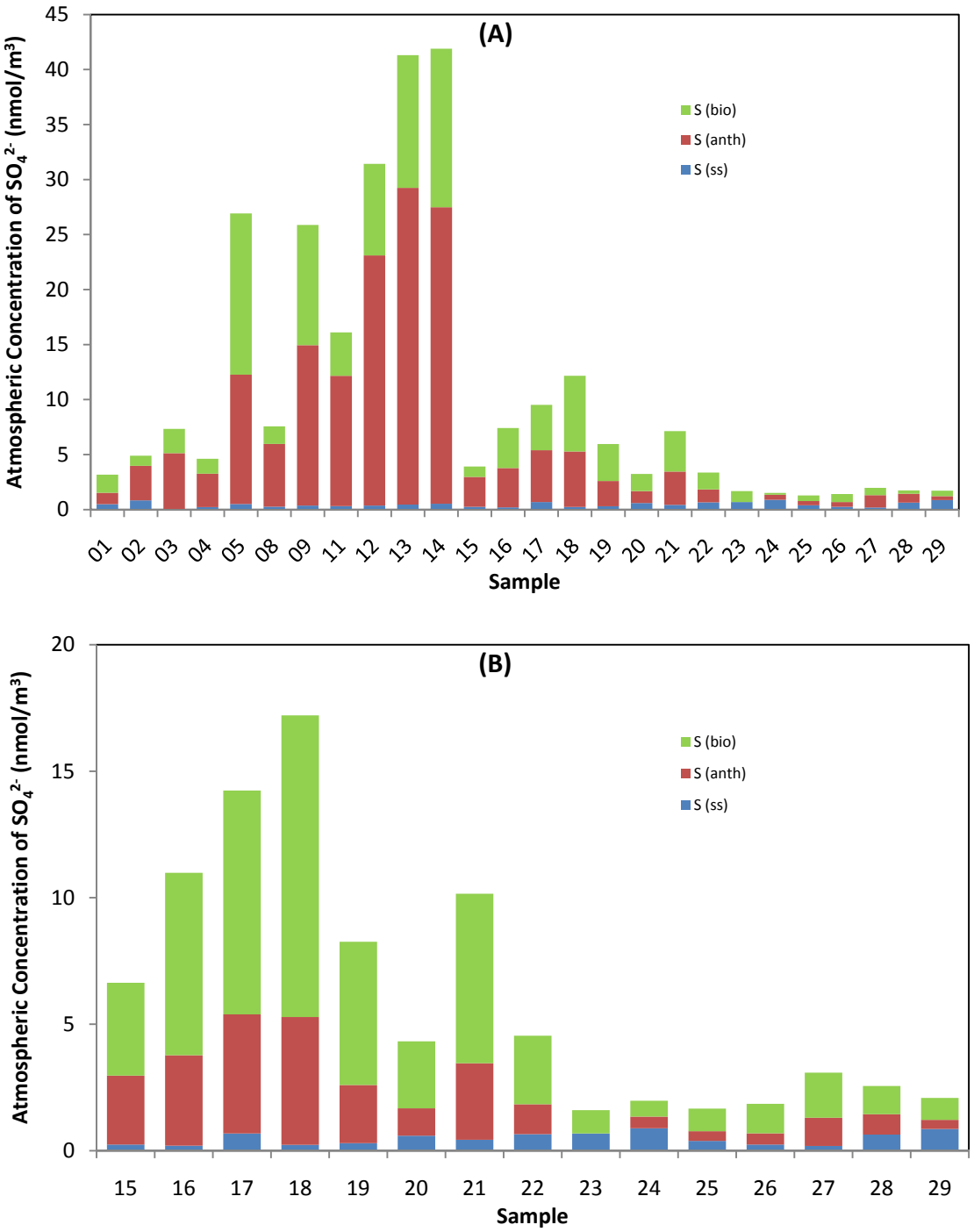

Figure 4.5 Concentration of SO_4^{2-} aerosols from cruise AMT15 displayed in bar charts. For each sample, total fine mode SO_4^{2-} is segregated into seasalt, anthropogenic and biogenic SO_4^{2-} using isotope data. Graph (A) presents all of the samples, and (B) enlarges the scale to show samples with low SO_4^{2-} concentration.

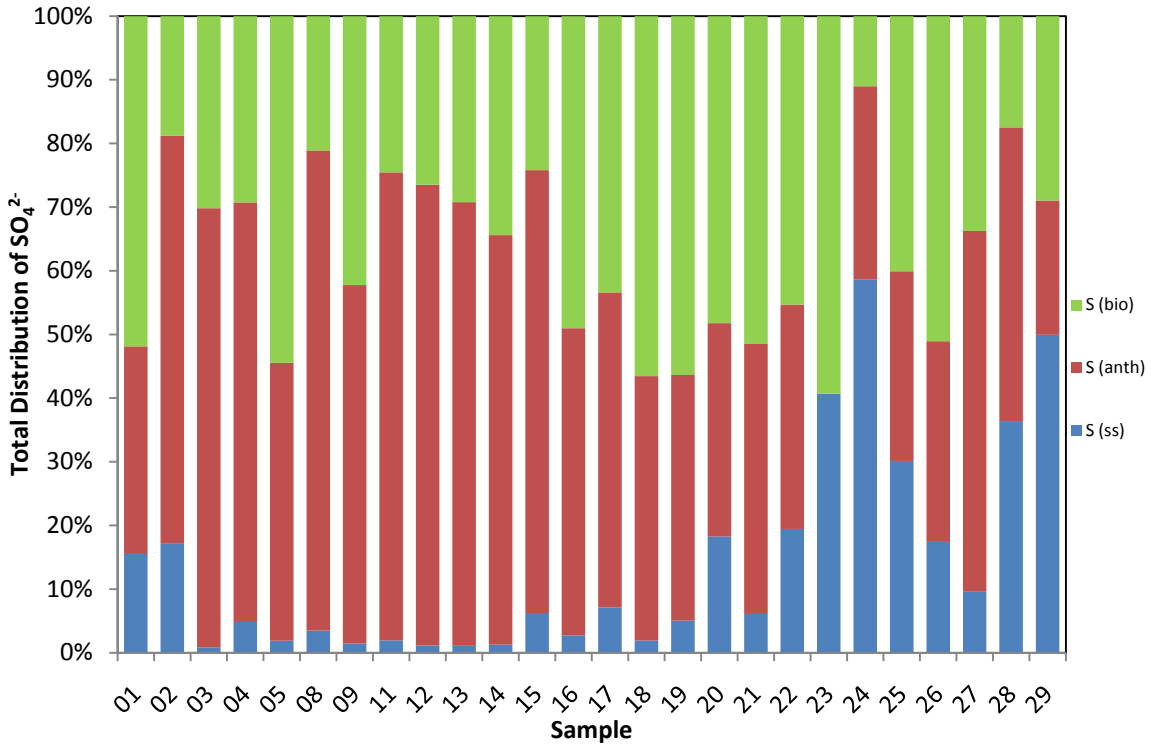

Figure 4.6 Percent contribution of different sources of sulfate towards total sulfate concentration for AMT15 samples, assuming the sum of seasalt, anthropogenic and biogenic sulfate equals total sulfate.

Although several studies have analysed aerosols using isotopic measurement as well as ion chromatography (McArdle et al., 1998; Wadleigh et al., 2001), few have attempted to segregate different components of sulfate from the total concentration, and none of these studies have done such analysis on a scale that cover such a wide range of ocean environments. It is therefore a relatively new approach in understanding the distribution of sulfate from different sources, in particular the contribution of biogenic and anthropogenic sulfate in non-seasalt sulfate.

Anthropogenic influence can be observed at the beginning of the cruise (sample 02 to 04, graph A, figure 4.5) despite the low sulfate concentrations. These samples originate near the North America continent according to five-day back trajectories after long range ocean transport as described in section 4.3.1. The relatively large proportion of anthropogenic

sulfur in Saharan air from samples 12 to 14 is also seen, consistent with impacts of European emissions as discussed in section 4.3.1. In addition, there could be an input from the desert region by air circulation near the equator (Jickells et al., 2003). It is worth noting that the high concentrations of sulfate could represent gypsum dust from the Saharan region which may dominate over the possible European source in the Saharan plume (graph A, figure 4.5). The isotopic composition of gypsum is influenced by the sources of sulfate available during variable formation process (Eckardt, 2001), hence it is difficult to determine an exact isotopic value for gypsum, making interpretations more complicated. Hence isotopes cannot separate these sources, but the similar increases in other anthropogenic tracers in these samples (e.g. ammonium and nitrate) suggest that European rather than gypsum sources are dominant. There is also evidence in figure 4.5 for an important contribution of biogenic sulfate, particularly in the SO region with lower total sulfate concentration (sample 26 to 29 in graph B, figure 4.5).

Figure 4.6 provides a different approach to the issue by considering the relative contribution of the three sulfate sources to total fine mode sulfate. Although the fluctuations in total sulfate concentration can no longer be observed, it presents the biogenic sulfate data in a way that is easier to interpret. As stated above, anthropogenic influences are similar in the European region and the Saharan region, but the important contributions of biogenic sulfate in samples such as 23 and 26 in the remote South Atlantic are highlighted by this plot. From samples 1 to 20, the biogenic input is less than 20% of the total sulfate concentration.

However, it increases to around 30-50% in samples 25-29 (except 24), which were collected around the South Atlantic Ocean, where high chlorophyll suggest substantial DMS emissions coupled with limited anthropogenic sources . The relatively high proportion of biogenic sulfate in sample 01 and 02 (originating from near Greenland according to the trajectories) can also be explained by the distance air travelled across the Atlantic Ocean, picking up biogenic signatures along the way, and the limited opportunity to acquire anthropogenic input, before been sampled near Europe. The anthropogenic component in samples 01 to 04 is consistent with the anthropogenic emissions from the North American continent. These emissions are removed and diluted during transport as noted earlier.

Those graphs derived from the sulfate isotope measurements therefore offer a useful way to trace biogenic and anthropogenic activities by measuring ionic concentration and isotopic composition of aerosols in the atmosphere.

Seasalt sulfate makes a very minor contribution to fine mode sulfate throughout the dataset, although its relative contribution increases in sample 23, 24, 28 and 29, where the overall concentration of SO_4^{2-} is low.

4.4 Cruise AMT 17

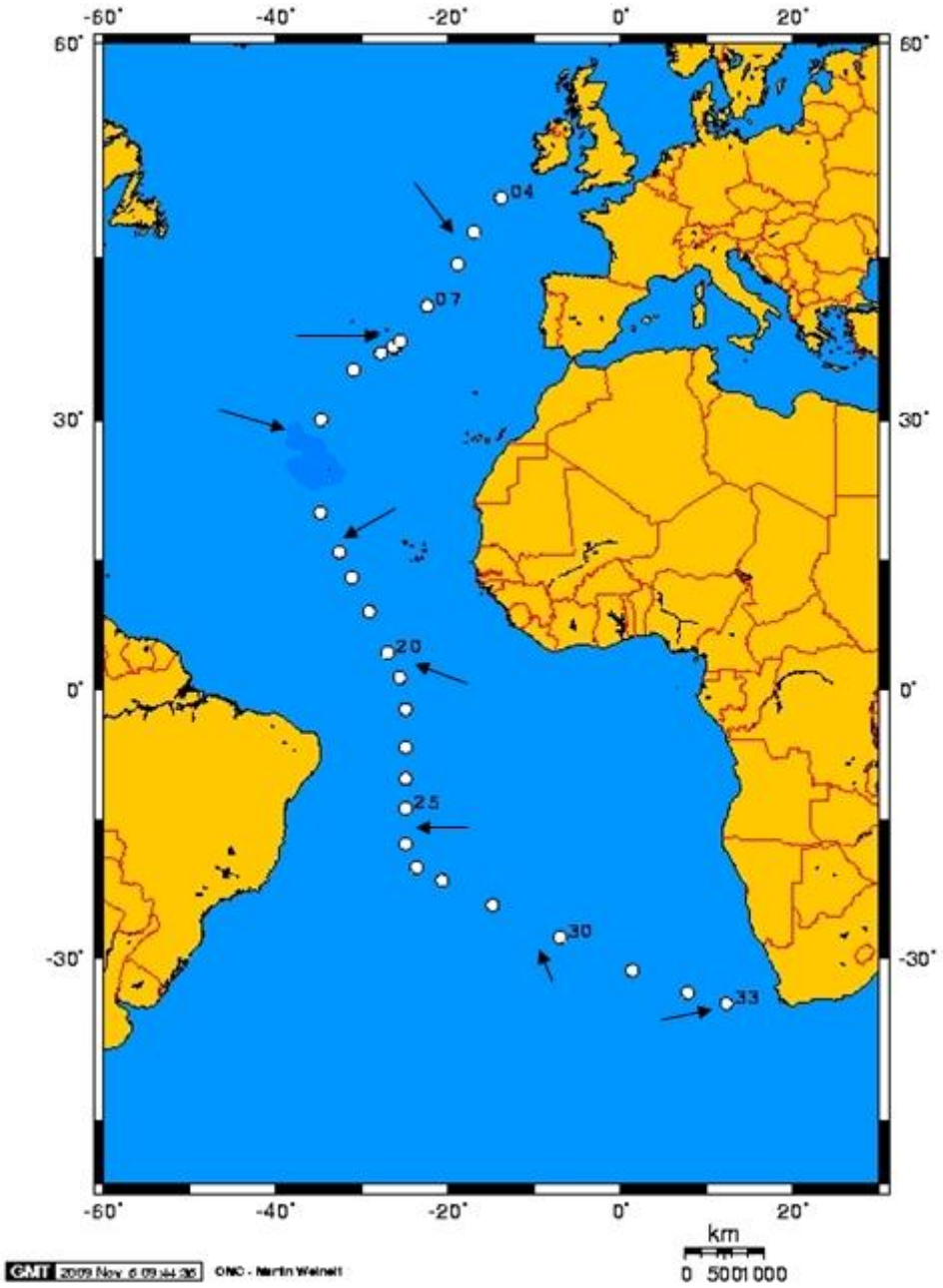

Figure 4.7 Cruise map for AMT17, starting from point 04 which is sampled near English Channel down to 33 near South Africa. Station 14 and 15 are analytical blanks and are not shown. This map is plotted in the same style as figure 4.1.

Figure 4.7 presents the location of the sampling stations based on the coordinates measured at the middle of a sampling period for each sample. Since MSA and sulfur isotope of sulfate are not measured in this dataset due to limitation in volume of samples, one graph plot will be used in an attempt to summarise patterns of some major ions. Note that AMT17 has a

more westerly cruise track than AMT15.

In general, concentrations of components of terrestrial origin are lower on AMT17 (figure 4.7) compared to AMT15 (figure 4.1), probably reflecting dilution / removal processes during longer transport over the oceans.

4.4.1 Major Ions

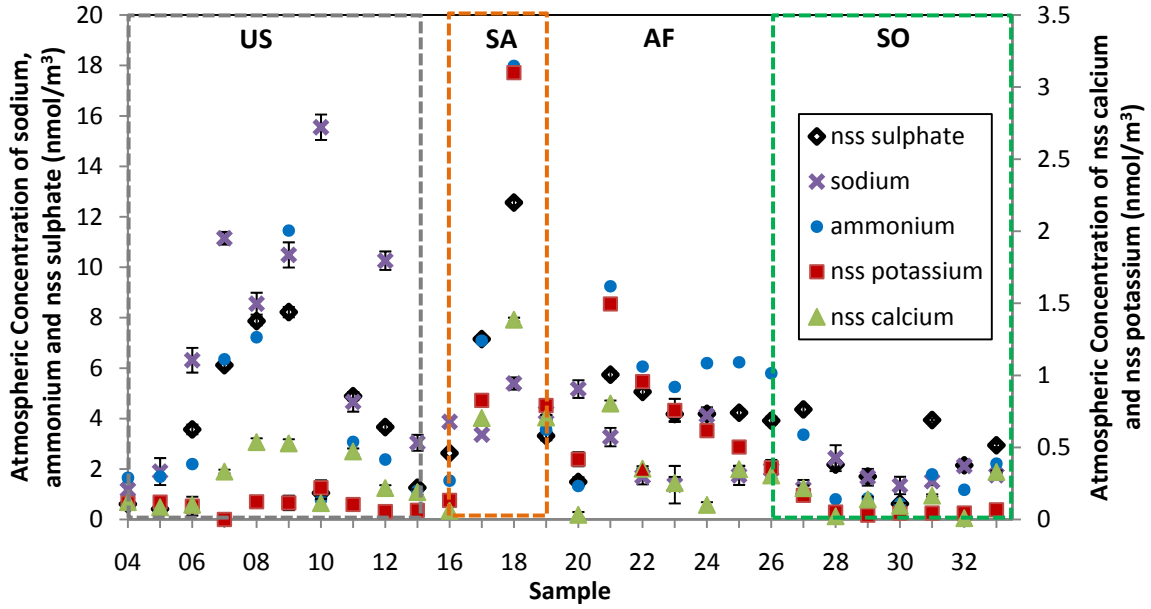

Figure 4.8 Atmospheric concentrations of sodium, ammonium, nss sulfate, nss potassium and nss calcium for individual samples. Concentrations of nss calcium & nss potassium have been plotted on the secondary y-axis to the right. Error bars of standard deviation are attached to each ion data point. Samples are categorized according to back trajectories, in the same way as in the previous AMT15 plots. Note that sample 14 and 15 are blanks and are not plotted.

The classification applied to figure 4.8 is identical to that used in chapter 4.3. According to figure 4.8, Zone US has air masses that travelled close to the North American Continent regions within the previous five days. Sample 4 is the only exception and sampled air masses that passed over Europe according to trajectories.

Some general pattern can still be observed compared to what is presented above for AMT15 dataset. High concentrations of nss sulfate and ammonium in samples 06 to 13 indicate

anthropogenic activities, and back trajectories suggest air that passed over North America. In zone SA, a distinctive increase in ammonium and nss ions from the Saharan desert indicates a similar contribution from the dust plume and European regions, which was already discussed above.

In zone SO, a large number of samples have trajectories that has air passing over the middle of the South Atlantic Ocean in the previous five days. As the cruise travels towards the Southern Ocean (sample 28-33), a comparatively pristine environment is indicated by the decrease in non-seasalt ion concentrations. As the cruise travels nearer to the Southern African continent, in sample 31-33, a small increase in ammonium and nss ions can again be observed, even though the trajectories are still suggesting a remote Southern Ocean origin.

4.5 Cruise 36 North

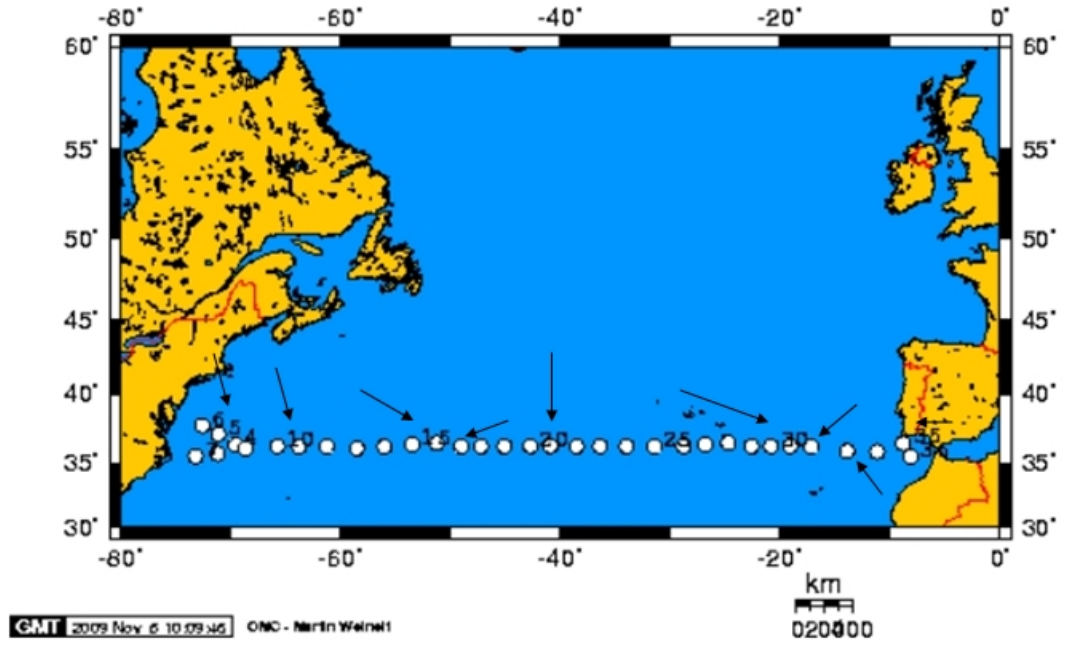

Figure 4.9 Cruise map for 36N, starting from sample 04 which is collected near the US across the Atlantic Ocean to sample 36 collected near Europe. The arrows indicate approximate trajectory directions. This map is plotted in the same style as figure 4.1 and 4.7.

Figure 4.9 can be slightly confusing due to the relatively short distance between sampling stations. The early section of this cruise involved a complex cruise track, and samples were taken further away from the coast of the United States (sample 04), then nearer the coast (sample 05 to 07) and then from sample 07 onwards across the North Atlantic Ocean.

4.5.1 Major non-seasalt ions

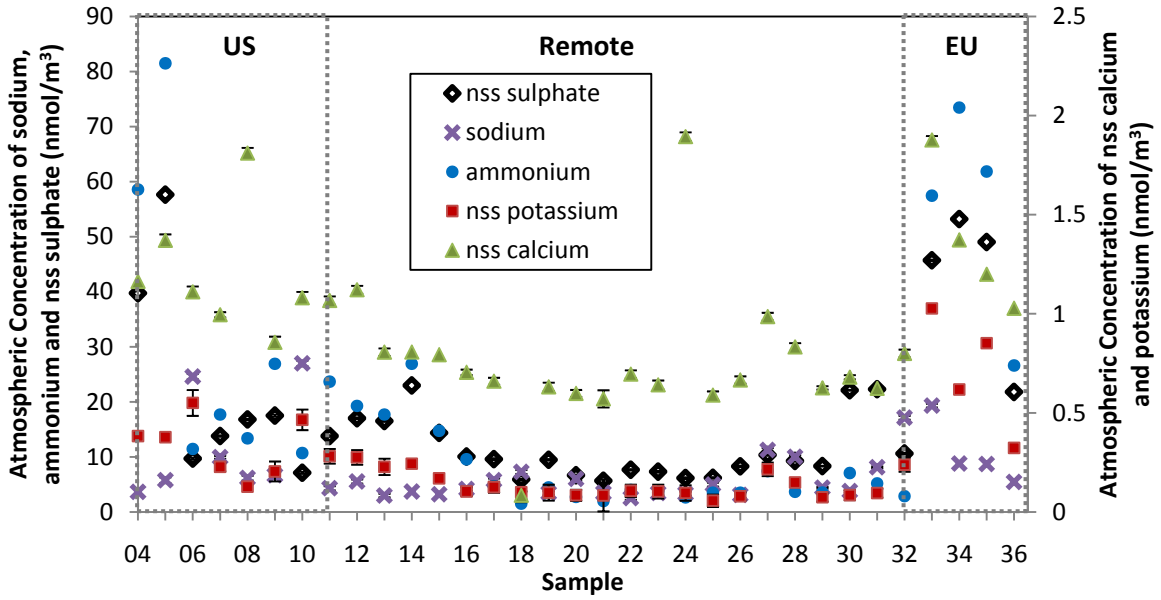

Figure 4.10 Atmospheric concentrations of sodium, ammonium, nss sulfate, nss potassium and nss calcium for individual samples. Concentrations of nss calcium & nss potassium have been plotted on the secondary y-axis to the right. Error bars of standard deviation are attached to each ion data point.

Figure 10 shares some common feature seen in AMT15 and 17. Due to the comparatively complex back trajectories in the dataset, samples classified as US and EU are samples of air which has travelled over or relatively near the two continents in the previous five days, and the remaining samples are classified as remote Atlantic, and did not reach the two continents within the five days before been sampled. In general, contributions from the US and Europe can be clearly seen at the two ends of the graph. Higher concentrations of nss ions are seen nearer the two continents and all show broadly similar patterns. However, the fluctuation of non-seasalt Ca is very difficult to interpret in two cases. The decrease at sample 18 and the peak in sample 24 cannot be explained by trajectories: the first one has air passing from near Europe in the previous five days, and the latter has air which was travelling down from Greenland.

4.5.2 Sulfate Aerosol and Different Sources

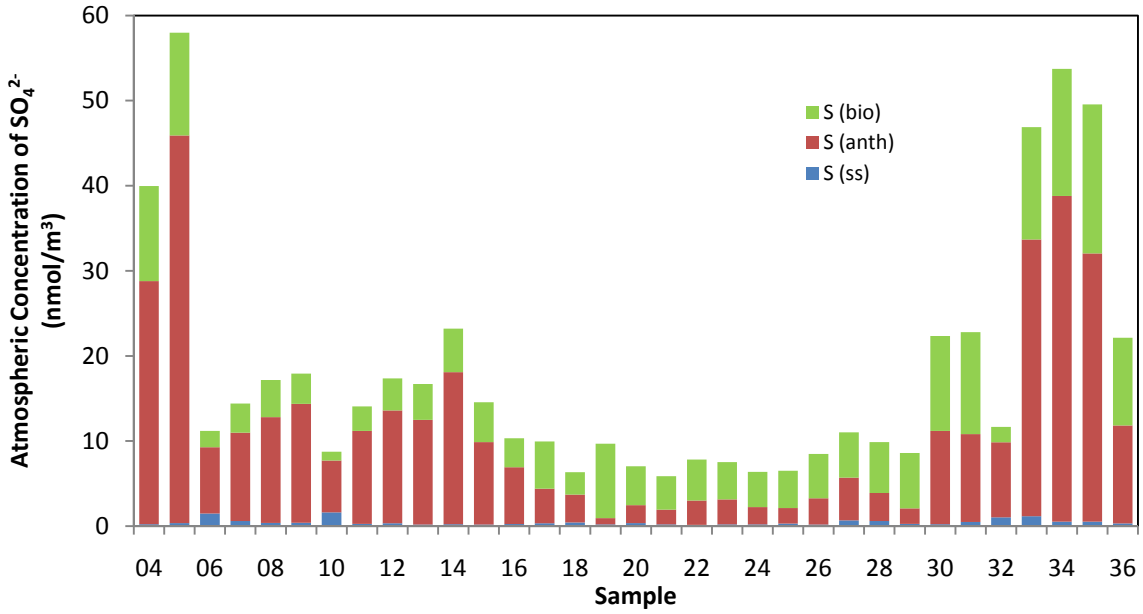

Figure 4.11 Concentrations of SO_4^{2-} displayed in bar charts. For each sample, total SO_4^{2-} is segregated into seasalt, anthropogenic and biogenic SO_4^{2-} using measured isotope data.

As for AMT15, sulfate isotope analyses allow the relative importance of different sulfur sources to be evaluated. Figure 4.11 shows the increase in anthropogenic sulfate nearer the two continents, logically linked with the increase of anthropogenic activities on those continents. The concentration of total sulfate is generally higher compared to the AMT cruises. Sea salt sulfate represents a very small component of the total sulfate compared to the other two sources throughout the cruise. The northern North Atlantic is nutrient rich and productive (figure 4.4), and this is presumably responsible for the comparatively high proportion of biogenic sulfate (figure 4.12). This trend is shown distinctively in sample 20 to 26, where trajectories indicate air masses passed over the productive regions during the five day period. During the middle of the cruise, although the overall concentration of sulfate decreases, the anthropogenic influences have decreased and the biogenic components become more significant, as shown below in fig 4.12.

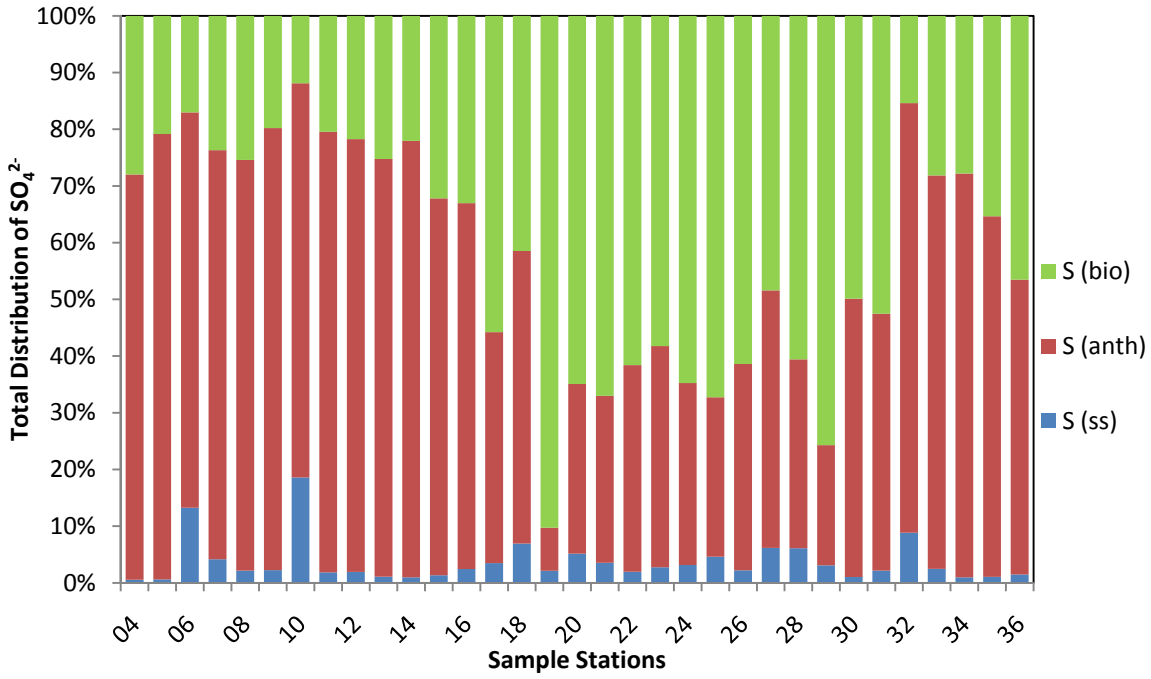

Figure 4.12 Contribution of different sources of sulfate towards total sulfate concentration, assuming the sum of seasalt, anthropogenic and biogenic sulfate equals total sulfate.

Figure 4.12 shows the percent contribution of the three sulfate component and illustrates the contribution of three sulfur sources more clearly than that in figure 4.11. It is clear that anthropogenic contribution is predominant near the US and Europe, contributing to around 70% and 50% of overall sulfate respectively (sample 04 to 14 and 32 to 36). The contribution from biogenic sulfate is higher around sample 17 to 30 (around 50% of total sulfate), where air that was sampled travel from the far north. Although not as pristine as the Southern Ocean, regions near the Arctic Ocean should still be expected to have relatively high biogenic activities and low anthropogenic emissions, consistent with figure 4.12.

4.6 Cruise JC18

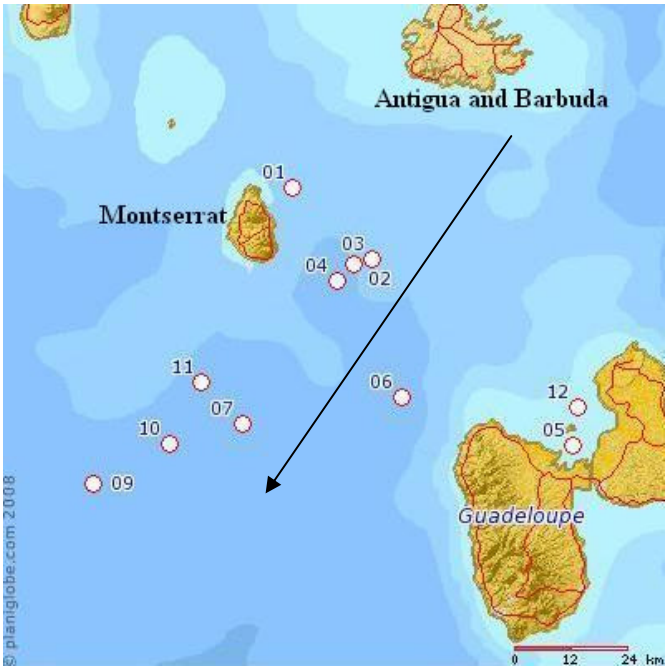

Figure 4.13 Cruise map for JC18 based on mid-point latitude coordinates. The sampling started at sample 01 near Montserrat, travelling down to Guadeloupe at sample 05. The cruise travelled west to sample 09 and back to Guadeloupe, finishing with collecting the last aerosol sample 12. The arrow indicates the five-day trajectory for all samples (except sample 09, see figure 4.14).

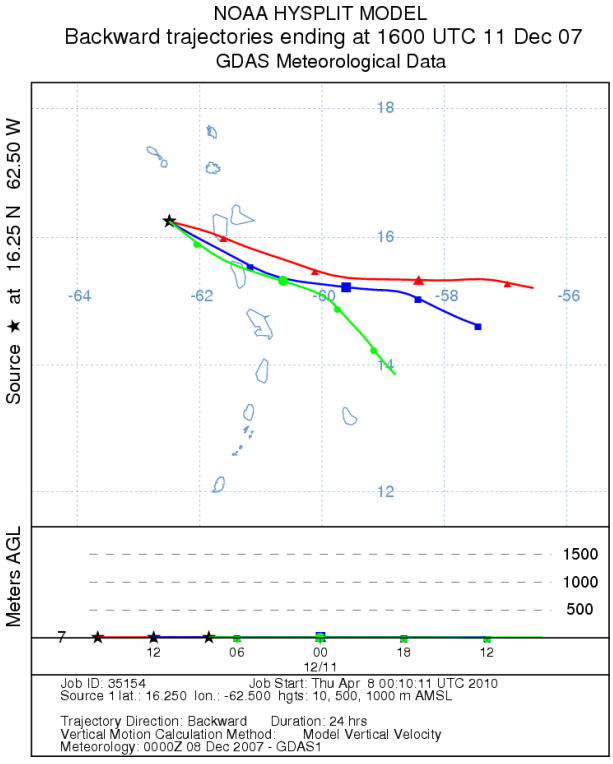

Figure 4.14 Five-day air parcel back trajectory for sample 09 from JC18 cruise.

This cruise provided an opportunity of samples from tropical areas and the potential to sample material associated with a volcanic plume of Montserrat. Volcanic plumes have been suggested to be a source of ammonium sulfate (Uematsu et al., 2004). Samples from this cruise were only analysed for major ions and ammonium isotopes.

4.6.1 Non-seasalt calcium, sulfate, potassium and ammonium

It should be noted that sample 01, 02, 08 and 12 are not available for ion concentration calculations, because mistakes have been made during the collection of aerosol samples, and the flow rate (for calculating atmospheric concentration) was not recorded.

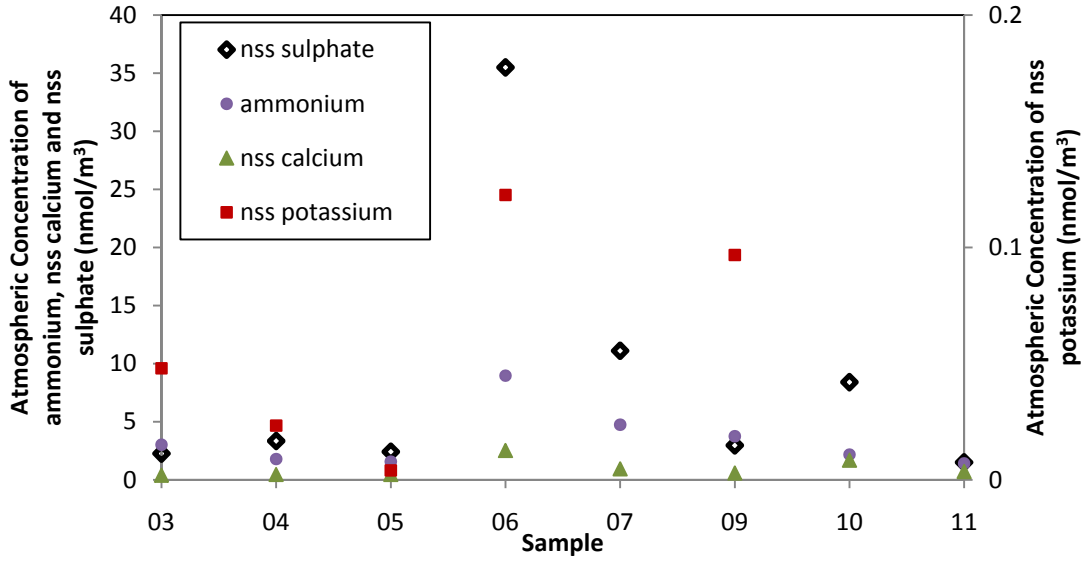

Figure 4.15 Atmospheric fine mode aerosol concentrations of ammonium non-seasalt calcium, sulfate and potassium for individual samples. The concentration of nss potassium is plotted on the secondary y-axis to the right.

Figure 4.15 shows atmospheric fine mode aerosol concentration for ammonium, non-seasalt calcium, potassium and sulfate. For sample 10, a negative nss potassium value was calculated due to the seasalt correction. Seasalt correction uses the ratio of desired ion over sodium in seawater, and in the case of potassium, the seasalt potassium calculated is

larger than the overall potassium concentration, therefore ending up with a negative nss potassium value. Similar values are obtained for sample 07 and 11, and cannot be explained using the data available. The three samples are therefore removed from the figure.

The five-day back trajectory can be used to explain some of the trends in ammonium, nss calcium, potassium and sulfate. It should be noted that for all eight samples, the trajectories all seem to have air travelling from the same direction (figure 4.13) except sample 09 (figure 4.14). By referring to the trajectories, most samples appear to be having little local influence, although the trajectories can of course be inaccurate. The chemical results for all the samples look rather similar apart from the higher values in sample 6. The higher value for sample 6 suggests some additional inputs from local sources, although the trajectories provide no evidence to support this suggestion. There is no evidence from the trajectories or the major ion analyses to suggest the samples were impacted by volcanic emissions from Montserrat.

Chapter 5: Synthesis - A Combination of Different Dataset

5.1 Introduction

In this section, different datasets will be brought together in an attempt to further utilize the variety of analysis done for aerosol samples e.g. non-seasalt sulfate against non-seasalt potassium. This should help to improve the understandings of the atmospheric transport/deposition of aerosols, in particular sulfur and nitrogen species. Sulfate and ammonium isotope data, which are presented in chapter 3, will also be used in order to further interpret the dataset. A number of graphs will be presented below, either to make comparison with available studies, or make some of the unique comparisons available in this study. It should be noted that within the text, ions will be referred directly (e.g. nitrate), and radicals will be stated where appropriate.

5.2 Ammonium and Nitrate in the Atmosphere

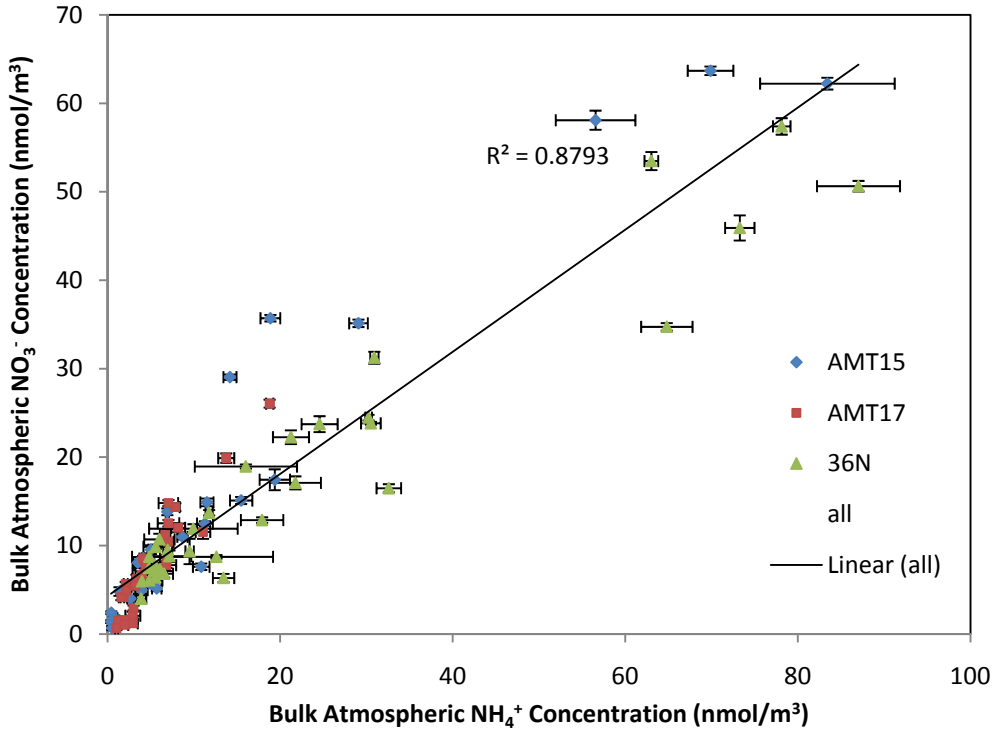

Figure 5.1 A plot of the atmospheric concentration of nitrate against ammonium in bulk (fine plus coarse mode) aerosol. Error bars of standard deviation attached to each data point.

In figure 5.1, a direct proportional relationship ($r_s = 0.83$, larger than the critical value at which P = 0.01 i.e. significant correlation) between bulk (fine + coarse mode aerosol) nitrate and ammonium is observed, showing that the ratio of oxidized to reduced species of inorganic N stays relatively constant regardless of their concentration [Baker et al. (2006), Johnson & Bell (2008), Prodi et al. (2009), Quinn et al. (1990)]. Different cruise tracks do not affect the relationship significantly, as shown above in figure 5.1, where AMT cruises share similar trend to 36N cruise that has a completely different sampling tracks. It can be observed that the relationship may be stronger at low concentrations of ammonium and nitrate, and become more scattered at higher concentrations. It should be noted that given that the percentage error is similar for all samples, samples with higher concentrations will

have a larger error bars with respect to those that have low concentrations, a pattern commonly observed in statistical analyses. According to five-day back trajectories, the five data points from cruise 36N with the highest concentrations of ammonium/nitrate have dominant anthropogenic sources from the United States and Europe regions, where there is intensive combustions of fossil fuel. Although the relationship stays relatively constant, there is no straight forward explanation of the cause of such trend. The most commonly studied and observed N species in the atmosphere are ammonium and nitrate, and from fig 5.1 it can be said that the ratio between ammonium to nitrate is relatively constant with varying concentrations (Baker et al., 2006). Nitrate is predominantly found in coarse mode aerosols, due to reaction between nitric acid and seasalt aerosol (Andreae and Crutzen, 1997). Ammonium comes from a range of sources which are already mentioned in chapter 1.4, and is mainly found in the fine mode aerosol. Between the two ions, nitrate is expected to be deposited more rapidly compared to ammonium, because nitrate is predominantly found in coarse mode aerosols and is removed at a faster rate than fine mode aerosols. Baker et al. (2010) prove that nitrate is the dominant nitrogen source to the surface ocean compared to ammonium. Since ammonium and nitrate have individual production/removal processes in the atmosphere, they may be expected to not be well related, which is different from what is observed. This may be explained by the presence of a dominant removal process over the differential removal between the two ions, resulting in this relationship. It could simply be physical processes such as dilution by wind/rainfall away

from broadly similar source regions at a global scale e.g. North America and Europe.

5.3 Correlation between MSA and Nitrate

In a model brought forward by Von Glasow & Crutzen (2004), hydroxide and nitrate radicals are the two dominant radicals in the first oxidation step of DMS, which produce MSA and other sulfur compounds as end products (see chapter 1.5). It is therefore worth considering MSA and nitrate ions together, in an attempt to understand the hypothesised process. The possibility of a relationship between these components does not appear to have been considered before. Unfortunately, only some samples from cruise AMT15 are analysed for both MSA and nitrate. Since nitrate is predominantly associated with the coarse mode via reaction of HNO_3 and NaCl, it is appropriate to consider total (coarse + fine mode) nitrate, since nitrate radical is found predominantly in the coarse mode aerosols.

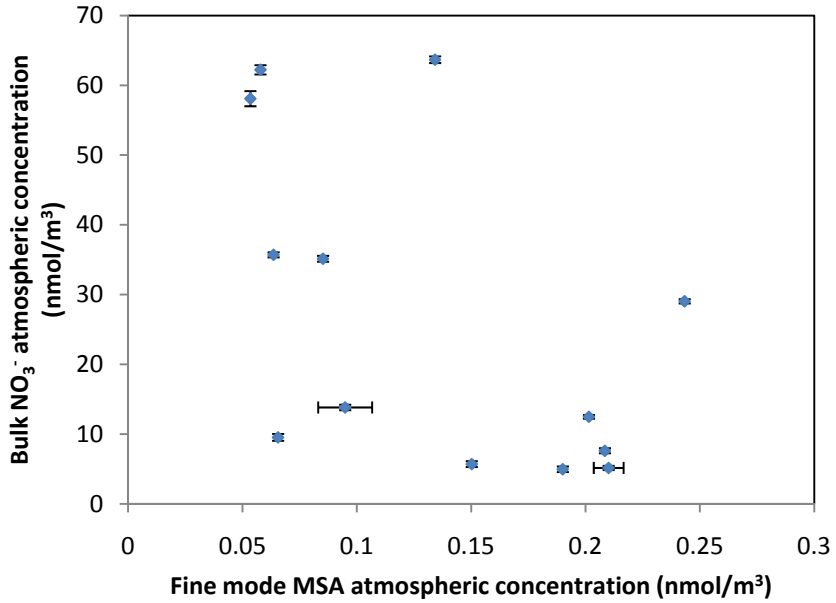

Figure 5.2 A plot of bulk atmospheric concentration of nitrate against fine mode MSA for AMT15 cruises. Error bars of standard deviation attached to each data point.

There is very little relationship between bulk nitrate and fine mode MSA in figure 5.2. Since the majority of nitrates are found in coarse mode aerosols, MSA cannot be plotted against fine mode nitrate, as most of the samples were below the calculated detection limit. Even though nitrate serves as an oxidation radical for DMS at night time (Prodi et al. 2009), little relationship is found between the radical and the end product. This suggests that nitrate will be a relatively poor indicator for DMS oxidation. This probably suggests that nitrate radical supply during the oxidation process is dominated by more complicated atmospheric cycling processes and not simply related to nitrate ion concentration. In addition, the atmospheric concentration of nitrate is also significantly higher than that of MSA. This suggests that the amount of nitrate available is in considerable excess of DMS concentrations, and can supply sufficient nitrate radicals for MSA and SO_2 production along the DMS oxidation pathway, while nitrate ion concentrations fluctuate due to other processes.

5.4 Ammonium and Sulfate Species

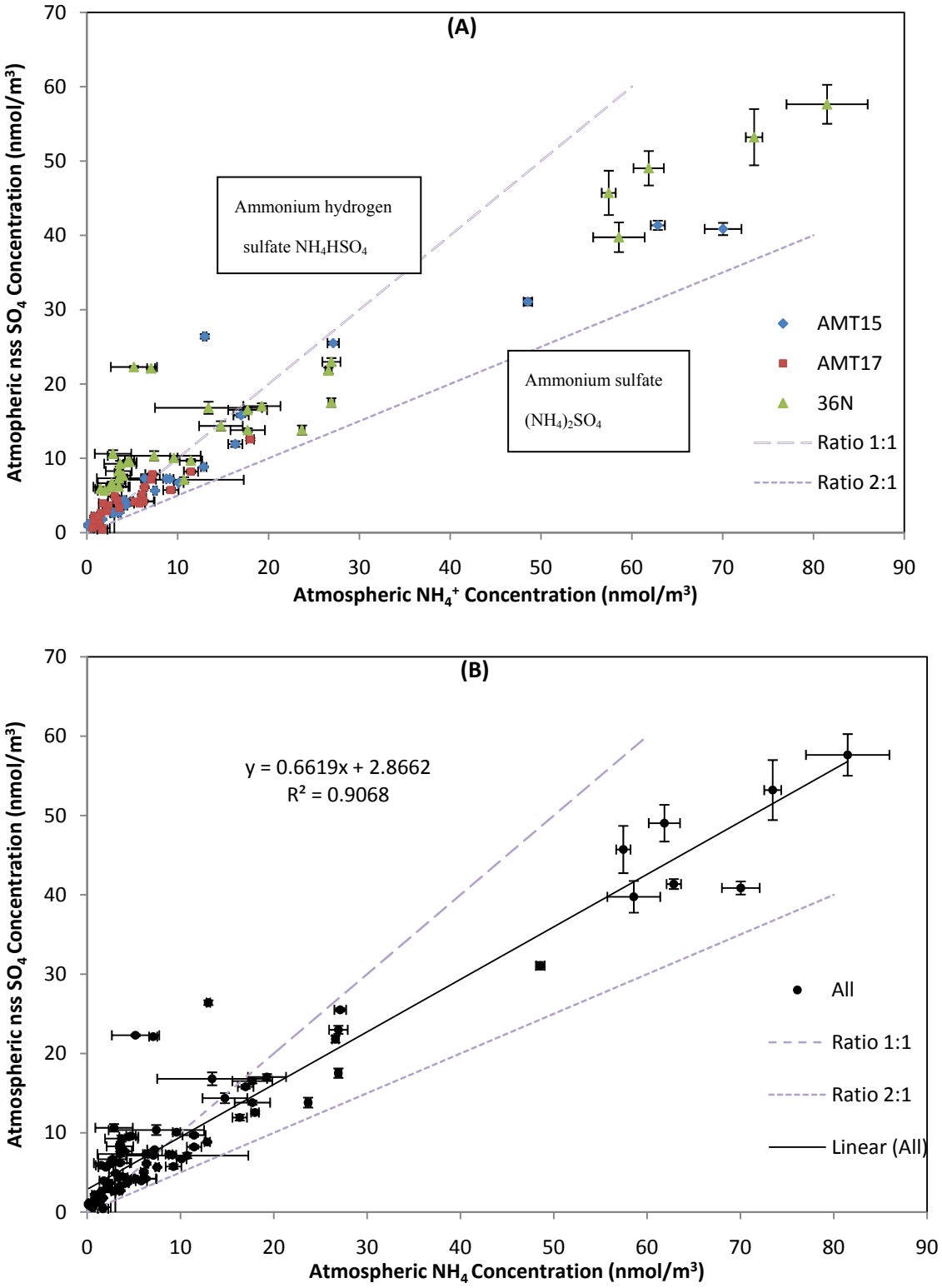

Figure 5.3 Relationship between atmospheric nss sulfate vs. fine mode ammonium. Error bars of standard deviation attached to each data point. Graph (A) separates data into three cruises and (B) groups all samples into one series for regression analysis. The dotted lines are described in the text.

As described in the introduction chapter, ammonium emissions are primarily associated

with fossil fuel combustion, with minor inputs from agricultural activities, biomass burning and a weak marine source (Baker et al., 2006, Quinn et al., 1990). Apart from the weak marine source, all other processes seem to be geographically linked to sulfate emission from anthropogenic activities. Figure 5.3 gives evidence to support this theory, indicating a direct proportional relationship ($r_s = 0.96$, larger than the $p = 0.01$ critical value i.e. significant correlation) between non-seasalt sulfate and ammonium in the atmosphere. At higher concentrations of ammonium and sulfate (top right of figure 5.3), cruise 36N samples were collected near the coast of Europe and the US. Similarly, for high concentration data point for AMT15 cruise, samples are taken from near the Saharan regions and near Senegal and Guinea. This correlation (graph B, figure 5.3) observed may be suggested partly as coming from similar anthropogenic sources, as discussed for nitrate (section 5.2), although they could be locally geographically separated and sulfate is formed after an oxidation step from SO_2 to sulfate. More importantly, ammonium and sulfate in the atmosphere tend to travel together with an ionic bond, produced from an acid-base chemical reaction between sulfuric acid and ammonium.

With the aid of sulfate isotope (only available for AMT15 and 36N), an additional approach can be taken. As described in chapter 4.1.3, with the aid of some calculation steps, it is possible to segregate non-seasalt sulfate into its components of anthropogenic and biogenic sulfate. An attempt is taken below to try and interpret the data in more detail. The comparatively weak marine biogenic source of ammonia is neglected in this attempt.

Both of graphs (A) and (B) from figure 5.3 have dotted lines drawn along with measured data points. These lines indicate the ratio between ammonium and nss sulfate; the 1:1 ratio represents NH_4HSO_4 particle composition and 2:1 ratio represents $(NH_4)_2SO_4$ particle composition, both particles are less volatile compared to ammonia/sulfuric acid in the atmosphere, and is produced from ammonia and sulfuric acid in a irreversible pathway (Johnson & Bell, 2008). The slope of the graph suggests global NH_3 and SO_2^- emission rates sufficient to partially neutralise the sulfuric acid formed (Quinn et al., 1990). Thus emissions of ammonia and SO_2 (H_2SO_4) in industrial regions are expected to become associated in the aerosol. It has recently been suggested that there could be a relationship between ammonia and DMS in marine atmosphere (Johnson & Bell, 2008).

Since ammonia gas in air has a short lifetime (Quinn et al., 1990), at remote regions ammonium and sulfate will be expected to have a biogeochemical relationship between the production of DMS and ammonium, even though no such trend is found in seawater (Johnson & Bell, 2008). The production of ammonium sulfate and ammonium hydrogen sulfate particles will remove acidic sulfate ions from the atmosphere. To put it in another way, the existence of any acidic sulfate particles will deposit any ammonia present. Since the process $NH_4^+{}_{(seawater)}$ <--> $NH_{3(seawater)}$ <-->$NH_{3\ (gas)}$ <--> $NH_4^+{}_{(particulate)}$ is in equilibrium, the removal of ammonium particulate will stimulate further release of ammonia gas from seawater into the air, therefore acting as a buffer to atmospheric acidity. On the other hand, removal of sulfate will not stimulate further release of nss sulfate, since

the oxidation of DMS is not reversible (Johnson & Bell, 2008). The observed linear relationship in figure 5.3 is consistent with the theory mentioned.

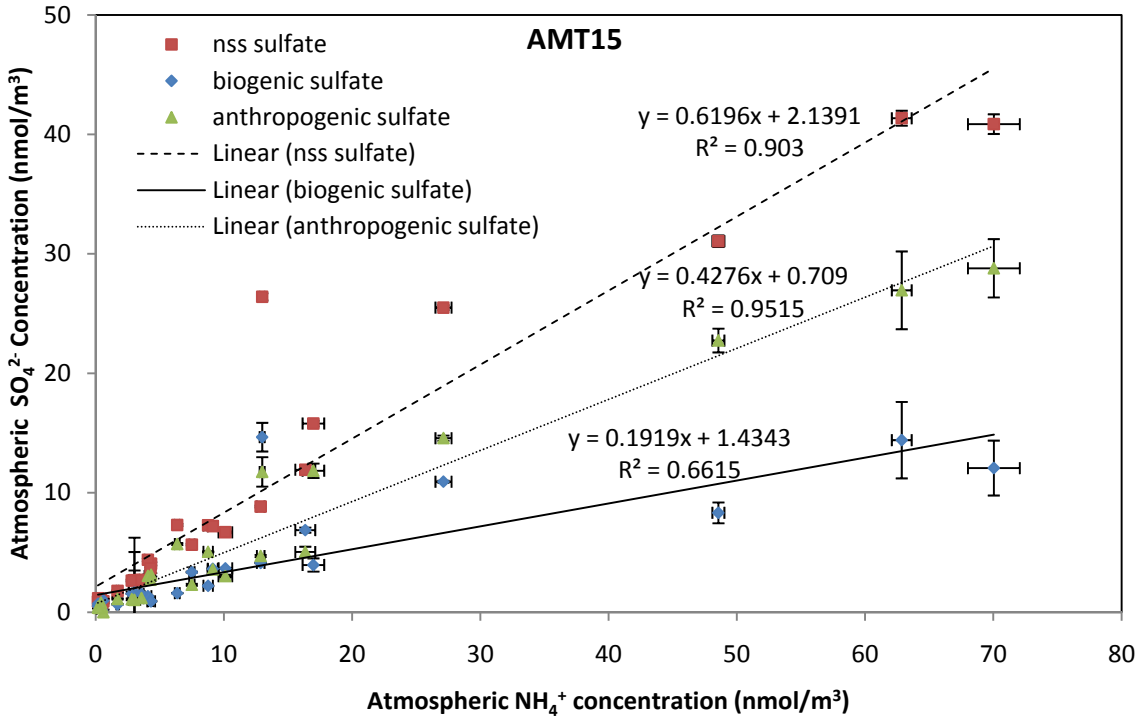

Figure 5.4 Relationship between nss sulfate and ammonium for AMT15 fine mode aerosols. The nss sulfates are segregated into two sulfate components: biogenic and anthropogenic. Error bars of standard deviation attached where available.

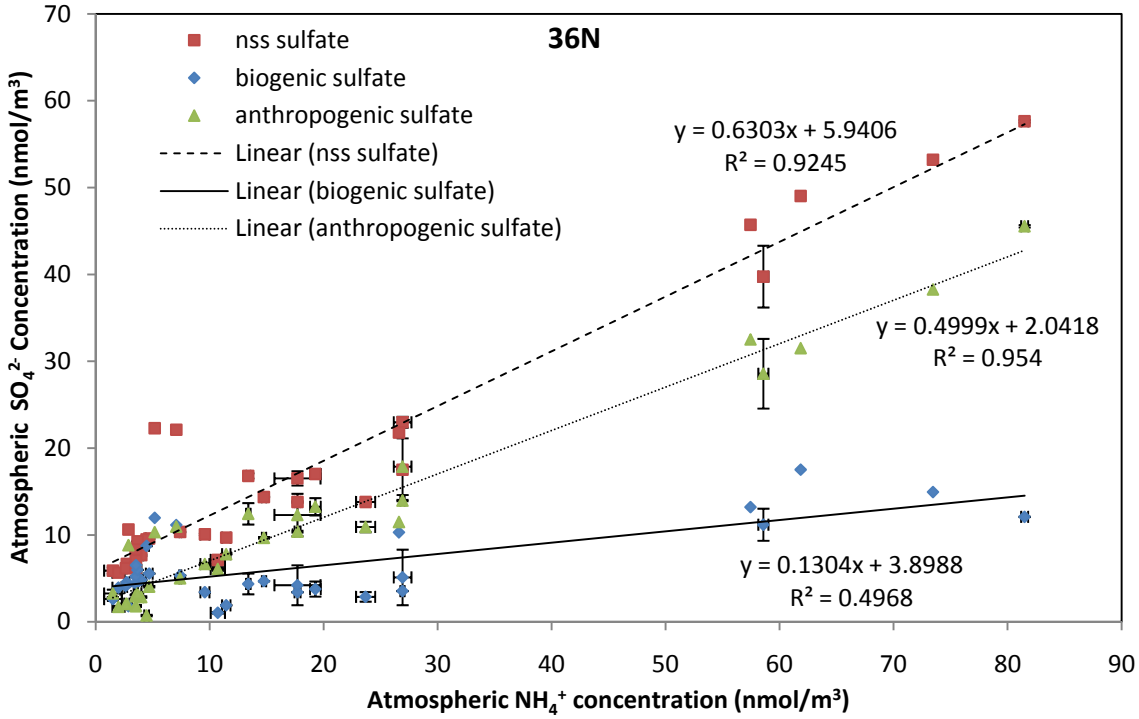

Figure 5.5 Relationship between nss sulfate and ammonium for 36N fine mode aerosols. The nss sulfates are segregated into two sulfate components: biogenic and anthropogenic. Error bars of standard deviation attached where available.

As mentioned at the beginning of this section, the relationship between ammonium and sulfate is likely to be due to similar sources and the acid-base reaction that results in the ionic bonding of two molecules. Cruise 36N and AMT15 have very different cruise tracks, and are expected to have different source contributions between the two sets of samples. However, the two sets of data have very similar correlation and gradient, which may support the chemical reaction mechanism as the dominant control. It should be noted that this suggestion will not explain the relationship between ammonium and nitrate (chapter 5.2). Segregating non-seasalt sulfate into anthropogenic and biogenic sulfate may provide more details on these relationships. Figure 5.5 shares similar characteristic as figure 5.4 above. The direct proportional relationship between total fine mode ammonium and sulfate

is also seen between total fine mode ammonium and anthropogenic sulfate (r = 0.98 for figure 5.4, r = 0.98 for figure 5.5). There is a relatively weak relationship between biogenic sulfate and total fine mode ammonium (r = 0.81 for figure 5.4, r = 0.7 for figure 5.5). This weaker relationship may reflect increased uncertainties in estimating biogenic sulfate compared to total sulfate and therefore does not necessarily contradict the suggestion of Johnson & Bell (2008). This representation of data also illustrates that ammonium aerosol concentrations (and presumably ammonia emissions) are greater than biogenic DMS emission.

5.5 Anthropogenic Tracers: Potassium and Sulfate

Both non-seasalt potassium and sulfate are effective tracers of anthropogenic activities. Non-seasalt potassium is predominantly linked to biomass burning (Andreae, 1983), and will be considered as anthropogenic in this context. Non sea-salt sulfate is known to be a product of anthropogenic activities such as the combustion of fossil fuels as well as biomass burning. A plot of these ions therefore offers an opportunity to consider the potential importance of biomass burning.

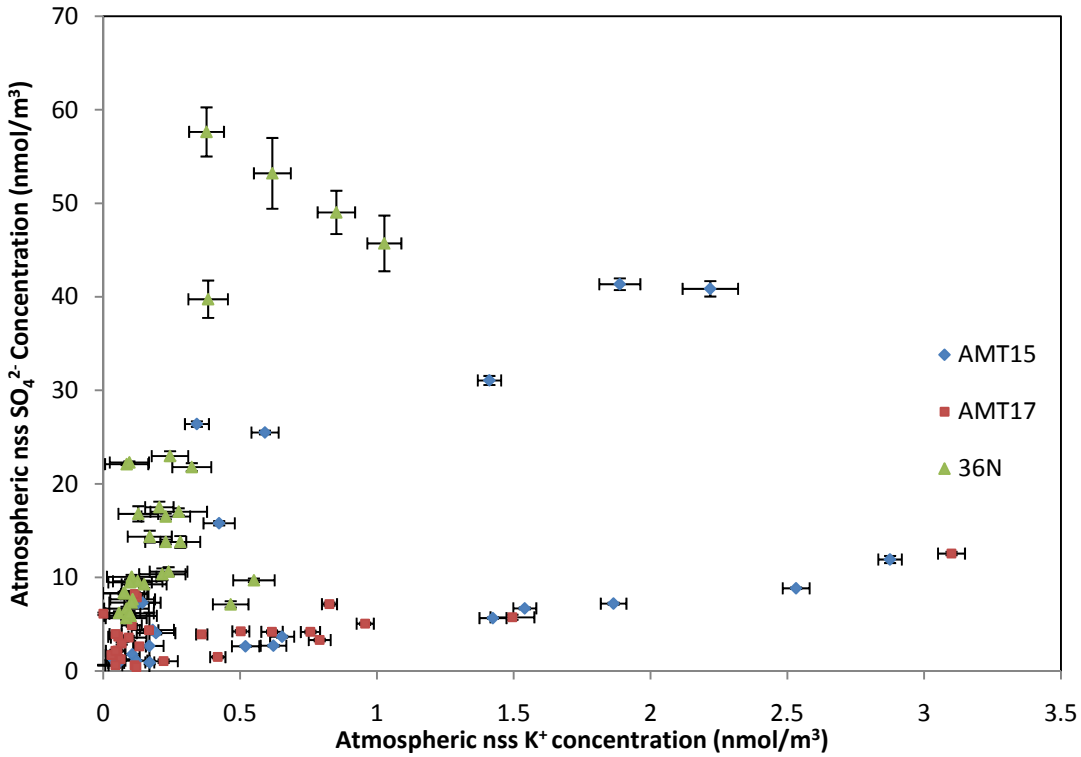

Figure 5.6 A plot of the atmospheric concentration of nss SO_4^{2-} against nss K^+ in fine mode aerosols. Error bars of standard deviation attached to each data point.

In figure 5.6, overall there is little evidence of a relationship. However, on closer inspection there are two distinctive trends that can be observed. For samples from 36N, larger increase in nss SO_4^{2-} and relative unchanged nss K^+ suggest relatively little biomass burning activities (low potassium) compare to other anthropogenic activities (high sulfate). Since both the North American and European continents are dominated by heavily developed countries, the trend provides evidence that the usage of fossil fuels is dominant (as a sulfate source) over the burning of biomass. In samples from AMT17, the concentration of potassium is higher than in samples from 36N. This may be due to a larger impact of biomass burning from deforestation in African countries and various other agricultural activities e.g. combustion of crops after harvests or forest fires. AMT15 samples, however, have a trend that seems to share characteristics from both cruises.

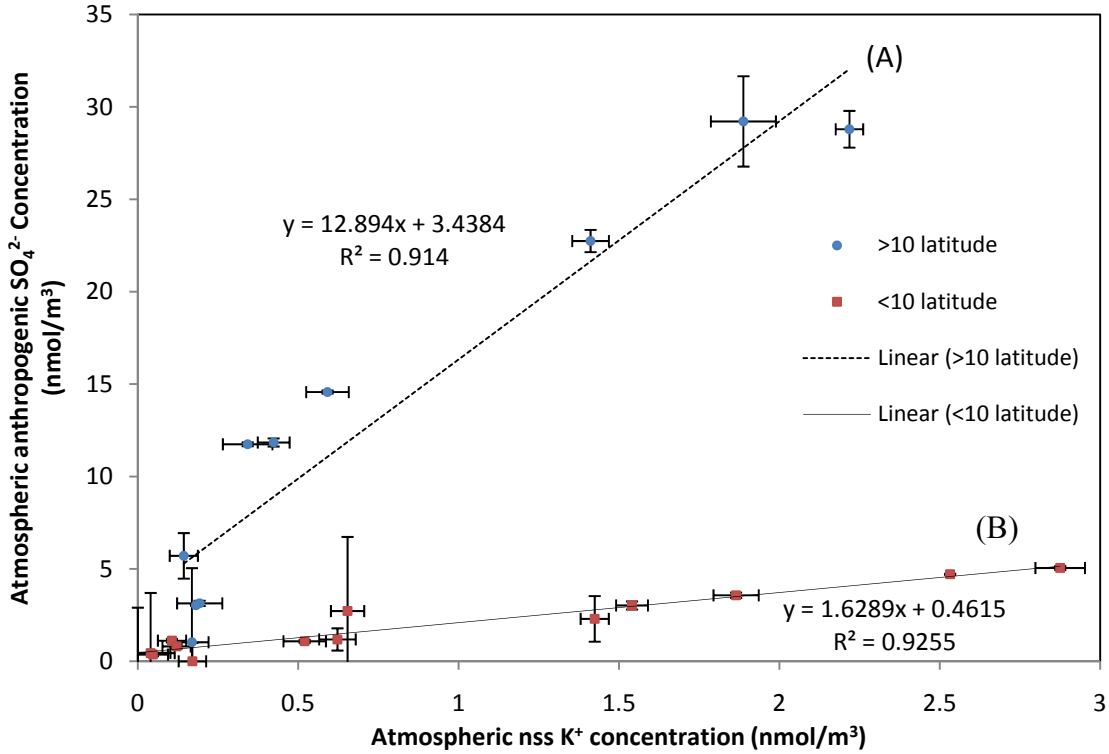

Figure 5.7 Plot of atmospheric nss K against anthropogenic SO_4 from AMT15 samples, separated above (A) and below (B) 10°N latitude, separated according to a proposed ITCZ circulation (Jickells et al., 2003). Error bars of standard deviation attached to each data point.

In figure 5.7, all three sets of data are presented, AMT15 samples have a unique two-way separation characteristic that is not seen in the rest of the dataset. From figure 5.7, it is observed that there are two distinctive trends from the same cruise track. Correlation (A) points to the pattern observed similarly in 36N samples (r = 0.96), where fossil fuel combustion is dominant. In correlation (B), the ratio between nss potassium and anthropogenic sulfate (r = 0.96) is significantly different with a much lower slope i.e. non-seasalt sulfate to non-seasalt potassium ratio. A student's t-test is performed, and P is found to be smaller than 0.05 (95% confidence level), therefore the hypothesis that the two groups (correlation A & B) are similar is rejected, and proved to be statistically different from each other. This can be described as a shift to another pattern where biomass burning

becomes predominant as a source of non-seasalt potassium and non-seasalt sulfate. Samples from AMT17 all fall close to correlation B. Five-day back trajectories for AMT17 samples indicate air masses sampled near Europe have come from the west of Europe i.e. North Atlantic. This explains the lack of samples that fall close to correlation A, as little European influence was captured by those samples.

According to Jickells et al. (2003), there is a theoretical separation of air masses around the inter-tropical convergence zone (ITCZ), which migrates seasonally from near the equator (0° latitude) in the northern hemisphere winter to approximately 10°N in the Northern Hemisphere summer (Baker et al. 2006, Sultan & Janicot 2000). This zone is believed to prevent mixing between the atmosphere of Northern and Southern hemisphere. In figure 5.7, assuming the boundary of ITCZ is at 10°N latitude, with the aid of sampling location coordinates, the data set is separated into two parts. One set above 10°N latitude represents European contribution, while the other set assumes contribution from regions below 10°N latitude (Africa in general). The two set of data plot well away from each other, with high anthropogenic sulfate to nss potassium ratio in Northern Hemisphere compared to the Southern Hemisphere that is already described. Activities from two regions are considered to be significantly different from each other, where one was dominated by sulfur and potassium emissions from developed countries with intensive usage of fossil fuels, and the other affected more by deforestation and agricultural activities associated with sulfate and potassium emissions. It is worth noting that there is seasonality to the biomass burning in

Southern African region (Baker et al., 2010). The seasonal variations must be taken into account when evaluating non-seasalt potassium and sulfate.

5.6 MSA / non-seasalt Sulfate Ratio

The ratio of MSA to non-seasalt SO_4^{2-} has been calculated in various studies [Gondwe et al. (2004), McArdle et al. (1995, 1998), Saltzman et al. (1986)] in an attempt to estimate the amount of sulfate derived from DMS oxidation, since MSA is a unique product of DMS oxidation. This requires that the relative proportion of MSA to nss sulfate derived from DMS oxidation is known. The relationship between MSA and nss biogenic sulfate from DMS is known from laboratory studies only. It is believed that this ratio is variable, including seasonal variations over the year (McArdle et al., 1995). The oxidation of DMS will produce sulfuric acid (which goes on to form ammonium sulfate) and MSA (Charlson et al., 1987), hence by calculating the ratio between biogenic nss sulfate and MSA the weighting between sulfate and MSA from DMS oxidation can be studied. The combination of sulfate isotope and MSA analysis here allows their ratio to be estimated from field sample for the first time, instead of the usual total nss sulfate (biogenic + anthropogenic) against MSA. Due to limitations in samples available, only sample 08, 15 and 19~29 from cruise AMT15 are measured for MSA in conjunction with the standard sulfate isotope analysis applied to all cruises.

Table 5.1 A short summary of the total nss SO_4^{2-}: MSA ratio calculated by some representative papers directly by analysing non-seasalt sulfate and MSA in marine aerosols.

MSA : nss SO_4^{2-} Ratio	Reference
0.13 ~ 0.23	Claeys et al. (2010)
0.015 ~ 0.67	Gondwe et al. (2004)
0.2 ~ 0.4	McArdle et al. (1995)
0.07 ~ 0.45	McArdle et al. (1998)
0.065	Saltzman (1986)

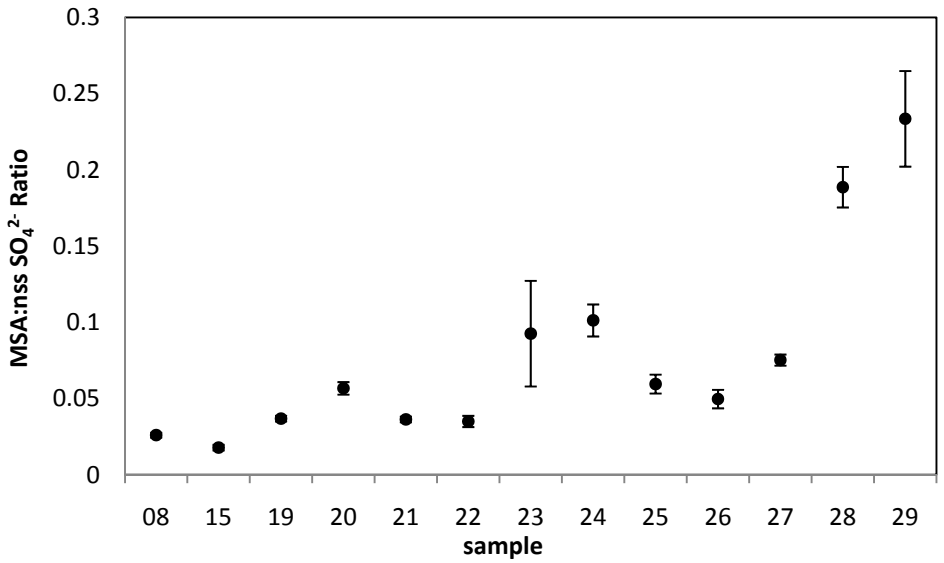

Figure 5.8 Variations in the nss SO_4: MSA ratio along AMT15 cruise track.

Figure 5.8 presents the changes in the total non-seasalt sulfate to MSA ratio in different sample stations. It can be seen that the ratio increases as the cruise travelled down the South Atlantic, into comparatively more pristine regions. The productivity at the South Atlantic/Southern Ocean is expected to be high (see chapter 4.3.2), therefore the production of DMS is expected to increase. The MSA / nss SO_4 ratio varies from 0.018 to 0.234, which agrees with the calculated range by studies summarized in table 5.1.

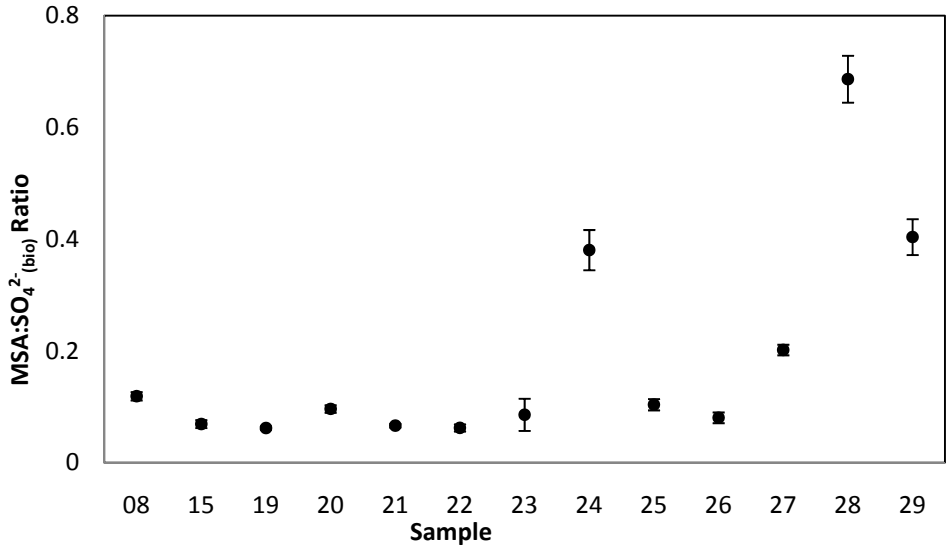

Figure 5.9 Variations in the biogenic SO_4: MSA ratio along AMT15 cruise track.

Using sulfate isotopes it is possible for the first time to calculate the ratio of MSA to biogenic sulfate, which are both believed to be produced entirely by the oxidation of DMS. From figure 5.9, it can be observed that the ratio between biogenic sulfate and MSA fluctuates in a similar way to figure 5.8, consistent with the comments made above. Sample 24 indicate high production of MSA over sulfuric acid in the air collected, and five day back trajectory show that air collected has travelled around high productive regions of the South Atlantic (figure 4.4, section 4.3.2). However, it should be noted that the increased productivity will not have an effect on the MSA to biogenic sulfate ratio. Referring back to figure 4.3 (section 4.3.2), it can be observed that sample 24 does not have high concentrations of MSA or non-seasalt sulfate, and five-day back trajectory suggests air has travelled near the South American continent before been sampled. Seasalt sulfate (60%) is dominant in sample 24, with very little biogenic sulfate (10%) and relatively unchanged amount (30%) of anthropogenic sulfate (figure 4.6, section 4.3.2).

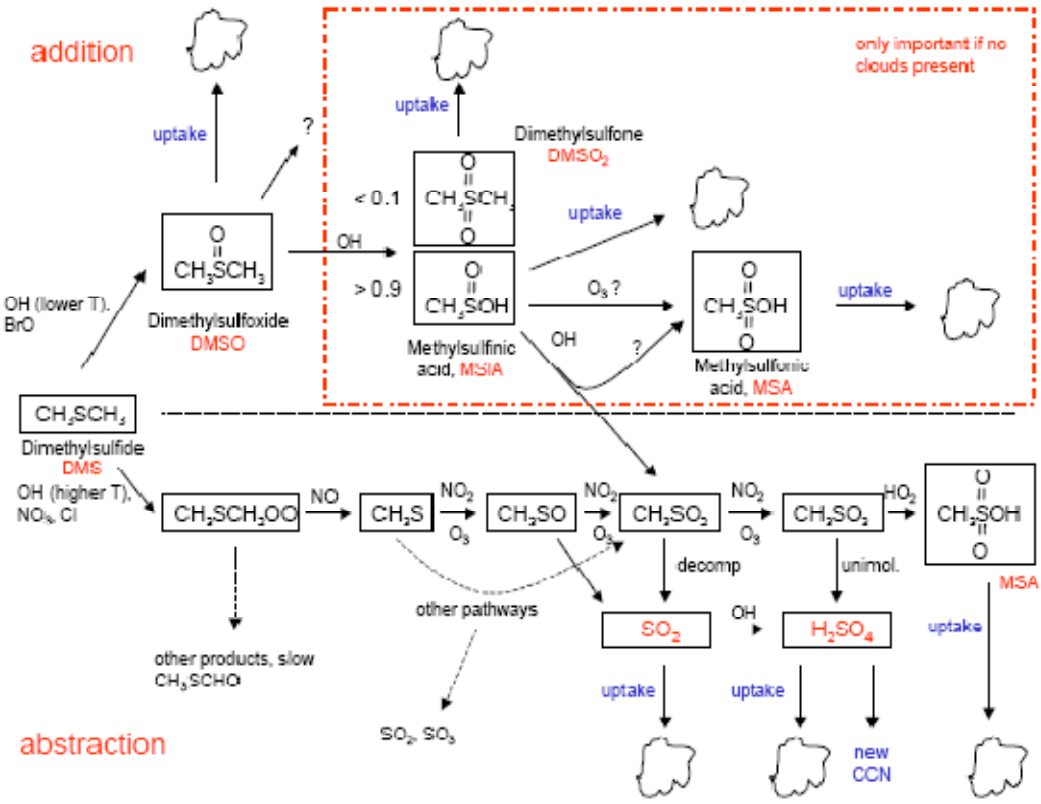

Figure 5.10 A schematic for the processes that take part in the oxidation of DMS, producing MSA and sulfuric acid (von Glasow & Crutzen, 2004).

A 20 month measurement campaign of aerosol measurements at Cape Grim, Tasmania by Andreae et al. (1999) reached the conclusion that the relative concentration of MSA is highest during summer, implying relatively more MSA production compared to SO_2 production from DMS oxidation. The concentrations of both components are strongly correlated with the relative population of cloud condensation nuclei, as suggested by the CLAW hypothesis (Charlson et al., 1987). However, by referring to figure 5.10, the proposed conclusion contradicts with the schematic produced by von Glasow & Crutzen (2004), where MSA should be expected to increase relative to SO_2 with lower temperature. Similar model results also indicate that the addition reaction pathway, which produces MSA over H_2SO_4, is favoured towards high latitudes i.e. lower temperatures (Koga &

Tanaka, 1996). This contradiction was addressed by von Glasow and Crutzen, and they concluded that there must be other controlling factors that overpower the temperature effect, or that that one or more of the processes described in figure 5.10 are wrong.

The significance of oxidant availability may be suggested to be more important than temperature. In the abstraction pathway, NO_x oxidants are only important during night times, and during day time hydroxyl radical is the dominant oxidant. Since the amount of NO_x is heavily influenced by anthropogenic activities (Galloway et al., 2003), as the cruise moves further down in to the Southern Atlantic, the environment is expected to become relatively pristine, hence less NO_x available (consistent with the aerosol nitrate data, figure 4.3, section 4.3.2) and therefore the abstraction pathway plays a less important role, producing less H_2SO_4. AMT15 travelled into the South Atlantic during October, 2004, and as the temperature is expected to be lower moving south down the South Atlantic, increased light intensity (seasonality involved) may stimulate production of MSA (addition pathway), because of the halogen radicals that are subsequently produced due to increased light (Vogt et al.1996). In addition, increasing amount of halogen available with increased light will oxidise NO_x into halogen nitrates, acting as a sink for NO_x species (Keene et al., 2009). It should be noted that although temperatures at the time of sample collection are known, the temperature at which DMS oxidation occurs is unknown. Since sample 24 to 29 all have trajectories near the Southern Ocean, it can be anticipated to be much cooler than sample 08 to 23 from Europe and Africa.

To sum up, the increased light intensity as well as low temperature is likely to encourage addition reaction between DMS and OH, which favours the production of MSA. Pristine regions of the Southern Atlantic will have less NO_x available for abstraction pathway that produces both H_2SO_4 and MSA. Finally, halogen radicals produced with increased light will remove NO_x species, as well as act as an oxidant in the addition pathway, which predominantly produces MSA. As a result, during summer periods at higher latitude regions, the addition pathway is favoured over abstraction, producing more MSA compared to H_2SO_4, agreeing with the increased MSA / biogenic sulfate ratio observed. It is also clear that the use of a single ratio for MSA / nss SO_4 from DMS oxidation is not appropriate. Instead, by segregating nss SO_4 into anthropogenic and biogenic sulfate, a better evaluation can be given when compared to MSA concentrations.

Chapter 6: Conclusion

This chapter will summarise some of the most important data presented and discussed in this thesis. A few figures from earlier chapters will be presented again and used to illustrate the summary of the main conclusions. Finally the limitations of this study will be noted and possible improvements that can be made for further studies considered.

6.1 Methods adapted

There is not much to comment on the methodology adapted to analyse the ionic concentration in aerosol samples. Most of the steps have been described in great detail in other studies, and no changes have been made in this study.

In the analysis of sulfur isotopic composition of sulfate a few steps were changed compared to earlier methods to minimize possible fractionation. The exclusion of filter paper, and instead the use of a centrifuge method is expected to have minimized the introduction of CO_2 and improved the data. However, due to time limitation, tests were not performed to compare the old and new methods once it was clear that the new method was accurate, precise and sensitive.

The method used to analyse nitrogen isotopic composition of ammonium in atmospheric aerosol samples is unique compared to other studies. A combination of methodologies described by Zhang et al. (2007) and McIlvin &Altabet (2005) for seawater has made sensitive measurements for aerosol ammonium isotopes possible. The results have

concluded that this combination of two methods can also be used to analyse atmospheric samples with similar extraction efficiency. In addition, since nitrite is insignificant in atmospheric aerosols, the step to remove excess nitrite can be ignored, hence potentially improving data and saving time. The resulting method is accurate, precise and sensitive.

6.2 Isotopic ammonium and sulfate data

The attempt to segregate isotopic data into different components is unique compared to other studies as well. Although ammonia is hypothesised to be coupled with DMS (Johnson & Bell, 2008), this study is the only one to date to have compared isotopic data of ammonium and sulfate together, supported by the atmospheric concentration data.

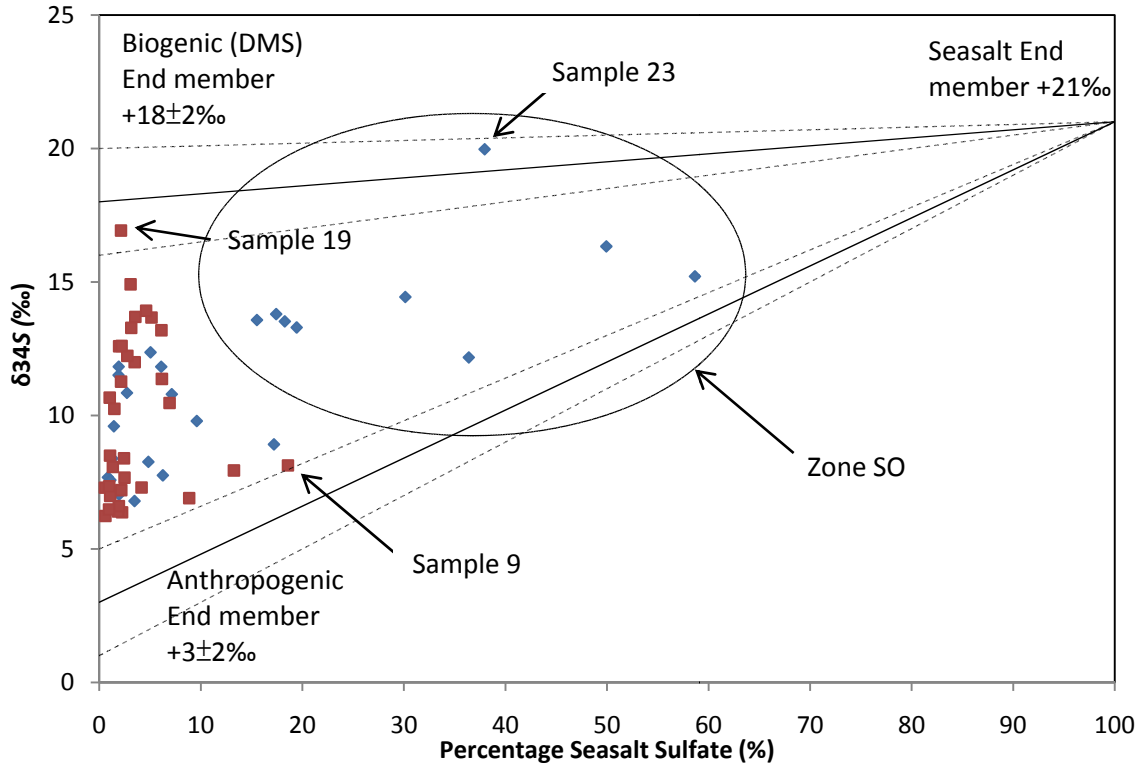

Figure 6.1 A plot showing the $\delta^{34}S$ value of measured aerosol samples from AMT15 (blue dot) and 36N (red square) against their calculated seasalt sulfate percentage.

Graphs similar to figure 6.1 are plotted in various studies as well, such as Wadleigh (2004). Such a plot identifies samples with a dominant single source, such as sample 23 from AMT15. However, this does not quantify the contribution from different sources of sulfate, which is achieved in this study.

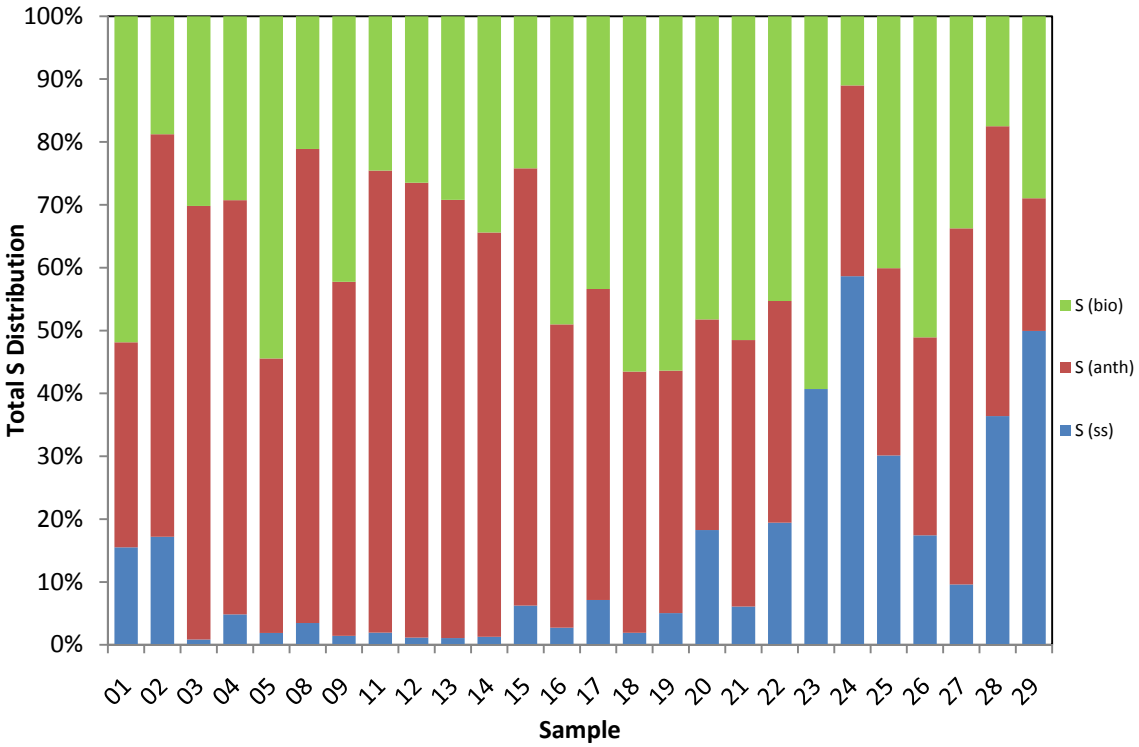

Figure 6.2 A histogram plotted to present the percentage contribution of three different components of sulfate in the atmosphere for cruise AMT15.

As shown in figure 6.2, the contribution from different sources of sulfate can be clearly observed. With a combination of atmospheric non-seasalt concentration data and five-day back trajectory data, the source of sulfate can be examined and traced accordingly.

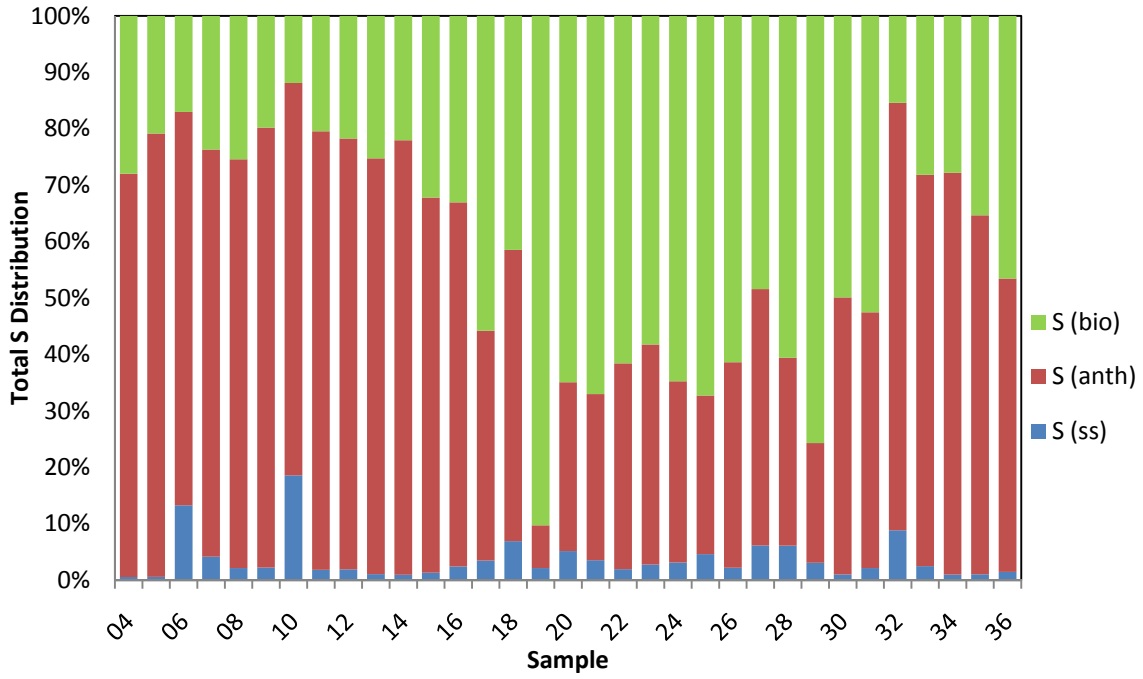

Figure 6.3 A histogram plotted to present the percentage contribution of three different components of sulfate in the atmosphere for cruise 36N. Error bars of uncertainty are not shown for clarity of the plot.

Similar to figure 6.2, figure 6.3 presents the contribution of different sulfate sources in the marine atmosphere in a very clear way for evaluation. It is worth noting that in fig 6.3 anthropogenic sulfate is relatively significant near continents (sample 04 to 14, 32 to 36), and biogenic sulfate is important over the remote North Atlantic Ocean (sample 16 to 31). For figures 6.2 and 6.3, the results demonstrate that over large areas of the open ocean biogenic sulfate is a major component of the aerosol.

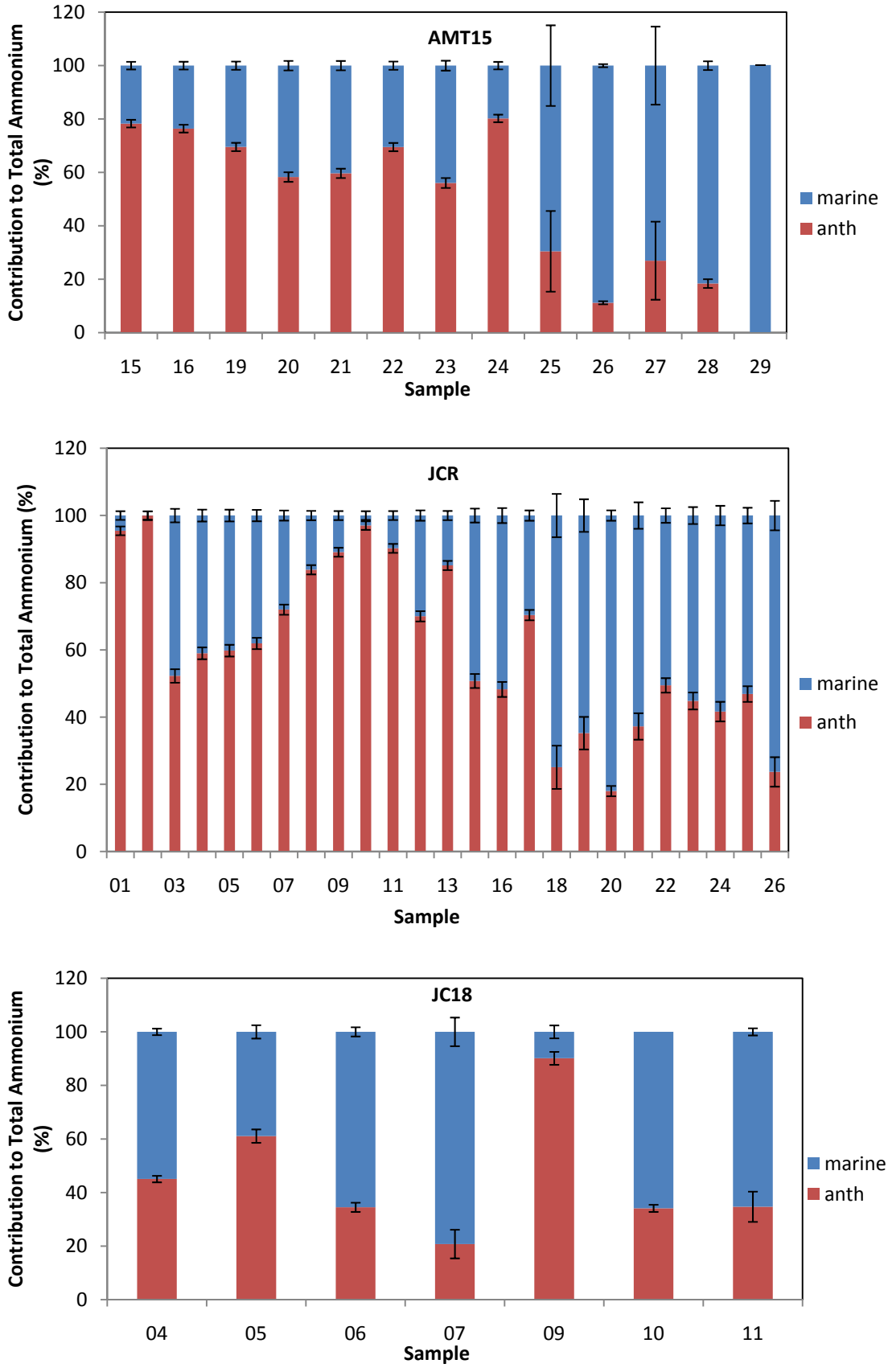

Figure 6.4 A series of histogram plotted to present the percentage contribution of marine and anthropogenic components of ammonium in the atmosphere for cruise AMT15, JCR and JC18. Error bars of uncertainty are attached to every sample.

The results presented here are used to estimate from isotopic data the relative importance of anthropogenic and marine biogenic ammonium in aerosol samples for the first time. This requires assumptions about the mechanisms driving the fractionation and about the end members of sources, and these require further evaluation. General trends can be observed from figure 6.4 for the relative importance of anthropogenic and marine biogenic ammonium. Anthropogenically dominated regions can be clearly distinguished on the graph. Given that the assumptions applied about end members are correct, it can be concluded that the remote South Atlantic is comparatively unaffected by anthropogenic ammonium (sample 25 to 29 for AMT15 and sample 18 to 26 for JCR).

The southern ocean is the region where biogenic ammonium and sulfate appear to be most significant. The absence of anthropogenic ammonium and SO_2 emission may also partially induce this observation. This is also a region of relatively high DMS emissions (Kettle et al., 1999) and this will therefore make this region dominated by biogenic sources. For ammonium, the assumptions are that the marine source is small compared to the anthropogenic source in the aerosol. However, Johnson et al. (2008) calculate from thermodynamic principles that the main marine ammonia emissions should be from warm tropical waters, which are in general low DMS sources (Kettle et al., 1999). On the other hand, high-latitude oceans become a sink for ammonia in the atmosphere (Johnson et al., 2008), while the remote North/South Atlantic will have a comparatively high DMS sources (Kettle et al., 1999). Hence the high contribution of biogenic ammonium and sulfate in the

Southern ocean samples may indicate a much less significant impact by anthropogenic sources compared to the remainder of the Atlantic, instead of a specific coupling between the two systems.

By considering $\frac{\text{biogenic S}}{\text{anthropogenic S}}$ vs. $\frac{\text{biogenic N}}{\text{anthropogenic N}}$

Although anthropogenic sulfate and ammonium have heavily perturbed the natural system and made evaluation for SO_4-NH_4 coupling difficult, it is possible to broadly define regional patterns in the importance of sources from the arguments above.

In the remote South Atlantic waters (high latitude):

$\frac{\text{biogenic S}}{\text{anthropogenic S}}$ increases compared to tropical areas since biogenic SO_4 increases and anthropogenic SO_4 decreases.

$\frac{\text{biogenic N}}{\text{anthropogenic N}}$ remain more or less stable, with a weak source of biogenic NH_4 and reduced anthropogenic emission for anthropogenic NH_4.

In tropical Atlantic waters:

$\frac{\text{biogenic S}}{\text{anthropogenic S}}$ decreases compared to the remote South Atlantic, with a weak biogenic SO_4 source and anthropogenic SO_4 increases

$\frac{\text{biogenic N}}{\text{anthropogenic N}}$ remain more or less stable, with a strong source of biogenic NH_4 and increased anthropogenic emission for anthropogenic NH_4.

The sulfate isotope source segregation has also suggested a strong latitudinal gradient in the MSA/$SO_4^{2-}{}_{(bio)}$ product ratio from DMS oxidation which needs to be considered when using MSA to trace biogenic sulfate.

The source separation for ammonium is less clear cut than for sulfur, mainly due to the wide range of anthropogenic ammonium by various sources, which overlaps with the range where marine biogenic ammonium is calculated. The AM15 and JCR data have both

suggested a significant anthropogenic source near continents and tropical waters, while marine biogenic ammonium being significant in the remote South Atlantic waters. If biogenic ammonia emissions are relatively strong in tropical waters, it will be difficult to identify this in the Atlantic where these waters are also subject to large inputs of anthropogenic emissions (figure 4.2 and 4.3) although the relatively high proportion of biogenic ammonium in the JC18 samples may be consistent with a tropical marine water ammonia source

It is much more difficult to separate the assumed two sources of ammonium from each other, because of difficulties in assigning end member source values. Results published for end member data from single source are variable, with the widest range measured been animal excreta ranges from -15 to 28‰ (Russell et al., 1998), although the results here seem to suggest a heavy isotopic signal proportional with a higher ammonium concentrations and more anthropogenic influence. Therefore, unlike end members of sulfate, which have precise isotopic values that are significantly different from one another, ammonium end members have large uncertainties relative to the observed range of aerosol ammonium composition. As commented in chapter 3.2, the uncertainties in the determination for ammonium end members dominate the overall uncertainties in the segregation.

6.3 Limitations in this study

There are various limitations that affect the data of this study, and can be grouped into two major factors: time and sample numbers.

Firstly, the system used to analyse sulfate isotope (Vario ELIII connected to the mass spectrometer PDZ-Europa 20-20, described in chapter 2.2.2) was freshly installed during the research period, and it took almost one year to optimise and tune to analytical accepted conditions. This significant drawback has affected the number of samples analysed.

It should also be noted that all samples are provided, not self-sampled. Although this conserves time spent on cruise travels, it has also limited the amount of samples allowed for the analysis. The isotopic analysis of sulfate requires a quarter of the sample filter, sometimes using up the last quarter of the filter available, before ammonium isotopic analysis took place. This makes measurements for ammonium isotopes impossible for some samples in this study.

6.4 Further research opportunities

By summarizing the data presented above and limitation described, some suggestions can be made in order to improve and provide statistical confidence to the data:

- Analyse more aerosol samples from various locations/ environments in order to better describe geographic variations in sulfate and ammonium isotopes.
- Obtain water column concentration data for DMS, which may be used to compare against aerosol MSA, sulfate isotopes and segregated biogenic sulfate data.
- Define end members of ammonium for segregation. This can be achieved by analyzing large number of samples from a variety of cruises sampling aerosols in different locations. Another option is to perform near-source analysis, which will help to determine specific isotopic data from individual sources.

Appendix 1: Five-day Air Mass Back Trajectories

NOAA HYSPLIT Model (http://ready.arl.noaa.gov/HYSPLIT_traj.php)
FNL Meteorological Data (except for JC18, GDAS Meteorological Data).
Three separate trajectory heights at 0 (sea level), 500 and 1000m.
Backward trajectory direction, with duration 120hrs (into 6hrs intervals).
Sample station number on the top left hand side corner.

I. AMT15

1

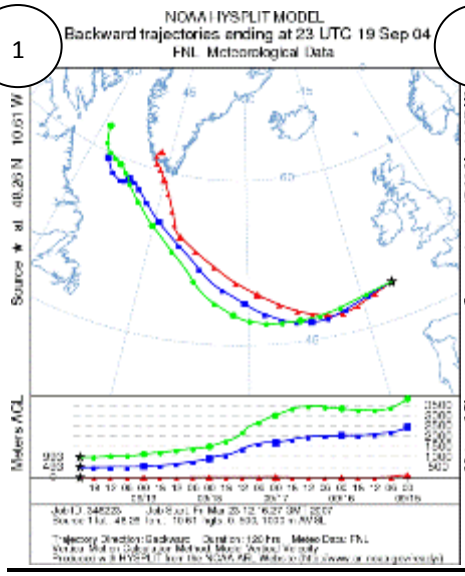

2

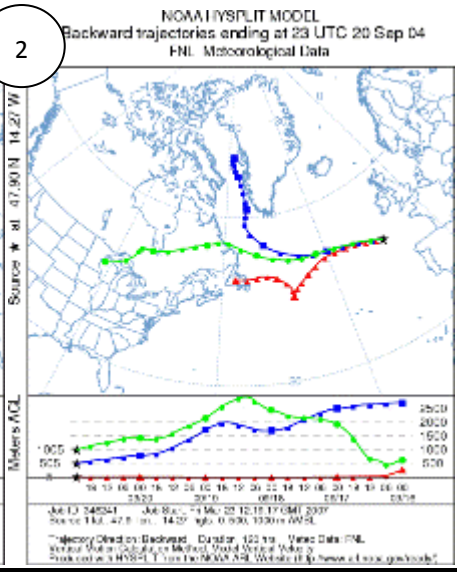

3

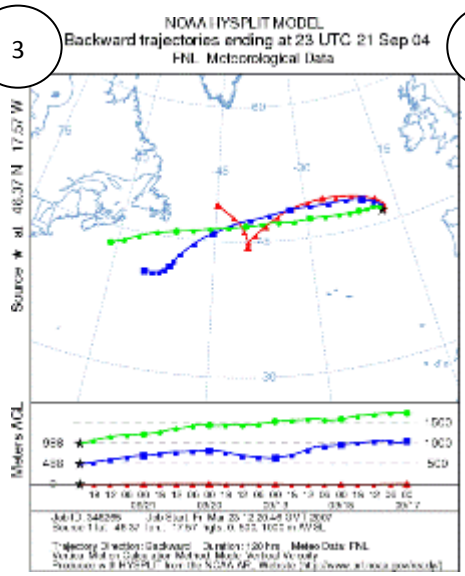

4

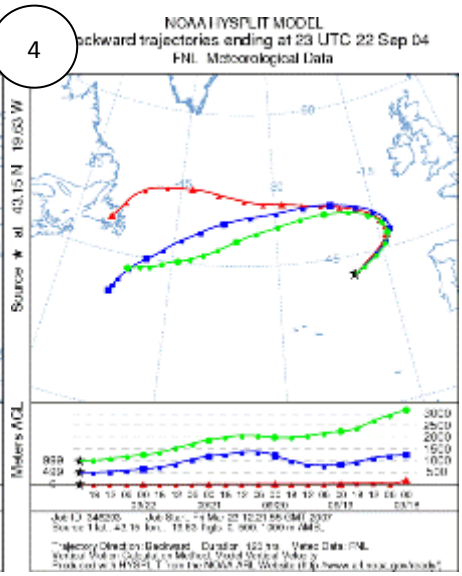

5

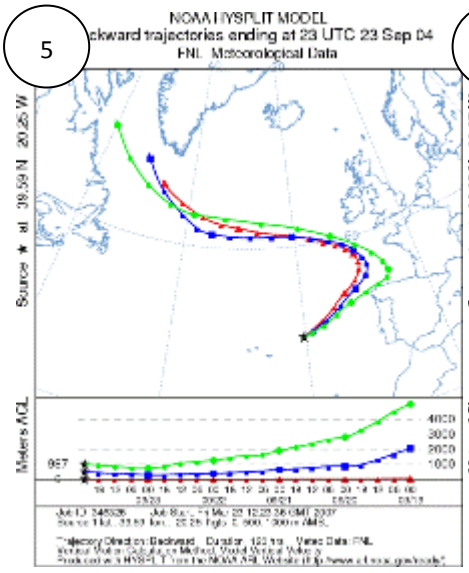
NOAA HYSPLIT MODEL
Backward trajectories ending at 23 UTC 23 Sep 04
FNL Meteorological Data
Source ★ at 39.59 N 20.25 W
Meters AGL

8

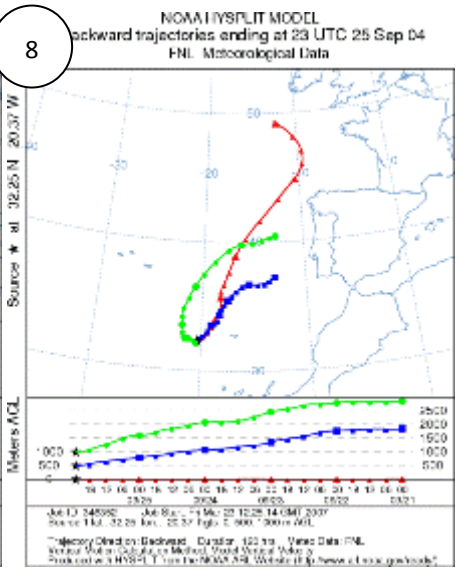
NOAA HYSPLIT MODEL
Backward trajectories ending at 23 UTC 25 Sep 04
FNL Meteorological Data
Source ★ at 32.25 N 20.37 W
Meters AGL

9

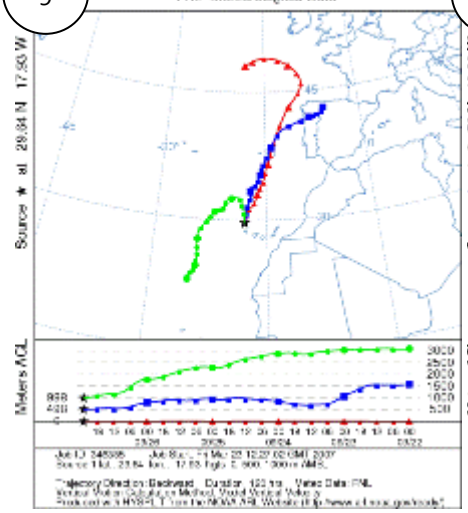
NOAA HYSPLIT MODEL
Backward trajectories ending at 23 UTC 26 Sep 04
FNL Meteorological Data
Source ★ at 29.84 N 17.50 W
Meters AGL

11

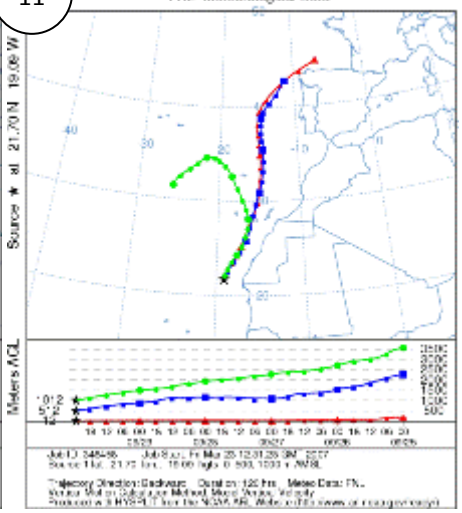
NOAA HYSPLIT MODEL
Backward trajectories ending at 23 UTC 29 Sep 04
FNL Meteorological Data
Source ★ at 21.70 N 19.08 W
Meters AGL

12

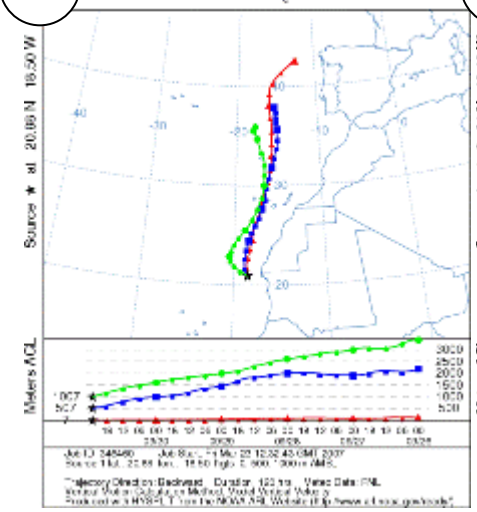
NOAA HYSPLIT MODEL
Backward trajectories ending at 23 UTC 30 Sep 04
FNL Meteorological Data
Source ★ at 20.89 N 18.50 W
Meters AGL

13

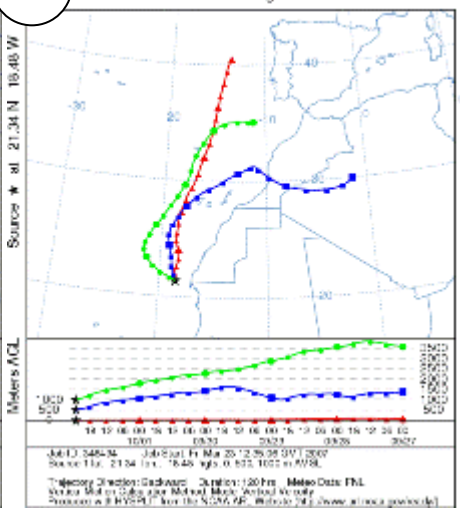
NOAA HYSPLIT MODEL
Backward trajectories ending at 23 UTC 01 Oct 04
FNL Meteorological Data
Source ★ at 21.34 N 18.48 W
Meters AGL

14

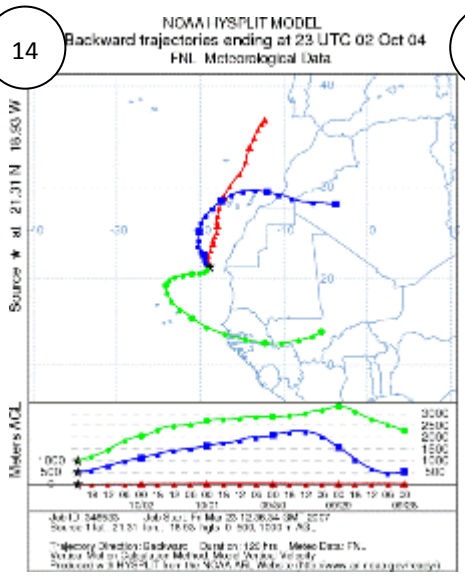

15

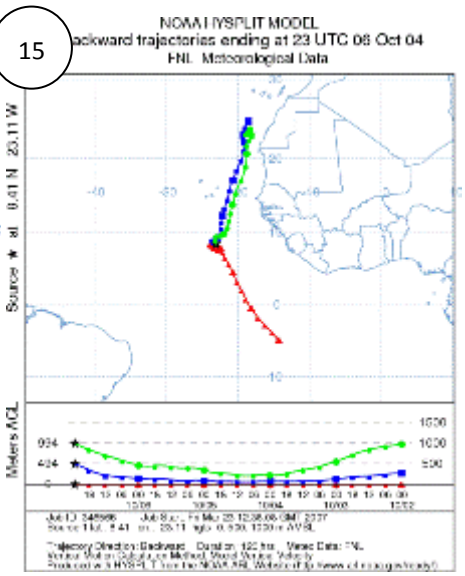

16

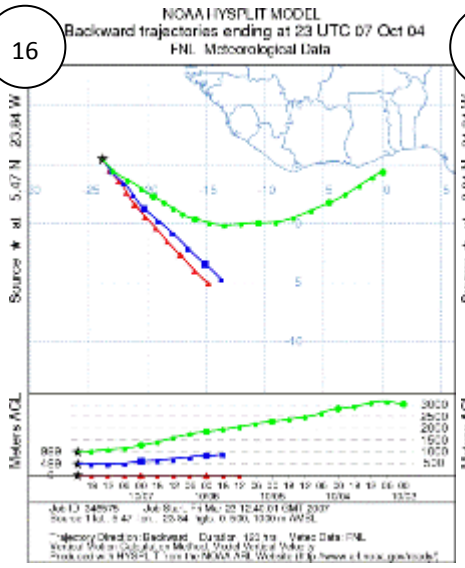

17

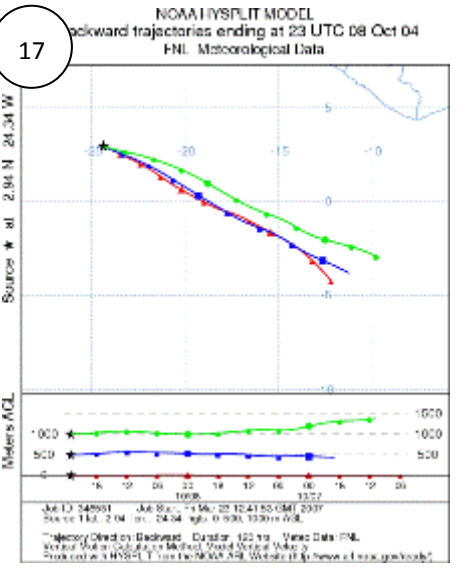

18

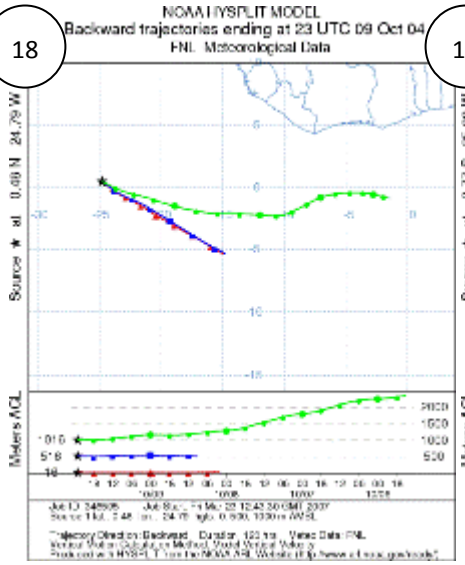

19

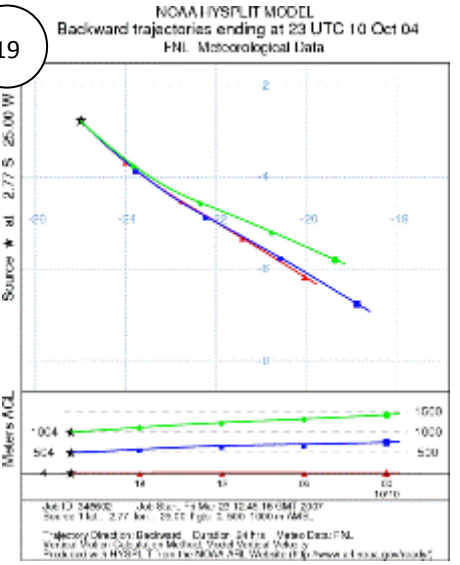

20

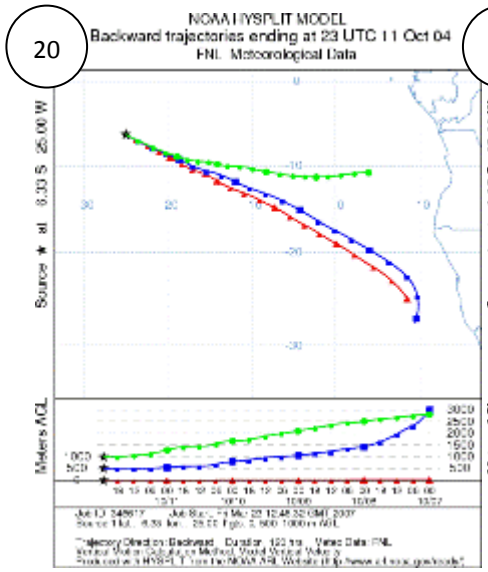

21

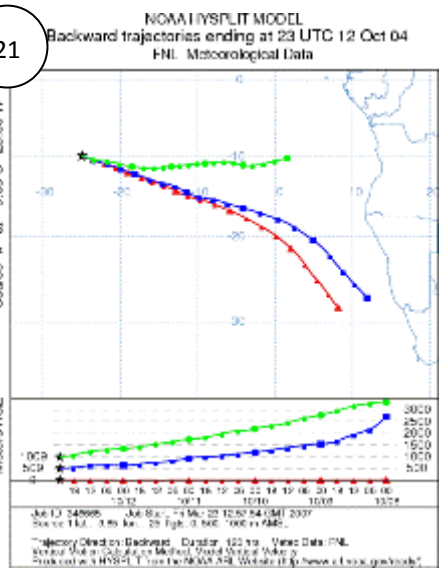

22

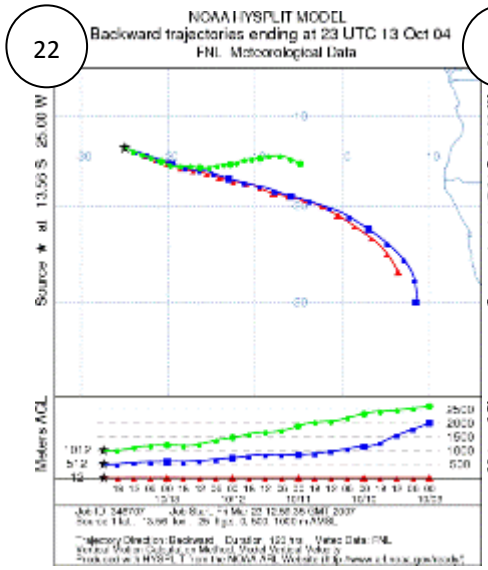

23

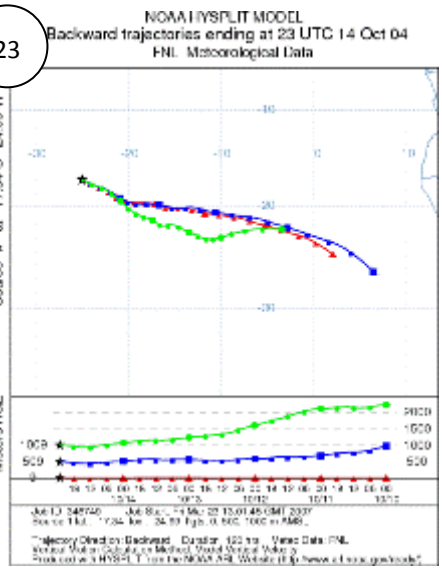

24

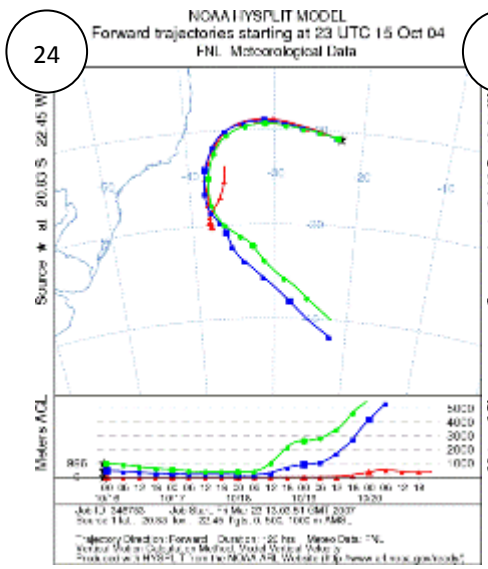

25

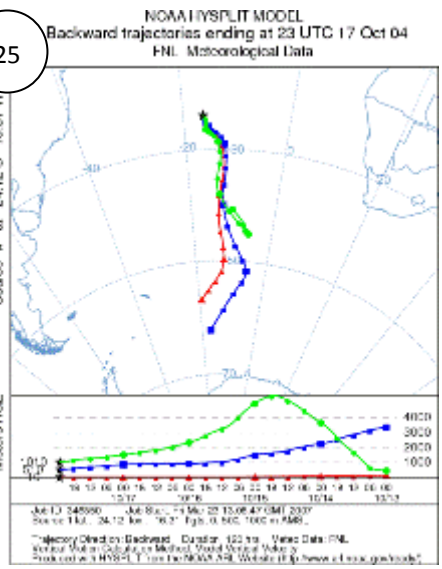

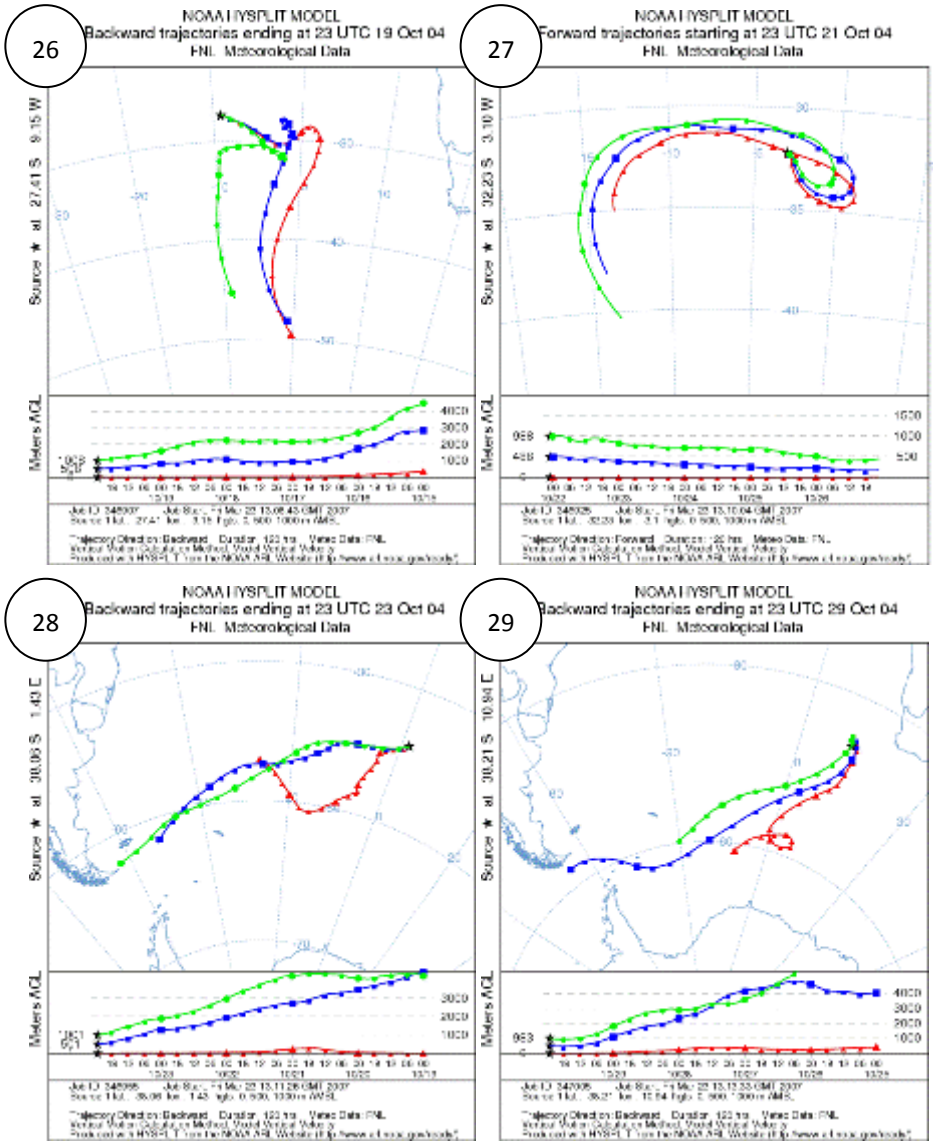

Diagram I A series of numbered five-day air mass back trajectories for aerosol samples collected during cruise AMT15.

II. AMT17

4

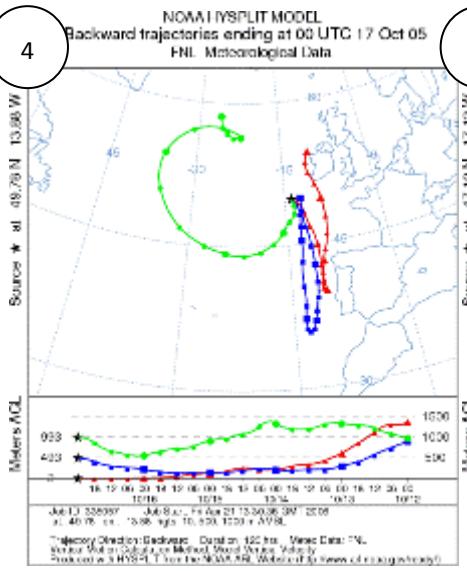

5

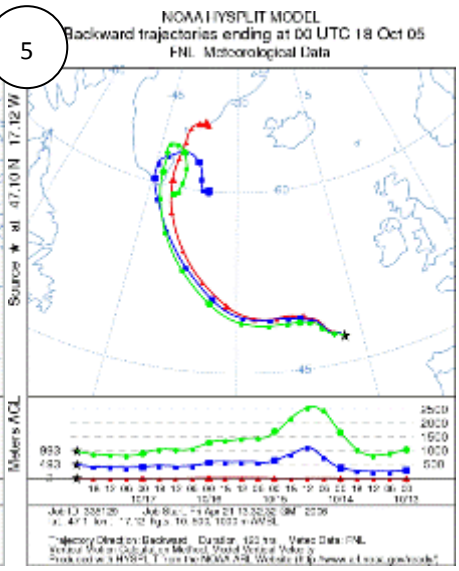

6

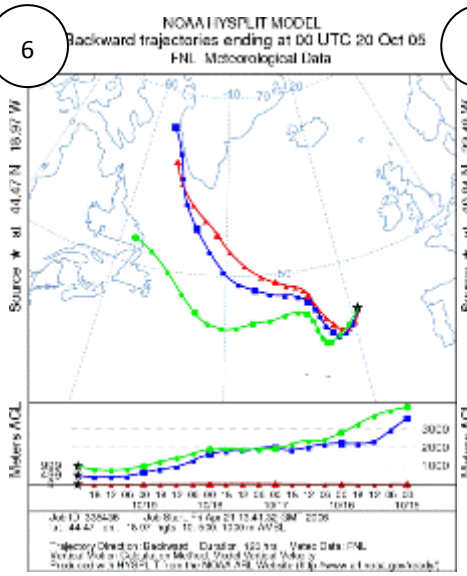

7

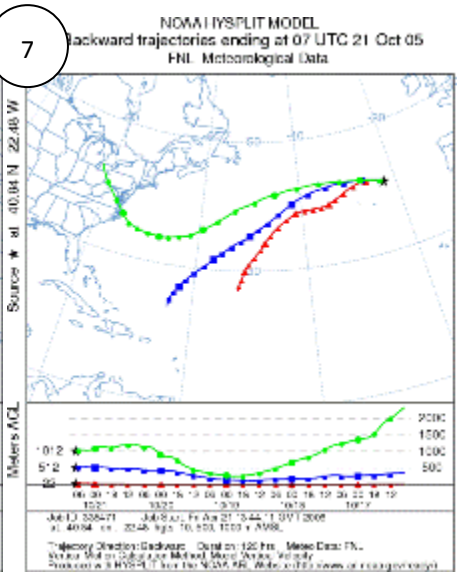

8

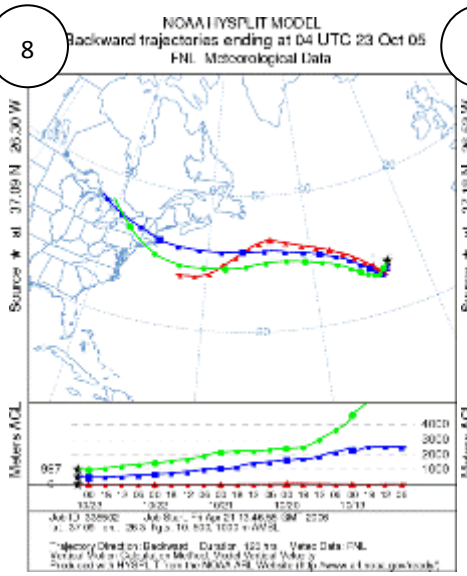

9

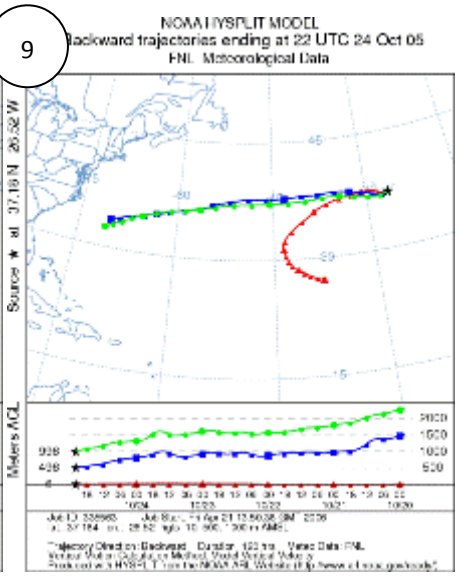

10

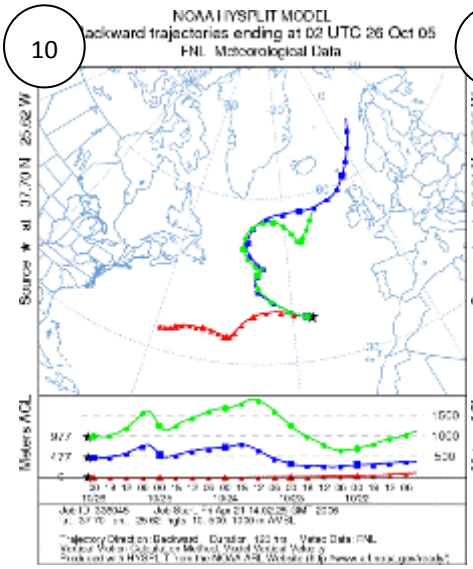

11

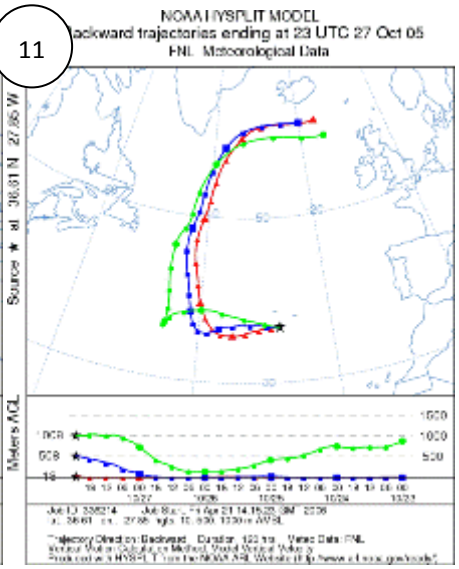

12

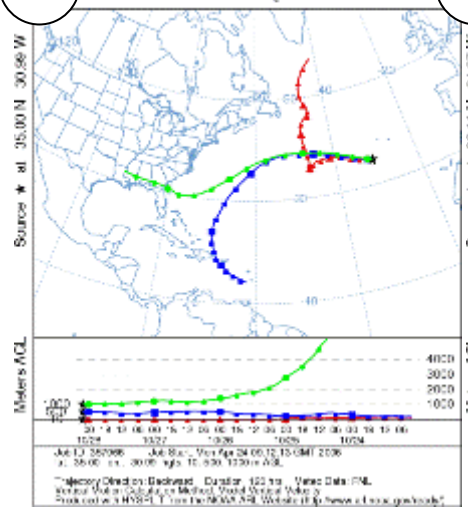

13

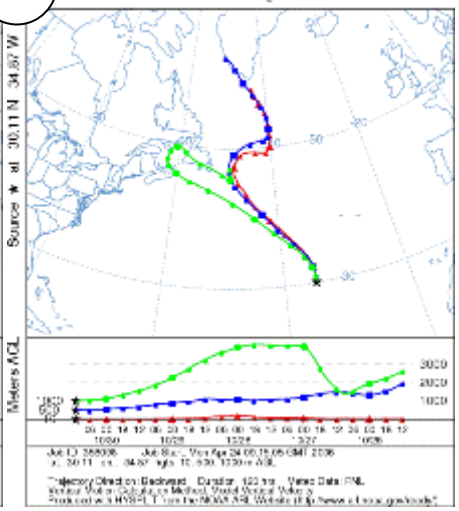

14

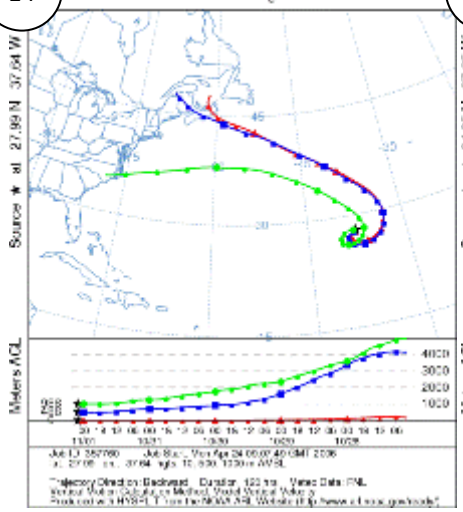

15

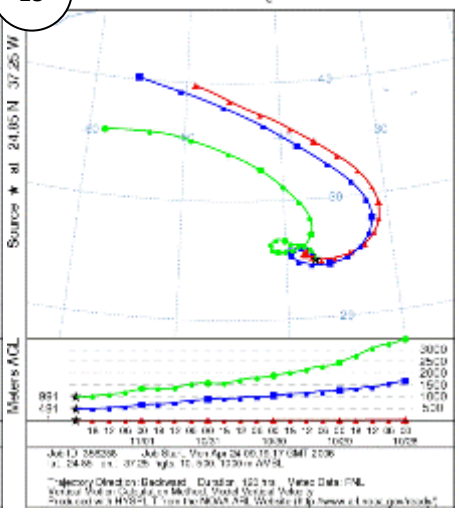

16

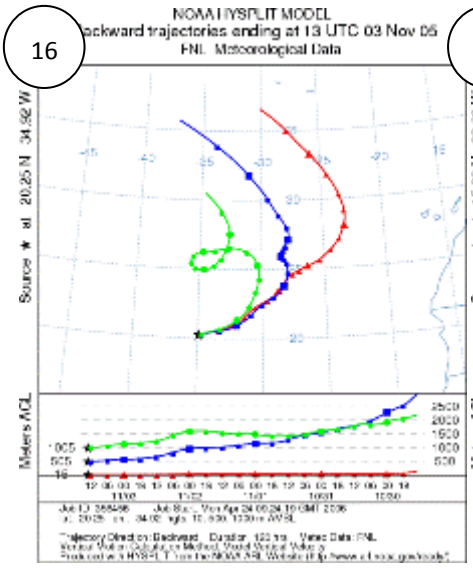

17

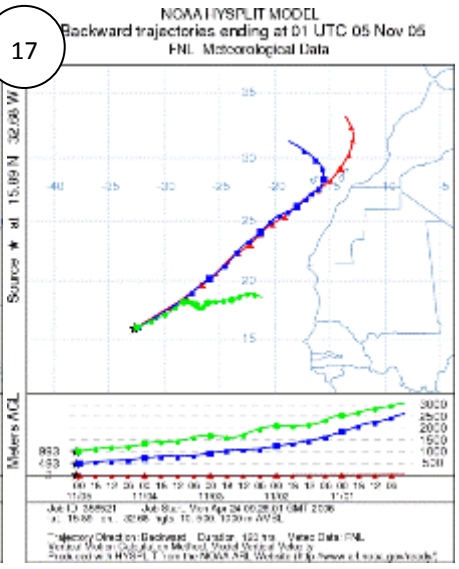

18

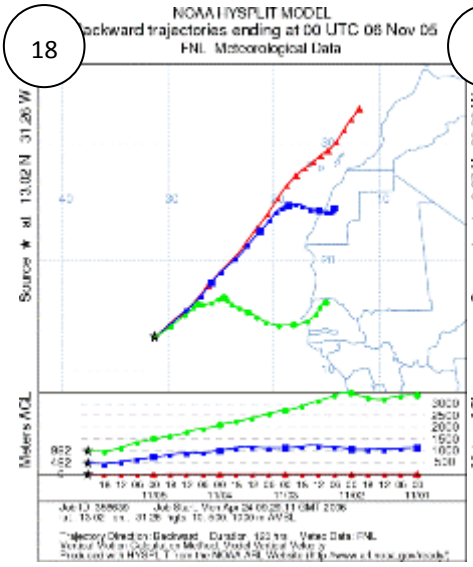

19

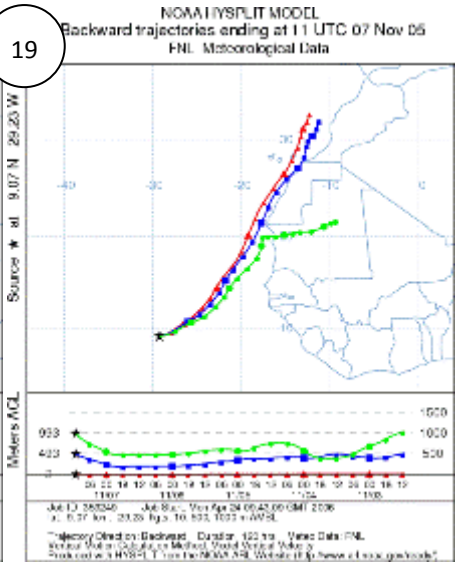

20

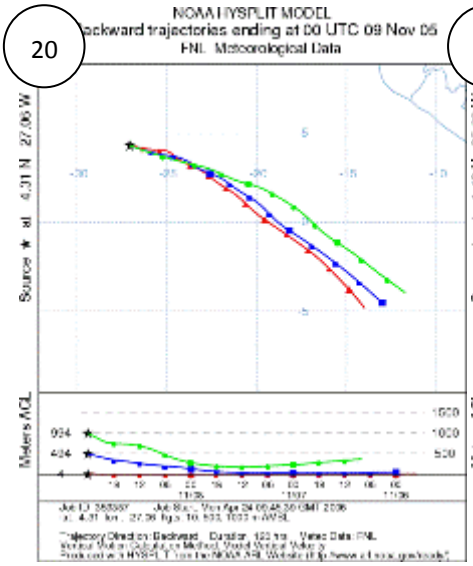

21

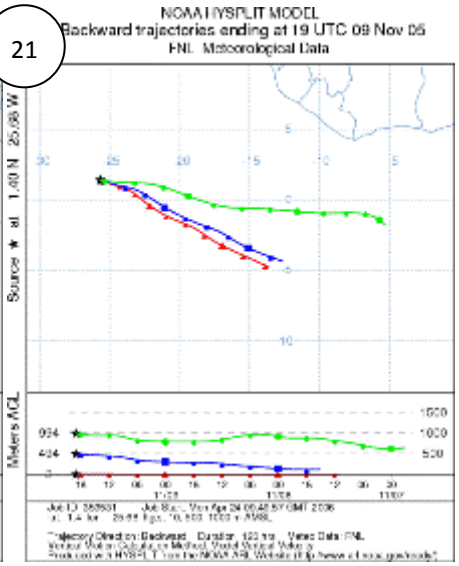

22

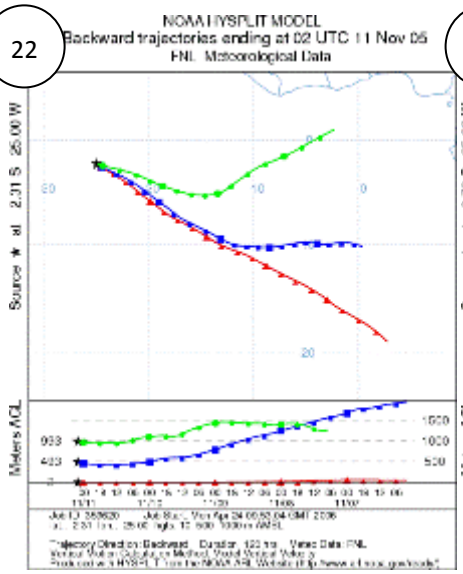

23

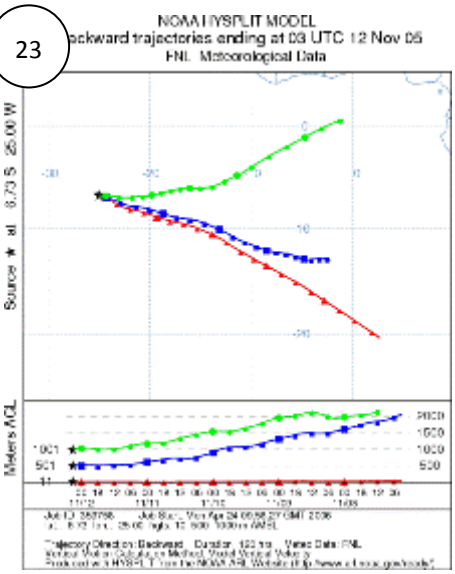

24

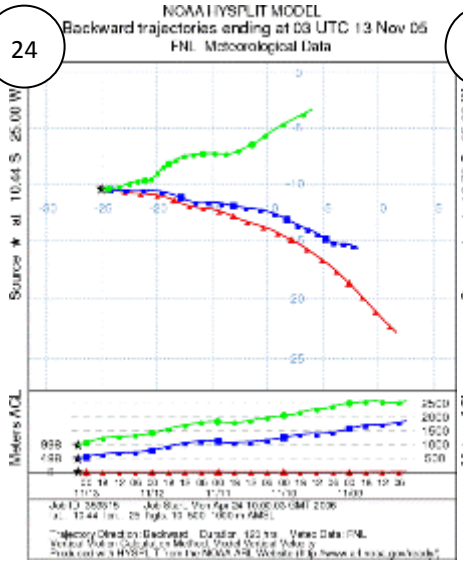

25

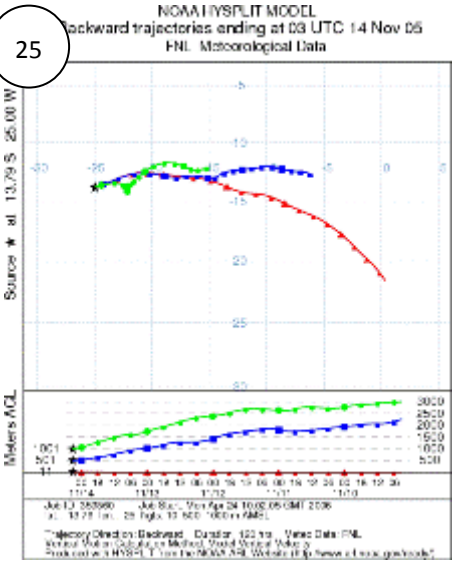

26

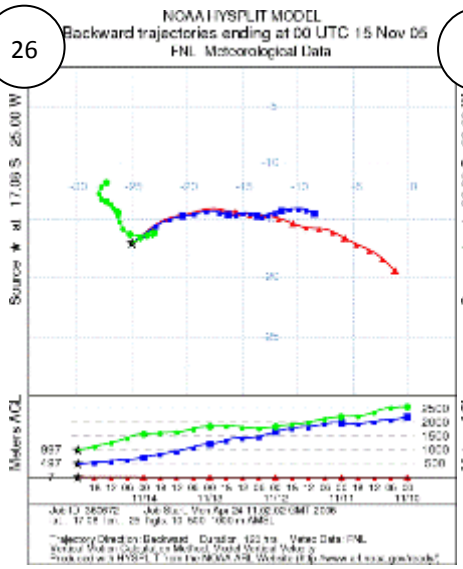

27

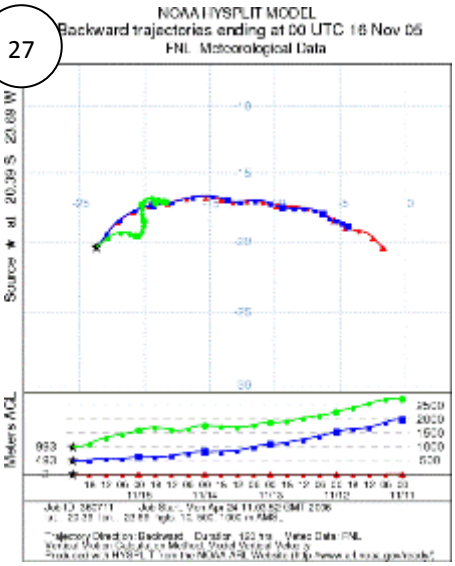

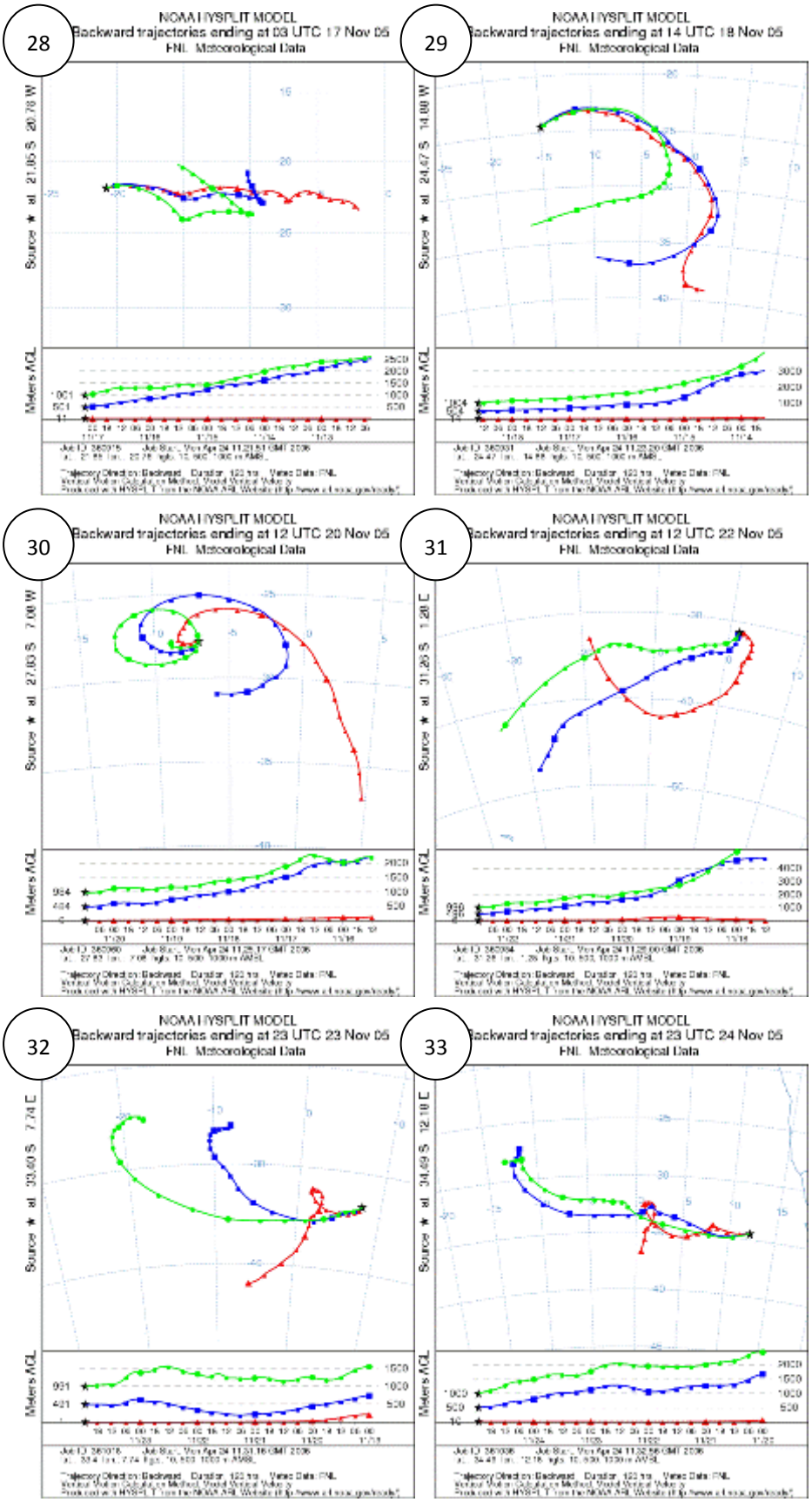

Diagram II A series of numbered five-day air mass back trajectories for aerosol samples collected during cruise AMT17.

III. 36N

4

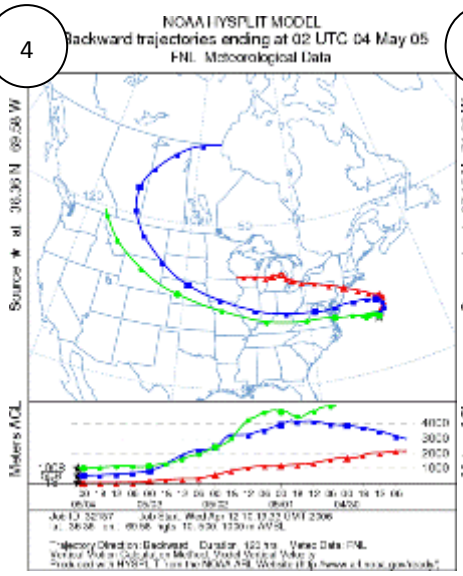

5

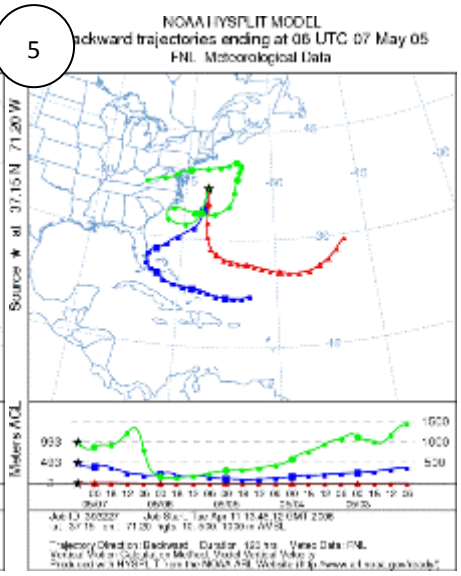

6

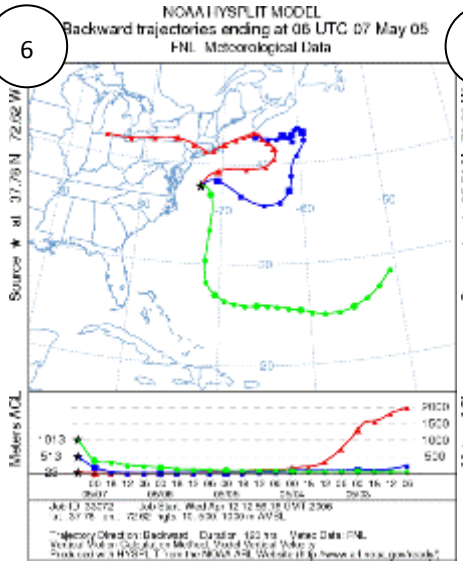

7

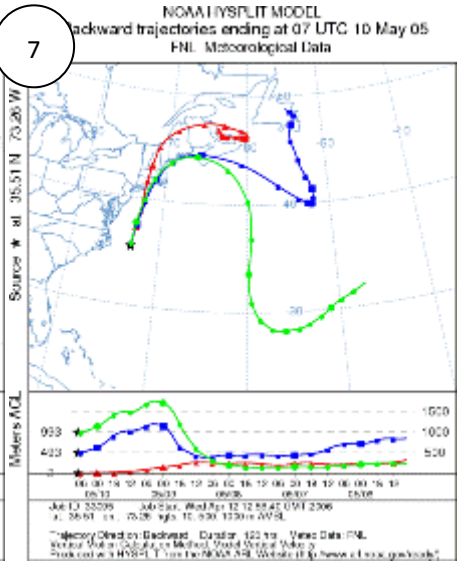

8

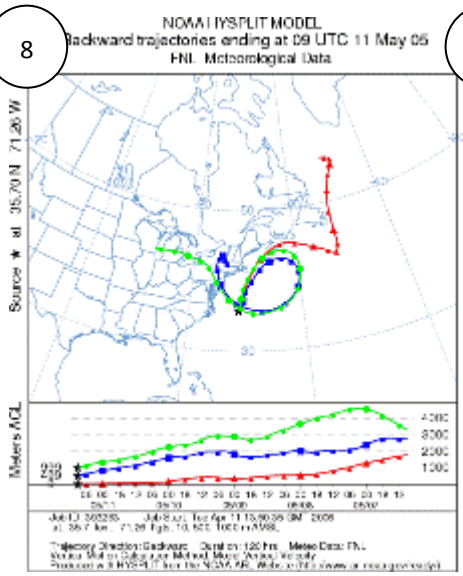

9

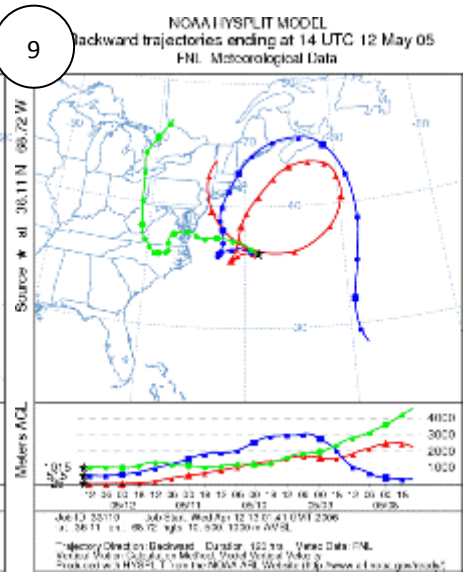

10

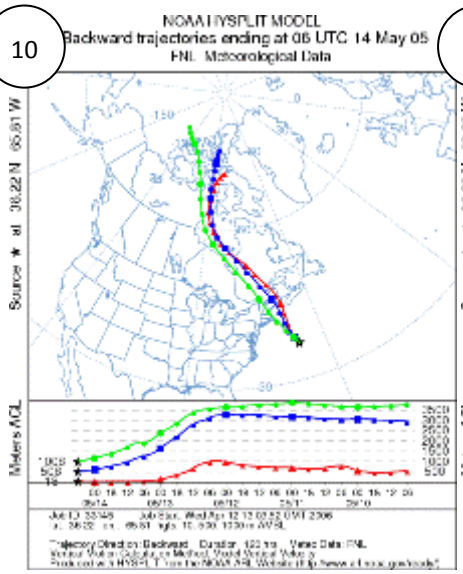

11

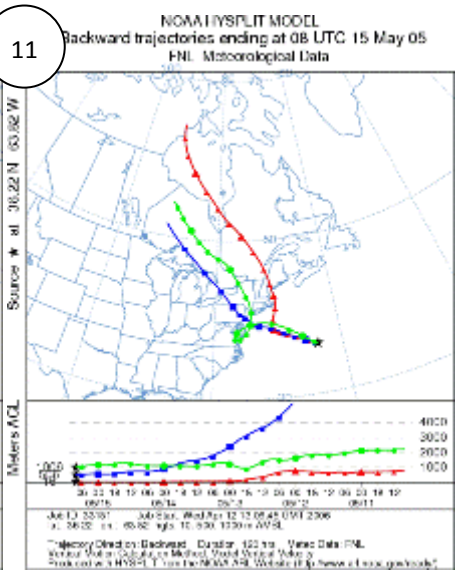

12

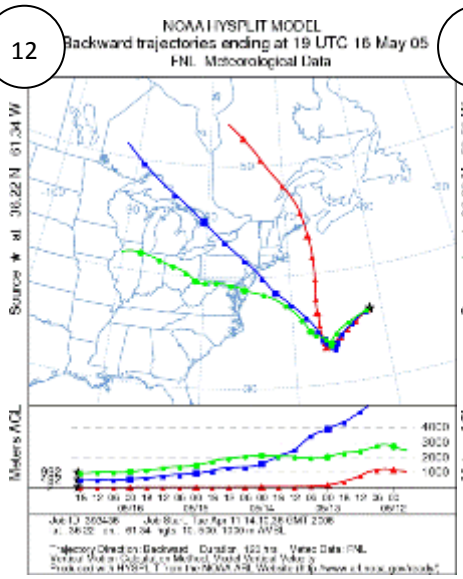

13

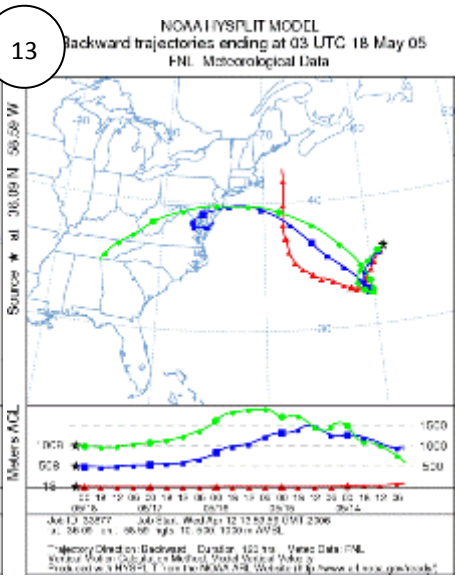

14

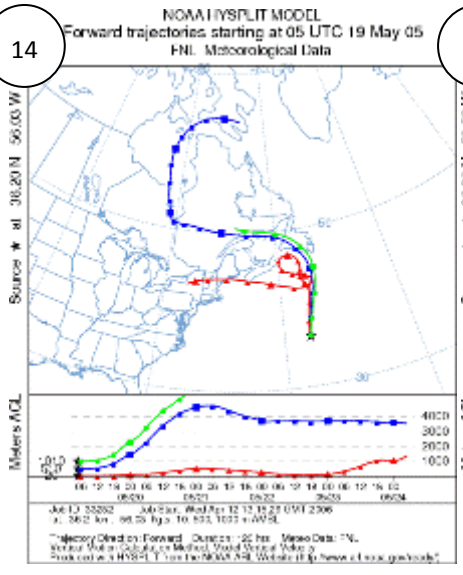

15

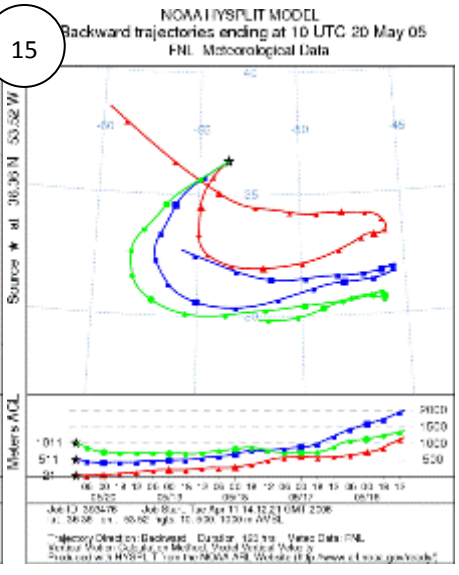

16

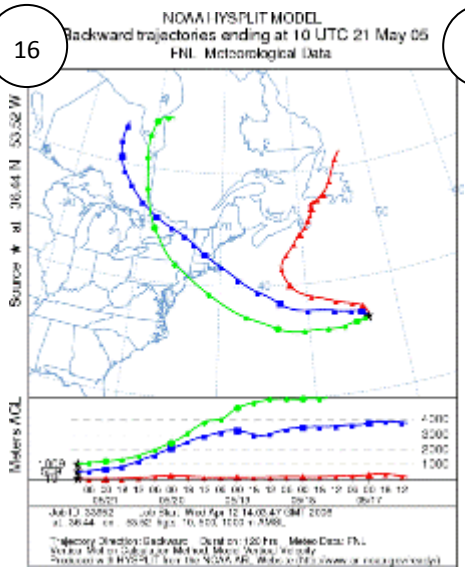

17

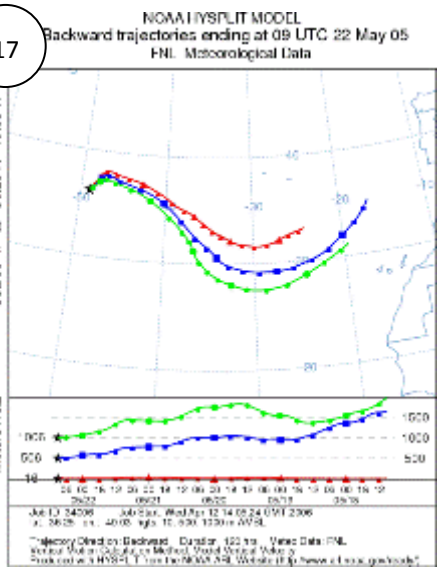

18

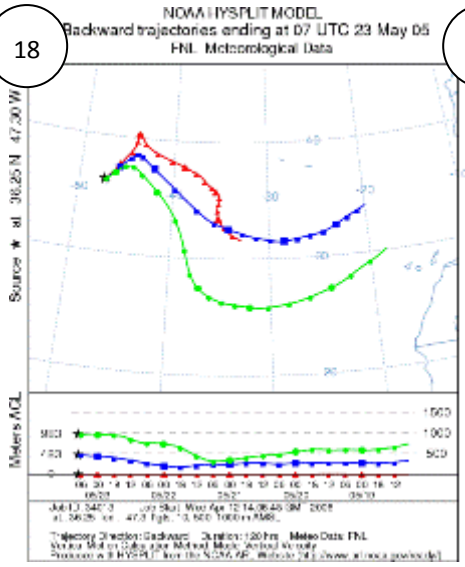

19

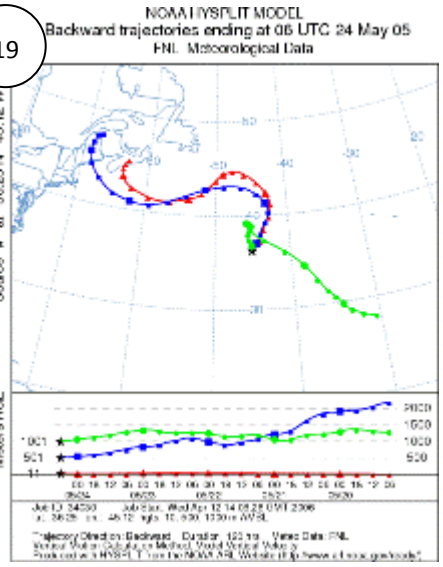

20

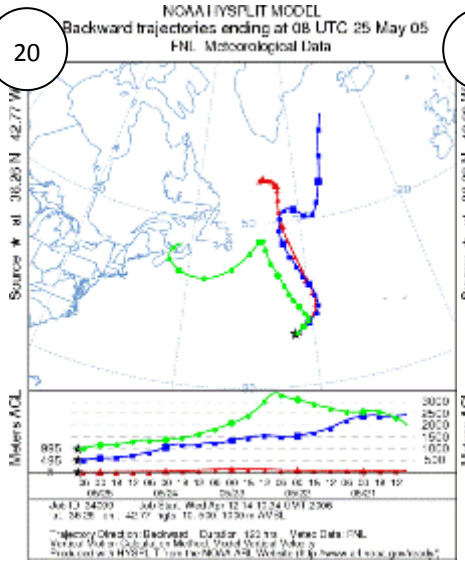

21

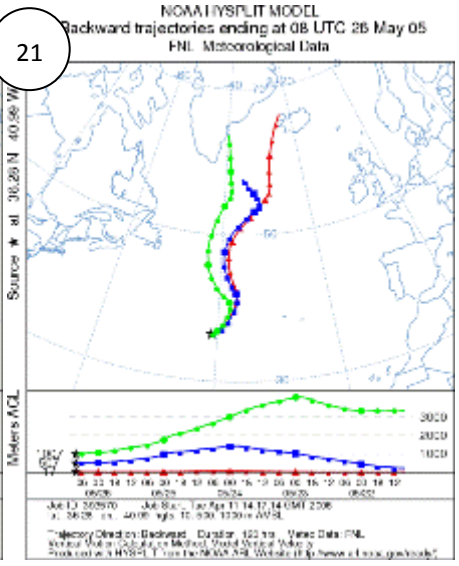

22

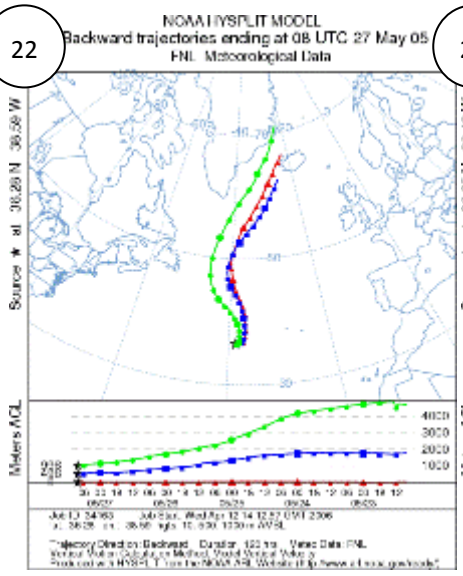

23

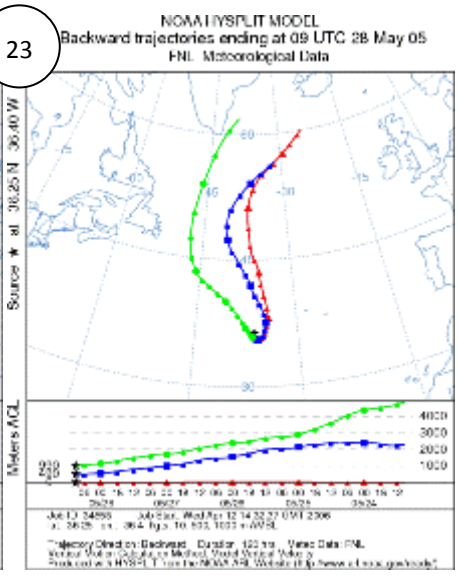

24

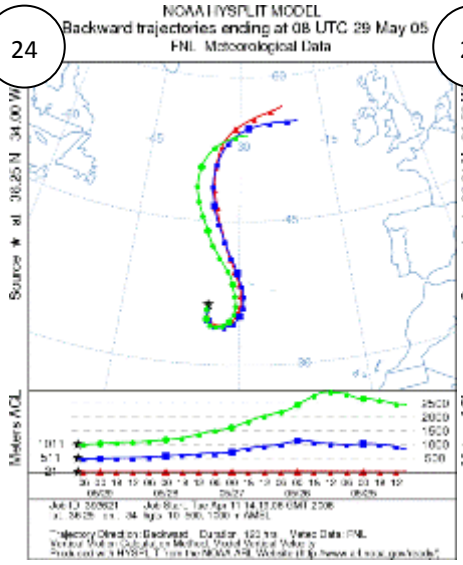

25

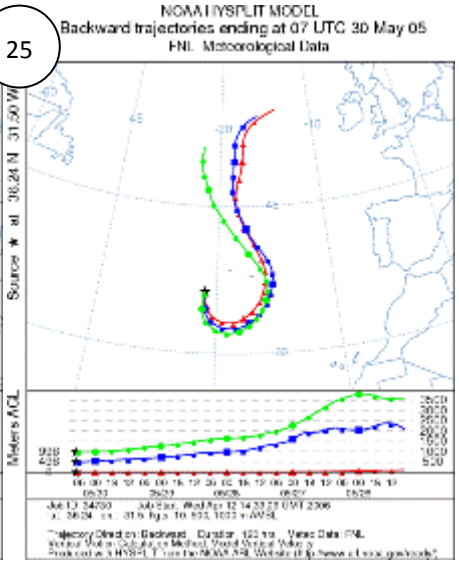

26

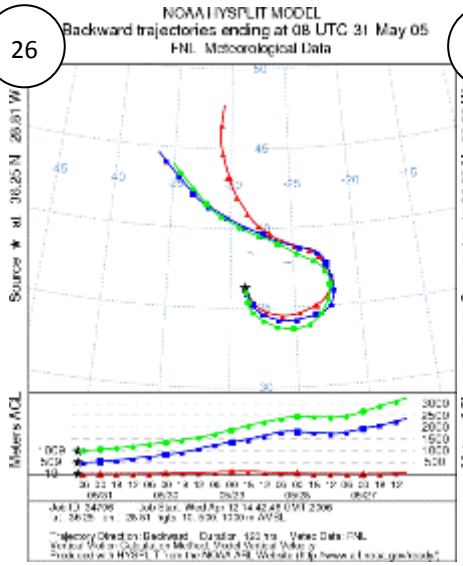

27

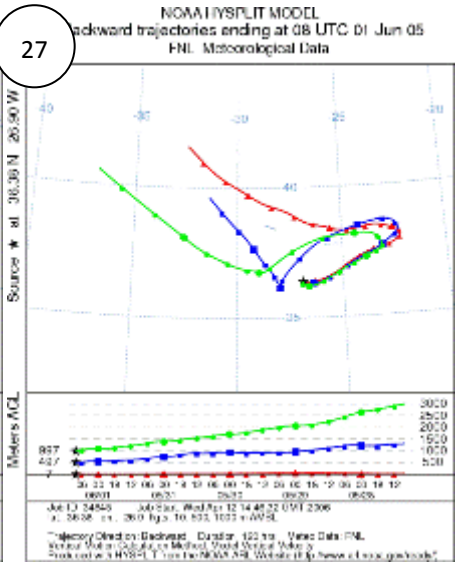

28

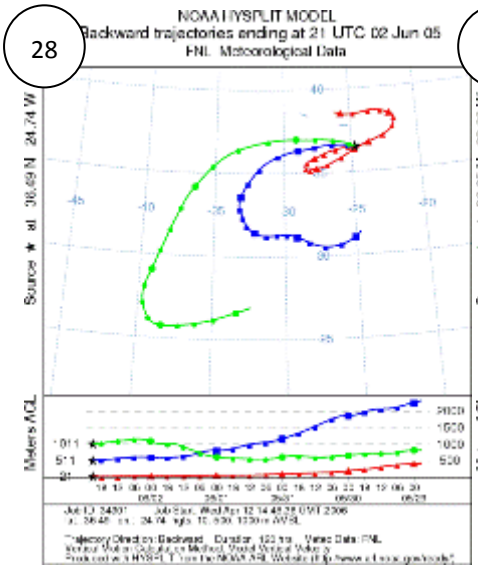

29

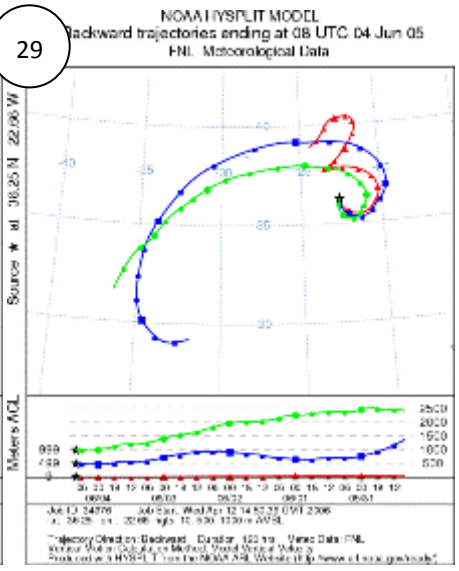

30

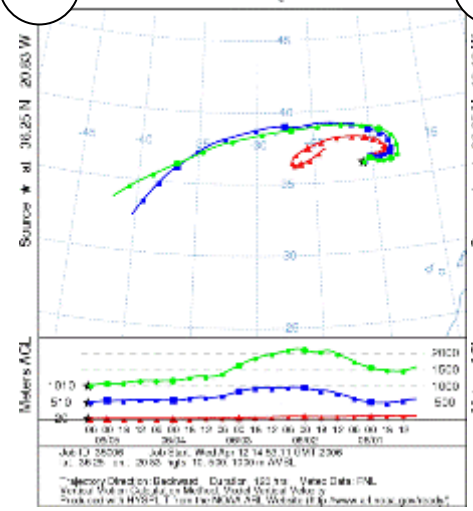

31

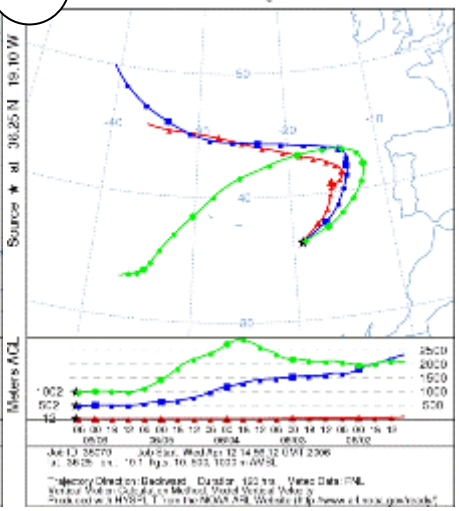

32

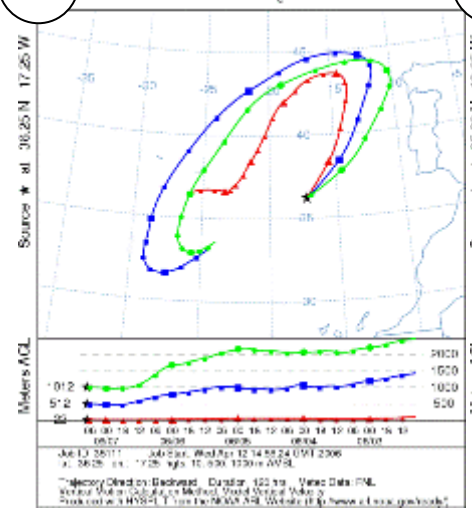

33

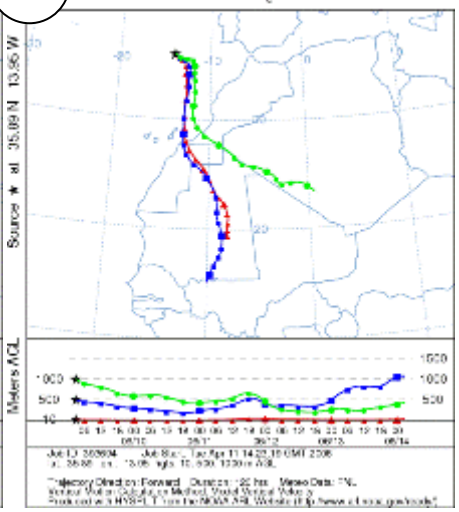

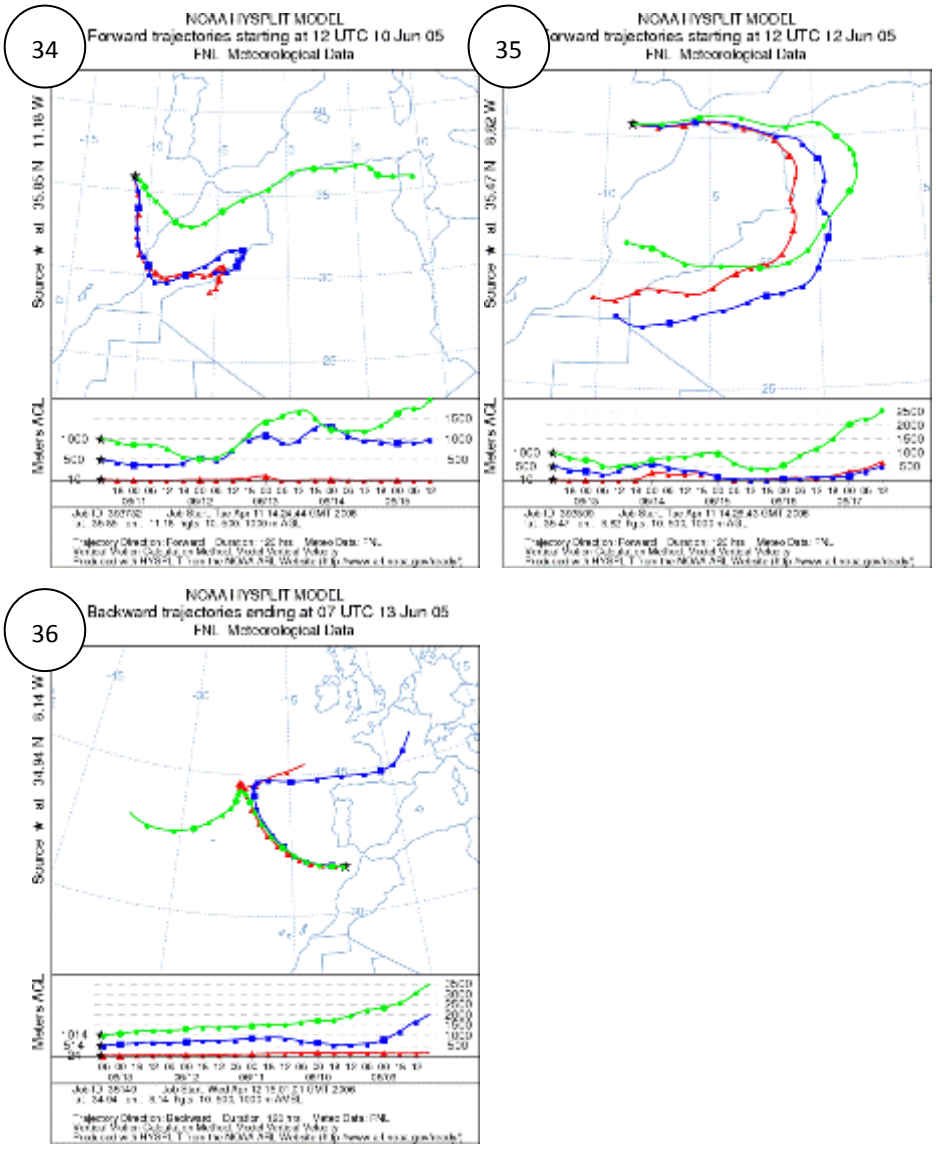

Diagram III A series of numbered five-day air mass back trajectories for aerosol samples collected during cruise 36N.

IV. JC18

3

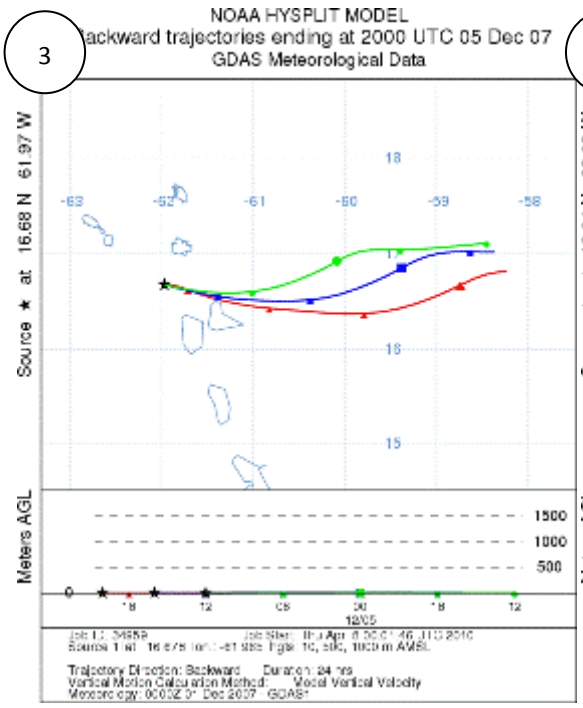
NOAA HYSPLIT MODEL
Backward trajectories ending at 2000 UTC 05 Dec 07
GDAS Meteorological Data
Source ★ at 16.68 N 61.97 W
Meters AGL
1500
1000
500
12/05
Trajectory Direction: Backward
Vertical Motion Calculation Method: Model Vertical Velocity

4

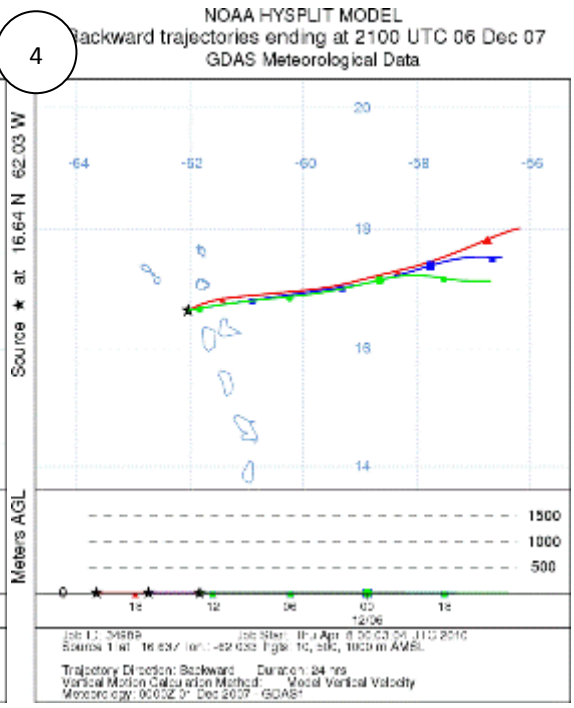
NOAA HYSPLIT MODEL
Backward trajectories ending at 2100 UTC 06 Dec 07
GDAS Meteorological Data
Source ★ at 16.64 N 62.03 W
Meters AGL
1500
1000
500
12/06
Trajectory Direction: Backward
Vertical Motion Calculation Method: Model Vertical Velocity

5

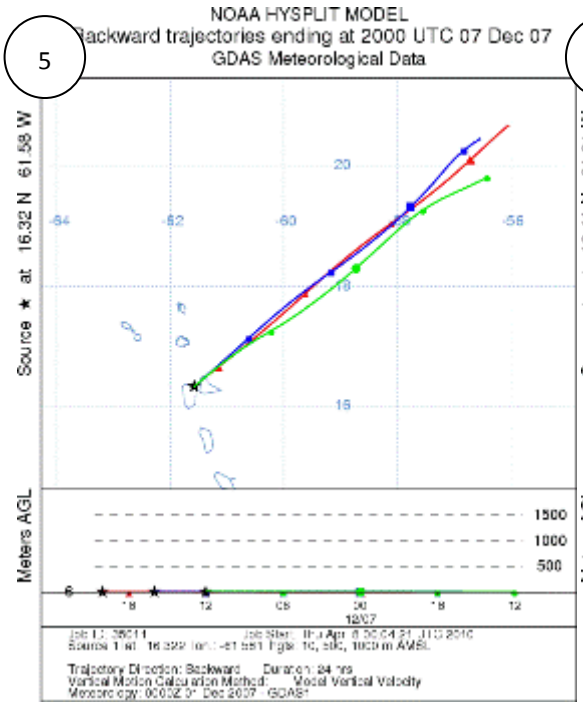
NOAA HYSPLIT MODEL
Backward trajectories ending at 2000 UTC 07 Dec 07
GDAS Meteorological Data
Source ★ at 16.32 N 61.58 W
Meters AGL
1500
1000
500
12/07
Trajectory Direction: Backward
Vertical Motion Calculation Method: Model Vertical Velocity

6

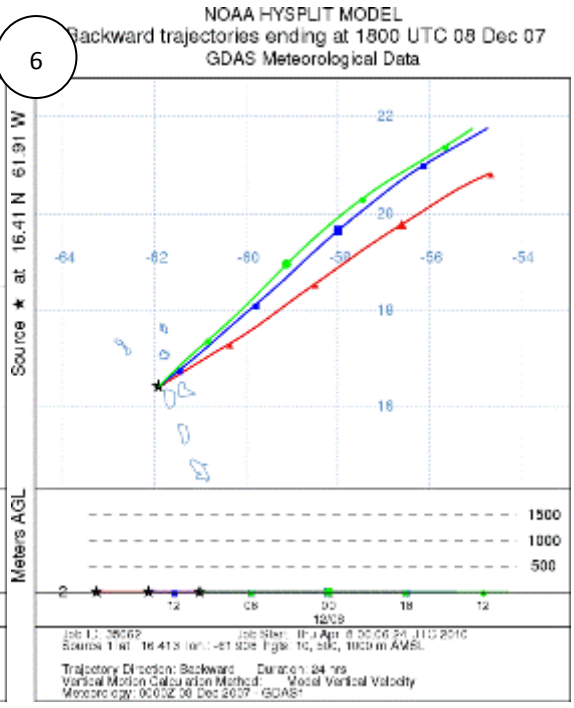
NOAA HYSPLIT MODEL
Backward trajectories ending at 1800 UTC 08 Dec 07
GDAS Meteorological Data
Source ★ at 16.41 N 61.91 W
Meters AGL
1500
1000
500
12/08
Trajectory Direction: Backward
Vertical Motion Calculation Method: Model Vertical Velocity

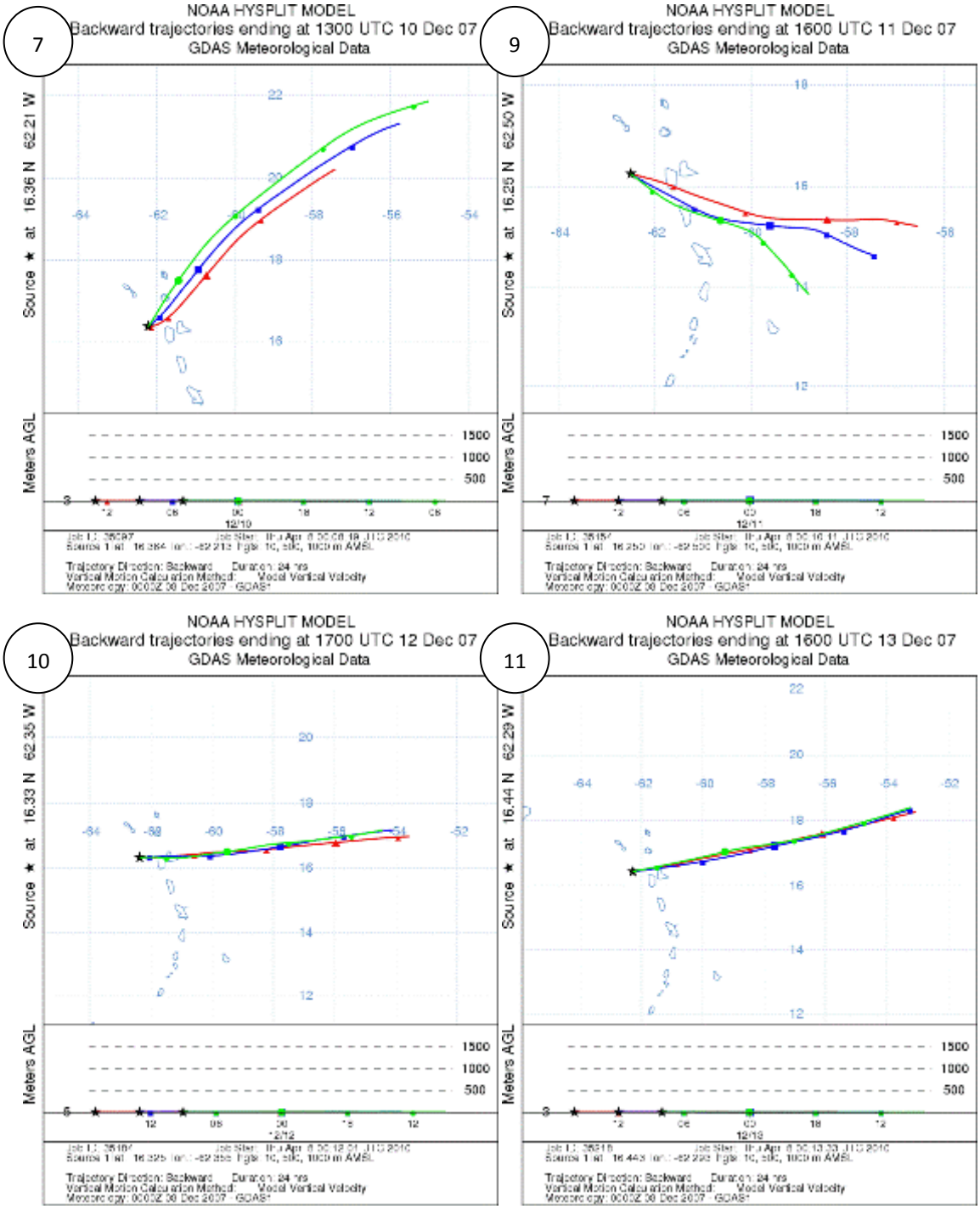

Diagram IV A series of numbered five-day air mass back trajectories for aerosol samples collected during cruise JC18.

V. JCR

1

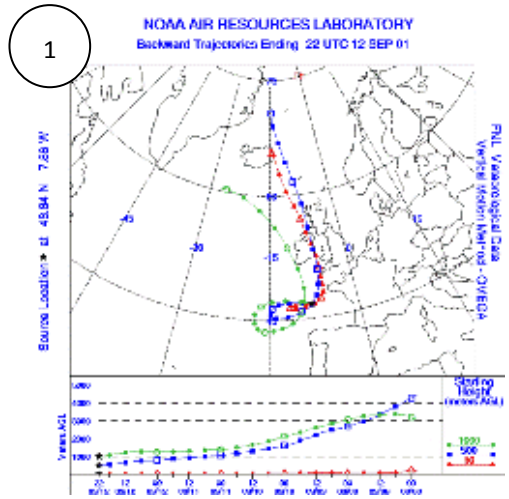
NOAA AIR RESOURCES LABORATORY
Backward Trajectories Ending 22 UTC 12 SEP 01

2

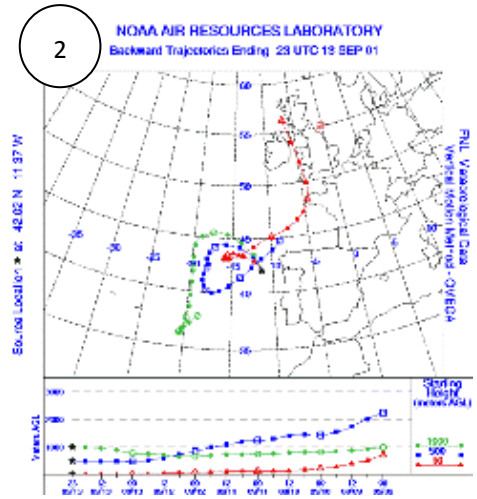
NOAA AIR RESOURCES LABORATORY
Backward Trajectories Ending 23 UTC 13 SEP 01

3

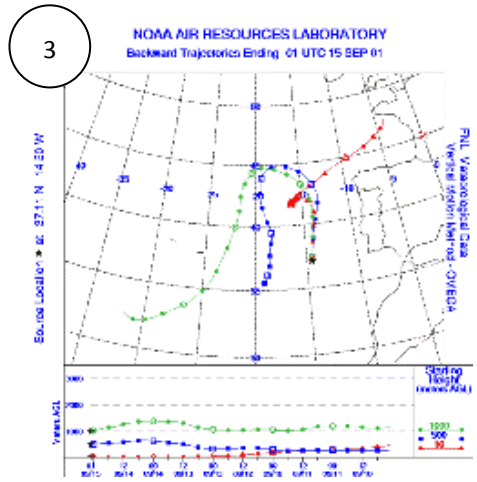
NOAA AIR RESOURCES LABORATORY
Backward Trajectories Ending 01 UTC 15 SEP 01

4

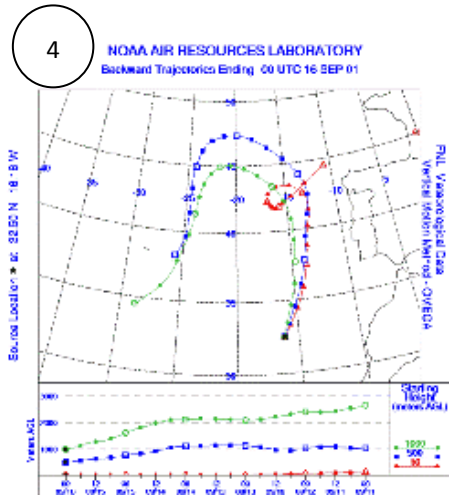
NOAA AIR RESOURCES LABORATORY
Backward Trajectories Ending 00 UTC 16 SEP 01

5

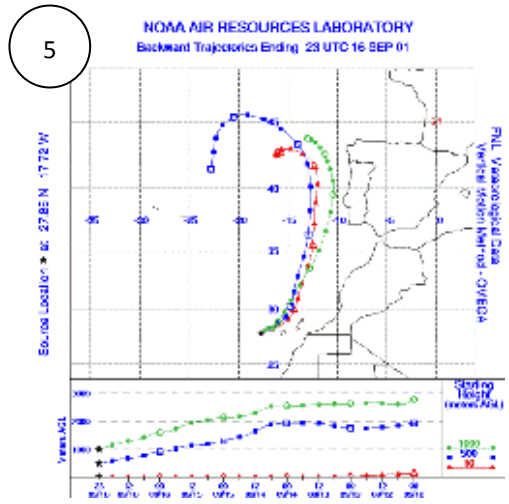
NOAA AIR RESOURCES LABORATORY
Backward Trajectories Ending 23 UTC 16 SEP 01

8

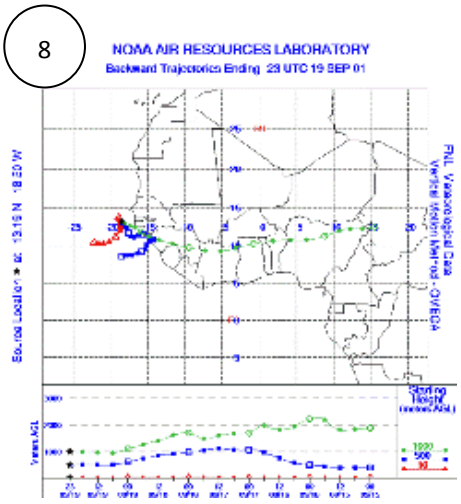
NOAA AIR RESOURCES LABORATORY
Backward Trajectories Ending 23 UTC 19 SEP 01

9

NOAA AIR RESOURCES LABORATORY

Backward Trajectories Ending 23 UTC 20 SEP 01

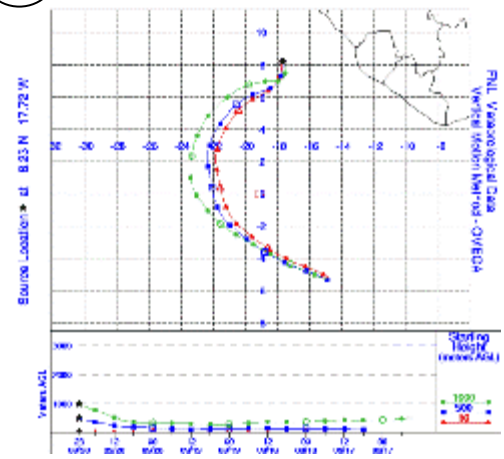

10

NOAA AIR RESOURCES LABORATORY

Backward Trajectories Ending 23 UTC 21 SEP 01

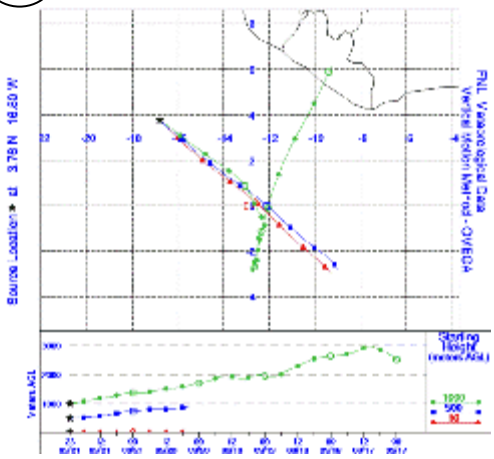

11

NOAA AIR RESOURCES LABORATORY

Backward Trajectories Ending 23 UTC 22 SEP 01

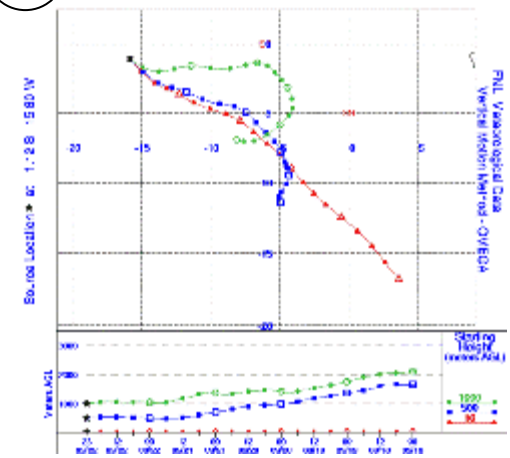

12

NOAA AIR RESOURCES LABORATORY

Backward Trajectories Ending 23 UTC 23 SEP 01

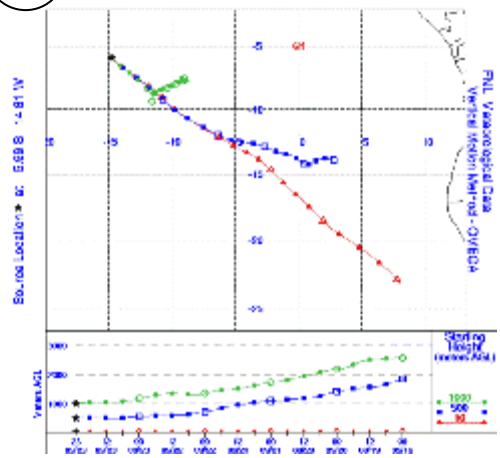

13

NOAA AIR RESOURCES LABORATORY

Backward Trajectories Ending 01 UTC 25 SEP 01

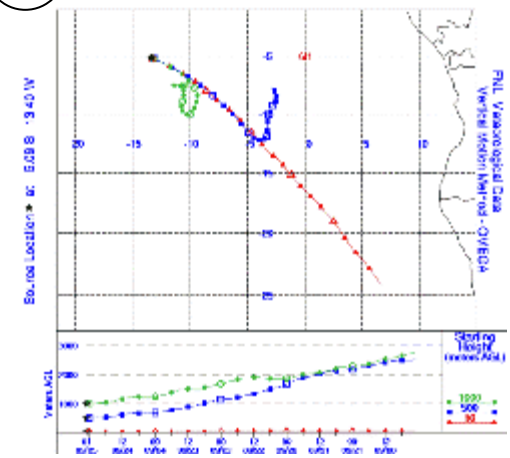

15

NOAA AIR RESOURCES LABORATORY

Backward Trajectories Ending 19 UTC 05 OCT 01

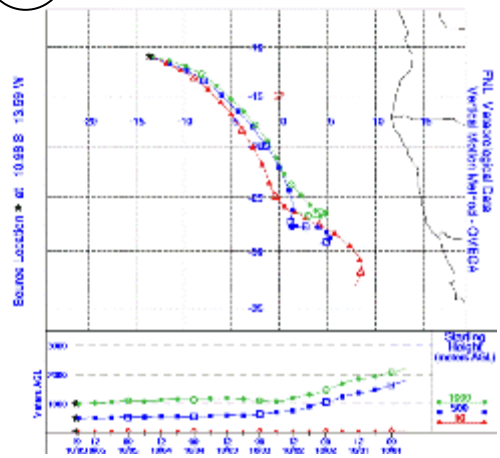

16

NOAA AIR RESOURCES LABORATORY

Backward Trajectories Ending 05 UTC 08 OCT 01

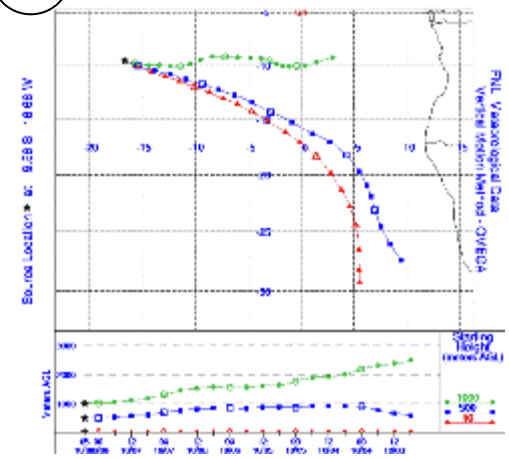

17

NOAA AIR RESOURCES LABORATORY

Backward Trajectories Ending 16 UTC 09 OCT 01

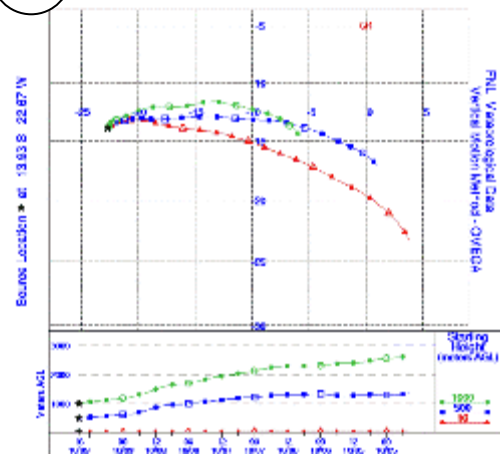

18

NOAA AIR RESOURCES LABORATORY

Backward Trajectories Ending 00 UTC 11 OCT 01

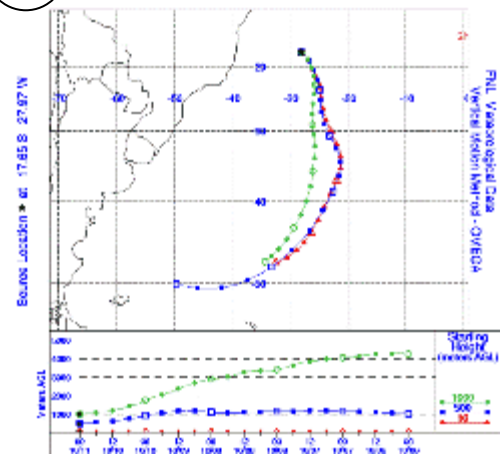

19

NOAA AIR RESOURCES LABORATORY

Backward Trajectories Ending 01 UTC 12 OCT 01

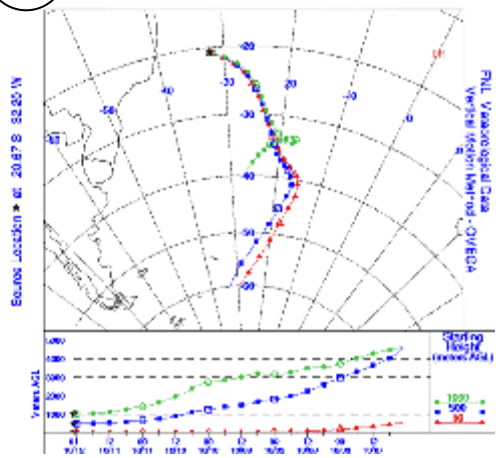

20

NOAA AIR RESOURCES LABORATORY

Backward Trajectories Ending 01 UTC 13 OCT 01

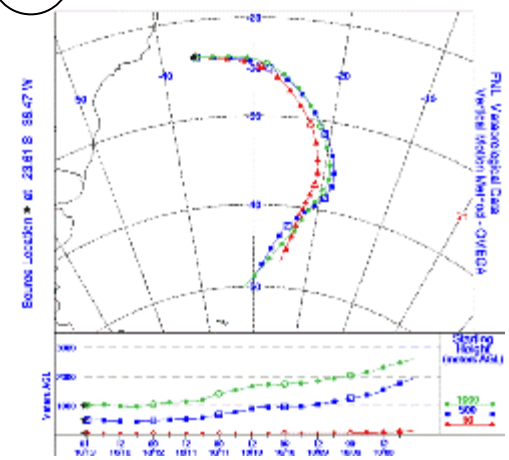

21

NOAA AIR RESOURCES LABORATORY

Backward Trajectories Ending 13 UTC 13 OCT 01

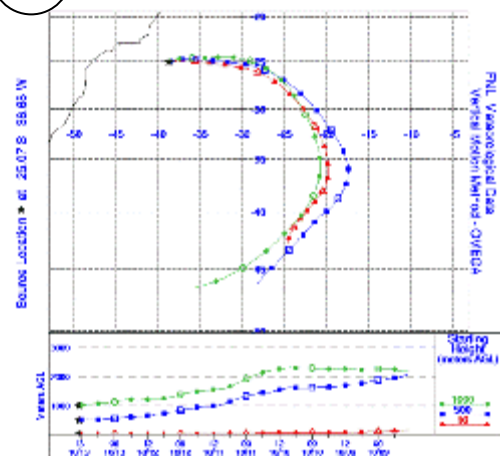

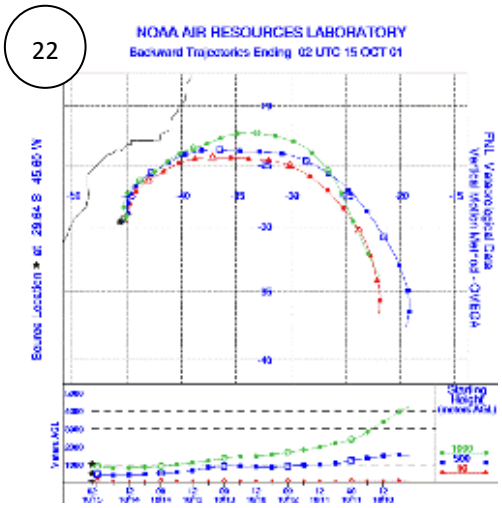

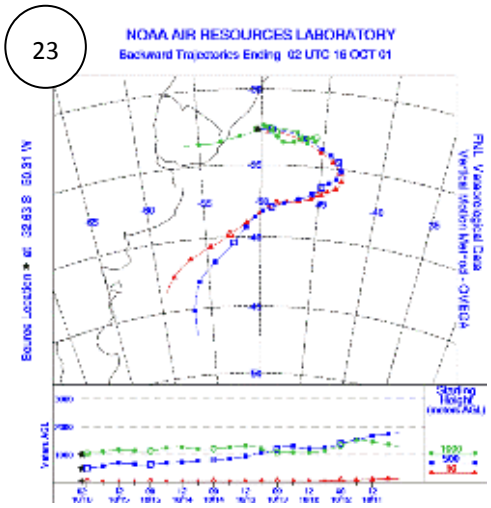

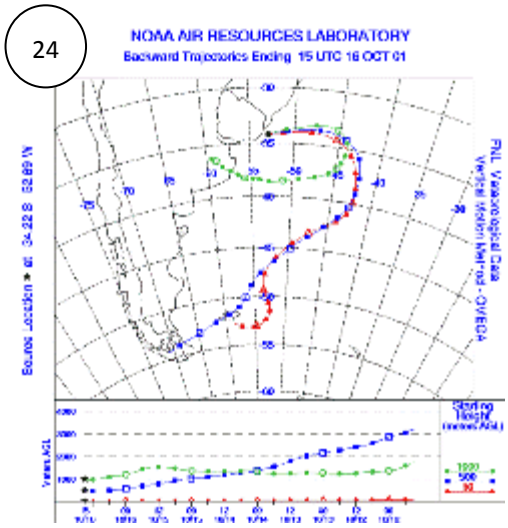

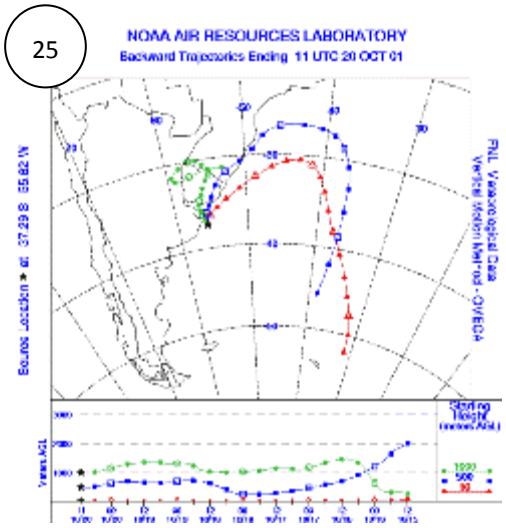

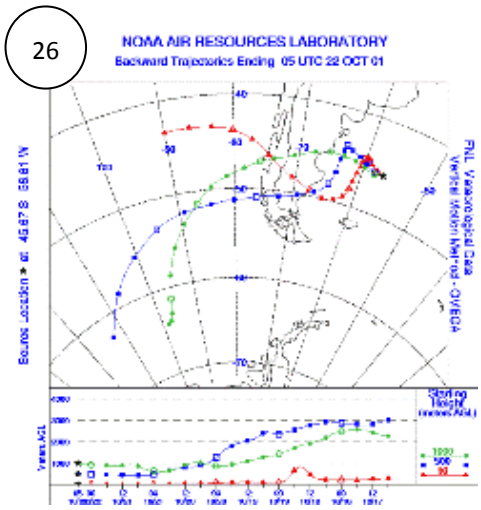

Diagram V A series of numbered five-day air mass back trajectories for aerosol samples collected during cruise JCR.

Appendix 2: Calculate the Relative Standard Deviation for Biogenic Sulfate

The calculation of the standard deviations for the calculated sulfate components can be derived by following the equations, based on Miller & Miller (2005):

For linear (addition/subtraction) combinations:

$$\text{If } y = k + k_a a + k_b b + k_c c + \cdots$$

$$\text{then } \sigma_y = \sqrt{(k_a\sigma_a)^2 + (k_b\sigma_b)^2 + (k_c\sigma_c)^2 + \cdots}$$

Where k, k_a, k_b etc are constants, the standard deviations of a, b, c etc. are defined as σ_a, σ_b, σ_c etc., and y indicates the derived value, σ_y the derived deviation.

For multiplicative (multiplication/division) combinations:

$$\text{If } y = kab/cd$$

$$\text{then } \frac{\sigma_y}{y} = \sqrt{(\frac{\sigma_a}{a})^2 + (\frac{\sigma_b}{b})^2 + (\frac{\sigma_c}{c})^2 + (\frac{\sigma_d}{d})^2}$$

Where identical terminologies apply.

Firstly, in order to calculate the sulfate components, in this case biogenic sulfate, three steps must be taken based on the atmospheric concentration and isotopic data: the calculation of non-seasalt sulfate i.e. seasalt correction, the calculation of seasalt sulfate fraction, and finally the calculation of biogenic sulfate (see chapter 3.1.3).

$$\text{Seasalt sulfate} = Na_{mea} \times \left(\frac{S}{Na}\right)_{sw} \qquad \textbf{Equation 1}$$

where Na_{mea} is the measured atmospheric concentration of sodium, multiplied by the average ratio of sulfates / sodium in seawater.

Then:

$$\text{Seasalt fraction} = \frac{\text{seasalt sulfate}}{\text{overall sulfate}} \qquad \textbf{Equation 2}$$

And finally:

$$\text{Conc. of S (bio)} = \text{Conc. of Total S} \times \left[\frac{(\text{S Isotope} - 3 - 18 * \text{Fraction of Seasalt})}{15}\right] \qquad \textbf{Equation 3}$$

From equation 3, the number

- +3 is the anthropogenic end member with an uncertainty of ±2‰ (sdA)
- +18 derives from 21‰ (seasalt end member, no deviation) minus +3‰ (anthropogenic end member, deviation ±2‰), and has a deviation of ±2‰ (sd1)
- +15 derives from +18‰ (biogenic end member, deviation 2‰) minus +3‰ (anthropogenic end member, deviation ±2‰), and should have deviation of $\sqrt{2^2 + 2^2} = 2.83$ (sd2)

All three equations must be used for biogenic sulfate calculation, and the relative deviation must be calculated cumulatively from equation 1 to 3.

Equation 3 can be separated into several parts in order to propagate error:
Assume standard deviation (sd) for
S Isotope = sdS
Anthropogenic end member (+3) = sdA
Seasalt end member – Anthropogenic end member (21-3=18) = sd1
Biogenic end member – Anthropogenic end member (18-3=15) = sd2
Fraction of seasalt sulfate = sdss
Total S = sdS

Part A: S Isotope − 3

$$\mathrm{SDa} = \sqrt{\mathrm{sdS}^2 + \mathrm{sdA}^2}$$

Part B: 18 ∗ Fraction of Seasalt

$$\mathrm{SDb} = \sqrt{\mathrm{sd1}^2 + \mathrm{sdss}^2}$$

Part C: (S Isotope − 3 − 18 ∗ Fraction of Seasalt)

$$\mathrm{SDc} = \sqrt{\mathrm{SDa}^2 + \mathrm{SDb}^2}$$

Part D: $\left[\frac{(\text{S Isotope} - 3 - 18 * \text{Fraction of Seasalt})}{15}\right]$

$$\frac{\mathrm{SDd}}{\mathrm{d}} = \sqrt{\left[\frac{\mathrm{sdc}}{(\text{S Isotope} - 3 - 18 * \text{Fraction of Seasalt})}\right]^2 + \left(\frac{\mathrm{sd2}}{15}\right)^2}$$

Part E: Conc. of Total S $\times \left[\frac{(\text{S Isotope} - 3 - 18 * \text{Fraction of Seasalt})}{15}\right]$

$$\frac{\mathrm{SDe}}{\mathrm{e}} = \sqrt{\left(\frac{\mathrm{sdS}}{\text{Total S}}\right)^2 + \left(\frac{\mathrm{SDd}}{\mathrm{d}}\right)^2}$$

By performing error propagation in several steps, the overall uncertainty for the concentration of biogenic sulfate can be calculated.

Appendix 3: Calculate the Relative Standard Deviation for Anthropogenic Ammonium

Similar to steps described in appendix 2, similar error propagation can be performed. The calculation for anthropogenic ammonium can be found in chapter 3.2.2

$$\%AN = \frac{(\delta^{15}N_T - \delta^{15}N_B)}{(\delta^{15}N_A - \delta^{15}N_B)} \times 100 \qquad \textbf{Equation 1}$$

Assume standard deviation (sd) for

$\delta^{15}N_T$ = sdT (standard deviation from replicate measurements)

$\delta^{15}N_B$ = sdB (estimated deviation, see chapter 3.2.2)

$\delta^{15}N_A$ = sdA (estimated deviation, see chapter 3.2.2)

Part A: $(\delta^{15}N_T - \delta^{15}N_B)$

$SDa = \sqrt{sdT^2 + sdB^2}$

Part B: $(\delta^{15}N_A - \delta^{15}N_B)$

$SDb = \sqrt{sdA^2 + sdB^2}$

Part C: $\frac{(\delta^{15}N_T - \delta^{15}N_B)}{(\delta^{15}N_A - \delta^{15}N_B)}$

$$\frac{SDc}{C} = \sqrt{\left(\frac{SDa}{a}\right)^2 + \left(\frac{SDb}{b}\right)^2}$$

Part D: $\frac{(\delta^{15}N_T - \delta^{15}N_B)}{(\delta^{15}N_A - \delta^{15}N_B)} \times 100$

$SDd = SDc \times 100$

By performing error propagation in several steps, the overall uncertainty for the percentage of anthropogenic ammonium can be calculated.

References

ALLAN, B. J., MCFIGGANS, G., PLANE, J. M. C., COE, H. & MCFADYEN, G. G. (2000) The nitrate radical in the remote marine boundary layer. *Journal of Geophysical Research D: Atmospheres,* 105**,** 24191-24204.

ANDREAE, M. O. (1983) Soot carbon and excess fine potassium: Long-range transport of combustion-derived aerosols. *Science,* 220**,** 1148-1151.

ANDREAE, M. O. & CRUTZEN, P. J. (1997) Atmospheric aerosols: Biogeochemical sources and role in atmospheric chemistry. *Science,* 276**,** 1052-1058.

ANDREAE, M. O., ELBERT, W., CAI, Y., ANDREAE, T. W. & GRAS, J. (1999) Non-sea-salt sulfate, methanesulfonate, and nitrate aerosol concentrations and size distributions at Cape Grim, Tasmania. *J. Geophys. Res.,* 104**,** 21695-21706.

ANDREAE, M. O. & MERLET, P. (2001) Emission of trace gases and aerosols from biomass burning. *Global Biogeochemical Cycles,* 15**,** 955-966.

ANDREWS, J. E., BRIMBLECOMBE, P., JICKELLS, T. D., LISS, P. S. & REID, B. (2004) *An Introduction to Environmental Chemistry*, Blackwell.

AYERS, G. P. & CAINEY, J. M. (2007) The CLAW hypothesis: A review of the major developments. *Environmental Chemistry,* 4**,** 366-374.

AYERS, G. P., IVEY, J. P. & GILLETT, R. W. (1991a) Coherence between seasonal cycles of dimethyl sulphide, methanesulphonate and sulfate in marine air. *Nature,* 349**,** 404-406.

AYERS, G. P. & GRAS, J. L. (1991b) Seasonal relationship between cloud condensation nuclei and aerosol methanesulphonate in marine air. *Nature,* 353**,** 834-835.

BAKER, A. R., JICKELLS, T. D., BISWAS, K. F., WESTON, K. & FRENCH, M. (2006) Nutrients in atmospheric aerosol particles along the Atlantic Meridional Transect. *Deep-Sea Research Part II: Topical Studies in Oceanography,* 53**,** 1706-1719.

BAKER, A. R., LESWORTH, T., ADAMS, C., JICKELLS, T. D. & GANZEVELD, L. (2010) Estimation of atmospheric nutrient inputs to the Atlantic Ocean from 50°N to 50°S based on large-scale field sampling: Fixed nitrogen and dry deposition of phosphorus *GLOBAL BIOGEOCHEMICAL CYCLES,* 24**,** GB3006.

BRISTOW, L. A. (2009) Tracing nitrogen flows acroos the southern North Sea : a stable isotope approach. *Thesis (Ph.D.), School of Environmental Sciences, University of East Anglia, Norwich*.

CALHOUN, J. A., BATES, T. S. & CHARLSON, R. J. (1991) Sulfur isotope measurements of submicrometer sulfate aerosol particles over the Pacific Ocean. *Geophysical Research Letters,* 18**,** 1877-1880.

CHARLSON, R. J., LOVELOCK, J. E., ANDREAE, M. O. & WARREN, S. G. (1987) Oceanic phytoplankton, atmospheric sulfur, cloud albedo and climate. *Nature,* 326**,** 655-661.

CLAEYS, M., WANG, W., VERMEYLEN, R., KOURTCHEV, I., CHI, X., FARHAT, Y., SURRATT, J. D., GÃ³MEZ-GONZÃ¡LEZ, Y., SCIARE, J. & MAENHAUT, W. (2010) Chemical characterisation of marine aerosol at Amsterdam Island during the austral summer of 2006-2007. *Journal of Aerosol Science,* 41**,** 13-22.

DUCE, R. A., LAROCHE, J., ALTIERI, K., ARRIGO, K. R., BAKER, A. R., CAPONE, D. G., CORNELL, S., DENTENER, F., GALLOWAY, J., GANESHRAM, R. S., GEIDER, R. J., JICKELLS, T., KUYPERS, M. M., LANGLOIS, R., LISS, P. S., LIU, S. M., MIDDELBURG, J. J., MOORE, C. M., NICKOVIC, S., OSCHLIES, A., PEDERSEN, T., PROSPERO, J., SCHLITZER, R., SEITZINGER, S., SORENSEN, L. L., UEMATSU, M., ULLOA, O., VOSS, M., WARD, B. & ZAMORA, L. (2008) Impacts of atmospheric anthropogenic nitrogen on the open ocean. *Science,* 320**,** 893-897.

ECKARDT, F. (2001) The origin of sulfates: An example of sulfur isotopic applications. *Progress in Physical Geography,* 25**,** 512-519.

FAURE, G. & MENSING, T. M. (2005) Isotopes: principles and applications. *3rd ed. Wiley*.

FRITZ, J. S. & GJERDE, D. T. (2000) Ion chromatography. *3rd ed. Wiley-VCH*.

GALLOWAY, J. N., ABER, J. D., ERISMAN, J. W., SEITZINGER, S. P., HOWARTH, R. W., COWLING, E. B. & COSBY, B. J. (2003) The nitrogen cascade. *BioScience,* 53**,** 341-356.

GONDWE, M., KROL, M., KLAASSEN, W., GIESKES, W. & DE BAAR, H. (2004) Comparison of modeled versus measured MSA: nss $SO_4^{=}$ ratios: A global analysis. *Global Biogeochemical Cycles,* 18**,** GB2006 1-18.

GRUBER, N. & GALLOWAY, J. N. (2008) An Earth-system perspective of the global nitrogen cycle. *Nature,* 451**,** 293-296.

HALAS, S. & SZARAN, J. (2001) Improved thermal decomposition of sulfates to SO_2 and mass spectrometric determination of $\delta^{34}S$ of IAEA SO-5, IAEA SO-6 and NBS-127 sulfate standards. *Rapid Communications in Mass Spectrometry,* 15**,** 1618-1620.

HEATON, T. H. E. (1986) Isotopic studies of nitrogen pollution in the hydrosphere and atmosphere: A review. *Chemical Geology,* 59**,** 87-102.

HEATON, T. H. E. (1987) $^{15}N/^{14}N$ ratios of nitrate and ammonium in rain at Pretoria, South Africa. *Atmospheric Environment,* 21**,** 843-852.

HOLMES, R. M., MCCLELLAND, J. W., SIGMAN, D. M., FRY, B. & PETERSON, B. J. (1998) Measuring 15N-NH4/+ in marine, estuarine and fresh waters: An adaptation of the ammonia diffusion method for samples with low ammonium concentrations. *Marine Chemistry,* 60**,** 235-243.

HUEBERT, B. (2007) Do i believe in CLAW? *Environmental Chemistry,* 4**,** 375-376.

JICKELLS, T. D., KELLY, S. D., BAKER, A. R., BISWAS, K., DENNIS, P. F., SPOKES, L. J., WITT, M. & YEATMAN, S. G. (2003) Isotopic evidence for a marine ammonia source. *Geophysical Research Letters,* 30**,** 27-1.

JOHNSON, M. T. & BELL, T. G. (2008) Coupling between dimethylsulfide emissions and the ocean-atmosphere exchange of ammonia. *Environmental Chemistry,* 5**,** 259-267.

JOHNSON, M. T., LISS, P. S., BELL, T. G., LESWORTH, T. J., BAKER, A. R., HIND, A. J., JICKELLS, T. D., BISWAS, K. F., WOODWARD, E. M. S. & GIBB, S. W. (2008) Field observations of the ocean-atmosphere exchange of ammonia: Fundamental importance of temperature as revealed by a comparison of high and low latitudes. *Global Biogeochemical Cycles,* 22.

KEENE, W. C., PSZENNY, A. A. P., GALLOWAY, J. N. & HAWLEY, M. E. (1986) Sea-Salt Corrections and Interpretation of Constituent Ratios in Marine Precipitation. *Journal of Geophysical Research D:*

Atmospheres, 91**,** 6647–6658.

KEENE, W. C., LONG, M. S., PSZENNY, A. A. P., SANDER, R., MABEN, J. R., WALL, A. J., O'HALLORAN, T. L., KERKWEG, A., FISCHER, E. V. & SCHREMS, O. (2009) Latitudinal variation in the multiphase chemical processing of inorganic halogens and related species over the eastern North and South Atlantic Oceans. *Atmospheric Chemistry and Physics,* 9**,** 7361-7385.

KELLY, S. D., STEIN, C. & JICKELLS, T. D. (2005) Carbon and nitrogen isotopic analysis of atmospheric organic matter. *Atmospheric Environment,* 39**,** 6007-6011.

KENDALL, C. & MCDONNELL, J. J. (1998) Isotope tracers in catchment hydrology. *1st ed. Elsevier Science*.

KOGA, S. & TANAKA, H. (1996) Simulations of seasonal variations of sulfur compounds in the remote marine atmosphere. *Journal of Atmospheric Chemistry,* 23**,** 163-192.

LEHMANN, M. F., BERNASCONI, S. M. & MCKENZIE, J. A. (2001) A method for the extraction of ammonium from freshwaters for nitrogen isotope analysis. *Analytical Chemistry,* 73**,** 4717-4721.

LESWORTH, T. (2007) Atmospheric nutrient inputs to the Atlantic Ocean. *Thesis (Ph.D.), School of Environmental Sciences, University of East Anglia, Norwich*.

LISS, P. S. & LOVELOCK, J. E. (2007) Climate change: The effect of DMS emissions. *Environmental Chemistry,* 4**,** 377-378.

LIU, X.-Y., XIAO, H.-Y., LIU, C.-Q., LI, Y.-Y. & XIAO, H.-W. (2008) Atmospheric transport of urban-derived NHx: Evidence from nitrogen concentration and $\delta^{15}N$ in epilithic mosses at Guiyang, SW China. *Environmental Pollution,* 156**,** 715-722.

MALIN, G. & KIRST, G. O. (1997) Algal production of dimethyl sulfide and its atmospheric role. *Journal of Phycology,* 33**,** 889-896.

MCARDLE, N. C. (1993) The use of stable sulfur isotopes to distinguish between natural and anthropogenic sulfur in the atmosphere. *PhD thesis, University of East Anglia, Norwich*.

MCARDLE, N. C. & LISS, P. S. (1995) Isotopes and atmospheric sulfur. *Atmospheric Environment,* 29**,** 2553-2556.

MCARDLE, N., LISS, P. & DENNIS, P. (1998) An isotopic study of atmospheric sulfur at three sites in Wales and at Mace Head, Eire. *Journal of Geophysical Research D: Atmospheres,* 103**,** 31079-31094.

MCARDLE, N., LISS, P. & DENNIS, P. (1998) An isotopic study of atmospheric sulfur at three sites in Wales and at Mace Head, Eire. *Journal of Geophysical Research D: Atmospheres,* 103**,** 31079-31094.

MCILVIN, M. R. & ALTABET, M. A. (2005) Chemical conversion of nitrate and nitrite to nitrous oxide for nitrogen and oxygen isotopic analysis in freshwater and seawater. *Analytical Chemistry,* 77**,** 5589-5595.

MILLER, J. N. & MILLER, J. C. (2005) Statistics and Chemometrics for Analytical Chemistry. *5th ed. Pearson Education Limited*.

NORMAN, A. L., ANLAUF, K., HAYDEN, K., THOMPSON, B., BROOK, J. R., LI, S. M. & BOTTENHEIM, J. (2006) Aerosol sulfate and its oxidation on the Pacific NW coast: S and O isotopes

in PM2.5. *Atmospheric Environment,* 40**,** 2676-2689.

O'DOWD, C. D. & DE LEEUW, G. (2007) Marine aerosol production: A review of the current knowledge. *Philosophical Transactions of the Royal Society A: Mathematical, Physical and Engineering Sciences,* 365**,** 1753-1774.

PARSONS, T. R., Y.MAITA & LALLI., C. M. (1984) A manual of biological and chemical methods for seawater analysis. *Pergamon Press (Oxford)*.

PATRIS, N., MIHALOPOULOS, N., BABOUKAS, E. D. & JOUZEL, J. (2000) Isotopic composition of sulfur in size-resolved marine aerosols above the Atlantic Ocean. *Journal of Geophysical Research D: Atmospheres,* 105**,** 14449-14457.

PELEGRI, J. L., CSANADY, G. T. & MARTINS, A. (1996) The North Atlantic nutrient stream. *Journal of Oceanography,* 52**,** 275-299.

PRODI, F., BELOSI, F., CONTINI, D., SANTACHIARA, G., DI MATTEO, L., GAMBARO, A., DONATEO, A. & CESARI, D. (2009) Aerosol fine fraction in the Venice Lagoon: Particle composition and sources. *Atmospheric Research,* 92**,** 141-150.

PURVAJA, R., RAMESH, R., RAY, A. K. & RIXEN, T. (2008) Nitrogen cycling: A review of the processes, transformations and fluxes in coastal ecosystems. *Current Science,* 94**,** 1419-1438.

QUINN, P. K., BATES, T. S., JOHNSON, J. E., COVERT, D. S. & CHARLSON, R. J. (1990) Interactions between the sulfur and reduced nitrogen cycles over the central Pacific Ocean. *Journal of Geophysical Research,* 95.

RAES, F., VAN DINGENEN, R., VIGNATI, E., WILSON, J., PUTAUD, J. P., SEINFELD, J. H. & ADAMS, P. (2000) Formation and cycling of aerosols in the global troposphere. *Atmospheric Environment,* 34**,** 4215-4240.

RAMASWAMY, V., O. BOUCHER, J. HAIGH, D. HAUGLUSTAINE, J. HAYWOOD, G. MYHRE, T. NAKAJIMA, G.Y. SHI, S. SOLOMON, R. BETTS, R. CHARLSON, C. CHUANG, J.S. DANIEL, A. DEL GENIO, R. VAN DORLAND, J. FEICHTER, J. FUGLESTVEDT, P.M. DE F. FORSTER, S.J. GHAN, A. JONES, J.T. KIEHL, D. KOCH, C. LAND, J. LEAN, U. LOHMANN, K. MINSCHWANER, J.E. PENNER, D.L. ROBERTS, H. RODHE, G.J. ROELOFS, L.D. ROTSTAYN, T.L. SCHNEIDER, U. SCHUMANN, S.E. SCHWARTZ, M.D. SCHWARZKOPF, K.P. SHINE, S. SMITH, D.S. STEVENSON, F. STORDAL, I. TEGEN, Y. ZHANG (2003) Chapter 6. Radiative Forcing of Climate Change. *IPCC Third Assessment Report - Climate Change 2001* Working Group I: The Scientific Basis.

REES, C. E. (1970) The sulfur isotope balance of the ocean: an improved model. *Earth and Planetary Science Letters,* 7**,** 366-370.

REES, C. E., JENKINS, W. J. & MONSTER, J. (1978) The sulfur isotopic composition of ocean water sulfate. *Geochimica et Cosmochimica Acta,* 42**,** 377-381.

ROBINSON, C., POULTON, A. J., HOLLIGAN, P. M., BAKER, A. R., FORSTER, G., GIST, N., JICKELLS, T. D., MALIN, G., UPSTILL-GODDARD, R., WILLIAMS, R. G., WOODWARD, E. M. S. & ZUBKOV, M. V. (2006) The Atlantic Meridional Transect (AMT) Programme: A contextual view 1995-2005. *Deep-Sea Research Part II: Topical Studies in Oceanography,* 53**,** 1485-1515.

ROLFF, C., ELMGREN, R. & VOSS, M. (2008) Deposition of nitrogen and phosphorus on the Baltic Sea: Seasonal patterns and nitrogen isotope composition. *Biogeosciences,* 5**,** 1657-1667.

RUSSELL, K. M., GALLOWAY, J. N., MACKO, S. A., MOODY, J. L. & SCUDLARK, J. R. (1998) Sources of nitrogen in wet deposition to the Chesapeake bay region. *Atmospheric Environment,* 32**,** 2453-2465.

SALTZMAN, E. S., SAVOIE, D. L., PROSPERO, J. M. & ZIKA, R. G. (1986) Methanesulfonic acid and non-sea-salt sulfate in Pacific air: Regional and seasonal variations. *Journal of Atmospheric Chemistry,* 4**,** 227-240.

SMIL, V. (2007) Global material cycles. The encyclopaedia of earth, viewed 20 January 2010, http://www.eoearth.org/image/Sulfur_cycle_flow_diagram.jpg

STUMM, W. & MORGAN, J. J. (1996) Aquatic chemistry: chemical equilibria and rates in natural waters. *3rd ed. Wiley*.

SULTAN, B. & JANICOT, S. (2000) Abrupt shift of the ITCZ over West Africa and intra-seasonal variability. *Geophysical Research Letters,* 27**,** 3353-3356.

THODE, H. G. (1991) Chapter 1: Sulfur Isotopes in Nature and the Environment: An Overview. *SCOPE43 Stable Isotopes - Natural and Anthropogenic Sulfur in the Environment*.

VALLINA, S. M. & SIMO, R. (2007) Re-visiting the CLAW hypothesis. *Environmental Chemistry,* 4**,** 384-387.

VOGT, R., CRUTZEN, P. J. & SANDER, R. (1996) A mechanism for halogen release from sea-salt aerosol in the remote marine boundary layer. *Nature,* 383**,** 327-330.

VON GLASOW, R. & CRUTZEN, P. J. (2004) Model study of multiphase DMS oxidation with a focus on halogens. *Atmospheric Chemistry and Physics,* 4**,** 589-608.

WADLEIGH, M. A., SCHWARCZ, H. P. & KRAMER, J. R. (2001) Areal distribution of sulfur and oxygen isotopes in sulfate of rain over eastern North America. *Journal of Geophysical Research D: Atmospheres,* 106**,** 20883-20895.

WADLEIGH, M. A. (2004) Sulfur isotopic composition of aerosols over the western North Atlantic Ocean. *Canadian Journal of Fisheries and Aquatic Sciences,* 61**,** 817-825.

WOODHOUSE, M. T., CARSLAW, K.S., MANN, G.W., VALLINA, S.M., VOGT, M., HALLORAN, P.R. AND BOUCHER, O. (2010) Low sensitivity of cloud condensation nuclei to changes in the sea-air flux of dimethyl-sulphide. *Atmospheric Chemistry and Physics,* 10(16)**,** 7545-7559.

XIAO, H. Y. & LIU, C. Q. (2002) Sources of nitrogen and sulfur in wet deposition at Guiyang, southwest China. *Atmospheric Environment,* 36**,** 5121-5130.

XIE, Y., XIONG, Z., XING, G., YAN, X., SHI, S., SUN, G. & ZHU, Z. (2008) Source of nitrogen in wet deposition to a rice agroecosystem at Tai lake region. *Atmospheric Environment,* 42**,** 5182-5192.

ZHANG, L., ALTABET, M. A., WU, T. & HADAS, O. (2007) Sensitive Measurement of NH_4^+ $^{15}N/^{14}N$ ($\delta^{15}NH_4^+$) at Natural Abundance Levels in Fresh and Saltwaters. *Analytical Chemistry,* 79**,** 5297-5303.